

# Association of MBL2 gene polymorphisms with pulmonary tuberculosis susceptibility: trial sequence meta-analysis as evidence

Raju K Mandal,<sup>1,\*</sup> Munawwar Ali Khan,<sup>2,\*</sup> Arif Hussain,<sup>3</sup> Sajad A Dar,<sup>1</sup> Sultan Aloufi,<sup>4</sup> Arshad Jawed,<sup>1</sup> Mohd Wahid,<sup>1</sup> Aditya K Panda,<sup>5</sup> Mohtashim Lohani,<sup>6</sup> Naseem Akhter,<sup>7</sup> Saif Khan,<sup>8</sup> Bhartendu Nath Mishra,<sup>9</sup> Shafiu Haque<sup>1</sup>

<sup>1</sup>Research and Scientific Studies Unit, College of Nursing and Allied Health Sciences, Jazan University, Jazan, Saudi Arabia; <sup>2</sup>Department of Life and Environmental Sciences, College of Natural and Health Sciences, Zayed University, Dubai, United Arab Emirates; <sup>3</sup>School of Life Sciences, Manipal Academy of Higher Education, Dubai, United Arab Emirates; <sup>4</sup>Department of Clinical Laboratory Sciences, College of Applied Medical Sciences, University of Ha'il, Ha'il, Saudi Arabia; <sup>5</sup>Centre for Life Sciences, Central University of Jharkhand, Ranchi, Jharkhand, India; <sup>6</sup>Department of Emergency Medical Services, College of Applied Medical Sciences, Jazan University, Jazan, Saudi Arabia; <sup>7</sup>Department of Laboratory Medicine, Faculty of Applied Medical Sciences, Al Baha University, Al Baha, Saudi Arabia; <sup>8</sup>Department of Basic Sciences, College of Dentistry, University of Ha'il, Ha'il, Saudi Arabia; <sup>9</sup>Department of Biotechnology, Institute of Engineering and Technology, Lucknow, Uttar Pradesh, India

\*These authors contributed equally to this work

**Background:** Mannose-binding lectin (MBL) or mannose-binding protein (MBP), encoded by MBL2 gene and secreted by the liver, activates complement system through lectin pathway in innate immunity against the host's infection. Conflictingly, a number of MBL2 variants, rs1800450 (A>B), rs1800451 (A>C), rs5030737 (A>D), rs7096206 (Y>X), rs11003125 (H>L), and rs7095891 (P>Q) allele, have been found to be associated with compromised serum levels and pulmonary tuberculosis (PTB) susceptibility. The present meta-analysis study was performed to evaluate the potential association of these MBL2 gene variants with PTB susceptibility.

**Materials and methods:** A quantitative synthesis was performed on PubMed (Medline), EMBASE, and Google Scholar web database searches. A meta-analysis was performed to calculate the pooled odds ratios and 95% CIs for all the genetic models.

**Results:** A total of 14 eligible studies were included to analyze their pooled data for associations between alleles, genotypes, and minor allele carriers. The statistical analysis revealed the significant reduced PTB risk with homozygous variant genotype of rs1800451 polymorphism (CC vs AA:  $P=0.043$ ; OR =0.828, 95% CI =0.689–0.994). Contrary to this, the variant allele of rs5030737 polymorphism showed association with increased PTB risk (D vs A:  $P=0.026$ ; OR =1.563, 95% CI =1.054–2.317). However, the other genetic models of rs1800450 (A>B), rs7096206 (Y>X), and rs11003125 (H>L) MBL2 gene polymorphisms did not divulge any association with PTB susceptibility.

**Conclusion:** The current meta-analysis concludes that rs1800451 (A>C) and rs5030737 (A>D) polymorphisms of MBL2 gene play a significant role in PTB susceptibility. Further, well-designed epidemiological studies with larger sample size including consideration of environmental factors are warranted for the future.

**Keywords:** meta-analysis, mannose-binding lectin, MBL2, pulmonary tuberculosis, PTB, polymorphism

## Introduction

Tuberculosis (TB), caused by *Mycobacterium tuberculosis*, is one of the most prevalent contagious airborne disease/infection, which is very harmful to the body tissues. In spite of good advancements in the treatment strategies, it is still a major health problem among the public. Lately, many reputed health reports reveal 10.4 million new cases and about 1.4 million deaths caused by TB, globally, in the year 2015. Among the two commonly found TB types, pulmonary tuberculosis (PTB) is one of the most devastating form and remains a leading cause of morbidity and mortality, globally.<sup>1</sup> PTB is a two-stage process including infection of *M. tuberculosis* and progression to the disease. It is a complex disease where both environmental and genetic factors play a role in

Correspondence: Shafiu Haque  
Research and Scientific Studies Unit,  
College of Nursing and Allied Health  
Sciences, Jazan University, Jazan 45142,  
Saudi Arabia  
Tel/Fax +966 17 317 4383  
Email shafiu.haque@hotmail.com

## Research Article

# Pharmacogenetic association between *NAT2* gene polymorphisms and isoniazid induced hepatotoxicity: trial sequence meta-analysis as evidence

Saif Khan<sup>1,\*</sup>, Raju K. Mandal<sup>2,\*</sup>, Abdulbaset Mohamed Elsbali<sup>3</sup>, Sajad A. Dar<sup>2</sup>, Arshad Jawed<sup>2</sup>, Mohd Wahid<sup>2</sup>, Harishankar Mahto<sup>4</sup>, Mohtashim Lohani<sup>5</sup>, Bhartendu Nath Mishra<sup>6</sup>, Naseem Akhter<sup>7</sup>, Ali A. Rabaan<sup>8</sup> and  Shafiul Haque<sup>2</sup>

<sup>1</sup>Department of Basic Science, College of Dental Sciences, University of Ha'il, Ha'il 2440, Saudi Arabia; <sup>2</sup>Research and Scientific Studies Unit, College of Nursing and Allied Health Sciences, Jazan University, Jazan 45142, Saudi Arabia; <sup>3</sup>Department of Clinical Laboratory Science, College of Applied Medical Sciences, Al Jouf University, Sakakah 72388, Saudi Arabia; <sup>4</sup>Centre for Life Sciences, Central University of Jharkhand, Ranchi 835205, Jharkhand, India; <sup>5</sup>Department of Emergency Medical Services, College Applied Medical Sciences, Jazan University, Jazan 45142, Saudi Arabia; <sup>6</sup>Department of Biotechnology, Institute of Engineering and Technology, Lucknow 226021, Uttar Pradesh, India; <sup>7</sup>Department of Laboratory Medicine, Faculty of Applied Medical Sciences, Albaha University, Albaha 65431, Saudi Arabia; <sup>8</sup>Molecular Diagnostic Laboratory, John Hopkins Aramco Healthcare, Dhahran 31311, Saudi Arabia

**Correspondence:** Shafiul Haque (shafiul.haque@hotmail.com)



Hepatotoxicity is a severe problem generally faced by tuberculosis (TB) patients. It is a well-known adverse reaction due to anti-TB drugs in TB patients undergoing long-term treatment. The studies published previously have explored the connection of N-acetyltransferase 2 (*NAT2*) gene polymorphisms with isoniazid-induced hepatotoxicity, but the results obtained were inconsistent and inconclusive. A comprehensive trial sequence meta-analysis was conducted employing 12 studies comprising 3613 controls and 933 confirmed TB cases using the databases namely, EMBASE, PubMed (Medline) and Google Scholar till December 2017. A significant association was observed with individuals carrying variant allele at position 481C>T (T vs. C:  $P = 0.001$ ; OR = 1.278, 95% CI = 1.1100–1.484), at position 590G>A (A vs. G:  $P = 0.002$ ; OR = 1.421, 95% CI = 1.137–1.776) and at position 857G>A (A vs. G:  $P = 0.0022$ ; OR = 1.411, 95% CI = 1.052–1.894) to higher risk of hepatotoxicity vis-à-vis wild-type allele. Likewise, the other genetic models of *NAT2* gene polymorphisms have also shown increased risk of hepatotoxicity. No evidence of publication bias was observed. These results suggest that genetic variants of *NAT2* gene have significant role in isoniazid induced hepatotoxicity. Thus, *NAT2* genotyping has the potential to improve the understanding of the drug–enzyme metabolic capacity and help in early predisposition of isoniazid-induced hepatotoxicity.

\* These authors contributed equally to this work.

Received: 28 May 2018  
Revised: 13 November 2018  
Accepted: 27 November 2018

Accepted Manuscript Online:  
03 December 2018  
Version of Record published:  
15 January 2019

## Introduction

*Mycobacterium tuberculosis* is the single most prominent species responsible for tuberculosis (TB) disease. This is a commonly prevalent disease present in almost all societies of the world. It causes a significant burden of morbidity and mortality on human population. The data from the year 2015 showed that almost 10.4 million people suffered from TB leading to 1.8 million deaths (<http://www.who.int/mediacentre/factsheets/fs104/en/>). The current most effective control is curing the patients with anti-TB drugs like isoniazid or isonicotinylhydrazide (INH), rifampicin (RMP) and pyrazinamide (PZA). These anti-TB drugs are used in combination for 6 or more months to cure the infection completely. The most common side effect associated with the use of anti-TB drugs is idiosyncratic hepatotoxicity, worldwide [1]. Hepatotoxicity



## Research Article

# A trial sequential meta-analysis of *TNF- $\alpha$* –308G>A (rs800629) gene polymorphism and susceptibility to colorectal cancer

Raju K. Mandal<sup>1,\*</sup>, Munawwar Ali Khan<sup>2,\*</sup>, Arif Hussain<sup>3</sup>, Naseem Akhter<sup>4</sup>, Arshad Jawed<sup>1</sup>, Sajad A. Dar<sup>1</sup>, Mohd Wahid<sup>1</sup>, Aditya K. Panda<sup>5</sup>, Mohtashim Lohani<sup>6</sup>, Bhartendu N. Mishra<sup>7</sup> and  Shafiul Haque<sup>1</sup>

<sup>1</sup>Research and Scientific Studies Unit, College of Nursing and Allied Health Sciences, Jazan University, Jazan-45142, Saudi Arabia; <sup>2</sup>Department of Life and Environmental Sciences, College of Natural and Health Sciences, Zayed University, P.O. Box 19282, Dubai, United Arab Emirates; <sup>3</sup>School of Life Sciences, Manipal Academy of Higher Education, P.O. Box 345050, Dubai, United Arab Emirates; <sup>4</sup>Department of Laboratory Medicine, Faculty of Applied Medical Sciences, Albaha University, Albaha 65431, Saudi Arabia; <sup>5</sup>Centre for Life Sciences, Central University of Jharkhand, Ranchi 835205, Jharkhand, India; <sup>6</sup>Department of Emergency Medical Services, College of Applied Medical Sciences, Jazan University, Jazan 45142, Saudi Arabia; <sup>7</sup>Department of Biotechnology, Institute of Engineering and Technology, Lucknow 226021, Uttar Pradesh, India

**Correspondence:** Shafiul Haque (shafiul.haque@hotmail.com)



**Purpose:** Tumor necrosis factor- $\alpha$  (*TNF- $\alpha$* ), secreted by the activated macrophages, may participate in the onset and progression of colorectal cancer (CRC). The association of *TNF- $\alpha$*  –308 G>A (rs1800629) single-nucleotide polymorphism (SNP) with CRC risk has been investigated by many studies but the results are inconclusive. A trial sequential meta-analysis was performed for precise estimation of the relationship between *TNF- $\alpha$*  –308 G>A gene polymorphism with CRC risk.

**Methods:** Medline (PubMed), EMBASE (Excerpta-Medica) and Google Scholar were mined for relevant articles. Odds ratios (ORs) and 95% confidence intervals (CIs) were calculated to estimate the significance of association.

**Results:** The pooled analysis indicated no risk associated with *TNF- $\alpha$*  –308 G>A SNP and overall CRC risk in five genetic comparison models, i.e. allelic (A vs. G:  $P = 0.524$ ; OR = 1.074, 95% CI = 0.863–1.335), homozygous (AA vs. GG:  $P = 0.489$ ; OR = 1.227, 95% CI = 0.688–2.188), heterozygous (AG vs. GG:  $P = 0.811$ ; OR = 1.024, 95% CI = 0.843–1.244), dominant (AA+AG vs. GG:  $P = 0.630$ ; OR = 1.055, 95% CI = 0.849–1.311) and recessive (AA vs. AG+GG:  $P = 0.549$ ; OR = 1.181, 95% CI = 0.686–2.033). Subgroup analysis revealed that *TNF- $\alpha$*  –308 G>A SNP is associated with reduced risk of CRC in Asian ethnicity. The study showed no publication bias.

**Conclusions:** No association of *TNF- $\alpha$*  –308 G>A SNP with overall CRC risk was found. This SNP is likely to be protective against CRC in Asian population when compared with Caucasian population. Larger prospective-epidemiological studies are warranted to elucidate the roles of *TNF- $\alpha$*  –308 G>A SNP in the etiology of CRC and to endorse the present findings.

\* These authors contributed equally to this work.

Received: 29 June 2018  
Revised: 29 October 2018  
Accepted: 29 November 2018

Accepted Manuscript Online:  
03 December 2018  
Version of Record published:  
15 January 2019

## Introduction

Approximately 608,000 people lose their life to colorectal cancer (CRC) worldwide [1]. According to the World Health Organization (WHO), millions of people will suffer from symptomatic as well as approximately the equal number from asymptomatic cases of CRC disease in the next decade.

CRC is a very heterogeneous and polygenic disease at a molecular level. It may be the result of interaction among different factors like environmental and genetic [2]. Early genome-wide association studies have shown contribution of many new single-nucleotide polymorphisms (SNPs) to increased



# Environmental factors associated with seasonal variations of night-time plant canopy and soil respiration fluxes in deciduous conifer forest, Western Himalaya, India

Nilendu Singh<sup>1</sup> · Bikash Ranjan Parida<sup>2</sup>

Received: 19 June 2018 / Accepted: 15 December 2018 / Published online: 2 January 2019  
© Springer-Verlag GmbH Germany, part of Springer Nature 2019

## Abstract

In situ carbon flux studies are typically rare over the Himalaya but are important to understand carbon (C) balance. We investigated night-time canopy respiration ( $R_{nc}$ ) and soil respiration ( $R_s$ ) of a deciduous coniferous forest in response to environmental factors. A comprehensive investigation has been carried out on C balance indicators by employing systematic and concurrent measurements over an annual growth cycle of pine (Nov 2010–Dec 2011). The study site consists of uniformly distributed young deciduous *Pinus roxburghii* plantation having understory as *Lantana camara* (an invasive shrub). Results underlined that both  $R_{nc}$  and  $R_s$  fluxes were highest in the post-monsoon season. Evaporative fraction (EF) and temperature explained maximum variability of fluxes during warm-moist monsoon. Our key finding depicts an inverse significant correlation between day-time canopy photosynthesis ( $A_c$ ) and  $R_{nc}$  across the seasons ( $r=0.83$ – $0.99$ ). This can be explained by the mechanistic physiological phase of optimal anabolism ( $A_c$ ) with favorable environmental conditions and minimum level of catabolism ( $R_{nc}$ ). The respiration-photosynthesis ratio ( $R_{nc}/A_c$ ) typically ranged from  $0.25 \pm 0.11$  (peak growing season) to  $0.71 \pm 0.16$  (winter season) with mean of  $0.26 \pm 0.10$ . The ratio  $R_s/A_c$  was highest during the winter season ( $2.69 \pm 0.43$ ), while minimum during peak growing season ( $0.64 \pm 0.29$ ). The  $R_{nc}/A_c$  ratio and night-time temperature (AT) also revealed that the ratio could increase when AT crossed 24 °C. These responses indicate that under climate warming, it may have a significant influence on net plant C uptake. Presence of understory shrub minimizes the  $R_{nc}/A_c$  ratio, and indicative of a more positive C-balance. Nevertheless, the observations could certainly lend useful insight into C-balance and ecological function in the region. Further, it may be useful in parameterizing and validating C-cycle models.

**Keywords** Night-time plant respiration · Soil respiration · *Pinus roxburghii* · Understory · Subtropical Himalaya · Respiration-photosynthesis ratio

## Abbreviations

$R_{nc}$  Night-time canopy respiration  
 $R_s$  Soil respiration

LE	Latent heat
SH	Sensible heat
ET	Evapotranspiration
EF	Evaporative fraction
AT	Air temperature
ST	Soil temperature
SM	Soil moisture
VPD	Vapor pressure deficit
RH	Relative humidity
C	Carbon
CO <sub>2</sub>	Carbon dioxide
$A_c$	Day-time canopy photosynthesis
GPP	Gross primary production
Rd <sub>day</sub>	Day-time plant respiration
$R_e$	Ecosystem respiration
LAI	Leaf area index

Communicated by Grams.


**Electronic supplementary material** The online version of this article (<https://doi.org/10.1007/s00468-018-1804-y>) contains supplementary material, which is available to authorized users.

✉ Bikash Ranjan Parida  
bikashrp@gmail.com

<sup>1</sup> Centre for Glaciology, Wadia Institute of Himalayan Geology, Dehradun 248001, India

<sup>2</sup> Department of Land Resource Management, School of Natural Resource Management, Central University of Jharkhand, Ranchi, Jharkhand 835205, India

# Paddy acreage mapping and yield prediction using sentinel-based optical and SAR data in Sahibganj district, Jharkhand (India)

Avinash Kumar Ranjan<sup>1</sup> · Bikash Ranjan Parida<sup>1</sup> 

Received: 18 October 2018/Revised: 9 January 2019/Accepted: 10 January 2019  
© Korean Spatial Information Society 2019

**Abstract** Rice is an important staple food for the billions of world population. Mapping the spatial distribution of paddy and predicting yields are crucial for food security measures. Over the last three decades, remote sensing techniques have been widely used for monitoring and management of agricultural systems. This study has employed Sentinel-based both optical (Sentinel-2B) and SAR (Sentinel-1A) sensors data for paddy acreage mapping in Sahibganj district, Jharkhand during the monsoon season in 2017. A robust machine learning Random Forest (RF) classification technique was deployed for the paddy acreage mapping. A simple linear regression yield model was developed for predicting yields. The key findings showed that the paddy acreage was about 68.3–77.8 thousand hectares based on Sentinel-1A and 2B satellite data, respectively. Accordingly, the paddy production of the district was estimated as 108–126 thousand tonnes. The paddy yield was predicted as 1.60 tonnes/hectare. The spatial distribution of paddy based on RF classifier and accuracy assessment of LULC maps revealed that the SAR-based classified paddy map was more consistent than the optical data. Nevertheless, this comprehensive study concluded that the SAR data could be more pronounced in acreage mapping and yield estimation for providing timely information to decision makers.

**Keywords** Acreage mapping · Yield estimation · Random Forest classifier · SAR data

## 1 Introduction

Agriculture plays a crucial role in the economy of many developing countries including India. The agriculture and allied sectors have contributed nearly 17–18% of India's Gross Domestic Product during 2017–2018 and engaged ~ 55% of the total population in agriculture and allied activities [1]. In the state of Jharkhand, nearly 80% of rural population has been involved in agriculture and allied activities. Rice (*Oryza Sativa*) plays a significant role by providing the nutritious need for the billions of world population [2]. As per the Directorate of Economics & Statistics, DAC&FW [1], Ministry of Agriculture, Government of India, India is the second largest rice producing country in the world after China, followed by Indonesia, Bangladesh, and Vietnam. The wide variation in landscape and the climatic condition of India, facilitate rice cultivation over multiple cropping seasons. Rice is primarily grown under the rainfed condition during kharif (monsoon) season (June–September) across the country. The kharif season accounts > 85% of the rice cultivation, whereas the remaining 15% grown during other seasons (summer and winter) [1].

Timely crop acreage estimation and yield prediction are vital information for making agricultural policies and national food security measures, which enables a way for governments and planners to make necessary decisions in terms of food security and ecological sustainability [3]. Early, reliable, and detailed acreage and yield estimation have great importance to the governmental agencies to facilitate the important decisions with respect to food

---

**Electronic supplementary material** The online version of this article (<https://doi.org/10.1007/s41324-019-00246-4>) contains supplementary material, which is available to authorized users.

---

✉ Bikash Ranjan Parida  
bikashrp@gmail.com

<sup>1</sup> Department of Land Resource Management, School of Natural Resource Management, Central University of Jharkhand, Ranchi, Jharkhand 835205, India



# Spatial distribution of mangrove forest species and biomass assessment using field inventory and earth observation hyperspectral data

Prem Chandra Pandey<sup>1,2</sup> · Akash Anand<sup>1,3</sup> · Prashant K. Srivastava<sup>1</sup>

Received: 17 September 2018 / Revised: 26 November 2018 / Accepted: 5 January 2019 /

Published online: 16 January 2019

© Springer Nature B.V. 2019

## Abstract

The objective of this research is to identify species, provide spatial distribution of the species and estimate the biomass in the mangrove Forest, Bhitarkanika India. Mangrove ecosystems play an important role in regulating carbon cycling, thus having a significant impact on global environmental change. Extensive studies have been conducted for the estimation of mangrove species identification and biomass estimation. However, estimation at a regional level with species-wise biomass distribution has been insufficiently investigated in the past because either research focuses on the species distribution or biomass assessment. Study shows that good relationship has been achieved between stem volume (field measured data) and Normalized Difference Vegetation Index (NDVI) and Enhanced Vegetation Index (EVI) derived from satellite image and further these two indices are employed to estimate the biomass in the study site. Three models- linear, logarithmic and polynomial (second degree) are used to estimate biomass derived from EVI and NDVI. The hyperspectral data (spatial resolution ~ 30 m) is utilised to identify ten mangrove plant species. We have prepared the spatial distribution map of these species using spectral angle mapper. We have also generated mangrove species-wise biomass distribution map of the study site along with areal coverage of each species. The results indicate that the *Sonneratia apetala* Buch.-Ham. and *Cynometra iripa* Kostel has the highest biomass among all ten identified species, 643.12 Mg ha<sup>-1</sup> and 652.14 Mg ha<sup>-1</sup>. Our study provided a positive relationship between NDVI, EVI, and the estimated biomass of Bhitarkanika Forest Reserve Odisha India. The study finds a similar results for both NDVI and EVI derived biomass, while linear regression has more significant results than the polynomial (second degree) and logarithmic regression derived biomass. The polynomial is found slightly better than the logarithmic when using the EVI as compared to NDVI derived biomass. The spatial distribution of species-wise biomass map obtained in this study using both, EVI and NDVI could be used to provide useful information for biodiversity assessment along with the sustainable solutions to different problems associated with the mangrove forest biodiversity. Thus, biomass assessment of larger regions can be achieved by utilization of remote sensing based indices as concluded in the present study.

---

Communicated by M. D. Behera, S. K. Behera and S. Sharma.

Extended author information available on the last page of the article



# Geoinformatics based assessment of coastal multi-hazard vulnerability along the East Coast of India

K. K. Basheer Ahammed<sup>1</sup>  · Arvind Chandra Pandey<sup>1</sup> 

Received: 15 September 2018/Revised: 27 December 2018/Accepted: 31 December 2018  
© Korean Spatial Information Society 2019

**Abstract** Climate change is one of the major threatens that coastal areas facing, and these coastal areas already stressed by large population. Past 4 decades tremendous tropical cyclones and associated flood are dismantled the coastline and resulted inundation and displacement of the coastal landforms. In the present study, coastal multi hazard vulnerability mapping has been carried out along the Krishna–Godavari deltaic plain, eastern coast of India. The study area consisting of four district include East Godavari, West Godavari, Krishna and Gundur which are the area affected by coastal hazards and climate variability. The area witnessed a high erosion rate up to 18 m/year in comparison to other regions in the state. Further this area exhibit low elevated topography, therefore sea level rise would lead to permanent inundation. In the study also identified about that 1147 sq km area is falling under multi hazard zone and around 102 coastal villages are under threat. This study revealed that the use of multi layer information combined with geospatial tools is most reliable and coast effective approach for disaster preparedness and adaptation. The result obtained from the present study may serve the baseline information for disaster management planning in the area.

**Keywords** Coastal multi-hazard · Climate change · Sea level · Shoreline change · Storm surge · Geospatial analysis

## 1 Introduction

Climate change<sup>1</sup> is a natural phenomena which has always been a dangerous threat to the habitants, ecology and life stocks [1], not only in the India, but all over the world. Sea level rise, land subsidence, and possible changes in storm climatology may cause more flood inundations, and economic losses to coastal cities in the future [2–4]. Around 40 million people are currently exposed to 100-year coastal floods and it is projected an increase in the exposed population by more than threefold and in exposed assets by more than tenfold worldwide by the 2070s [5, 6]. The increasing flood risk in coastal cities calls for immediate actions. Although, climate change impacts are difficult to prevent, however the intensity can be reduced by developing suitable preparedness plans and mitigation strategies. Research and development should not to be limited to major coastal hazard<sup>2</sup> like cyclone and tsunami, but the risk reduction plans should be compatible for multiple hazards [7]. Mitigating the effects of potential disasters and having the appropriate infrastructure in place for response requires detailed knowledge on the vulnerability of the places to a wide range of environmental hazards [8]. Federal Emergency Management Agency (FEMA) developed a tool to first of its kind called Multi-Hazard Mapping Initiative (MMI) in 1997 [9] for maintain a living atlas of hazard data and map services for advisory purposes.

---

✉ Arvind Chandra Pandey  
arvindchandrap@yahoo.com

K. K. Basheer Ahammed  
basheer.kk@yahoo.com

<sup>1</sup> Department of Land Resource Management, Central University of Jharkhand, Ranchi 835 205, India

<sup>1</sup> Climate change refers to a change in the state of the climate that can be identified by changes in the mean and/or the variability of its properties, and that persists for an extended period, typically decades or longer. It refers to any change in climate over time, whether due to natural variability or as a result of human activity.

<sup>2</sup> Hazard is a potential source of harm or adverse health effect on a person or persons.



# Mixed lineage kinase 3 promotes breast tumorigenesis via phosphorylation and activation of p21-activated kinase 1

Subhasis Das<sup>1</sup> · Rakesh Sathish Nair<sup>1</sup> · Rajakishore Mishra<sup>2</sup> · Gautam Sondarva<sup>1</sup> · Navin Viswakarma<sup>1</sup> · Hazem Abdelkarim<sup>3</sup> · Vadim Gaponenko<sup>3</sup> · Basabi Rana<sup>1,4,5</sup> · Ajay Rana<sup>1,4,5</sup>

Received: 17 August 2018 / Revised: 28 November 2018 / Accepted: 7 December 2018  
© Springer Nature Limited 2019

## Abstract

Mixed lineage kinase 3 (MLK3), a MAP3K member has been envisioned as a viable drug target in cancer, yet its detailed function and signaling is not fully elucidated. We identified that MLK3 tightly associates with an oncogene, PAK1. Mammalian PAK1 being a Ste20 (MAP4K) member, we tested whether it is an upstream regulator of MLK3. In contrast to our hypothesis, MLK3 activated PAK1 kinase activity directly, as well as in the cells. Although, MLK3 can phosphorylate PAK1 on Ser133 and Ser204 sites, PAK1S133A mutant is constitutively active, whereas, PAK1S204A is not activated by MLK3. Stable overexpression of PAK1S204A in breast cancer cells, impedes migration, invasion, and NFκB activity. In vivo breast cancer cell tumorigenesis is significantly reduced in tumors expressing PAK1S204A mutant. These results suggest that mammalian PAK1 does not act as a MAP4K and MLK3-induced direct activation of PAK1 plays a key role in breast cancer tumorigenesis.

## Introduction

Mixed lineage kinase 3 (MLK3) also known as MAP3K11 belongs to a large family of MAP3Ks, called the mixed lineage kinases (MLKs) because their catalytic domains contain signature sequences of both Ser/Thr and Tyr kinases [1, 2]. The biochemical analyses hitherto, have shown that MLKs are functional Ser/Thr kinases and activate

downstream MAPK pathways, however their tyrosine kinase activities if any, are still not known [1, 3]. There are nine mammalian MLK members and based on the functional domains and sequence similarities, they are classified in three sub-groups: the mixed lineage kinases (MLKs), dual-leucine zipper kinases (DLKs), and zipper sterile- $\alpha$ -motif kinases (ZAKs) [1]. MLK3 belongs to the MLK sub-group and has been implicated in various cancers [4–6] and neurodegenerative diseases [7, 8]. The pan-MLK inhibitor went to clinical trials for Parkinson's disease, however the trial was abruptly stopped due to unknown reasons [8]. The role of MLK3 in cancer is an emerging area and earlier we reported that MLK3 kinase activity and transcripts were downregulated by estrogen in breast cancer, providing a survival advantage to ER+ breast cancer cells [4]. We also reported that the kinase activity of MLK3 was downregulated by HER2 amplification and MLK3 activity was essential to promote cell death in HER2+ breast cancer cells by anti-HER2 therapies [9]. However, in triple-negative breast cancer cells, MLK3 activation promotes migration and invasion, and MLKs inhibitor blocked cancer cell migration/invasion [10]. Conceivably, MLK3 and other MLK family members are important therapeutic targets in various diseases, including cancer, yet, their upstream regulators and downstream signaling pathways are not fully elucidated.

These authors contributed equally: Subhasis Das, Rakesh Sathish Nair

**Supplementary information** The online version of this article (<https://doi.org/10.1038/s41388-019-0690-0>) contains supplementary material, which is available to authorized users.

✉ Ajay Rana  
arana@uic.edu

- <sup>1</sup> Department of Surgery, Division of Surgical Oncology, University of Illinois at Chicago, Chicago, IL 60612, USA
- <sup>2</sup> Center for Life Sciences, School of Natural Sciences, Central University of Jharkhand, Ranchi, Jharkhand 835205, India
- <sup>3</sup> Department of Biochemistry and Molecular Genetics, University of Illinois at Chicago, Chicago, IL 60607, USA
- <sup>4</sup> University of Illinois Hospital & Health Sciences System Cancer Center, University of Illinois at Chicago, Chicago, IL 60612, USA
- <sup>5</sup> Jesse Brown VA Medical Center, Chicago, IL 60612, USA

# Fabrication and characterization of thin targets of Nickel ( $^{61,62}\text{Ni}$ ) isotopes by physical vapour deposition technique for nuclear reaction studies

Nabendu Kumar Deb<sup>a</sup>, Kushal Kalita<sup>a,\*</sup>, S.R. Abhilash<sup>b</sup>, Pankaj K. Giri<sup>c</sup>,  
Rohan Biswas<sup>b</sup>, G.R. Umapathy<sup>b</sup>, D. Kabiraj<sup>b</sup>, S. Chopra<sup>b</sup>

<sup>a</sup>*Department of Physics, Gauhati University, Guwahati-781014, Assam, India*

<sup>b</sup>*Inter University Accelerator Centre, Aruna Asaf Ali Marg, New Delhi - 110067, India*

<sup>c</sup>*Centre for Applied Physics, Central University of Jharkhand, Ranchi-835205, India*

---

## Abstract

To perform nuclear reaction experiments at HIRA, IUAC, New Delhi, thin (100 - 150  $\mu\text{g}/\text{cm}^2$ ) and pure  $^{61,62}\text{Ni}$  targets of uniform thickness are required. Self supporting targets are preferable for such case but, instead, carbon-backed isotopic targets are fabricated by adapting physical vapour deposition technique as it was comparatively more stable and consistent. Around 25 thin targets of both  $^{61,62}\text{Ni}$  isotopes are prepared using the limited amount of available enriched target material (less than 100 mg). The carbon-backed slides along with the parting agents are prepared using a diffusion pump based coating unit and the target material is deposited over the carbon-backed slides in the turbopump based coating unit. To obtain consistent and intact targets, some trials were done with deposited slides and was found that the material degrades in any of the slides when kept idle for few days. The thicknesses of the targets are verified using profilometer,  $\alpha$  energy loss technique, and RBS technique. They were found to be in good agreement with each other using the three techniques. The purity and the uniformity of the fabricated targets are further confirmed after verification using the RBS, the EDS and the XRD techniques.

**Keywords:** Physical vapor deposition, Nuclear reaction studies, the RBS, the

---

\*Kushal Kalita

Email address: [ku\\_kalita@yahoo.com](mailto:ku_kalita@yahoo.com) (Kushal Kalita)



# Impact of nitrogen fertilization and tillage practices on nitrous oxide emission from a summer rice ecosystem

Nirmali Bordoloi<sup>a</sup>, Kushal Kumar Baruah<sup>b</sup>, Pradip Bhattacharyya<sup>c</sup>  
and Prabhat Kumar Gupta<sup>d</sup>

<sup>a</sup>Department of Environmental Sciences, Central University of Jharkhand, Brambe, India; <sup>b</sup>Department of Environmental Science, Tezpur University, Tezpur, India; <sup>c</sup>Agricultural and Ecological Research Unit, Indian Statistical Institute, Giridih, Jharkhand, India; <sup>d</sup>Sophisticated and Analytical Instrumentation Division, National Physical Laboratory, New Dehli, India

## ABSTRACT

Identification of the combination of tillage and N fertilization practices that reduce agricultural Nitrous oxide (N<sub>2</sub>O) emissions while maintaining productivity is strongly required in the Indian subcontinent. This study investigated the effects of tillage in combination with different levels of nitrogen fertilizer on N<sub>2</sub>O emissions from a rice paddy for two consecutive seasons (2013–2014 and 2014–2015). The experiment consisted of two tillage practices, i.e., conventional (CT) and reduced tillage (RT), and four levels of nitrogen fertilizer, i.e., 0 kg N ha<sup>-1</sup> (F1), 45 kg N ha<sup>-1</sup> (F2), 60 kg N ha<sup>-1</sup> (F3) and 75 kg N ha<sup>-1</sup> (F4). Both tillage and fertilizer rate significantly affected cumulative N<sub>2</sub>O emissions ( $p < 0.05$ ). Fertilizer at 45 and 60 kg N ha<sup>-1</sup> in RT resulted in higher N<sub>2</sub>O emissions over than did the CT. Compared with the recommended level of 60 kg N ha<sup>-1</sup>, a 25% reduction in the fertilizer to 45 kg N ha<sup>-1</sup> in both CT and RT increased nitrogen use efficiency (NUE) and maintained grain yield, resulting in the lowest yield-scaled N<sub>2</sub>O-N emission. The application of 45 kg N ha<sup>-1</sup> reduced the cumulative emission by 6.08% and 6% in CT and RT practices, respectively, without compromising productivity.

## ARTICLE HISTORY

Received 19 July 2018  
Accepted 3 January 2019

## KEYWORDS

Nitrous oxide; nitrogen use efficiency; photosynthesis; rice field

## Introduction

Nitrous oxide (N<sub>2</sub>O) is a powerful greenhouse gas (GHG) that contributes to global warming and stratospheric ozone depletion (Sutton et al. 2014). The concentration of atmospheric N<sub>2</sub>O increases at a rate of 0.2–0.3% annually, and it had risen from the pre-industrial value of 270 ppb to 324 ppb by 2011 (IPCC 2013). N<sub>2</sub>O contributes to 10% of the radiative forcing, making it the third largest well-mixed climate forcing agent. The 'Ozone Depletion Potential' (ODP) of N<sub>2</sub>O is 0.017 which is comparable to the ODPs of other ozone-depleting chemicals (Ravishankara et al. 2009). The emission of N<sub>2</sub>O has recently received attention owing to its contribution to global climate change with long atmospheric lifetime (approximately 120 years) and high global warming potential that is 298 times higher than that of carbon dioxide (CO<sub>2</sub>) in a time horizon of 100 years (IPCC 2013).

Agricultural soil is the major source of N<sub>2</sub>O emission and is responsible for 66% of the total gross anthropogenic emission of N<sub>2</sub>O (UNEP 2013). The application of synthetic nitrogen (N) fertilizer in rice fields, a common practice among farmers, is likely to contribute to global warming through an increase in N<sub>2</sub>O emissions (Bouwman et al. 2002). The potency of these emissions is affected by the form, amount, timing, and method of fertilizer application (McSwiney and Robertson 2005; Lin



# In-situ Observation and Nitrate-N Load Assessment in Madhubani District, Bihar, India

Binita Kumari<sup>1</sup>, Pankaj Kumar Gupta<sup>2\*</sup> and Deepak Kumar<sup>3</sup>

<sup>1</sup>Centre for Landuse Management, Central University of Jharkhand, Ranchi- 835 205, India

<sup>2</sup>Department of Hydrology, IIT Roorkee, Roorkee - 247 667, India

<sup>3</sup>Department of Soil and Water Conservation Engineering, College of Technology, G.B. Pant University of Agriculture and Technology, Pantnagar- 263 153, India

**E-mail:** [binita.kumari@cuja.ac.in](mailto:binita.kumari@cuja.ac.in); [pankajkumarpsc@gmail.com](mailto:pankajkumarpsc@gmail.com); [deepak.civil.iitdelhi@gmail.com](mailto:deepak.civil.iitdelhi@gmail.com)

## ABSTRACT

Fertilizers may leach through the vadose zone and eventually reach groundwater in agriculturally intensive areas. Thus, the main focus of this study was to investigate Nitrate-N load and vulnerability of groundwater resources using in-situ observed hydrogeological data. Soil water flow and contaminant transport equation was numerically simulated using HYDRUS 1D for constant head and atmospheric top boundary conditions. Sub-surface materials were distributed based on the lithologs of the target area. Observed water table locations were considered as bottom boundary condition to respective numerical domain. The time taken by Nitrate-N to reach groundwater table was considered to estimate vulnerability index. The results show that Nitrate-N load is higher in constant head boundary conditions than atmospheric boundary conditions. The eastern part of the study area shows high vulnerability than northern part followed by western part. In-situ observed nitrate concentrations were well matched with simulated results. The high vulnerability in eastern and northern part is due to alluvial sandy lithologs and very shallow groundwater table. These findings are in line with the observed low water table depths, less runoff, and higher hydraulic conductivity of the vadose zone material in these area. In western part, forest cover dominated land use causes low pollution vulnerabilities to groundwater resources. This study may help to frame agricultural and soil-water conservation practices with more sustainable remedial techniques.

## INTRODUCTION

The groundwater which is the largest reservoir of fresh water is currently at a critical state as it is depleting very rapidly and becoming unsafe for drinking. Non-point source (NPS) pollutants like excess fertilizers, pesticides, livestock wastes, and salts are continuing to be a major source of contamination for underground water resources (Harter et al. 2005). Compared to point source contamination, the NPS pollution is more difficult to monitor and mitigate due to the inherent heterogeneity of the vadose zone. Therefore, a better understanding of moisture flow and the NPS contaminant transport through vadose zone is essential to assess the long term impacts on groundwater quality especially where irrigation return flow is a major component of recharge passing through the overlying deep and heterogeneous vadose zone to local groundwater resources. The precise understanding of flow and the NPS contaminant fate and transport processes in the vadose zone is also a crucial in designing efficient fertilizer management protocols for enhancing agricultural production while safeguarding groundwater from NPS contamination.

Considerable research has been conducted to study the NPS pollutants mass balance in the variably saturated root zones (Stenger

et al. 2002). The NPS budgeting in the root zone have been widely used in agronomy to determine the fate of solutes in soils and the potential for contaminant leaching to groundwater. Commonly it is believed that the unsaturated zone below the root zone acts as a buffer where pollutants are fully or partly get attenuated before reaching the water table (Kumar et al. 2013; Gupta and Yadav, 2017; Gupta et al. 2018). In contrarily, preferential flow paths in the vadose zone might occur and have been thought to accelerate contaminants migration in the deep unsaturated zone and ultimately reducing their arrival time in groundwater (Simunek et al., 2003). In many agricultural areas, particularly in river deposition area, groundwater is found at shallow depths and therefore, consideration of the entire variably saturated zone is the key parameter in predicting accurate NPS emissions to groundwater (Mustapha et al. 2018; Gupta et al. 2018; Ranjan et al. 2018). But the deep vadose zone and its inherent spatial variability are rarely considered in earlier groundwater quality assessment studies. Further, the earlier studies that accounted spatial variability of deep vadose zone, only considered simplified steady-state and gravity dominated flow conditions (Russo and Fiori 2009). In the present study, vulnerability assessment is performed by simulating the moisture flow equation coupled with the contaminant transport equation numerically for the stratified vadose zone considering the site specific top boundary conditions at different locations of the study area.

## STUDY AREA

Madhubani of north Bihar (Fig 1) was considered for Nitrate-N leaching study and groundwater vulnerability assessment. The area is about 3440.64 sq km. The area of different land use/land cover of all the districts is listed in Table 1. Figure 2 shows land use and land cover of the study area. Average annual rainfall in study area ranges from 1142-1290 mm (Indian Meteorological Department, IMD). While, Kumar et al. (2016) reported a daily evapotranspiration of 2-6 mm in study area. Groundwater information booklet of Madhubani district issued by CGWB (2013) reported that daily maximum and minimum temperature are around 36°C and 24°C respectively in summer, which reaches upto 43°C in some cases. Sandy alluvium soil is dominating subsurface media, generally found in flood plains. Madhubani (northern parts) are in touch with the Tarai zone of Nepal and slopping towards Darbhanga (in south). The major drainages

**Table 1.** Classification of land use and land cover of study area

Land Use and Cover	Madhubani
Agriculture	982.59
Barren Land	857.87
Tree Cover	1047.03
Urban Built up	301.43
Water Bodies	251.72

## All optical NOT and NOR gates using interference in the structures based on 2D linear photonic crystal ring resonator

Alok kumar and Sarang Medhekar

E-mail: [smedhekarbit@gmail.com](mailto:smedhekarbit@gmail.com)

Department of Physics, Central University Jharkhand, Ranchi-835205, Jharkhand (INDIA)

### Abstract:

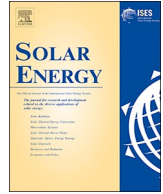
All optical NOT and NOR logic gates using structures based on linear photonic crystal ring resonator (LPhCRR) are proposed in this paper. The switching function of the proposed gates can be obtained at very small power levels as it relies on the interference effect. Moreover, their functioning is possible with wide range of input powers and tolerant to input power fluctuations (as those work in linear optics regime). Optical behavior of the purposed structures is demonstrated by using Two Dimensional Finite Difference Time Domain (2DFDTD) method and dispersion diagram is extracted by Plane Wave Expansion (PWE) method. Performance of the proposed structures is found to be very good in terms of response time and contrast ratio.

**Keywords:** All-optical logic gate; photonic crystal.

### 1 Introduction

Optical devices have high demand recently. Among various optical devices, all optical logic gates or optical switches play important role in the development of optical network, optical computer and signal analysis [1]. Demand of miniaturization and high speed has made exploration of optical gates of extreme importance.

The photonic crystals (PC) are composed of periodic dielectric or metallo - dielectric nanostructures that have alternating low and high dielectric constant in one, two and three dimensions [2]. PC based optical devices are currently the subject of intense research because they provide fascinating platform for new generation of integrated optical devices and component of ultra-compact size, high speed and low power consumption [3]. Proposal of several PC based all optical devices are available in literature such as optical filter [4-5], optical multiplexer [6], optical decoder [7] optical junction [8], asymmetric reflector [9], three port asymmetric router [10] and all optical logic gates [11-13]



## Ensuring the completion of solar cooking process under unexpected reduction in solar irradiance



Atul A. Sagade<sup>a,1</sup>, S.K. Samdarshi<sup>a,b,\*</sup>, P.J. Lahkar<sup>c,2</sup>

<sup>a</sup> Department of Energy Engineering, Central University of Jharkhand, Ranchi 835205, Jharkhand, India

<sup>b</sup> Centre of Excellence in Green and Efficient Energy Technology, Central University of Jharkhand, Ranchi 835205, Jharkhand, India

<sup>c</sup> Dept. of Energy, Tezpur University, Assam, India

### ARTICLE INFO

#### Keywords:

Solar cookers  
Cooker Opto-Thermal Ratio  
Heat retention  
Thermal performance of solar cookers  
Thermal cooling  
Completion of solar cooking process

### ABSTRACT

One of the big challenges in the solar cooking process is ensuring the completion of cooking process under unexpected reduction in the sunshine due to cloudiness. The popularity of solar cookers is hindered because of the uncertainty in the accomplishment of cooking process, resulting in spoilage of food and wastage of time, leading to inconvenience and loss. The completion of cooking activity certainly requires a definite amount of stored heat at above the cooking temperature and a parameter to provide the related information for design incorporation. Because of the complex nature of the cooking process, the present work considers rice as the food item. In the process, it proposes an alternative to heating based test procedure to determine more realistic value of thermal performance parameter (TPP) for the solar cookers. The relevant parameter is determined utilizing novel cooling test. Two different designs of cookers have been tested to establish the proposal.

### 1. Introduction

Out of different cooking methodologies of food, the boiling water cooking is one of the basic and most popular methods in the developing world. In this method, the food is heated using different heat supply sources to complete the process of cooking. Solar radiation is one of them. It is well-known that cooking is a complex process. It involves the heating of a food item to the temperature suitable for onset of the chemical changes till completion of cooking process. If the heat addition to the food is irregular, then there will be disruption in the chemical process. It may hamper the completion of the cooking process leading to spoilage of food.

A number of attempts have been made to develop solar cookers that work during off sunshine hours. A suitable storage system for the purpose needs to be carefully designed as per the requirement of the temperature of heat flow for storing-in and extracting out, the rate of storing and extraction, and the stability cycle of the system. Any solution to these issues not only adds to the gravimetric/volumetric energy/power requirements but also to the cost which limits its affordability. Thus, a holistic solution to this appears to be quite involved.

In fact, there is another issue which needs attention prior to this. The existing designs of solar cooker, although work successfully in the

cooking of food during sunshine hours, often fail when there is a sudden reduction in solar irradiance. This leads to wastage of time and spoilage of food and thus, loss of faith/reliability in the solar cooking technology.

Therefore, it is essential that the cooking, employing a solar cooker, ensures the completion of the cooking of a specified food on normal sunshine day. Even if there is a sudden and unexpected drop in solar radiation, the solar cooker should maintain a minimum temperature for a known duration for completion of cooking process. It needs the minimum temperature and duration to be identified for a given food item. Hence, it is mandatory that a particular solar cooker must retain sufficient amount of heat to make up for the heat loss during the period within the temperature range to ensure completion of solar cooking process after its onset, even under intermittent weather conditions.

Thus, an objective parameter characterizing the heat retention and quantifying the time component for ensuring the accomplishment of the solar cooking process for a given design of solar cooker at a given location (meteorological condition) is defined as a *heat retention time* (Lahkar and Samdarshi, 2010). Heat retention time ( $\tau_{hr}$ ) is the duration for which temperature of the test load/food item is maintained between two (upper and lower) reference temperatures under sudden uncontrolled reduction in clearness and radiation at the location. It

\* Corresponding author at: Department of Energy Engineering, Central University of Jharkhand, Ranchi 835205, Jharkhand, India.

E-mail address: [drksamdarshi@rediffmail.com](mailto:drksamdarshi@rediffmail.com) (S.K. Samdarshi).

<sup>1</sup> Current affiliation: Solar Energy Research Laboratory, Pandharpur 413304, Maharashtra, India.

<sup>2</sup> Current affiliation: Dhemaji Polytechnic, Silapathar, Assam, India.

**Anisotropic compact stars in the Buchdahl model: A comprehensive study**

S. K. Maurya\*

*Department of Mathematical and Physical Sciences, College of Arts and Science,  
University of Nizwa, Nizwa, Sultanate of Oman*

Ayan Banerjee†

*Astrophysics and Cosmology Research Unit, University of KwaZulu Natal, Private Bag X54001,  
Durban 4000, South Africa*

M. K. Jasim‡

*Department of Mathematical and Physical Sciences, University of Nizwa, Nizwa 616, Sultanate of Oman*

J. Kumar and A. K. Prasad§

*Department of Applied Mathematics, Central University of Jharkhand, Ranchi 835205, India*

Anirudh Pradhan||

*Department of Mathematics, Institute of Applied Sciences & Humanities, GLA University,  
Mathura 281 406, Uttar Pradesh, India*

(Received 24 November 2018; published 15 February 2019)

In this article we present a class of relativistic solutions describing spherically symmetric and static anisotropic stars in hydrostatic equilibrium. For this purpose, we consider a particularized metric potential, namely, Buchdahl ansatz [Phys. Rev. D **116**, 1027 (1959).] which encompasses almost all the known analytic solutions to the spherically symmetric, static Einstein equations with a perfect fluid source, including, in particular, the Vaidya-Tikekar and Finch-Skea. We developed the model by considering an anisotropic spherically symmetric static general relativistic configuration that has a significant effect on the structure and properties of stellar objects. We have considered eight different cases for generalized Buchdahl dimensionless parameter  $K$  and analyzed them in a uniform manner. As a result it turns out that all the considered cases are valid at every point in the interior spacetime. In addition to this, we show that the model satisfies all the energy conditions and maintains the hydrostatic equilibrium equation. In the frame work of anisotropic hypothesis, we consider analogue objects with similar mass and radii, such as LMC X-4, SMC X-1, EXO 1785-248 etc. to restrict the model parameter arbitrariness. Also, establishing a relation between pressure and density in the form of  $P = P(\rho)$ , we demonstrate that equation of state (EoS) can be approximated to a linear function of density. Despite the simplicity of this model, the obtained results are satisfactory.

DOI: [10.1103/PhysRevD.99.044029](https://doi.org/10.1103/PhysRevD.99.044029)**I. INTRODUCTION**

In astrophysics, studying the structural properties and formation of compact objects, such as neutron stars (NSs) and quark stars (Qs), has attracted much attention to the researchers in the context of General Relativity (GR), as well as widely developing modified theories of gravity. Crudely, compact stars are the final stages in the evolution of ordinary stars which become an excellent test bed for the

study of highly dense matter in extreme conditions. In recent times, a number of compact objects with high densities have been discovered [1], which are often observed as pulsars, spinning stars with strong magnetic fields. Our theoretical understanding about compact stars is rooted in the Fermi-Dirac statistics, which are responsible for the high degeneracy pressure that holds up the star against gravitational collapse and was proposed by Fowler in 1926 [2]. Shortly afterwards, using Einstein's special theory of relativity and the principles of quantum physics, Chandrasekhar showed that [3,4] white dwarfs are compact stars, which are supported solely by a degenerate gas of electrons, to be stable if the maximum size of a stable white dwarf is approximately  $3 \times 10^{30}$  kg (about 1.4 times the mass of the Sun).

\*sunil@unizwa.edu.om

†ayan\_7575@yahoo.co.in

‡mahmoodkhalid@unizwa.edu.om

§jitendark@gmail.com

||pradhan.anirudh@gmail.com





## Hybrid mean value of $2k$ -th power inversion of $L$ -functions and general quartic Gauss sums

SHIKHA SINGH\* and JAGMOHAN TANTI

Centre for Applied Mathematics, Central University of Jharkhand, Ranchi 835 205, India

\*Corresponding author.

E-mail: shikha.singh@cuja.ac.in

MS received 8 November 2017; revised 14 December 2017;  
accepted 18 December 2017; published online 25 February 2019

**Abstract.** In this paper, we find the  $2k$ -th power mean of the inversion of  $L$ -functions with the weight of the general quartic Gauss sums. We establish the results with the help of Dirichlet characters and properties of classical Gauss sums. We also describe asymptotic behaviour for it.

**Keywords.** Dirichlet  $L$ -functions; Gauss sum; hybrid power mean; asymptotic formula.

**Mathematics Subject Classification.** 11L05.

### 1. Introduction

Let  $r \geq 3$  be an integer and  $\chi$  a Dirichlet character modulo  $r$ . For any positive integer  $m$ , the general  $k$ -th Gauss sums  $G(m, k, \chi; r)$  is defined as

$$G(m, k, \chi; r) = \sum_{b=1}^r \chi(b) e\left(\frac{mb^k}{r}\right),$$

where  $e(t) = e^{2i\pi t}$ .

For  $k = 4$  and  $\chi = \chi_0$ ,

$$G(m, 4; r) = \sum_{b=1}^r ' e\left(\frac{mb^4}{r}\right),$$

where  $\sum_{b=1}^r '$  denotes the summation over all  $1 \leq b \leq r$  such that  $(b, r) = 1$ .

A Dirichlet  $L$ -function is defined by the series

$$L(l, \chi) = \sum_{m=1}^{\infty} \frac{\chi(m)}{m^l},$$

where  $l = \rho + iw$  is a complex number,  $\rho > 1$ .

The problem of finding the  $n$ -th power mean of the Dirichlet  $L$ -functions is already there in the literature. Yi and Zhang [5, 6] studied the first power mean and the  $2k$ -th power mean by using the method with the weight of Gauss sums.



# Simple and cost-effective sonochemical preparation of ternary NZnO–Mn<sub>2</sub>O<sub>3</sub>@rGO nanohybrid: a potential electrode material for supercapacitor and ammonia sensing

Benjamin Raj<sup>1</sup> · Ramesh Oraon<sup>2</sup> · Arun Kumar Padhy<sup>1</sup>

Received: 5 December 2018 / Revised: 21 January 2019 / Accepted: 29 January 2019 / Published online: 9 February 2019  
© Springer-Verlag GmbH Germany, part of Springer Nature 2019

## Abstract

The present work deals with a simple and cost-effective sonochemical assisted synthesis of binary transition metal oxide (BTMOs) (NZnO–Mn<sub>2</sub>O<sub>3</sub>) and NZnO–Mn<sub>2</sub>O<sub>3</sub>@rGO ternary nanohybrid using a imidazole derivative as an organic precursor aimed at the application in supercapacitor and sensing of ammonia in aqueous medium. Morphological analysis using various physicochemical techniques, like FESEM, TEM, XRD, and BET, revealed surface enriched property (high surface area and porous nature) with uniform decoration of binary metal oxides (NZnO–Mn<sub>2</sub>O<sub>3</sub>) over reduced graphene oxide (rGO). Formation and synergistic interaction of nanohybrid materials were confirmed from FTIR and Raman analysis. Electrochemical measurements showed maximum capacitance performance via cyclic voltammetry (CV) achieved by ternary nanohybrid NZnO–Mn<sub>2</sub>O<sub>3</sub>@rGO (252.77 Fg<sup>-1</sup> at scan rate 50 mV s<sup>-1</sup>) which is in good agreement with the charging–discharging (GCD) and electrochemical impedance spectroscopy (EIS) analysis. Further, the ternary nanohybrid material exhibited good sensing of ammonia in aqueous medium as indicated by continuous amperometric response with a lowest sensitivity of 0.47 ppm.

**Keywords** Nanohybrid · Supercapacitor (SCs) · Specific capacitance · Sensor · Porous

## Introduction

In periodic intricate technological/industrial developments, it is a challenge for the scientific community to provide healthy environment, developing not only green way of energy harvesting/storage but also the awareness of existence of hazardous gases in the atmosphere. Continuous depletion of fossil fuels and severe emission of hazardous gases has led to energy and environmental crisis [1]. Thus, growing ecological concern with an imminent shortage of fossil fuels has stimulated extensive research efforts towards the replacement of environment unfriendly resources to exploit sustainable, clean, and highly efficient technologies [2, 3]. Advancement of nanotechnology with supercapacitor (SCs) and sensor has attracted enormous research attention from both academic and

industry worldwide [4, 5]. While SCs take the advantage of long lifetime, environmental friendliness, safety with high energy, and power density to overcome energy issues, on the other hand, sensors are prevalent for detection of trace level of chemicals or hazardous gas at ppm level having deteriorating influence. Hence, it is highly crucial for the harmonious survival of mankind as well as an ecosystem at large [6–9]. The universal and practical applications of SCs and sensor heavily rely on the design and preparation of nanostructured electrode material possessing extremely large surface to volume ratio with tuneable physical and chemical properties, superior redox activity, and large natural abundance [10–12].

Binary transition metal oxides (BTMOs) are of greatest importance and demonstrated to be an effective solution for yielding improved overall performance of material [13]. Typically, BTMOs have composed of at least one transition metal ion and one or more electrochemically active/inactive ions in a closely packed system. In addition, low-cost synthesis, surface enriched property, and strong surface interaction can be conferred for potential application in SCs and sensor [14–16]. There are several reports on the fabrication of BTMOs with different synthetic routes like microwave irradiation [17], hydrothermal/solvothermal [18, 19],

✉ Arun Kumar Padhy  
arun.padhy@uj.ac.in

<sup>1</sup> Department of Chemistry, Central University of Jharkhand, Brambe, Ranchi 835205, India

<sup>2</sup> Department of Nanotechnology, Central University of Jharkhand, Brambe, Ranchi 835205, India



# Assessment of recent changes in planform of river Ganga from Mirapur Khadar to Narora barrage, Uttar Pradesh, India

Prachi Singh<sup>1</sup> · R. G. Patil<sup>2</sup> · Ajai Singh<sup>3</sup>

Received: 27 May 2017 / Accepted: 27 January 2018 / Published online: 2 February 2018  
© Springer International Publishing AG, part of Springer Nature 2018

## Abstract

Present study was undertaken to assess the vast changes in the behavior of the course of the Ganga river by the identification of recent changes in planform and dynamic fluvial characteristics of the river and quantification of the meandering indices as well as braiding index for the region Mirapur Khadar to Narora, Uttar Pradesh. Narora barrage is located on the banks of river Ganga and its construction was completed in 1966. After its construction, the braiding index was increased from 0.17 to 0.41 from 1975 to 2015. Meandering indices were observed to be increased from 1.26 to 1.36 within a chronological period from 1975 to 2015. This shows that streams are exhibiting braiding as well as meandering pattern. The construction of Bijnor as well as Narora barrages has affected the planform geometry of river Ganga. The study reveals that the natural as well as anthropogenic factors are responsible for the oscillating nature of river Ganga. The study further reveals that Landsat images can be successfully used to identify the meandering indices, braiding index and planform change.

**Keywords** Ganga River · Sinuosity Index · Braiding Index · Tortuosity · Landsat · Mirapur Khadar · Narora

## Introduction

One of the most important sources of water is rivers. Rivers have played an important place in human life. River is a natural waterway that flows across landscape from higher to lower elevation (Sinha and Ghosh 2011). River Ganga is the longest river in India and flows approximately 1569 miles (2525 km) from Himalayan Mountains to the Bay of Bengal. The Ganga River emerges from Himalayan Mountains and flows into the Indo Gangetic plain of Uttar Pradesh,

Bihar and West Bengal finally end at Bay of Bengal. The Ganga River is extremely important to the people of India and it acts as a lifeline for millions of people (Singh 2014). It has a number of tributaries such as Yamuna, Ramganga and has two distributaries Padma and Bhagirathi-Hoogly. Location of tributaries and distributaries is shown in Fig. 1. The Gangetic basin in India is very fertile and densely populated and it faces problems of frequent occurrence of flood, soil erosion and shifting of river channels which hinders the economic development of the whole basin area.

There are three segments of river Ganga, namely upper Ganga (Gaumukh to Haridwar); middle Ganga (Haridwar to Varanasi); lower Ganga (Varanasi to Ganga Sagar). The River in the upper segment flows on steep and narrow bed, mostly rocks and boulders, carries cold water, is subjected to less anthropogenic pollution, and has highly sensitive and fragile ecosystem and biodiversity. The River in the middle segment enters and flows in plains, meandering mostly on bed of fine sand, has wide river bed and flood plain, and most importantly modified through human interventions in terms of huge quantities of water diversion and subjected to high degree of pollutant loads from domestic, industrial and agricultural activities. The river in the third segment has experienced considerable changes in the sediment transport and deposition, causes wide-spread flooding, undergoes

---

✉ Ajai Singh  
ajai.singh@uj.ac.in  
Prachi Singh  
prachisingh1407@gmail.com  
R. G. Patil  
rsrgpscdrh@gmail.com

<sup>1</sup> Centre for Water Engineering and Management, Central University of Jharkhand, Ranchi, Jharkhand, India

<sup>2</sup> River Hydraulics Division, Central Water and Power Research Station, Ministry of Water Resources, River Development and Ganga Rejuvenation, Pune, Maharashtra, India

<sup>3</sup> Centre for Water Engineering and Management, Central University of Jharkhand, Ranchi, Jharkhand, India



# Effect of indentation load on mechanical properties and evaluation of tribological properties for zirconia toughened alumina

Ayush Pratap<sup>a,b,1</sup>, Piyush Kumar<sup>a,b,1</sup>, G.P. Singh<sup>b</sup>, Nilrudra Mandal<sup>a</sup>, B.K. Singh<sup>a,c</sup>

<sup>a</sup> Materials Processing & Microsystems Laboratory, Central Mechanical Engineering Research Institute, Durgapur 713209, India

<sup>b</sup> Department of Nano-technology, Central University of Jharkhand Brambe Ranchi, 835205 Jharkhand, India

<sup>c</sup> Mechanical Engineering Department, National Institute of Technology Durgapur, Durgapur 713209, India

## ARTICLE INFO

### Article history:

Received 8 January 2020

Accepted 13 February 2020

Available online 18 March 2020

### Keywords:

ZTA

Co-precipitation

Hardness

Toughness

Co-efficient of friction (COF)

Specific wear rate

## ABSTRACT

In this study, co-precipitation processing route has been opted to prepare the ZTA composites. The well homogenized powders are compacted in a circular shape die-punch arrangement using hydraulic press. The mechanical properties of developed composites are evaluated on Vickers testing machine. In this study, a wide range of test load (0.5–50 N) has been applied on the samples to see its effect on hardness. A significant decrease in the value of hardness and fracture toughness has been observed with increasing load. An interesting result has been observed beyond 25 N loads, where stagnation in the said properties is observed. After evaluation of mechanical properties the ZTA composites are used to investigate the tribological properties. A comparative study has been made between alumina and ZTA ceramics at a load of 20 N with sliding velocity of 0.5 m/s. The observed results show an improvement of 57.8% in case of specific wear rate, whereas 19.78% improvement has been achieved in case of coefficient of friction for ZTA ceramics as compared to alumina ceramics. The improvements in tribological properties are attributed to the soft phase of zirconia reinforced inside hard matrix of alumina which provides a toughening effect.

© 2019 Elsevier Ltd. All rights reserved.

Selection and peer-review under responsibility of the scientific committee of the 10th International Conference of Materials Processing and Characterization.

## 1. Introduction

Now a day's environment friendly materials are emphasized due to stricter enforcement of new standards, imposed by United Nations Environment Programmes (UNEP). In this context, ceramic materials, specially zirconia toughened alumina (ZTA) are one of the best alternatives to replace the conventional one due to high hardness, fracture toughness, environment friendly and nontoxic in nature. The rough and tumble properties of ceramics gained its importance in structural applications in many industries like manufacturing medical aerospace etc. Alumina based ceramic has been widely known to industries due to its better thermo-mechanical properties and high resistance to thermal and chemical attack. Recently, many researchers dedicated their research to counterbalance the demerits associated with alumina ceramics. In this regard, Bindal et al. [1] showed a significant improvement in hardness (~46%) and fracture toughness (~53%) of alumina

matrix with incorporation of 10 wt% yttria stabilized zirconia (YSZ) inside alumina. The powders were synthesized through co-precipitation method, the size of the powder ranging from 100 to 300 nm. Bindal et al. also demonstrated that the presence of zirconia restrict the abnormal grain growth and helps in formation of equiaxed and homogeneous grain growth. Recently, a comparative study was carried out by Singh et al. [2,3] for different percentage of YSZ inside alumina. The investigation clearly demonstrated that 90:10 wt% ratio of alumina:YSZ has high mechanical properties among all composites. The incorporation of additives like MgO [4], Cr<sub>2</sub>O<sub>3</sub> [5] and CeO<sub>2</sub> [6] inside alumina matrix also showed significant improvement in the mechanical properties of alumina ceramics. The effect of indentation load on the mechanical properties to developed proportional specimen resistance model (SPM) was well illustrated by Gong et al. [7]. Researcher illustrated that the indentation size effect (ISE) at low loading condition, the value of hardness is high and at high loading condition the hardness is low.

In the application of any advance materials, which are used in harsh environmental condition for a prolong time the tribological

<sup>1</sup> These authors contributed equally to this work.

E-mail address: [bipinmech2008@gmail.com](mailto:bipinmech2008@gmail.com) (B.K. Singh)



## ARTICLE

**Core-shell structured Zero-valent Manganese (ZVM): A novel nanoadsorbent for efficient removal of As(III) and As(V) from drinking water**Received 00th January 20xx,  
Accepted 00th January 20xx

DOI: 10.1039/x0xx00000x

Amulya Prasad Panda,<sup>a</sup> Priyanka Rout,<sup>a</sup> Kishore K. Jena,<sup>b</sup> Saeed M. Alhassan,<sup>b</sup> Sanjukta A. Kumar,<sup>c</sup> Usha Jha,<sup>a</sup> R. K. Dey,<sup>d</sup> S. K. Swain<sup>\*e</sup>

This work describes the preparation of core shell structured zero valent manganese (ZVM) for sequestration of total arsenic from drinking water. The material was synthesized using ultra-sonication assisted hydrothermal route and the prepared material was characterized by using various analytical instruments such as FTIR, XRD, FE-SEM, EDS, AFM, TEM, TGA-DTA, BET and XPS. Combination of data shows successful fabrication of core-shell structured ZVM which consist of core zero-valent manganese (Mn<sup>0</sup>) encapsulated by layers of manganese oxides (Mn<sub>3</sub>O<sub>4</sub>-MnO<sub>2</sub>). XPS analysis provides the information regarding the surface interaction of arsenic species with the adsorbent material. The adsorbent was tested for arsenic removal with variation of solution parameters in a batch technique. Both As(III) and As(V) could be removed over a wide pH range where the maximum sorption capacity was found to be of 30.9 mg g<sup>-1</sup> and 72.5 mg g<sup>-1</sup> for As(III) and As(V), respectively. It was observed that the sorption kinetics and adsorption isotherm follows pseudo second order kinetic model and D-R isotherm model, respectively. Presence of co-anions in a competitive environment had little effect on the arsenic removal properties of material. Moreover, the exceptional arsenic adsorption capacity of ZVM in ground water and high reusability make it a promising adsorbent material in removal of total arsenic from aqueous solution.

**1. Introduction**

Consumption of arsenic contaminated drinking water poses a serious threat to human health and presently occurs as a global outbreak. Argentina was the first country to report about the incidences of arsenic poisoning in 1930 followed by Taiwan in 1960. However, it was only in the late 1990s, arsenic in drinking water was identified as a grave concern and since then there is a significant boost in the number of arsenic-tainted countries.<sup>1</sup> Arsenic in natural water mainly occurs as oxyanions compounds of inorganic species i.e. arsenite (As(III) as H<sub>3</sub>AsO<sub>3</sub>, H<sub>2</sub>AsO<sub>3</sub><sup>-</sup>) and arsenate (As(V) as H<sub>2</sub>AsO<sub>4</sub><sup>-</sup>, HAsO<sub>4</sub><sup>2-</sup>, AsO<sub>4</sub><sup>3-</sup>).<sup>2</sup> Arsenite is more prevalent in reducing conditions and is more toxic and mobile compared to arsenate which predominates under the oxidizing condition.<sup>3</sup> As the reduction and oxidation reactions concerning these arsenic species are

very slow, both the oxidation states can co-exist in natural water irrespective of the redox condition.<sup>4</sup> Inorganic arsenic is considered as a powerful human carcinogen and it is believed that even low concentration of arsenic in drinking water can cause dire consequences on human health. These include skin lesions, hypertension, diabetes, lung cancer, bladder cancer and many more.<sup>2,3,5</sup> Keeping in view, the lethal impact of arsenic on human health; the World Health Organization (WHO) has taken stringent action recommending 0.01mgL<sup>-1</sup> arsenic as the maximum contamination limit in drinking water.<sup>6</sup> In order to meet this benchmark of arsenic in drinking water, diverse approaches were explored for arsenic elimination including various techniques such as coagulation/precipitation, adsorption, reverse osmosis, membrane filtration, electrodialysis, photo-oxidation and biological remediation.<sup>7,8</sup> Among these, adsorption has evolved as the most promising technique for arsenic sequestration as arsenic species have higher affinity towards the adsorbent surface (particularly metal oxides) which inevitably controls its mobility in the environment.<sup>3,4,9</sup> To date several metal oxide sorbents were developed for efficient arsenic removal from drinking water such as ZrO<sub>2</sub>, TiO<sub>2</sub>, CuO and MgO nanoparticles but among them iron based oxides were the most extensively studied sorbents. This was because of their higher affinity towards the inorganic arsenic.<sup>5,8,9,10</sup> Iron based oxides can potentially remove arsenic from drinking water by either acting as a reductant, sorbent, co-precipitant or behaving as a contaminant-immobilizing agent.

<sup>a</sup> Department of Chemistry, Birla Institute of Technology, Mesra, Ranchi, Jharkhand, 835215, India

<sup>b</sup> Department of Chemical Engineering, Khalifa University, SAN Campus, Abu Dhabi, 2533, United Arab Emirates (UAE)

<sup>c</sup> Analytical Chemistry Division, Bhabha Atomic Research Centre, Trombay, Mumbai, 400085, India

<sup>d</sup> Department of Chemistry, Central University of Jharkhand, Ranchi, Jharkhand, 835205, India

<sup>e</sup> Central Instrumentation Facility, Birla Institute of Technology, Mesra, Ranchi, Jharkhand 835215, India

\* Email: [skswain@bitmesra.ac.in](mailto:skswain@bitmesra.ac.in)

Electronic Supplementary Information (ESI) available: [details of any supplementary information available should be included here]. See DOI: 10.1039/x0xx00000x

**p73 induction by *Abrus* agglutinin facilitates Snail ubiquitination to inhibit epithelial to mesenchymal transition in oral cancer**

Niharika Sinha<sup>a</sup>, Biswa Ranjan Meher<sup>b</sup>, Prajna Paramita Naik<sup>a</sup>, Prashanta Kumar Panda<sup>a</sup>, Subhadip Mukhapadhyay<sup>a</sup>, Tapas K Maiti<sup>c</sup> and Sujit K Bhutia<sup>a,\*</sup>

<sup>a</sup>Department of Life Science, National Institute of Technology Rourkela, Rourkela-769008, Odisha, India

<sup>b</sup>Centre for Life Science, Central University of Jharkhand, Brambe, Ranchi-835205, Jharkhand, India

<sup>c</sup>Department of Biotechnology, Indian Institute of Technology, Kharagpur, Kharagpur-721302, India

*\*Corresponding author*

Sujit Kumar Bhutia, PhD  
Department of Life Science  
National Institute of Technology Rourkela  
Rourkela-769008, Odisha, India  
Phone: 91-6612462686, Fax: 91661-2472926  
E-Mail address: [sbhutia@nitrkl.ac.in](mailto:sbhutia@nitrkl.ac.in), [bhutiask@gmail.com](mailto:bhutiask@gmail.com)

**ABSTRACT**

*Background:* Epithelial-to-mesenchymal transition (EMT), a key step in oral cancer progression, is associated with invasion, metastasis, and therapy resistance, thus targeting the EMT represents a critical therapeutic strategy for the treatment of oral cancer metastasis. Our previous study showed that *Abrus* agglutinin (AGG), a plant lectin, induces both intrinsic and extrinsic apoptosis to activate the tumor inhibitory mechanism.

*Objective:* This study aimed to investigate the role of AGG in modulating invasiveness and stemness through EMT inhibition for the development of antineoplastic agents against oral cancer.

*Methods:* The EMT- and stemness-related proteins were studied in oral cancer cells using Western blot analysis and fluorescence microscopy. The potential mechanisms of Snail downregulation through p73 activation in FaDu cells were evaluated using Western blot analysis, immunoprecipitation, confocal microscopy, and molecular docking analysis. Immunohistochemical staining of the tumor samples of AGG-treated FaDu-xenografted nude mice was performed.

*Results:* At the molecular level, AGG-induced p73 suppressed Snail expression, leading to EMT inhibition in FaDu cells. Notably, AGG promoted the translocation of Snail from the nucleus to the cytoplasm in FaDu cells and triggered its degradation through ubiquitination. In this setting, AGG inhibited the interaction between Snail and p73 in FaDu cells, resulting in p73 activation and EMT inhibition. Moreover, in epidermal growth factor (EGF)-stimulated FaDu cells, AGG abolished the upregulation of extracellular signal-regulated kinase (ERK)1/2 that plays a pivotal role in the upregulation of Snail to regulate the EMT phenotypes. In immunohistochemistry analysis, FaDu xenografts from AGG-treated mice showed decreased expression of Snail, SOX2, and vimentin and increased expression of p73

## Systematic study of incomplete-fusion dynamics below 8 MeV/nucleon energy

Harish Kumar,<sup>1,\*</sup> Suhail A. Tali,<sup>1</sup> M. Afzal Ansari,<sup>1,†</sup> D. Singh,<sup>2</sup> Rahbar Ali,<sup>3</sup> Asif Ali,<sup>1</sup> Siddharth Parashari,<sup>1</sup> Pankaj K. Giri,<sup>2</sup> Sneha B. Linda,<sup>2</sup> R. Kumar,<sup>4</sup> R. P. Singh,<sup>4</sup> and S. Muralithar<sup>4</sup>

<sup>1</sup>*Nuclear Physics Laboratory, Department of Physics, Aligarh Muslim University, Aligarh 202002, India*

<sup>2</sup>*Centre for Applied Physics, Central University of Jharkhand, Ranchi 835205, India*

<sup>3</sup>*Department of Physics, Gandhi Faiz-E-Aam College, Shahajhanpur 242001, India*

<sup>4</sup>*Nuclear Physics Group, Inter University Accelerator Centre, New Delhi 110067, India*



(Received 23 June 2018; revised manuscript received 17 January 2019; published 18 March 2019)

An attempt has been made to provide crucial information about the dependence of incomplete-fusion dynamics on various entrance channel parameters below 8 MeV/nucleon energy. The forward recoil range distributions of several evaporation residues produced in the  $^{13}\text{C} + ^{175}\text{Lu}$  system have been measured at  $\approx 88$ -MeV energy and examined in the framework of the code SRIM. Owing to the fractional linear momentum transfer from the projectile to the target nucleus, incomplete-fusion (ICF) products are observed to be trapped at lower cumulative thickness than that of complete fusion products. In order to study the incomplete-fusion behavior with various entrance channel parameters, the incomplete-fusion fraction ( $F_{\text{ICF}}$ ) has also been deduced and compared with those obtained for the systems available in the literature. The reinvestigation of the Coulomb factor ( $Z_p Z_T$ ) dependence of incomplete fusion indicates that it is somehow projectile structure dependent. No systematic trend is observed with the target deformation parameter ( $\beta_2$ ) dependent study of ICF. A systematic linear growth in the incomplete-fusion probability function ( $F_{\text{ICF}}$ ) is observed with increasing the parameters  $Z_p Z_T \beta_2$  and  $Z_p Z_T / (1 - \beta_2)$ , but separately for  $\alpha$ - and non- $\alpha$ -cluster structured projectiles with different targets. The present findings explore the role of Coulomb interaction on ICF dynamics more effectively. Moreover, the projectile  $\alpha$ - $Q$  value is found to be a suitable parameter which explains effectively the observed trend in the study of ICF with the above-mentioned parameters. The incomplete-fusion existence below critical angular momentum ( $\ell_{\text{crit}}$ ), i.e.,  $\ell \leq \ell_{\text{crit}}$ , is also observed for the present  $^{13}\text{C} + ^{175}\text{Lu}$  system.

DOI: [10.1103/PhysRevC.99.034610](https://doi.org/10.1103/PhysRevC.99.034610)

### I. INTRODUCTION

Efforts are continuously being made to investigate the incomplete-fusion (ICF) process in collisions of heavy ions at lower projectile energies [1–5]. In the interaction of two heavy ions, several reaction channels may open up, which further leads to the transfer of cluster of the nucleons. Fusion suppression based studies have also explored the ICF dynamics, using weakly bound projectiles around the barrier [6–9]. Nevertheless, the study of ICF is still an active area of research due to complexity in the mass transferred from the projectile to the target. Thereby, it requires further investigation to unfold the ICF dependence on various entrance channel parameters. It is now a well-understood fact that the ICF process is also one of the dominant reaction modes other than complete fusion (CF) at energies near and well above the Coulomb barrier ( $V_{\text{CB}}$ ), which contributes significantly to the total fusion cross sections [10–13]. In the case of CF, the entire projectile fuses with the target nucleus. On the other hand, the incident projectile may break up into its fragments in the case of ICF, wherein only one of the parts fuses with the target and the remnant moves as a spectator.

The experimental features of the ICF in the breakup of projectiles like  $^{12}\text{C}$ ,  $^{14}\text{N}$ , and  $^{16}\text{O}$  into  $\alpha$  clusters were first observed by Britt and Quinon [14]. However, Inamura *et al.* [15] provided the major advances in the study of the ICF process from the extracted information based on the particle- $\gamma$  coincidence measurements. Udagawa and Tamura [16] explained the projectile breakup into  $\alpha$  clusters in the vicinity of the target nuclear field. Several theoretical models [16–20] were proposed using tightly bound projectiles to explain the ICF process. The CF and the ICF processes have also been categorized on the basis of imparted angular momentum ( $\ell$ ) in the system. For the ICF process, the attractive nuclear potential is no longer strong enough to capture the projectile entirely by the target nucleus and the CF gives way to the ICF process. As per predictions of the SUMRULE model of Wilczynski *et al.* [17], the ICF process exists only for input angular momentum values ( $\ell$ ) greater than critical angular momentum values ( $\ell_{\text{crit}}$ ). However, in contradiction to the SUMRULE model approach, a substantial contribution of ICF below  $\ell_{\text{crit}}$  has also been observed in recent studies [12,13,21–23]. As the projectile partially fuses with the target, less nucleonic degrees of freedom participate in the case of ICF. Hence, owing to the linear momentum transfer (LMT), the ICF products are observed to traverse the shorter path in the stopping medium compared with that of CF products [4,12,22,23]. The studies available in the literature show noticeable ICF contribution in the

\* amu.harish@gmail.com

† drmafzalansari@yahoo.com



# Analysis of dielectric and magnetic phase transitions in $\text{Yb}(\text{Fe}_{0.5}\text{Cr}_{0.5})\text{O}_3$ bulk perovskite

Tirupathi Patri<sup>1</sup> · Ponnaiah Justin<sup>2</sup> · P. D. Babu<sup>3</sup> · Avijit Ghosh<sup>4</sup>

Received: 4 November 2018 / Accepted: 25 February 2019 / Published online: 4 March 2019  
© Springer-Verlag GmbH Germany, part of Springer Nature 2019

## Abstract

A comprehensive investigation of dielectric and magnetic phase transitions in  $\text{Yb}(\text{Fe}_{0.5}\text{Cr}_{0.5})\text{O}_3$  bulk ceramics has been presented. The co-existence of orthorhombic phase (*Pbnm*) along with minor hexagonal (*P6<sub>3</sub>cm*) phase is detected through Rietveld refinement technique, whereas the presence of  $\text{Fe}^{3+}/\text{Fe}^{2+}$  and  $\text{Cr}^{3+}/\text{Cr}^{2+}$  species is also encountered under XPS study. The dielectric broad-band spectroscopic study (5–500 K) reveals that two dielectric transition peaks: (1) at 370 K, first order ferroelectric transition for induced local non-centrosymmetry, and (2) at 462 K, diffuse like relaxor transition because of formation of polar nano-regions and, Schottky barriers at sample-electrode interface, respectively. The complex impedance spectroscopic study exhibits the non-Debye type dielectric relaxation phenomena at lower temperatures, while at high temperatures, oxygen ion vacancies are found to contribute the conduction progression. Furthermore, dc-magnetization plot in FC-ZFC mode detects the strong interactions between  $\text{Cr}^{3+}/\text{Fe}^{3+}$  sublattices also with  $\text{Yb}^{3+}$  ions and  $\text{Yb}^{3+}-\text{Yb}^{3+}$  ions. This results into an antiferromagnetic ordering at  $T_N \sim 271$  K for  $\text{Cr}^{3+}-\text{Cr}^{3+}/\text{Fe}^{3+}-\text{Fe}^{3+}$  or  $\text{Cr}^{3+}-\text{Fe}^{3+}$  spins followed by weak ferromagnetic ordering at 41 K for the occurrence of progressive spin reorientation and further at 11.2 K due to onset interactions of ferromagnetic  $\text{Cr}^{3+}/\text{Fe}^{3+}$  sub-lattices with paramagnetic  $\text{Yb}^{3+}$  ions.

## 1 Introduction

Over the past few decades, there has been renewed interest in the field of multiferroics for possible applications in magnetoelectric (ME) coupling devices [1–3]. Recently, rare earth families including ortho-ferrites, manganites, and chromites have been most extensively studied to search for possible large value of ME coupling parameter [4–9]. The rare earth-chromites  $\text{RCrO}_3$  (R = rare earth or Yttrium) i.e., orthorhombic distorted perovskite ( $\text{ABO}_3$ -type) systems exhibit strong magnetic properties due to the interaction between  $\text{R}^{3+}$  and

$\text{Cr}^{3+}$  ions. The possible interaction between  $\text{R}^{3+}$  and  $\text{Cr}^{3+}$  ions denoted as  $\text{R}^{3+}-\text{R}^{3+}$ ,  $\text{Cr}^{3+}-\text{R}^{3+}$  and  $\text{Cr}^{3+}-\text{Cr}^{3+}$ , are significant in the region of low temperature. These interactions are generally predicted to be consisting of the isotropic and symmetric, as well as antisymmetric and anisotropic exchange interactions of  $\text{Cr}^{3+}-\text{Cr}^{3+}$ ,  $\text{Cr}^{3+}-\text{R}^{3+}$ , and  $\text{R}^{3+}-\text{R}^{3+}$  ions, respectively [5, 10–12]. Again, it is well known that octahedral tilt or rotation produces an orthorhombic distortion by the reduction of Cr-O-Cr bond angle in  $\text{RCrO}_3$  system. This octahedral ( $\text{CrO}_6$ ) tilting can produce canted antiferromagnetic (c-AFM) order of  $\text{Cr}^{3+}$  spins [13]. It is also reported that signature of weak ferromagnetic (FM) properties arising due to small canting of  $\text{Cr}^{3+}$  spins, while the coupling of R-ions and the  $\text{Cr}^{3+}$  spins responsible for ordering below Néel temperature [14]. Furthermore, the spin-phonon coupling arising from complex magnetic ordering with nearest neighbour and next nearest neighbour exchange interactions is predicted [15]. But, there is no serious consensus on magnetic ordering in  $\text{RCrO}_3$  system.

Among all the members of  $\text{RCrO}_3$  system,  $\text{YbCrO}_3$  provides the excellent physical properties for strong anisotropic exchange interaction between the  $\text{Yb}^{3+}$  and  $\text{Cr}^{3+}$  ions. The strong anisotropic exchange interaction ( $3d-4f$  orbital) between  $\text{Yb}^{3+}$  and the  $\text{Cr}^{3+}$  spins in  $\text{YbCrO}_3$  system

✉ Avijit Ghosh  
avijitphy@gmail.com

<sup>1</sup> Department of Physics, Rajiv Gandhi University of Knowledge Technologies-R K Valley Campus, Kadapa, Andhra Pradesh 516330, India  
<sup>2</sup> Department of Chemistry, Rajiv Gandhi University of Knowledge Technologies-R K Valley Campus, Kadapa, Andhra Pradesh 516330, India  
<sup>3</sup> UGC-DAE Consortium for Scientific Research, Mumbai Center, BARC, Mumbai 400085, India  
<sup>4</sup> Department of Physics, Central University of Jharkhand, Ranchi, Jharkhand 835205, India



# Evaluating urban growth and its implication on flood hazard and vulnerability in Srinagar city, Kashmir Valley, using geoinformatics

Tauseef Ahmad<sup>1</sup> · Arvind Chandra Pandey<sup>1</sup> · Amit Kumar<sup>1</sup>

Received: 20 December 2018 / Accepted: 1 April 2019 / Published online: 1 May 2019  
© Saudi Society for Geosciences 2019

## Abstract

The present study investigates the urban growth in the Srinagar city of Kashmir Valley during 1972–2014 and the effect of 2014 Kashmir flood on the urban environment. Srinagar is the capital city in Kashmir Valley which has been affected by the devastating flood in 2014. The built-up growth for the past 42 years was 1565% with concomitant population growth of 224% in the Srinagar city. The built-up development was more pronounced in the central part of the city and along the river Jhelum during 1972–1989 which later on spread largely in the southernmost part of Srinagar city during the period of 1996–2014. High-Resolution Satellite (HRS) data-based observations indicated that 2014 flood inundation occupied 108 sq. km area within the Srinagar municipal limits. The increase of built-up inundation was monitored from 1972 to 2014, which reveals that the built-up inundation was 3.7 sq. km and increased to 39.2 sq. km. The spatial analysis revealed that nine wards located in the topographically low regions and in the proximity to Jhelum river were completely (100%) inundated during the flood. The past built-up inundation spatial analysis with reference to 2014 flood inundation indicated decrease in the percentage built-up area inundation (72.4% in 1972 to 46% in 2014) which reveals that the new built-up growth in the Srinagar city mostly occurred in the relatively safer zones. It is also observed that very high flood hazard and vulnerability zones were located in the western, southern, and central parts of the city in only 10 wards which rendered these wards with very high flood risk. The study demonstrated that geoinformatics-based spatial analysis of flood inundation can be effectively used for flood risk and related strategic planning.

**Keywords** Urban growth · Urban flood · Srinagar city · Flood risk · Geoinformatics

## Introduction

Urbanization and urban growth are vital spatio-social processes (United Nations 2005), which leads to changes in human societies and relationship between social, economic, physical, and environmental dimensions (Dadras et al. 2015). Urban growth

is acknowledged by the physical and functional changes due to the transformation of rural landscape into urban forms (Xiao et al. 2006), which has an important influence on the cities worldwide on its social changes and environs (Dewan and Yamaguchi 2008; Van Ginkel 2008; Carter 1981). Urban sprawl is primarily provoked by uncoordinated, uncontrolled, haphazard, and unplanned growth and represented the low-density built-up growth with the most widespread effect on the environment (Muniz et al. 2008; Poelmans and Van Rompaey 2009; Diksha and Kumar 2017). This leads to land conversion to non-natural area that substantiates fast population growth (Barnes et al. 2001; Sudhira and Ramachandra 2007). The sequence of uncontrolled urban growth and advancement strains the capacity to deliver basic services (Zhang 2004). It also induces irretrievable land alteration (Luck and Wu 2002; Aguilera et al. 2011), which affects forest lands, wetlands, and agricultural practices (Kumar and Pandey 2016; Rahman et al. 2008; Galster et al. 2001).

Editorial handling: Candan Gokceoglu

✉ Arvind Chandra Pandey  
arvindchandrap@yahoo.com

Tauseef Ahmad  
tauseef@live.in; tauseef@cuja.ac.in

Amit Kumar  
amit.kumar@cuja.ac.in; amit.iirs@gmail.com

<sup>1</sup> Department of Geoinformatics, Central University of Jharkhand, Ranchi, India





# Simple Synthesis of End Functionalized Regioregular Poly(3-Hexyl thiophene) by Catalytic-Initiated Kumada Catalyst Transfer Polymerization

Koomkoom Khawas,<sup>1</sup> Soumili Daripa,<sup>2</sup> Pallavi Kumari,<sup>1</sup> Manas K. Bera,<sup>3</sup> Sudip Malik,<sup>3</sup> Biplab K. Kuila <sup>2</sup>

<sup>1</sup>Department of Chemistry, Central University of Jharkhand, Brambe, Ranchi 835205, Jharkhand, India

<sup>2</sup>Department of Chemistry, Institute of Science, Banaras Hindu University, Varanasi 221005, Uttar Pradesh, India

<sup>3</sup>School of Applied and Interdisciplinary Sciences, Indian Association for the Cultivation of Science, 2A&2B Raja S. C. Mullick Road, Kolkata 700032, West Bengal, India

Correspondence to: B. K. Kuila (E-mail: bkkuila.chem@bhu.ac.in)

Received 2 January 2019; accepted 17 February 2019

DOI: 10.1002/pola.29349

**KEYWORDS:** conjugated polymer; poly(3-hexyl thiophene); Kumada catalyst transfer polymerization (KCTP); end-functionalized polymer

**INTRODUCTION**  $\pi$ -conjugated polymers have attained significant research attention within the burgeoning field of organic electronic and optoelectronic research.<sup>1–5</sup> Among these polymers, poly(3-hexyl-thiophene) (P3HT) remains frontrunner in the research of conjugated polymers and work horse for organic electronic devices, such as photovoltaics, organic field-effect transistors, and so on.<sup>6,7</sup> With the rapid development of nanotechnology and block copolymer science, there is a tremendous demand of simple and novel strategies for the preparation of P3HTs with well-defined end functional groups as they can be used for the synthesis of more complex polymer structures of P3HT like star polymers, polymer brushes, block copolymers (BCP), polymer nanohybrids, and so on.<sup>8–19</sup> The synthesis of P3HT-based BCP or their complex architectures is sometimes necessary in order to manipulate the P3HT chains arrangement, assembly, or orientation in nanoscale level in thin-film devices to obtain better device performance.<sup>8,20–22</sup> Generally, three different synthetic strategies are adopted for the synthesis of end-functionalized P3HT: (a) Grignard metathesis (GRIM) for in situ modification of reactive P3HT end groups, (b) postpolymerization modification of the terminal aromatic moiety or functional group relying on the conversion of aryl bromides or other groups installed using GRIM to achieve the desired functionality, and (c) use of Ni-based catalytic initiators in combination with Kumada catalyst-transfer polymerization (KCTP).

End functionalization via GRIM involves in situ quenching of living end of the resulting polymer by KCTP with different types of

Grignard reagents including allyl, vinyl, aryl, alkyl, and so forth.<sup>23,24</sup> In this case, the degree of end-functionalization is determined solely by the nature of the Grignard reagent where allyl, ethynyl, and vinyl groups produce monofunctional polymers, while other Grignard reagents result primarily in bis-end-functionalized polymers.<sup>8</sup> The extent of end functionality is solely dependent on polymerization mechanism and reactivity of the Grignard reagents used for end functionalization. Any undesired chain termination during polymerization results in P3HT without end functionality. In post-functionalized approach, synthesized P3HT having mainly bromo or hydrogen group at one or both chain ends was further converted into suitable functional group by appropriate single or a multiple chemical transformations.<sup>12,25–31</sup> Although the postpolymerization strategy is versatile, the multistep nature and need for specific coupling reagents are the limitation of this method and should be factored into any design scheme.<sup>8</sup> In the third and most elegant approach, Ni-based functional initiators equipped with functional moiety are utilized for the synthesis of P3HT with well-defined end-functional groups.<sup>32–35</sup> Successful synthesis of different end functional P3HTs with (protected) alcohol, ethynyl, carboxylic acid, amine, or phosphonate groups proves the versatility of this approach.<sup>36–38</sup> Recently, the concept of Ni-based external initiators was introduced and has been successfully employed for the preparation of P3HTs with different end groups, hybrid materials using a variety of inorganic nanoparticles, and complex polymeric architectures including brushes and BCPs.<sup>13,17,39</sup> In spite of great success, there are still very limited number of approaches for the synthesis of Ni initiator and their further use for successful synthesis of well-defined end-terminated regioregular poly(3-hexyl thiophene)

Additional supporting information may be found in the online version of this article.

© 2019 Wiley Periodicals, Inc.



# Local convergence analysis for Chebyshev's method

Chandni Kumari<sup>1</sup> · P. K. Parida<sup>1</sup>

Received: 6 December 2017

© Korean Society for Computational and Applied Mathematics 2018

**Abstract** In this work, we are working to present a local convergence analysis for Chebyshev's method by using majorizing sequence. The given method is a third order iterative process, used in order to approximate a zero of an nonlinear operator equation in a Banach space. Here we are using a new type of majorant conditions to prove the convergence. We will also try to establish relations between this majorant conditions with results of based on Kantorovich-type and Smale-type assumptions.

**Keywords** Chebyshev's method · Newton's method · Banach space · Convex majorant · Ball convergence · Radius of convergence

**Mathematics Subject Classification** 65G99 · 65J15 · 47H17 · 47J05

## 1 Introduction

Let  $U_1$  and  $U_2$  be two Banach spaces and  $\Omega$  be a non empty open convex subset of  $U_1$ . Setup  $F : \Omega \subseteq U_1 \longrightarrow U_2$ , where  $F$  is a non-linear operator. Solving the non-linear equation

$$F(u) = 0 \tag{1.1}$$

is one of the most commonly occurring problem in the scientific and engineering computing area. In the present study, we will consider the problem of finding a local

---

✉ P. K. Parida  
pkparida@cuj.ac.in

Chandni Kumari  
mar93chandni@gmail.com

<sup>1</sup> Centre for Applied Mathematics, Central University of Jharkhand, Ranchi 835205, India

1 **BaZrO<sub>3</sub> and Cs-BaZrO<sub>3</sub> catalysed transesterification of *Millettia Pinnata* oil and**  
2 **optimisation of reaction variables by response surface Box-Behnken design**

3  
4 Dipesh Kumar and <sup>a</sup>Bhaskar Singh

5 Centre for Environmental Sciences, Central University of Jharkhand  
6 Ranchi, India-835205

7  
8 <sup>a</sup>corresponding author: [bhaskar.singh@cuja.ac.in](mailto:bhaskar.singh@cuja.ac.in)  
9

---

10 **Abstract**

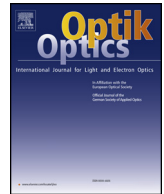
11  
12 Perovskite BaZrO<sub>3</sub> was synthesised via a relatively mild solid-state reaction route by using  
13 nitrate precursors. Thermal behaviour, the presence of crystalline phases and functional  
14 groups, specific surface area, microstructural characteristics, elemental composition, and  
15 basic strength of the synthesised material was examined. Further, the partial ionic exchange  
16 of Ba ions in BaZrO<sub>3</sub> was attempted to synthesise Cs modified BaZrO<sub>3</sub>. Characterization  
17 results revealed the synthesis of phase pure and strongly basic materials. BaZrO<sub>3</sub> was tested  
18 as a transesterification catalyst for the synthesis of biodiesel. Transesterification reaction  
19 variables for BaZrO<sub>3</sub> catalysed transesterification were optimised using response surface  
20 methodology based Box-Behnken designing approach. Under the suggested optimal  
21 conditions the predicted conversion was 94.12%, and the experimentally determined  
22 conversion of 93.2±0.3 % confirmed the validity of the generated quadratic model. Cs  
23 modification of BaZrO<sub>3</sub> enhanced its basic strength. Under the optimised conditions for  
24 pristine BaZrO<sub>3</sub>, the effect of Cs modification on BaZrO<sub>3</sub> was assessed, and it led to a  
25 conversion of 97.27±0.4 %. Both the materials were effective in catalysing the  
26 transesterification of *M. pinnata* oil, however; only Cs-BaZrO<sub>3</sub> catalysed oil met the EN  
27 14214:2003 specification for minimum ester content in biodiesel.  
28  
29  
30  
31  
32  
33  
34  
35  
36  
37  
38

39 **Keywords:** *Biodiesel, Transesterification, Heterogeneous Catalyst, Perovskite, BaZrO<sub>3</sub>*  
40  
41  
42  
43  
44



Contents lists available at ScienceDirect

Optik

journal homepage: [www.elsevier.com/locate/ijleo](http://www.elsevier.com/locate/ijleo)

Original research article

# Transition from two-photon absorption to saturable absorption in gold patterned ruby thin film

Satchi Kumari<sup>a,\*</sup>, Shompa Kumari<sup>a</sup>, Avesh Kumar<sup>b</sup>, Vijay Kumar<sup>b</sup>, R.P. Singh<sup>b</sup><sup>a</sup> Centre for Applied Physics, Central University of Jharkhand, Ranchi, 835205, India<sup>b</sup> Physical Research Laboratory, Navrangpura, Ahmedabad, 380009, Gujarat, India

## ARTICLE INFO

## Keywords:

Z-scan  
Two-photon absorption  
Saturable absorption  
Ruby  
Surface plasmon resonance

## ABSTRACT

Nonlinear behaviour of gold micro disks patterned Ruby film has been investigated via Z-scan technique. Open Z-scan was performed for Ruby and Ruby/gold thin film using 532 nm Laser source. Two-photon absorption (TPA) and Saturable absorption (SA) have been observed in pure Ruby and Ruby/gold thin film respectively. The expression for normalized transmittance in open Z-scan was obtained by Gaussian decomposition method for fitting. The values for nonlinear absorption coefficient ( $\beta$ ) for Ruby/gold ( $7.41 \times 10^{-7} m/W$ ) was two orders of magnitude higher than that of Ruby ( $1.41 \times 10^{-9} m/W$ ). Further, TPA and SA were confirmed by open Z-scan on these films, performed using 633 nm Laser source.

## 1. Introduction

Ruby has potential applications in the field of nonlinear optics [1–9]. Various nonlinear effects viz. as slowing down of light [4–6], non-degenerate two wave mixing [3,7], spectral hole [8] has been experimentally as well as theoretically studied in Ruby. Among above mentioned applications, slowing down of light in Ruby has emerged as a promising field for nonlinear optics application [4,6]. Slow light has been generated in Ruby by a very simple technique, using a single beam of laser, known as coherent population oscillation (CPO) [6,9]. The observed delay of  $\sim 1.26$  ms and corresponding  $v_g \sim 45$  m/s has been demonstrated in Ruby crystal via CPO [4]. Nearly all experiments of slow light in Ruby has been performed in bulk, while for applications it has to be achieved in thin film geometry. For this purpose, Ruby thin film has been deposited via Pulsed Laser deposition (PLD) technique on sapphire substrate (thickness  $\sim 3.5$   $\mu$ m) [10]. The slowing down of light has been studied in PLD Ruby film via degenerate two-wave mixing technique (DTWM) [11]. For a 200 ns pulse (derived from 2<sup>nd</sup> harmonic of Nd:YAG laser), the observed delay was  $\sim 17$  ns and corresponding group velocity was,  $v_g \sim 205.88$  m/s. This delay was very small as compared to the delay in case of bulk Ruby [4,11]. The reduction of delay in thin film geometry was due to smaller interaction length as compared to the bulk. In order to enhance the interaction in Ruby, gold micro disks patterned onto the Ruby thin film.

The interaction of laser light with the gold micro disks patterned Ruby film shows higher energy transfer and hence better pump-probe coupling [12]. This can be attributed to Fabry-Perot and surface plasmon modes [13–15]. Such changes in non-linear response after coupling with surface plasmon has been observed in other experiments as well [16–20]. To understand change in optical nonlinearity it is important to estimate the NLO coefficients. These coefficients can be estimated by using Z-scan technique [11,21]. It is a simple, highly sensitive and a popular technique for understanding and estimating nonlinear coefficients [21–27]. Recently, this technique has been successfully used to investigate nonlinear properties of even metallic films [28,29]. The optical nonlinearity of

\* Corresponding author.

E-mail address: [satchikumarisingh@gmail.com](mailto:satchikumarisingh@gmail.com) (S. Kumari).



# Relativistic model for anisotropic compact stars using Karmarkar condition

A.K. Prasad<sup>1</sup> · J. Kumar<sup>1</sup> · S.K. Maurya<sup>2</sup> · B. Dayanandan<sup>2</sup>

Received: 25 September 2018 / Accepted: 8 April 2019 / Published online: 19 April 2019  
© Springer Nature B.V. 2019

**Abstract** In this work we have obtained some families of relativistic anisotropic compact stars by solving of Einstein's field equations. The field equations have been solved by suitable particular choice of the metric potential  $e^\lambda$  and embedding class one condition. The physical analysis of this model indicates that the obtained relativistic stellar structure for anisotropic matter distribution is physically reasonable model for compact star whose energy density of the order  $10^{15}$  g/cm<sup>3</sup>. Using the Tolman-Oppenheimer-Volkoff equations, we explore the hydrostatic equilibrium and the stability of the compact stars like PSR J1614-2230, 4U 1608-52, SAX J1808.4-3658, LMC X-4, RX J1856-37, Vela X-1, 4U 1820-30, EXO 1785-248, PSR J1903+327, 4U 1538-52, SMC X-1, Her X-1 and Cen X-3. We also estimated the mass and radius of such compact stars.

**Keywords** Compact star · Anisotropic fluid sphere · General Relativity · Karmarkar condition

## 1 Introduction

The non-zero anisotropy is an important component in relativistic stellar systems in the absence of an electric field. Bowers and Liang (1974) highlighted the anisotropic sphere in general relativity. There has been many work done the physical related to anisotropic pressure. Dev and Gleiser (2002, 2003) have discussed that pressure anisotropy influence the mass, structure and physical properties of compact sphere. Also it was shown by Herrera and Santos (1997) that the effect of anisotropy in pressure. They have proposed physical mechanism in low and very high density system for astrophysical compact objects. Böhmer and Harko (2006) derived upper and lower limits for the basic physical parameters viz. mass-radius ratio, anisotropy, redshift and total energy for arbitrary anisotropic general relativistic matter distributions in the presence of cosmological constant. They have shown that anisotropic compact stellar type objects can be much more compact than the isotropic ones, and their radii may be close to their corresponding Schwarzschild radii.

Anisotropy in fluid pressure usually arise due to presence of mixture of different types of fluids, magnetic field or external field, rotation, existence of super-fluid, viscosity and phase transitions etc. Ruderman (1972) has studied the stellar models and argued that the nuclear matter at very high densities of the order  $10^{15}$  g/cm<sup>3</sup> may have anisotropic features and their interactions are relativistic. The paper of many authors (Maurya and Gupta 2013; Maurya et al. 2015) suggest that the anisotropic is a crucial component in the description of dense objects with nuclear matter. Here we would like to mention that Mak and Harko (2003), and Sharma et al. (2001) suggest that anisotropy is a sufficient condition in the study of dense nuclear matter with strange star. In fact, several kinds of literature (Bhar 2015;

---

✉ J. Kumar  
jitendark@gmail.com

A.K. Prasad  
amitkarun5@gmail.com

S.K. Maurya  
sunil@unizwa.edu.om

B. Dayanandan  
baiju@unizwa.edu.om

<sup>1</sup> Department of Mathematics, Central University of Jharkhand, Ranchi 835205, India

<sup>2</sup> Department of Mathematical and Physical Sciences, College of Arts and Science, University of Nizwa, Nizwa, Sultanate of Oman

## Measurement of excitation functions in $^{14}\text{N}$ - ion induced reactions

Amritraj Mahato<sup>a</sup>, D Singh<sup>a\*</sup>, Pankaj K Giri<sup>a</sup>, Sneha B Linda<sup>a</sup>, Harish Kumar<sup>b</sup>, Suhail A Tali<sup>b</sup>, M Afzal Ansari<sup>b</sup>,  
R Kumar<sup>c</sup>, S Muralithar<sup>c</sup> & R P Singh<sup>c</sup>

<sup>a</sup>Department of Physics, Central University of Jharkhand, Ranchi 835 205, India

<sup>b</sup>Department of Physics, Aligarh Muslim University, Aligarh 202 002, India

<sup>c</sup>Inter University Accelerator Centre, Aruna Asaf Ali Marg, New Delhi 110 067, India

Received 8 April 2019

Excitation functions of nine evaporation residues populated through complete and/or incomplete fusion in  $^{14}\text{N} + ^{124}\text{Sn}$  system in the projectile energy range  $\approx 4-7$  MeV/nucleon have been measured. Recoil catcher activation technique using offline  $\gamma$ -ray spectrometry has been employed in these measurements. The evaporation residues produced through xn and pxn channels are found to be well reproduced by the theoretical predictions of PACE-4. In case of evaporation residues produced through  $\alpha$ -emitting channels, significant enhancement in the measured excitation functions over their theoretical predictions has been observed. This enhancement indicates that these  $\alpha$ -emitting channels are attributed to the incomplete fusion process. The comparison of present study with literature data also shows that the ICF probability depends on various entrance channel parameters. A new combined parameter  $\left(\frac{Z_p Z_T}{1-\beta_2}\right)^{\mu_{IC}}$  has been found to explain more precisely the ICF dynamics than other entrance channel parameters.

**Keywords:** Excitation functions, Stacked foil activation technique, Complete and incomplete fusion, Incomplete fusion fraction, Projectile structure

### 1 Introduction

The study of heavy ion induced reactions mainly completes fusion (CF) and incomplete fusion (ICF) has been a subject of resurgent interest to the nuclear physicists. In case of complete fusion (CF) process, entire projectile fuses with the target and the highly excited compound system decays by evaporating low energy nucleons and  $\alpha$ -particles at the equilibrium stage. Whereas in case of ICF reactions, only a part of the projectile fuses with the target nucleus, leading to transfer of a fraction of the incident momentum to the target nucleus, while the remainder (generally  $\alpha$ -particle) behaves as a spectator and moves in the forward cone. The first experimental evidence of ICF was observed by Britt and Quinton<sup>1</sup>. Major advances in the understanding of ICF dynamics took place after the charged particle- $\gamma$  coincidence measurements by Inamura *et al.*<sup>2</sup> for  $^{14}\text{N} + ^{159}\text{Tb}$  system at beam energy about  $\approx 7$  MeV/nucleon. Several theoretical models have been proposed to explain the characteristic features of ICF dynamics. Some of the most widely used models to explain ICF data are the Sumrule model<sup>3</sup>, breakup fusion model<sup>4</sup>, promptly emitted

particles model<sup>5</sup>, exciton model<sup>6</sup> and overlap model<sup>7</sup>. These theoretical models satisfactorily reproduce the contribution of ICF in some cases at higher energy, i.e., greater than 10 MeV/nucleon. But none of these models can satisfactorily explain the gross features of ICF data at low projectile energy below 7 MeV/nucleon. Hence, a clear picture of the mechanism of ICF dynamics has yet to be established at low bombarding energy. This makes the study of low energy incomplete fusion dynamics still an unsolved area of investigation. The presence of low energy ICF reactions and their dependence on various entrance channel parameters have been studied during the last couple of decades. Morgenstern *et al.*<sup>8</sup> found that the contribution of ICF to total fusion cross section increases with entrance channel mass asymmetry at relatively higher energies greater than 10 MeV/nucleon. Recently, several investigators have shown great interest to study the dependence of ICF dynamics on various entrance channel parameters<sup>9-11</sup>. Their studies show that the onset of ICF dynamics does not depend on a single entrance channel parameter, while it depends on various entrance channel parameters.

The present work has been carried out with a motivation to understand the dependence of ICF dynamics on various entrance channel parameters.

\*Corresponding author (E-mail: dsinghcuj@gmail.com)



# Vertical structure of atmospheric boundary layer over Ranchi during the summer monsoon season

Sagarika Chandra<sup>1</sup> · Nishi Srivastava<sup>1</sup> · Manoj Kumar<sup>2</sup>

Received: 19 April 2016 / Accepted: 29 March 2018 / Published online: 7 April 2018  
© Springer-Verlag GmbH Austria, part of Springer Nature 2018

## Abstract

Thermodynamic structure and variability in the atmospheric boundary layer have been investigated with the help of balloon-borne GPS radiosonde over a monsoon trough station Ranchi (Lat. 23°45'N, Long. 85°43'E, India) during the summer monsoon season (June–September) for a period of 2011–2013. Virtual potential temperature gradient method is used for the determination of mixed layer height (MLH). The MLH has been found to vary in the range of 1000–1300 m during the onset, 600–900 m during the active and 1400–1750 m during the break phase of monsoon over this region. Inter-annual variations noticed in MLH could be associated with inter-annual variability in convection and rainfall prevailing over the region. Along with the MLH, the cloud layer heights are also derived from the thermodynamic profiles for the onset, active and break phases of monsoon. Cloud layer height varied a lot during different phases of the monsoon. For the determination of boundary-layer convection, thermodynamic parameter difference ( $\delta\theta = \theta_{es} - \theta_e$ ) between saturated equivalent potential temperature ( $\theta_{es}$ ) and equivalent potential temperature ( $\theta_e$ ) is used. It is a good indicator of convection and indicates the intense and suppressed convection during different phases of monsoon.

## 1 Introduction

The atmospheric boundary layer (ABL) is the lowest part of the troposphere. It is influenced by the Earth's surface in addition to insolation, soil moisture, presence of clouds, advection of air mass and high/low pressure. ABL plays an essential role in regulating the transport of energy and moisture from the surface to the free atmosphere. Surface heating and radiative cooling create instability and turbulence in the ABL and are responsible for the formation of the mixed layer (Stull 1988; Oke 1988; Garratt 1992). The ABL height depends on different factors such as prevailing meteorological conditions, local time of observation and geographical location (Srivastava et al. 2010). The turbulence of ABL could be formed by buoyancy forces or mechanical forces, though buoyantly generated ABL tends to be more

uniformly mixed than does mechanically driven. The ABL height variations are largely driven by the seasonal changes in prevailing meteorological conditions such as temperature, humidity, wind and clouds. The structure of the ABL during Indian summer monsoon of India differs from other seasons due to the influence of large-scale monsoon features, such as the formation of the monsoon trough, depression and low-level jet. However, the influence of these factors on the ABL height is not well understood (Holt and Sethuraman 1987). The practical and theoretical problems involved in the determination of the ABL height are reflected in the literature (Stull 1988; Garratt 1992; Seibert et al. 2000). The estimation of ABL height is one of the crucial meteorological calculations in the monsoon season due to the presence of clouds and the strong wind circulation.

The ABL characteristics in the monsoon season have been studied by researchers using meteorological tower, numerical simulations over land (Raman et al. 1990) and radiosonde observations over ocean (Bhat et al. 2000). Several experiments in the past were conducted over the oceanic part of India to study the ABL along with station data, also radiosonde observation were used in few cases. The experiments in the Indian Ocean and Arabian Sea have included the International Indian Soviet Monsoon Experiment (ISMEX, 1973), MONSOON-77 and Monsoon

Responsible Editor: S. Trini Castelli.

✉ Nishi Srivastava  
nishi.bhu@gmail.com

<sup>1</sup> Department of Physics, Birla Institute of Technology Mesra, Ranchi 835215, India

<sup>2</sup> Centre for Environmental Sciences, Central University of Jharkhand, Ranchi 835205, India



Article

# Net Ecosystem Exchange of CO<sub>2</sub> in Deciduous Pine Forest of Lower Western Himalaya, India

Nilendu Singh <sup>1</sup>, Bikash Ranjan Parida <sup>2,\*</sup> , Joyeeta Singh Charakborty <sup>3</sup> and N.R. Patel <sup>4</sup> 

<sup>1</sup> Centre for Glaciology, Wadia Institute of Himalayan Geology, Dehradun 248001, India; nilendu\_singh@yahoo.com

<sup>2</sup> Department of Geoinformatics, School of Natural Resource Management, Central University of Jharkhand, Ranchi 835205, India

<sup>3</sup> Forest Research Institute, Dehradun 248001, India; joyeeta.u@gmail.com

<sup>4</sup> Indian Institute of Remote Sensing, Dehradun 248001, India; nrpatel@iirs.gov.in

\* Correspondence: bikashrp@gmail.com or bikash.parida@uj.ac.in

Received: 19 April 2019; Accepted: 17 May 2019; Published: 20 May 2019



**Abstract:** Carbon cycle studies over the climate-sensitive Himalayan regions are relatively understudied and to address this gap, systematic measurements on carbon balance components were performed over a deciduous pine forest with an understory layer. We determined annual net carbon balance, seasonality in components of carbon balance, and their environmental controls. Results indicated a strong seasonality in the behavior of carbon exchange components. Net primary productivity (NPP) of pine forest exceeded soil respiration during the growing phase. Consequently, net ecosystem exchange exhibited a net carbon uptake. In the initial phase of the growing season, daily mean uptake was  $-3.93 (\pm 0.50) \text{ g C m}^{-2} \text{ day}^{-1}$ , which maximizes  $(-8.47 \pm 2.3)$  later during post-monsoon. However, a brief phase of carbon release was observed during peak monsoon (August) owing to an overcast condition. Nevertheless, annually the forest remained as a carbon sink. The understory is extensively distributed and it turned out to be a key component of carbon balance because of sustained NPP during the pine leafless period. Temperature and evaporative fraction exhibited a prime control over the seasonal carbon dynamics. Our observations could lend certain useful insights into the application of coupled climate-carbon cycle models for the Himalaya and ecological functions in the region.

**Keywords:** net primary productivity; soil respiration; carbon use efficiency; *Pinus roxburghii*; understory; subtropical Himalaya

## 1. Introduction

During the last two centuries, anthropogenic CO<sub>2</sub> emissions and deforestation have increased the surface temperature significantly. The built-up CO<sub>2</sub> in the atmosphere causes global warming, whose future extent will not only depend on the size of future emissions, but also on the development of future carbon (C) sinks of the terrestrial biosphere and ocean. Terrestrial biosphere, together with the ocean help by drawing down more than 50% of the annual anthropogenic CO<sub>2</sub> emissions, and their C sink strength have continuously improved over the past five decades [1]. However, the future trend of C sink largely depends on the responses of terrestrial ecosystems to increasing CO<sub>2</sub> concentrations and climate change [2]. Further, the terrestrial C sink is mostly controlled by the forest ecosystems and associated environmental drivers [3].

The C balance of terrestrial ecosystems can be represented by both the net ecosystem productivity (NEP) and net ecosystem carbon exchange (NEE). The balance between ecosystem respiration (*Re*) and gross primary productivity (GPP) determines NEE, which can be positive (i.e., carbon source) or

Article

# Spatio-Temporal Rainfall Variability and Flood Prognosis Analysis Using Satellite Data over North Bihar during the August 2017 Flood Event

Gaurav Tripathi , Bikash Ranjan Parida \*  and Arvind Chandra Pandey

Department of Geoinformatics, School of Natural Resource Management, Central University of Jharkhand, Ranchi 835205, Jharkhand, India; gauravtripathi3135gt@gmail.com (G.T.); arvindchandrap@yahoo.com (A.C.P.)

\* Correspondence: bikashrp@gmail.com; Tel.: +91-7992257184

Received: 24 January 2019; Accepted: 13 May 2019; Published: 17 May 2019



**Abstract:** Flooding is one of the most common natural disasters in India. Typically, the Kosi and Gandak river basins are well-known for lingering flood affected basins in North Bihar every year, which lies in the eastern part of India. There were no such comprehensive studies available in North Bihar that discussed flood progression and regression at shorter time-scales like two day intervals. So in this study, we employed high temporal resolution data to capture inundation extent and further, the flood extent has been validated with high spatial resolution data. The specific objective of this study was to analyze the satellite-derived Near Real Time (NRT) MODIS flood product for spatiotemporal mapping of flood progression and regression over the North Bihar. The synthetic aperture RADAR (SAR) data were also used to validate the MODIS NRT Flood data. As a case study, we selected a recent flood event of August–September 2017 and captured the flood inundation spatial extent at two day intervals using the 2 day composite NRT flood data. The flood prognosis analysis has revealed that during the peak flooding period, 12% to 17% of the area was inundated and the most adversely affected districts were Darbhanga and Katihar in North Bihar. We estimated that in total nearly 6.5% area of the North Bihar was submerged. The method applied was simple, but it can still be suitable to be applied by the community involved in flood hazard management, not necessarily experts in hydrological modeling. It can be concluded that the NRT MODIS flood product was beneficial to monitor flood prognosis over a larger geographical area where observational data are limited. Nevertheless, it was noticed that the flood extent area derived from MODIS NRT data has overestimated areal extent, but preserved the spatial pattern of flood. Apparently, the present flood prognosis analysis can be improved by integrating microwave remote sensing data (SAR) and hydrological models.

**Keywords:** flood progression and regression; satellite-derived rainfall; MODIS NRT Flood product; Kosi and Gandak River; water levels

## 1. Introduction

Flooding is one of the most devastating and recurring events in the Indian subcontinent because of its geographical and riverine structure, which makes various parts of the nation prone to floods. The causative factors of frequent floods in India are intense rainfall, dam breach, unplanned urbanization, and land use/land cover (LU/LC) changes, that typically leads to the loss of lives and properties. As flood events have been increasing over the last three decades [1], the development of flood mapping using satellite data and application of flood inundation models become crucial to monitor and assess flood impact. Mostly in densely populated countries like India, an effective flood monitoring and forecasting system has been lacking due to inadequate resources [2]. Satellite remote sensing data can

## Sustainable Chemistry

## Exploring Nanostructured Zr/Cu Composite Oxide (NZCO) as an Efficient Adsorbent for Removal of As(III) and As(V) from Aqueous Solution

Priyanka Rout<sup>+</sup>,<sup>[a]</sup> Amulya Prasad Panda<sup>+</sup>,<sup>[a]</sup> Kishore K. Jena,<sup>[b]</sup> Saeed M. Alhassan,<sup>[b]</sup> Sanjukta A. Kumar,<sup>[c]</sup> Usha Jha,<sup>[a]</sup> R. K. Dey,<sup>[d]</sup> and S. K. Swain<sup>\*[e]</sup>

Consumption of arsenic contaminated water induces and aggravates major health problems in humans. In this report, we have successfully synthesized nanostructured Zr/Cu composite oxide (NZCO) by ultrasonically assisted hydrothermal process for total arsenic sequestration. Various batch experiments were performed with NZCO to determine its adsorption efficacy for As(III) and As(V) species. NZCO demonstrated outstanding performance in removing arsenic species from water with maximum adsorption capacities of 72.25 mg g<sup>-1</sup> and 107.5 mg g<sup>-1</sup> for As (III) and As (V) respectively under optimized conditions. The adsorption kinetics was closely fitted to pseudo-second order model and adsorption isotherms were

well described by D–R isotherms model. Meanwhile, the adsorption tests performed on naturally occurring ground water samples confirmed the effectiveness of NZCO in remediating total arsenic level below the prescribed limit of WHO-MCL (0.01 mg L<sup>-1</sup>). The adsorption mechanisms study exhibits a single-step arsenic treatment option involving electrostatic interaction and ligand exchange reactions. Various analytical techniques were used to characterize the material. Facile synthesis route combined with excellent performance make NZCO a novel adsorbent in total arsenic removal from drinking water.

## Introduction

Arsenic contamination is of great concern in drinking water as its lethal dose creates havoc in the lives of people. Due to its toxicological and carcinogenic nature it has evoked great heed of several researchers in the past years.<sup>[1]</sup> Long-term intake of arsenic contaminated water poses dire consequences on human health like lungs and kidney diseases, blackfoot disease, mental disorder in children and various other dermal effects.<sup>[2–4]</sup> Inorganic arsenic in natural water is normally present as As(III) (Arsenite) (*i.e.*, H<sub>3</sub>AsO<sub>3</sub>, H<sub>2</sub>AsO<sub>3</sub><sup>-</sup>) and As(V) (Arsenate) (*i.e.*, H<sub>2</sub>AsO<sub>4</sub><sup>1-</sup>, HAsO<sub>4</sub><sup>2-</sup>).<sup>[3,5,6]</sup> The toxicity, mobility and bioavailability of arsenic species are highly dependent on their oxidation states.<sup>[7,8]</sup> Below pH 9.2 As(III) exists as non-charged species and

have greater toxicity and mobility compared to As(V).<sup>[9,10]</sup> To abate the detrimental impacts of arsenic, the World Health Organization (WHO) has set an unflinching standard of 0.01 mg L<sup>-1</sup> arsenic in drinking water which consequently spurred the development of numerous arsenic treatment technologies.<sup>[3,11]</sup> Unfortunately, many of the technologies snagged behind due to one or more issues like sludge formation, in-efficient arsenic removal, large number of chemical requirement.<sup>[12]</sup> However, on account of simplicity, easy sludge free operation, regeneration propensity and cost-effectiveness, adsorption was considered to be the most propitious method for arsenic removal from aqueous solution.<sup>[3,13,14]</sup>

To date, several adsorbent materials were developed to remove arsenic from drinking water.<sup>[10,15,16]</sup> But either their kinetics were slow or had low arsenic adsorption capacity. Some involved stability issues and lead to secondary pollution of treated water. Thus, development of sustainable and effective sorbents for arsenic decontamination from drinking water is the utmost priority of research. To palliate the consequences of arsenic contaminated water, nano-metal oxide sorbents were introduced in the recent years owing to their unique properties of high specific area, high reactivity and high specificity.<sup>[17,18]</sup> For example, TiO<sub>2</sub> nanoparticles,<sup>[19]</sup> MgO nanoflakes,<sup>[20]</sup> CuO nanoparticles<sup>[21]</sup> and hydrous amorphous ZrO<sub>2</sub> nanoparticles<sup>[22]</sup> were reported for the remediation of both As(III) and As(V). A common feature among all the aforementioned metal oxides sorbents was that; they have higher affinity for the negatively charged As(V) over As(III) as As(III) occur as a non-ionic species in most of the pH range. Therefore, for efficient removal of both the arsenic species from

[a] P. Rout,<sup>+</sup> A. P. Panda,<sup>+</sup> Prof. U. Jha  
Department of Chemistry, Birla Institute of Technology, Mesra, Ranchi, Jharkhand, 835215, India


[b] Dr. K. K. Jena, Dr. S. M. Alhassan  
Department of Chemical Engineering, Khalifa University, SAN Campus, Abu Dhabi, 2533, United Arab Emirates (UAE)

[c] Dr. S. A. Kumar  
Analytical Chemistry Division, Bhabha Atomic Research Centre, Trombay, Mumbai, 400085, India

[d] Prof. R. K. Dey  
Department of Chemistry, Central University of Jharkhand, Ranchi, Jharkhand, 835205, India

[e] Dr. S. K. Swain  
Central Instrumentation Facility, Birla Institute of Technology, Mesra, Ranchi, Jharkhand 835215, India  
E-mail: skswain@bitmesra.ac.in

[<sup>+</sup>] Co-first authors

 Supporting information for this article is available on the WWW under <https://doi.org/10.1002/slct.201901094>

# Climatic controls of decomposition drive the global biogeography of forest–tree symbioses

B. S. Steidinger<sup>1,15</sup>, T. W. Crowther<sup>2,15\*</sup>, J. Liang<sup>3,4,15\*</sup>, M. E. Van Nuland<sup>1</sup>, G. D. A. Werner<sup>5</sup>, P. B. Reich<sup>6,7</sup>, G. J. Nabuurs<sup>8,182</sup>, S. de-Miguel<sup>9,10</sup>, M. Zhou<sup>3</sup>, N. Picard<sup>11</sup>, B. Herault<sup>12,13</sup>, X. Zhao<sup>4</sup>, C. Zhang<sup>4</sup>, D. Routh<sup>2</sup>, GFBI consortium<sup>14</sup> & K. G. Peay<sup>1\*</sup>

**The identity of the dominant root-associated microbial symbionts in a forest determines the ability of trees to access limiting nutrients from atmospheric or soil pools<sup>1,2</sup>, sequester carbon<sup>3,4</sup> and withstand the effects of climate change<sup>5,6</sup>. Characterizing the global distribution of these symbioses and identifying the factors that control this distribution are thus integral to understanding the present and future functioning of forest ecosystems. Here we generate a spatially explicit global map of the symbiotic status of forests, using a database of over 1.1 million forest inventory plots that collectively contain over 28,000 tree species. Our analyses indicate that climate variables—in particular, climatically controlled variation in the rate of decomposition—are the primary drivers of the global distribution of major symbioses. We estimate that ectomycorrhizal trees, which represent only 2% of all plant species<sup>7</sup>, constitute approximately 60% of tree stems on Earth. Ectomycorrhizal symbiosis dominates forests in which seasonally cold and dry climates inhibit decomposition, and is the predominant form of symbiosis at high latitudes and elevation. By contrast, arbuscular mycorrhizal trees dominate in aseasonal, warm tropical forests, and occur with ectomycorrhizal trees in temperate biomes in which seasonally warm-and-wet climates enhance decomposition. Continental transitions between forests dominated by ectomycorrhizal or arbuscular mycorrhizal trees occur relatively abruptly along climate-driven decomposition gradients; these transitions are probably caused by positive feedback effects between plants and microorganisms. Symbiotic nitrogen fixers—which are insensitive to climatic controls on decomposition (compared with mycorrhizal fungi)—are most abundant in arid biomes with alkaline soils and high maximum temperatures. The climatically driven global symbiosis gradient that we document provides a spatially explicit quantitative understanding of microbial symbioses at the global scale, and demonstrates the critical role of microbial mutualisms in shaping the distribution of plant species.**

Microbial symbionts strongly influence the functioning of forest ecosystems. Root-associated microorganisms exploit inorganic, organic<sup>2</sup> and/or atmospheric forms of nutrients that enable plant growth<sup>1</sup>, determine how trees respond to increased concentrations<sup>6</sup> of CO<sub>2</sub>, regulate the respiratory activity of soil microorganisms<sup>3,8</sup> and affect plant species diversity by altering the strength of conspecific negative density dependence<sup>9</sup>. Despite the growing recognition of the importance of root symbioses for forest functioning<sup>1,6,10</sup> and the potential to integrate symbiotic status into Earth system models that predict functional changes to the terrestrial biosphere<sup>10</sup>, we lack spatially explicit quantitative maps of root symbioses at the global scale. Quantitative maps of tree symbiotic states would link the biogeography of functional traits

of belowground microbial symbionts with their 3.1 trillion host trees<sup>11</sup>, which are spread across Earth's forests, woodlands and savannahs.

The dominant guilds of tree root symbionts—arbuscular mycorrhizal fungi, ectomycorrhizal fungi, ericoid mycorrhizal fungi and nitrogen-fixing bacteria (N-fixers)—are all based on the exchange of plant photosynthate for limiting macronutrients. Arbuscular mycorrhizal symbiosis evolved nearly 500 million years ago, and ectomycorrhizal, ericoid mycorrhizal and N-fixer plant taxa have evolved multiple times from an arbuscular-mycorrhizal basal state. Plants that are involved in arbuscular mycorrhizal symbiosis comprise nearly 80% of all terrestrial plant species; these plants principally rely on arbuscular mycorrhizal fungi for enhancing mineral phosphorus uptake<sup>12</sup>. In contrast to arbuscular mycorrhizal fungi, ectomycorrhizal fungi evolved from multiple lineages of saprotrophic ancestors and, as a result, some ectomycorrhizal fungi are capable of directly mobilizing organic sources of soil nutrients (particularly nitrogen)<sup>2</sup>. Associations with ectomycorrhizal fungi—but not arbuscular mycorrhizal fungi—have previously been shown to enable trees to accelerate photosynthesis in response to increased concentrations of atmospheric CO<sub>2</sub> when soil nitrogen is limiting<sup>6</sup>, and to inhibit soil respiration by decomposer microorganisms<sup>3,8</sup>. Because increased plant photosynthesis and decreased soil respiration both reduce atmospheric CO<sub>2</sub> concentrations, the ectomycorrhizal symbiosis is associated with buffering the Earth's climate against anthropogenic change.

In contrast to mycorrhizal fungi, which extract nutrients from the soil, symbiotic N-fixers (Rhizobia and Actinobacteria) convert atmospheric N<sub>2</sub> to plant-usable forms. Symbiotic N-fixers are responsible for a large fraction of biological soil-nitrogen inputs, which can increase nitrogen availability in forests in which N-fixers are locally abundant<sup>13</sup>. Symbioses with either N-fixers or ectomycorrhizal fungi often demand more plant photosynthate than does arbuscular mycorrhizal symbiosis<sup>12,14,15</sup>. Because tree growth and reproduction are limited by access to inorganic, organic and atmospheric sources of nitrogen, the distribution of root symbioses is likely to reflect environmental conditions that maximize the cost:benefit ratio of symbiotic exchange as well as physiological constraints on the different symbionts.

One of the earliest efforts<sup>16</sup> to understand the functional biogeography of plant root symbioses categorically classified biomes by their perceived dominant mycorrhizal type, and hypothesized that seasonal climates favour hosts that associate with ectomycorrhizal fungi (owing to the ability of these hosts to compete directly for organic nitrogen). By contrast, it has more recently been proposed that sensitivity to low temperatures has prevented N-fixers from dominating outside of the tropics, despite the potential for nitrogen fixation to alleviate nitrogen limitation in boreal forests<sup>15,17</sup>. However, global-scale tests of

<sup>1</sup>Department of Biology, Stanford University, Stanford, CA, USA. <sup>2</sup>Department of Environmental Systems Science, ETH Zürich, Zürich, Switzerland. <sup>3</sup>Department of Forestry and Natural Resources, Purdue University, West Lafayette, IN, USA. <sup>4</sup>Research Center of Forest Management Engineering of State Forestry and Grassland Administration, Beijing Forestry University, Beijing, China. <sup>5</sup>Department of Zoology, University of Oxford, Oxford, UK. <sup>6</sup>Department of Forest Resources, University of Minnesota, St Paul, MN, USA. <sup>7</sup>Hawkesbury Institute for the Environment, Western Sydney University, Penrith, New South Wales, Australia. <sup>8</sup>Wageningen University and Research, Wageningen, The Netherlands. <sup>9</sup>Department of Crop and Forest Sciences - Agrotecnio Center (UdL-Agrotecnio), Universitat de Lleida, Lleida, Spain. <sup>10</sup>Forest Science and Technology Centre of Catalonia (CTFC), Solsona, Spain. <sup>11</sup>Food and Agriculture Organization of the United Nations, Rome, Italy. <sup>12</sup>Cirad, UPR Forêts et Sociétés, University of Montpellier, Montpellier, France. <sup>13</sup>Department of Forestry and Environment, National Polytechnic Institute (INP-HB), Yamoussoukro, Côte d'Ivoire. <sup>182</sup>Forest Ecology and Forest Management Group, Wageningen University and Research, Wageningen, The Netherlands. <sup>14</sup>A list of participants and their affiliations appears in the online version of the paper. <sup>15</sup>These authors contributed equally: B. S. Steidinger, T. W. Crowther, J. Liang. \*e-mail: tom.crowther@usys.ethz.ch; albeca.liang@gmail.com; kpeay@stanford.edu

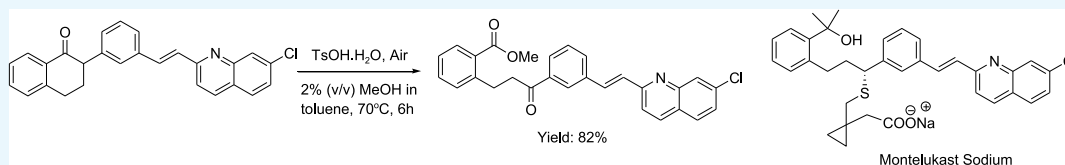


# Acid-Catalyzed Air-Oxidative Fragmentation of the Carbon–Carbon Bond in 2-Aryl-1-tetralones

Partha Ghosh\*<sup>1</sup>

Department of Chemistry, Central University of Jharkhand, Brambe, Ranchi 835205, India

**S** Supporting Information



**ABSTRACT:** Catalytic auto-oxidation with air is a highly desirable method for green synthesis. Described here is a method for acid-catalyzed one step air-oxidative fragmentation of 2-aryl-1-tetralones to alkyl-2-(3-oxo-3-aryl) benzoates in the presence of alcohol. This method was then demonstrated using concise synthesis of a key intermediate of antiasthma drug Montelukast sodium. Moreover, the paradoxical nature of the reaction in which ester forms but only within a low concentration threshold of alcohol helps in understanding the mechanism of the reaction.

## INTRODUCTION

Fragmentation reactions are highly efficient in building molecular complexity from simpler molecular assembly.<sup>1</sup> These aesthetically pleasing reactions are efficient by virtue of their high atom economy and step minimization potential in a synthetic sequence.<sup>2</sup> On the other hand, auto-oxidation reaction is used as the green synthetic method in which air oxygen is a renewable oxidant.<sup>3</sup> Hence, the synthetic method involving auto-oxidative fragmentation is highly desirable for efficient green synthesis.<sup>4</sup> O<sub>2</sub> is widely used as economic and environment-friendly oxidant in the production of bulk chemical from simpler petroleum-derived hydrocarbons.<sup>5</sup> However, because of lack of selectivity and control, O<sub>2</sub> is not commonly used as oxidant in chemical laboratory and pharmaceutical industry.<sup>6</sup> It is known that carbonyl compounds undergo auto-oxidation under basic conditions to form  $\alpha$ -hydroperoxides, which undergo C–C bond cleavage in both acidic and alkaline condition.<sup>7,8</sup> Ishikawa et al. while reporting aryl migration in air oxidation of 2-aryl-1-tetralone also mentioned few examples in which the fragmentation product was obtained, most notably 2-phenyl-1-tetralone **1** was converted to benzoic acid derivative **2** as sole product in the presence of the TsOH catalyst (Scheme 1).<sup>9</sup>

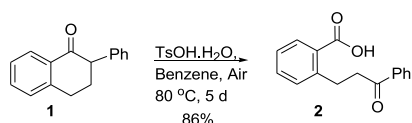
The abovementioned one step reaction slowly proceeded to form a diarylpropane framework without any sensitizer, light or pure oxygen. Intrigued by these reported findings, and because of the absence of further reports in the literature for this

transformation, a study was conducted to find out the synthetic scope for acid-catalyzed air-oxidative fragmentation of 2-aryl-1-tetralones, which were easily accessed from 1-tetralone via palladium-catalyzed  $\alpha$ -arylation methods.<sup>10</sup>

## RESULTS AND DISCUSSION

Reaction optimization with **1** under various conditions was performed which is summarized in Table 1. When the reaction was performed in toluene at 80 °C the reaction was complete within 72 h and the benzoic acid derivative **2** formed in 88% yield. Temperature of 80 °C in toluene was found to be optimum as increasing (entry 2) or decreasing (entry 3) reaction temperature, the reaction became slower and yield went down. The reaction also proceeded in tetrahydrofuran (THF) with good yield. Trifluoroacetyl in toluene and HCl in THF also catalyze the conversion with good yield. When relatively weak acetic acid was used as solvent, the reaction proceeded but with only 38% yield of **2** (other byproducts formed was not characterized). No reaction was observed when the reaction was run either in methanol or in mixed solvents of 10% (v/v) of methanol in THF (entry 9) and 10% (v/v) of methanol in toluene (entry 10). Interestingly, when 5% (v/v) methanol in toluene was used as solvent, low yield of methyl ester product **3a** instead of **2** was obtained. This result prompted to run the reaction in even lower alcohol concentration in toluene. Accordingly, reaction was run in 2% (v/v) methanol and surprisingly within 8 h starting ketone **2** was consumed completely and **3a** formed in 90% yield. Further lowering of methanol concentration resulted incomplete reaction (data not shown). On the other hand switching

Scheme 1



Received: March 18, 2019

Accepted: April 23, 2019

Published: May 2, 2019



## Corrigendum

## Corrigendum to “PUMA dependent mitophagy by *Abrus* agglutinin contributes to apoptosis through ceramide generation” [Biochim. Biophys. Acta Mol. Cell Res. 1865 (2018) 480–495]



Prashanta Kumar Panda<sup>a</sup>, Prajna Paramita Naik<sup>a</sup>, Biswa Ranjan Meher<sup>b</sup>, Durgesh Nandini Das<sup>a</sup>, Subhadip Mukhopadhyay<sup>a</sup>, Prakash Priyadarshi Praharaj<sup>a</sup>, Tapas K. Maiti<sup>c</sup>, Sujit K. Bhutia<sup>a,\*</sup>

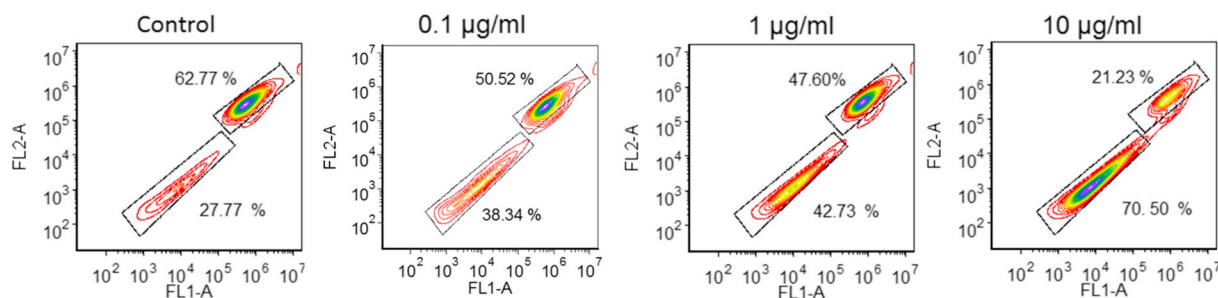
<sup>a</sup> Department of Life Science, National Institute of Technology, Rourkela, India

<sup>b</sup> Centre for Life Sciences, Central University of Jharkhand, Brambe, Ranchi, Jharkhand, India

<sup>c</sup> Department of Biotechnology, Indian Institute of Technology, Kharagpur, India

The authors regret as control is identical to 0.1 µg/ml in Fig. 4a. The authors now display a corrected version of 0.1 µg/ml in Fig. 4a. This corrected figure does not alter the conclusions of the study. The figure legend remains the same for this corrected figure.

The authors would like to apologise for any inconvenience caused.



DOI of original article: <https://doi.org/10.1016/j.bbamcr.2017.12.002>

\* Corresponding author at: Department of Life Science, National Institute of Technology Rourkela, Rourkela 769008, Odisha, India.

E-mail address: [sujitb@nitrrkl.ac.in](mailto:sujitb@nitrrkl.ac.in) (S.K. Bhutia).

<https://doi.org/10.1016/j.bbamcr.2019.05.002>

Available online 16 May 2019

0167-4889/ © 2019 Elsevier B.V. All rights reserved.





# Wheat Acreage Mapping and Yield Prediction Using Landsat-8 OLI Satellite Data: a Case Study in Sahibganj Province, Jharkhand (India)

Bikash Ranjan Parida<sup>1</sup> · Avinash Kumar Ranjan<sup>1</sup>

Received: 25 September 2018 / Revised: 24 December 2018 / Accepted: 18 April 2019 / Published online: 7 May 2019  
© Springer Nature Switzerland AG 2019

## Abstract

The emergence of remote sensing technologies and availability of satellite data over three decades have facilitated to monitor and understand the agricultural systems in many intensive agricultural regions. Here, we performed a comprehensive study on utilization of multi-temporal satellite data (i.e., Landsat-8 and MODIS) for wheat acreage and yield estimation during winter season (2016–2017) over the Sahibganj District in Jharkhand (India). Phenological variables were derived using the time-series normalized difference vegetation index (NDVI), which helps to understand the phenological transitions of wheat. The NDVI profile was used to derive rules for decision tree classifier to map the acreage of wheat. The key findings indicate that the acreage of wheat was estimated as ~3870 ha. Further, the long-term wheat statistics data were used to derive a yield model. Based on this model, wheat production was predicted as ~4523 t for the winter season 2016–2017, while, the mean was 3482 t. Predicted wheat yield was as ~1.17 t/ha, which was underestimated by 0.07 t/ha. Thus, it can be concluded that the accuracy of yield prediction depends on the precision of wheat acreage map derived from remote sensing data. A significant challenge for accurate acreage mapping could be the coarser spatial resolution of satellite data as the average plot sizes of Indian farmers can be far smaller than pixel sizes of the satellite data. Nevertheless, this comprehensive case study inferred that satellite-derived wheat acreage can be preferred to predict yield instead of traditional-based survey estimates.

**Keywords** Phenology · Decision tree · Wheat acreage · Yield prediction · Remote sensing

## 1 Introduction

Agriculture plays a key role in India's economy by contributing 17.3% of India's gross domestic product (GDP) in 2016–2017 and over 55% of the population is engaged in agricultural activity. Given the importance of agricultural sector, India becomes a leading producer of rice and wheat over the years. India is the second biggest producer of wheat in the world with ~30 million hectares of cultivation land. As per the Directorate of Economics & Statistics, DAC&FW [6], Ministry of Agriculture, Government of India, wheat production was ~96.50 million tons in 2016–2017. There are two key agricultural seasons, namely, Kharif (monsoon season) and Rabi (winter season). Wheat is the Rabi season's main crop that sown in November and harvested in March. During Rabi season

(winter), wheat is grown in several states of India, namely, Jammu and Kashmir, Himachal Pradesh, Uttarakhand, Punjab, Chandigarh-Haryana-Delhi, Uttar Pradesh, Bihar, Jharkhand, and Rajasthan. These aforementioned states contributed ~99.5% of total wheat production in the country. Remaining states such as Karnataka, Assam, Chhattisgarh, and other North Eastern states have contributed only ~0.5% of the total wheat production in the country (DES 2017). In the state of Jharkhand (JH), wheat crop plays an imperative role for livelihood of farming communities that supports food security for ~80% of total population of the state [17].

The information on crop acreage and yield is very essential for planning and sustainable development of agriculture system. Reliable and timely detailed information on crop acreage provides valuable information to the planner and policy makers for making decision with respect to procurement, storage, public distribution, export-import, and finally the food security of nation [28]. Many developing countries including India have been used the traditional method (i.e., survey-based) of data collection for crop monitoring and yield estimation, wherein Crop Cutting Experiment (CCE) typically conducted under a complex sampling design (i.e., stratified

✉ Bikash Ranjan Parida  
bikashrp@gmail.com

<sup>1</sup> Department of Geoinformatics, School of Natural Resource Management, Central University of Jharkhand, Ranchi 835205, India

# Characterization of pH Dependent Growth Response of Agriculturally Important Microbes for Development of Plant Growth Promoting Bacterial Consortium

Anil Kumar\* , Menka Kumari, Preeti Swarupa and Shireen

Department of Life Sciences, School of Natural Sciences, Central University of Jharkhand, Brambe, Ranchi - 835 205, Jharkhand, India.

## Abstract

Soil microbial community structure is influenced by both biotic and abiotic factors prevailing in the soil milieu. The pH is one of the noticeable abiotic factors that affect soil microbial community. Different species prefer different range of pH for their optimal growth; however they can tolerate a wide range around acidic, neutral or alkaline pH. Microbes with broad range of pH tolerance i.e. from acidic to alkaline soil have better survival rate or opportunity as compared to other microbes which have narrow range of pH tolerance. So, in the present study growth response of plant growth promoting bacteria (PGPB) from rhizosphere and rhizoplane of different groups of plant has been characterized at broad range of pH (3.0-13.0) and hence can be applied in soils of different pH range to enhance plant growth and yield. Ten bacterial isolates, which exhibited *in-vitro* plant growth promoting traits i.e. phosphate solubilisation, biological nitrogen fixation, Indole acetic acid (IAA) production and siderophore production, revealed differential growth response to pH. Some isolates showed good response in broad pH range from acidic to alkaline (~3.5 to ~12.5). These plant growth promoting bacterial groups therefore can be potentially used as bacterial consortium for application in agricultural fields to enhance crop productivity.

**Keywords:** pH, growth, response, PGPB, consortium, tolerance.

\*Correspondence: anil.kumar@cuja.ac.in; +91-9955273226

(Received: 10 March 2019; accepted: 30 May 2019)

**Citation:** Anil Kumar, Menka Kumari, Preeti Swarupa and Shireen, Characterization of pH Dependent Growth Response of Agriculturally Important Microbes for Development of Plant Growth Promoting Bacterial Consortium, *J Pure Appl Microbiol.*, 2019; **13**(2): 1053-1061. doi: 10.22207/JPAM.13.2.43

© The Author(s) 2019. **Open Access.** This article is distributed under the terms of the Creative Commons Attribution 4.0 International License which permits unrestricted use, sharing, distribution, and reproduction in any medium, provided you give appropriate credit to the original author(s) and the source, provide a link to the Creative Commons license, and indicate if changes were made.

**Total Synthesis of ( $\pm$ )-4,8,14-trihydroxyilludala-2,6,8-triene**

Muthiah Suresh, Anusueya Kumari, and Raj Bahadur Singh\*

Department of Chemistry, Central University of Jharkhand, Brambe, Ranchi-835 205, India.

Corresponding author's e-mail address: [rajbahadur.iitb@gmail.com](mailto:rajbahadur.iitb@gmail.com), [raj.singh@cuja.ac.in](mailto:raj.singh@cuja.ac.in)**ABSTRACT**

The first total synthesis of 4,8,14-trihydroxyilludala-2,6,8-triene **1** in racemic form was achieved in six steps from the indanone **5**. The key feature of the synthesis is keto ester formation,  $\alpha$ -methylation, silane mediated reduction, Friedel–Crafts acylation and demethylation to provide the crucial precursor **11**. LAH was found to be a suitable reducing agent that helps to directly transform **11** into target molecule **1**.

Keywords:

4,8,14-trihydroxyilludala-2,6,8-triene

Indanone

 $\alpha$ -methylation

silane mediated reduction

Friedel–Crafts acylation

## Seasonal glacier surface velocity fluctuation and contribution of the Eastern and Western Tributary Glaciers in Amery Ice Shelf, East Antarctica

Shridhar Digambar Jawak<sup>1,2</sup>, Shubhang Kumar<sup>3</sup>, Alvarinho Joaozinho Luis<sup>1</sup>, Prashant Hemendra Pandit<sup>4\*</sup>, Sagar Filipe Wankhede<sup>1</sup>

<sup>1</sup>Earth System Science Organization (ESSO), National Centre for Polar and Ocean Research (NCPOR), Ministry of Earth Sciences (MoES), Headland Sada, Goa 403804, India

<sup>2</sup>Svalbard Integrated Arctic Earth Observing System (SIOS), SIOS Knowledge Centre, Svalbard Science Park, P.O. Box 156, N-9171, Longyearbyen, Svalbard, Norway

<sup>3</sup>Centre for Land Resource Management, Central University of Jharkhand, Ranchi 835205, India

<sup>4</sup>National Bureau of Soil Survey and Land Use planning (NBSS & LUP) - Indian Agriculture Research Institute (IARI), New Delhi 110012, India

### Abstract

Glaciers play a crucial role in the study of the climate change pattern of the Earth. Remote sensing with access to large archives of data has the ability to monitor glaciers frequently throughout the year. Therefore, remote sensing is the most beneficial tool for the study of glacier dynamics. Fed by many tributaries from different sides, the Amery Ice Shelf (AIS) is one of the largest ice shelves that drains ice from the Antarctic ice sheet into the Southern Ocean. This study focuses on the eastern and the western tributaries of the AIS. The primary objective of the study was to derive the velocity of the tributary glaciers and the secondary objective was to compare variations in their velocities between the summer and winter season. This study was carried on using the European Space Agency's (ESA) Sentinel-1 satellite's Synthetic Aperture Radar (SAR) data acquired from the Sentinel data portal. Offset tracking method was applied to the Ground Range Detected (GRD) product of the Sentinel-1 interferometric wide (IW) swath acquisition mode. The maximum velocity in summer was observed to be around 610 m/yr in the eastern tributary glacier meeting the ice shelf near the Pickering Nunatak, and around 345 m/yr in the Charybdis Glacier Basin from the western side. The maximum velocity in the winter was observed to be 553 m/yr in the eastern side near the Pickering Nunatak whereas 323 m/yr from the western side in the Charybdis Glacier Basin. The accuracy of the derived glacier velocities was computed using bias and root mean square (RMS) error. For the analysis, the publicly available velocity datasets were used. The accuracy based on RMS error was observed to be 85-90% for both seasons with bias values up to 25 m/yr and root mean square error values up to 30 m/yr.

**Key words:** Antarctic, glacier velocity, offset tracking, synthetic aperture radar

**DOI:** 10.5817/CPR2019-1-5

Received May 7, 2019, accepted June 3, 2019.

\*Corresponding author: P. H. Pandit <sh.prashantpandit@gmail.com>; <alvluis@ncaor.gov.in>

**Acknowledgements:** The authors would like to thank European Space Agency (ESA) for providing Sentinel-1 images available online. We would like to acknowledge Dr. M. Ravichandran, Director, ESSO-NCPOR for his encouragement to carry out the work. The whole study was carried out at the Polar Remote Sensing Division of NCPOR, Goa.

# Evolution of Indigenous Rights Under International Law: Analysis from TWAIL Perspective

The Oriental Anthropologist  
19(1) 7–24, 2019  
© 2019 Oriental Institute of Cultural and  
Social Research and SAGE  
Reprints and permissions:  
[in.sagepub.com/journals-permissions-india](http://in.sagepub.com/journals-permissions-india)  
DOI: 10.1177/0972558X19835387  
[journals.sagepub.com/home/oan](http://journals.sagepub.com/home/oan)



Rashwet Shrinkhal<sup>1</sup>

## Abstract

Indigenous people are the most socially, politically, and economically marginalized groups in the world. They are the most oppressed on account of the fact that the values sustaining the moral roots of their culture are considered incompatible with the values of modern culture. This article traces the evolution of rights of indigenous people in international law. It argues that discrimination against indigenous people was maintained under international law based on differences on scale of civilization. It will demonstrate how 'universal standards' may be applied not as an agent of liberation but dominance. In doing so, Third World Approaches to International Law (TWAIL) perspective is adopted to deconstruct international law.

## Keywords

Indigenous people, international law TWAIL perspective, marginalized groups

## Introduction

Legal system as an institution is a social and historical construct, a structure built of words and meanings, and designed to promote certain values in an ordering system. The overall character of a legal system itself is based on a vision of how

---

<sup>1</sup> The Centre for Contemporary and Tribal Customary Law, Central University of Jharkhand, Ranchi Dist, Jharkhand, India.

**Disclaimer:** This article is based upon author's doctoral thesis submitted at the Centre for International Legal Studies, SIS, JNU, New Delhi.

---

### Corresponding author:

Rashwet Shrinkhal, The Centre for Contemporary and Tribal Customary Law, Central University of Jharkhand, Ratu-Lohardaga Road, Ranchi Dist, Brambe, Jharkhand 835205, India.

E-mail: [rashwetshrinkhal@gmail.com](mailto:rashwetshrinkhal@gmail.com)

## Tree Diversity Assessment and Above Ground Forests Biomass Estimation using SAR Remote Sensing: A case study of Higher Altitude Vegetation of North-East Himalayas, India

Amit Kumar<sup>1</sup>, B.S.P.C. Kishore<sup>1</sup>, P. Saikia<sup>1\*</sup>, J. Deka<sup>2</sup>, S. Bharali<sup>3</sup>, L. B. Singha<sup>4</sup>, O.P. Tripathi<sup>4</sup> and M.L. Khan<sup>5</sup>

<sup>1</sup>*School of Natural Resource Management, Central University of Jharkhand, Brambe-835205, Ranchi, Jharkhand, India* (AK: [amit.kumar@cuja.ac.in](mailto:amit.kumar@cuja.ac.in), [amit.iirs@gmail.com](mailto:amit.iirs@gmail.com) orcid.org/0000-0002-4582-5677; PS: [purabi.saikia@cuja.ac.in](mailto:purabi.saikia@cuja.ac.in), [purabi.saikia83@gmail.com](mailto:purabi.saikia83@gmail.com) orcid.org/0000-0001-5481-282X; BPSCK: [bspckishore@gmail.com](mailto:bspckishore@gmail.com))

<sup>2</sup>*Department of Environmental Sciences, Gauhati University, Guwahati-781014, India*

<sup>3</sup>*Rubber Board of India, Regional Office, Dimapur-797112, Nagaland, India*

<sup>4</sup>*Department of Forestry, North Eastern Regional Institute of Science & Technology (Deemed University), Nirjuli-791109, Itanagar, Arunachal Pradesh, India*

<sup>5</sup>*Department of Botany, Dr. Harisingh Gour Central University, Sagar - 470003, Madhya Pradesh, India* ([khanml61@gmail.com](mailto:khanml61@gmail.com) orcid.org/0000-0001-6849-0307)

\*Corresponding author: P. Saikia (+91 9546757390)

### Abstract

Forest biomass is one of the significant components for assessing the productivity and sustainability of the forest's ecosystem. In the present study, the mapping and estimation of above ground biomass (AGB) was performed using field observations employing allometric equations and C band Sentinel 1A and L band Advanced Land Observation System (ALOS) Phased Array L-band Synthetic Aperture Radar (PALSAR) remote sensing satellite images for the parts of north eastern Himalayan forests, Arunachal Pradesh. Total 57 transects of 500 m x 10 m size was laid in West Kameng and Tawang districts (altitude range: 1047 to 4161m) of Arunachal Pradesh, in which a total of 12203 individuals of 67 tree species (Diameter at Breast Height (DBH) range: 3.18 to 235.45 cm) was recorded. The study exhibited higher tree density (428 individuals' ha<sup>-1</sup>) and basal cover (7658.63 m<sup>2</sup>ha<sup>-1</sup>) in the studied forests. The highest above ground biomass was contributed by *Castanopsis indica* (103.82 t ha<sup>-1</sup>) followed by *Pinus roxburghii* (46.24 t ha<sup>-1</sup>) and *Quercus semicarpifolia* (23.14 t ha<sup>-1</sup>). Further, AGB was estimated using the Horizontal-Horizontal (HH), Horizontal-Vertical (HV) polarizations acquired by the ALOS PALSAR 50 m mosaic (2008) dataset and Vertical-Vertical (VV), Vertical-Horizontal (VH) polarizations acquired by the Sentinel 1A dataset. The relationship between field based AGB and radar backscatter for selected sample plots was established using pair wise correlation. While comparing the two satellite-based SAR images, it is observed that high correlation between radar backscatter and field based AGB was observed in ALOS PALSAR as compared to Sentinel 1A SAR. This is due to higher sensitive to backscatter values and higher penetration level of L band ALOS PALSAR as compared to C band Sentinel 1A SAR. The correlation study indicates high correlation of HV polarizations in ALOS PALSAR (HV polarization R<sup>2</sup>=0.63; HH polarization R<sup>2</sup>=0.58) as compared to Sentinel 1A (VV polarization R<sup>2</sup>= 0.054 and VH polarization R<sup>2</sup>= 0.044). The most accurate and reliable method to estimate AGB is the field based method, but it is time consuming and tedious. Whereas, AGB estimation by L band SAR remote sensing is time effective and can be used for larger area in comparatively less



## MAPPING VELOCITY OF THE POTSDAM GLACIER, EAST ANTARCTICA USING LANDSAT-8 DATA

S. D. Jawak<sup>1</sup>, M. Joshi<sup>2,3,\*</sup>, A. J. Luis<sup>4</sup>, P. H. Pandit<sup>5</sup>, S. Kumar<sup>6</sup>, S. F. Wankhede<sup>4</sup>, Anirudh T. Somadas<sup>7</sup>

<sup>1</sup>Svalbard Integrated Arctic Earth Observing System (SIOS), SIOS Knowledge Centre, University Centre in Svalbard (UNIS), P.O. Box 156, N-9171, Longyearbyen, Svalbard, Norway; shridhar.jawak@gmail.com

<sup>2</sup>Department of Geoinformatics, Mangalore University, Mangalore, Karnataka—574199, India

<sup>3</sup>Divecha Centre for Climate Change, Indian Institute of Science, Bangalore, Karnataka – 560012; mansijoshi692@gmail.com <sup>4</sup>Earth System Science Organization - National Centre for Polar and Ocean Research, Ministry of Earth Sciences, Government of India, Headland Sada, Vasco-da -Gama, Goa 403804, India; alvluis@ncaor.gov.in, swankhede436@gmail.com

<sup>5</sup>National Bureau of Soil Survey and Land Use planning (NBSS & LUP) - Indian Agriculture Research Institute (IARI), New Delhi, India; sh.prashantpandit@gmail.com

<sup>6</sup>Centre for Land Resource Management, Central University of Jharkhand, Ranchi – 835205, India; shubh30195@gmail.com

<sup>7</sup>University of Twente, Faculty ITC, P. O. Box 217, 7500 AE Enschede, Netherlands; a.tharaventhedathsomadas@student.utwente.nl

**KEY WORDS:** Glacier velocity, image matching, pixel tracking, Landsat-8 OLI, Antarctic glacier

### ABSTRACT:

Most of the glaciers have been retreating and thinning globally due to climate change. Glacier velocity is one such important parameter of glacier dynamics, which helps to understand the mass balance. The variations in velocity at different areas of the glacier can be used to identify the zones of ablation and accumulation. Zones of accumulation are identified as areas with higher velocity. This data is useful to incorporate in the glacier mass balance analysis. This study aims to derive the glacier velocity, using feature tracking technique for Potsdam glacier, east Antarctica. Feature tracking is an efficient way to derive glacier velocity, which is based on a cross-correlation algorithm that seeks offsets of the maximal correlation window on repeated satellite images. In this technique, two temporally different images are acquired for the same area and a distinct feature on both images is identified and the velocity is calculated with respect to the movement of that particular feature from one image to the other. Landsat-8 data for the year 2016 was used to derive velocity. Finer resolution promotes better feature tracking so the panchromatic band (band 8) of Landsat-8 OLI with a resolution of 15 m was utilized for deriving velocity. This technique was performed using COSI-Corr module in ENVI. This tool calculates displacement between the east-west and north-south directions, and the resultant velocity is calculated using the displacement in both directions and the temporal difference of two images. The velocity map generated at a resolution of 240 m showed that the resultant velocity ranged between 18.60 and 285.28 ma<sup>-1</sup>. Bias and root mean square error (RMSE) have been calculated with respect to the point-by-point MEASUREs data provided by National Snow and Ice Data Centre at 1000 m resolution. The RMSE was found to be 78.06 ma<sup>-1</sup> for 2016. The velocity for Potsdam glacier was also pictorially validated with the DGPS measurements from literature.

### 1. INTRODUCTION

Glacier ice deforms under the force of gravity and is able to slide on the ground. The resulting ice flow observed at the surface represents the mass transport between areas with predominant snow accumulation and those with prevailing mass loss by ice melt or break-off. The effects of climate warming are for instance evident in the continuous retreat of glaciers. Thus, measuring glacier flow-fields decisively contributes to understanding glaciers and related hazards (Kääb et al., 2002). Glacier velocities can be measured using different remote sensing techniques such as, Interferometric Synthetic Aperture Radar (InSAR), Differential Interferometric SAR (DInSAR), offset tracking, feature tracking with GPS, speckle tracking, feature tracking, etc. These techniques work on different time scales and have different strengths and shortcomings, and so they complement each other in glaciological studies (Heid et al., 2011). Like GPS based tracking, It is more advantageous when only small features are available for tracking in a study area because these features may not be discernible on the images. On the other hand, GPS is disadvantaged by the problem of accessibility. Remotely sensed data helps in handling the issues of inaccessibility.

Although glacier-surface velocities can be measured directly on the glacier with high accuracy at arbitrary spatial and temporal

resolutions, observations over long periods involve frequent revisits of the survey points, which can only be located on the accessible parts of a glacier. Therefore, field measurements commonly result in very sparse spatial coverage. Because of the huge degree and troublesome openness of high rugged landscape, remote-sensing strategies give an effective method to gather information in disparate regions. In contrast, remote sensing-based measurements provide the opportunity to achieve large and possibly complete spatial coverage, even in very remote areas. Remotely sensed imagery can provide detailed and timely data for Earth observation across both time and space, which enhances the ability to map and monitor glacier flow on a nearly global scale (Pandit et al., 2018). Optical satellite image-based ice-velocity measurement using feature tracking is a well-established method (Jawak et al., 2018). Feature tracking involves tracking identifiable features between pairs of optical satellite images using an image-matching algorithm such as normalized cross-correlation (NCC), cross-correlation operated in the frequency domain on orientation images (CCF-O), and co-registration of optically sensed images and correlation (COSI-Corr) (Liu et al., 2017). Cross correlation is also applied to provide in image registration in areas devoid the bedrock exposure. The use of cross-correlation software is a significant improvement over previous manually-based

## SEASONAL COMPARISON OF VELOCITY OF THE EASTERN TRIBUTARY GLACIERS, AMERY ICE SHELF, ANTARCTICA, USING SAR OFFSET TRACKING

S. D. Jawak<sup>1</sup>, S. Kumar<sup>2,\*</sup>, A. J. Luis<sup>3</sup>, P. H. Pandit<sup>4</sup>, S. F. Wankhede<sup>3</sup>, T. S. Anirudh<sup>5</sup>

<sup>1</sup>Svalbard Integrated Arctic Earth Observing System (SIOS), SIOS Knowledge Centre, University Centre in Svalbard (UNIS), P.O. Box 156, N-9171, Longyearbyen, Svalbard, Norway; shridhar.jawak@gmail.com

<sup>2</sup>Centre for Land Resource Management, Central University of Jharkhand, Ranchi – 835205, India; shubh30195@gmail.com

<sup>3</sup>Earth System Science Organization- National Centre for Polar and Ocean Research, Ministry of Earth Sciences, Government of India, Headland Sada, Vasco-da -Gama, Goa 403804, India; alvluis@ncaor.gov.in; swankhede436@gmail.com

<sup>4</sup>National Bureau of Soil Survey and Land Use planning (NBSS & LUP) - Indian Agriculture Research Institute (IARI), New Delhi, India; sh.prashantpandit@gmail.com

<sup>5</sup>University of Twente, Faculty ITC, P. O. Box 217, 7500 AE Enschede, Netherlands; a.tharaventhedathsomasdas@student.utwente.nl

**KEY WORDS:** Amery Ice Shelf, Glacier Surface Velocity, Offset Tracking, SAR, Remote Sensing

### ABSTRACT:

Antarctica and Greenland are two major Earth's continental ice shelves which play an important role in influencing Earth's energy balance through their high albedo. The ice sheets comprise of grounded ice or the continental glaciers and their associated ice shelves. Surface velocity is an important parameter that needs to be monitored to understand the glacier dynamics. Marine terminating glaciers have higher velocity than land terminating glaciers. Therefore, ice shelves are generally observed to have higher velocity as compared to continental glaciers. The focus of this study is Amery ice shelf (AIS) which is the third largest ice shelf located in east Antarctica terminating into the Prydz Bay on the eastern Antarctica. The surface ice-flow velocity of AIS is very high compared to its surrounding glaciers which flows at a rate of 1400  $\text{ma}^{-1}$  and drains about 8% of the Antarctic ice sheet. AIS is fed by different glaciers and ice streams at the head, as well as from the western and eastern side of the ice shelf before it terminates into the ocean. The primary objective of this study was to compute velocity of the eastern tributary glaciers of AIS using SAR from Sentinel-1 data. The secondary objective was to compare the winter and summer velocities of the glaciers for 2017-2018. The offset tracking method has been applied to the ground range detected (GRD) product obtained from Sentinel-1 satellite. This method is suitable for regions with higher glacier velocity where interferometry is generally affected by the loss of coherence. The offset tracking method works by tracking the features on the basis of another feature and calculates the offset between the two features in the images. Two tributary glaciers near the Clemence massif and another glacier near the Pickering Nunatak feed into this ice shelf from the eastern glacial basin region that drains ice from the American Highland, east Antarctica. The glaciers near the Clemence massif showed low annual velocity which ranged from 100  $\text{ma}^{-1}$  at the head to  $\sim 300 \text{ma}^{-1}$  near the end of the glacier, where it merges with AIS. The glaciers flowing near the Pickering Nunatak exhibited moderate velocity ranging from 150  $\text{ma}^{-1}$  at its head and reaching up to 450  $\text{ma}^{-1}$  near the tongue. The summer velocity (March 2018) was observed to be higher than the velocity in winter (July 2017) and the difference between the summer and the winter velocities was found to be between 50  $\text{ma}^{-1}$  and 130  $\text{ma}^{-1}$ . The results for the velocity were obtained at 120 m resolution and were compared with the previous MEaSURES (Making Earth System Data Records for Use in Research Environments) yearly velocity at 450 m and 1 km resolution provided by National Snow and Ice Data Center portal. The results were evaluated using statistical measure- bias and the accuracy was derived using the root mean square error. The bias did not exceed 20  $\text{ma}^{-1}$  for the three glaciers and the accuracy was observed to be more than 85% for most of the regions. The accuracy of the results suggests that the offset tracking technique is useful for future velocity estimation in the regions of high glacier velocity.

### 1. INTRODUCTION

The ice and snow in the Polar Regions play a crucial role in Earth's radiation budget as the cryosphere reflects about 90% of the incoming solar radiation (Jawak and Luis, 2014). The continental shelves of Antarctica and Greenland are almost completely covered by ice (Jawak et al., 2018). In the southern hemisphere Antarctica hosts larger ice mass and in the northern hemisphere Greenland contains relatively less ice mass, both of which could contribute to sea level rise of 66 m, if completely melted. Most of the cryospheric regions are situated in severe weather conditions and accessibility to these regions is limited due to their rough terrain, harsh weather conditions, sometimes all year round and high logistic cost. The inaccessibility due to various factors make remote sensing the best and most affordable

technique that could be used for monitoring different dynamics of the glaciers in these regions (Jeong et al., 2017; Jawak et al., 2017; Pandit et al., 2017; Jawak et al., 2018). The availability of satellite remote sensing technology and its progress in recent decades has enhanced our capability to monitor these regions at regular time intervals over a long period of time (Jawak and Luis, 2014).

The mass balance of glaciers is pivotal to understanding the accumulation of ice and its subsequent drain into the sea due to ablation (Lugli and Vittuari, 2017). Various factors that cause glacier ablation are surface melt, surface melt water runoff, sublimation, avalanching and windblown snow. The velocity of

\* Corresponding author.



# Highly Water-Soluble Rod–Coil Conjugated Block Copolymer for Efficient Humidity Sensor

Koomkoom Khawas, Soumili Daripa, Pallavi Kumari, Santanu Das, Ratan Kumar Dey, and Biplab Kumar Kuila\*

In this report, the preparation of highly water-soluble rod–coil conjugated block copolymer poly(3-hexylthiophene)-*b*-polystyrenesulfonic acid (P3HT-*b*-PSSA) is demonstrated using a facile method with its moisture sensing properties. The block copolymer synthesis method comprises Kumada catalyst transfer polymerization and atom transfer radical polymerization from a bifunctional initiator followed by sulfonation of polystyrene using moderate reaction conditions. The polymerization results in the synthesis of well-defined block copolymers with controllable block length. The successful synthesis of the block copolymer is studied by NMR and FTIR spectroscopy while optical and structural properties of the block copolymer are investigated using UV–vis, photoluminescence spectroscopy, XRD, and FESEM. In water, the block copolymer shows aggregated structure with crystalline core formed by rod-like P3HT chain with absorption maxima at 558 nm, whereas in solid state the absorption maxima is blue shifted to 548 nm. The proton conductivity of the block copolymer P3HT-*b*-PSSA with ≈91% of PSSA (by weight) is measured from impedance study, and the values for bulk and grain conductivities are  $5.25 \times 10^{-4}$  and  $4.66 \times 10^{-6} \text{ S cm}^{-1}$ , respectively, at room temperature. The as-synthesized block copolymer shows a very high water uptake with maximum ≈80% in comparison with its initial weight. The I–V measurement of the device made from block copolymer shows nonlinear, rectifying characteristic and the current increases with increase of relative humidity (RH%). The block copolymer device shows well-correlated systemic and reversible resistance change with RH both in doped and undoped state. It is believed that the interesting and highly reversible moisture-sensitive electronic properties of this block copolymer will be useful for the fabrication of moisture-sensitive polymer-based flexible electronic devices.

## 1. Introduction

Design and synthesis of new conjugated polymeric materials or their block copolymers have attracted tremendous research attentions due to their enormous potential applications in many fields including sensors, energy storages, corrosion inhibition, and optoelectronic devices.<sup>[1–7]</sup> Poly(3-hexylthiophene) (P3HT) is one of the extensively studied conjugated polymers and has been used as an active material in various electronic devices such as photovoltaics, organic field effect transistors, and light emitting diodes (LED).<sup>[8]</sup> Another important core issue with conjugated polymers which is of great concern is their solubility or processability from the real applications point of view. Additionally, there is a great demand of water-soluble conjugated polymeric materials in applications that would benefit from environmentally friendly steps and applications centered on their use in biological environments.<sup>[9]</sup> P3HT has been coupled with various types of blocks in order to manipulate its solubility, structure, and optical and electronic properties.<sup>[10–16]</sup> Particularly, block copolymers consisting of rod block and non-conductive coil block have attracted great interest in view of their wide varieties of applications like flexible and less expensive organic opto-

electronic devices, biotechnology, and high-performance composites.<sup>[15,17–20]</sup> Depending on the solvent composition and regioregularity, rod–coil conjugated block copolymers can self-assemble into different nano-scaled morphologies like lamellae, spheres, cylinders, vesicles, and nanofibres both in solution and solid state.<sup>[17–23]</sup> Different techniques have been applied to synthesize the non-conducting coil block, ranging from anionic polymerization to ring-opening metathesis polymerization and controlled radical polymerization (i.e., atom transfer radical polymerization [ATRP], nitroxide-mediated polymerization [NMP], and reversible addition fragmentation chain transfer [RAFT] polymerization).<sup>[16,24–26]</sup> The alternative synthetic route is a coupling reaction between two end-functionalized homopolymers by “click chemistry” and some work has been done in this direction.<sup>[27,28]</sup> Poly(styrenesulfonate) (PSS) or

K. Khawas, P. Kumari, R. K. Dey  
Department of Chemistry  
Central University of Jharkhand  
Brambe, Ranchi 835205, Jharkhand, India

S. Daripa, Dr. B. K. Kuila  
Department of Chemistry  
Institute of Science  
Banaras Hindu University  
Varanasi 221005, Uttar Pradesh, India  
E-mail: bkkuila.chem@bhu.ac.in

S. Das  
Department of Ceramic Engineering  
Indian Institute of Technology (BHU)  
Varanasi 221005, Uttar Pradesh, India

The ORCID identification number(s) for the author(s) of this article can be found under <https://doi.org/10.1002/macp.201900013>.

DOI: 10.1002/macp.201900013

## Energy Technology &amp; Environmental Science

## Kinetics of Thermal Degradation of Non-Woven Plastics: Model-Free Kinetic Approach

Satyanarayan Patnaik,<sup>[a]</sup> Sachin Kumar,<sup>[b]</sup> and Achyut K. Panda<sup>\*,[c]</sup>

The thermo-degradative behaviour of non-woven plastics was studied in order to analyze their thermal stability and subsequent recycling method. Non-isothermal thermogravimetric experiments using wide range of heating rates of 10, 20, 40, 60, 80, 100 °C min<sup>-1</sup> have been performed from ambient to 900 °C in a thermo-balance with the objective of determining the kinetic parameters. Four model free kinetic approaches such as Friedman method, Coats-Redfern (modified) method, Flynn-Wall-Ozawa (FWO) method and Kissinger method have been used to determine kinetic parameters for the two stage

degradation of the non-woven plastic sample including the thermal degradation of synthetic plastics in the first step followed by the subsequent degradation of inorganic fillers in the second step. The activation energy obtained for first stage degradation is found significantly lower (106-112 kJ/mol) compared to the second stage degradation (191-202 kJ/mol). This result would help design a process for the valorisation of synthetic polymer and segregation of the filler materials in the plastic sample to be reused further.

## Introduction

As the life span of commonly used synthetic plastics is very small, the uses of non-woven plastics are gradually increasing as a substitute as these plastics are designed to last long, thus reach the waste stream later than ordinary plastics. Non-woven plastics are broadly web or sheet like structures in which fibre or filaments are entangled mechanically, thermally or chemically.

Interlocking of layers or networks of fibres/ filaments or film-like filamentary structures results in non-woven plastics. Non-woven fabrics are flat and flexible.<sup>[1]</sup> Raw materials used in non-woven are different in different industries, covering the entire spectrum from synthetic to natural fibres. Different fibres including Polypropylene 63%, Polyester 23%, Viscose rayon 8%, Acrylic 2% Polyamide 1.5%, other speciality fibres 3% are used in production of non-woven plastics.<sup>[2]</sup> In addition to plastics, non-woven plastic materials also contain higher amounts of fillers as compared to other plastic materials. The advantage of using non-woven bags is that they are 100% reusable and recyclable, i.e. they can be used a number of times before they get worn out and are the best alternative to ordinary plastic bags in the present context. There are numerous applications

of non-woven plastics, which may be the production of baby diapers or industrial high-performance textiles. Traditional textiles are substituted by non-wovens plastics in many areas such as geo textiles, materials for building, thermal and sound insulating materials, cover stocks, agriculture, aerospace, home furnishings, hygienic and health care textiles, automotive industries etc.<sup>[3]</sup> Large scale utilisation of non-woven plastics in different applications would result in the accumulation of such wastes in the solid waste stream creating environmental issues owing to their non-biodegradability nature, and thus need attention for recycling. As the major component of the non-woven plastics are polypropylene and other thermoplastics, the most suitable recycling method for such plastics is pyrolysis yielding fuels and/or lubricants. Numerous works on the thermal degradation of different thermoplastics are reported by various researchers.<sup>[4]</sup> As the composition and manufacturing process of non-woven plastics are different than ordinary synthetic plastics, their pyrolysis may require different process conditions and different process design approaches. The design of such industrial process needs the input of kinetics parameters as has been reported by different researchers are summarized as follows.

The kinetic analysis of thermal degradation of waste polypropylene (PP) and High density polyethylene (HDPE) was carried out by thermogravimetric (TG) experiments and the activation energy of blended plastic was found lower than those of individual plastic samples.<sup>[5]</sup> Thermal degradation behaviour of PP and HDPE (non-degraded and degraded) were studied in order to analyse their thermal stability and calculate kinetic parameters. The kinetic parameters were determined by using different integral and differential methods. PP was found to reduce the activation energy ( $E_a$ ) significantly when mixed with non-degraded HDPE.<sup>[6]</sup> The activation energy and the reaction model of the pyrolysis of HDPE, low density polyethylene (LDPE) and PP have been estimated from non-

[a] S. Patnaik

Research Scholar, Department of Chemistry, Veer Surendra Sai University of Technology Burla, Odisha, India, PIN: 768018

[b] Dr. S. Kumar

Centre for Excellence in Green and Efficient Energy Technology (GEFT), School of Engineering and Technology, Central University, Ranchi, Jharkhand, India PIN: 835205, India

[c] Dr. A. K. Panda

Department of Chemistry, Veer Surendra Sai University of Technology Burla, Odisha, India, PIN: 768018, Tel.: 09437132916  
E-mail: achyut.panda@gmail.com

Supporting information for this article is available on the WWW under <https://doi.org/10.1002/slct.201901114>

Materials Science inc. Nanomaterials &amp; Polymers

# Aligned Proton-Conducting Graphene Sheets via Block Copolymer Supramolecular Assembly and Their Application for Highly Transparent Moisture-Sensing Conductive Coating

Soumili Daripa,<sup>[a]</sup> Koomkoom Khawas,<sup>[b]</sup> Santanu Das,<sup>[c]</sup> Ratan Kumar Dey,<sup>[b]</sup> and Biplab Kumar Kuila\*<sup>[a]</sup>

Here, we have demonstrated a well-defined strategy to prepare highly sulphonated reduced graphene oxide (S-rGO) sheets via non-covalent modification of rGO with water soluble rod-coil conjugated block copolymer poly(3-hexylthiophene)-block-poly(4-styrenesulfonic acid) (P3HT-b-PSSA) carrying a long PSSA block. S-rGO sheets are highly water soluble and its aqueous solution can be used to fabricate highly transparent conductive thin film coating on versatile smooth substrate surfaces like glass, indium tin oxide (ITO), quartz and flexible PET. The successful anchoring of sulfonic acid group on rGO surface via non-covalent modification by P3HT-b-PSSA was confirmed and analyzed by FTIR and XRD study. The bulk morphology of S-rGO reveals sheet like morphology where individual sheets are aligned with each other in a parallel arrangement through intercalation of PSSA chains driven by block copolymer self-assembly. AFM image of the thin film also supports nice parallel alignment of S-rGO sheets of average thickness ~100 nm on substrate surface. S-rGO sample shows very high water uptake

(~91% in comparison to its initial weight) and proton conductivity 0.5 S/cm after water vapor exposure for 1 hour. Such high proton conductivity is due to the synergy of alignment of graphene sheets with a continuous network of proton conducting nanochannels created by block copolymer microphase separation on the rGO surface. Nyquist plot with two semicircles suggested the presence of grain boundaries in the sample. I–V measurement of transparent thin film device fabricated from S-rGO sheets shows linear behavior with systematic increase of current on increasing water vapor exposure time. The block copolymer device shows well correlated, systematic and reversible resistance change with relative humidity (RH) confirming its efficient sensing capability towards moisture. We believe that high proton conductivity and interesting, reversible moisture sensitive electrical property of this material will be useful in fabricating transparent and flexible moisture sensors, flexible electronics, moisture induced energy storage, fuel cell, biological applications and others.

## Introduction

Development of new sole proton conducting or both proton and electronic conducting materials attain considerable research interests worldwide due to their wide range potential applications in the area of fuel cells, sensors, biological systems and chemical filters.<sup>[1–4]</sup> Primarily, researches are focused on designing inert and faster proton conductor, which basically relies on the efficient chemical network for rapid propagation of proton.<sup>[5]</sup> Till date, various types of proton conducting materials have been developed based on either organic

materials or coordination-polymers. Those materials include acid doped polymers, hydrocarbon ionomers, metal organic frameworks, nanocomposites and ionic liquids with a broad range of ionic conductivity from  $10^{-1}$  to  $10^{-8} \text{Scm}^{-1}$ .<sup>[6–12]</sup> Graphene/reduced graphene oxide (rGO) which is atomically thin two dimensional (2D) novel carbon materials with  $sp^2$  hybridized carbon, possesses extraordinary electrical, optical, mechanical and thermal properties. Hence, 2D graphene has been proposed as emerging material for varieties of potential devices such as electronics and optoelectronics, memory, sensors, energy harvesting, storage and biomedical devices.<sup>[13–16]</sup> Because of the specific and interesting properties of GO, such as a two-dimensional (2D) platform structure with numerous oxygen functional groups like -O-, -OH, -COOH and epoxy groups extended outward, GO-based materials are considered to be good candidates for fabricating proton conducting and efficient humid sensing materials.<sup>[5,12,16,17]</sup> Hayami et al.<sup>[5]</sup> reported the proton conductivity of bulk graphite oxide, graphene oxide/proton hybrid and graphene oxide nanosheets with 100% humidity in the range of  $10^{-4} \text{Scm}^{-1}$  to  $10^{-2} \text{Scm}^{-1}$ . However, unavoidable aggregation of the individual nanosheets due to strong stacking force and limited solution

[a] S. Daripa, Dr. B. K. Kuila

Department of Chemistry, Institute of Science, Banaras Hindu University, Varanasi, Uttar Pradesh-221005, India  
E-mail: bkkuila.chem@bhu.ac.in

[b] K. Khawas, Prof. R. K. Dey

Department of Chemistry, Central University of Jharkhand, Brambe, Ranchi, Jharkhand -835205, India

[c] Dr. S. Das

Department of Ceramic Engineering, Indian Institute of Technology (BHU), Varanasi Uttar Pradesh-221005, India

Supporting information for this article is available on the WWW under <https://doi.org/10.1002/slct.201900662>



# Effect of pressure anisotropy on Buchdahl-type relativistic compact stars

S. K. Maurya<sup>1</sup> · S. D. Maharaj<sup>2</sup>  · Jitendra Kumar<sup>3</sup> · Amit Kumar Prasad<sup>3</sup>

Received: 31 October 2018 / Accepted: 1 July 2019 / Published online: 8 July 2019  
© Springer Science+Business Media, LLC, part of Springer Nature 2019

## Abstract

We consider exact models for dense relativistic stars with anisotropic pressures and containing Buchdahl-type spacetime geometry. The Buchdahl condition can be transformed to an Euler–Cauchy equation for the gravitational potentials. We solve this condition to find a new exact solution to the Einstein field equations with anisotropic matter distribution. We show that the exact solution produces a realistic model of a compact relativistic star satisfying all physical requirements. The regularity, equilibrium, causality, stability, energy conditions and compactness limits for a well behaved compact sphere are satisfied.

**Keywords** Einstein field equations · Anisotropic fluids · Compact stars

## 1 Introduction

When seeking a model of a relativistic compact object in astrophysics we first need to find an exact solution of the Einstein field equations. Delgaty and Lake [1], in their detailed listing, pointed out that several families of exact solutions have been found over the last century. However only a handful of these solutions satisfy the physical requirements for a realistic stellar model in general relativity. An example of a spacetime geometry that meets all requirements of physical acceptability is that of Buchdahl [2]. It is for this reason that the Buchdahl metric is utilized to study dense stars in strong gravitational fields. A recent example is the analysis of the Buchdahl metric in a spherically symmetric charged anisotropic matter distribution by Singh et

---

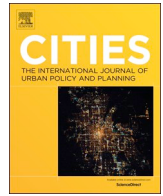
✉ S. D. Maharaj  
maharaj@ukzn.ac.za

<sup>1</sup> Department of Mathematical and Physical Sciences, College of Arts and Science, University of Nizwa, Nizwa, Oman

<sup>2</sup> Astrophysics and Cosmology Research Unit, School of Mathematics, Statistics and Computer Science, University of KwaZulu-Natal, Private Bag X54001, Durban 4000, South Africa

<sup>3</sup> Department of Applied Mathematics, Central University of Jharkhand, Ranchi 835205, India





# Monitoring and modelling spatio-temporal urban growth of Delhi using Cellular Automata and geoinformatics

Pratyush Tripathy<sup>a,b</sup>, Amit Kumar<sup>a,\*</sup>

<sup>a</sup> Department of Land Resource Management, Central University of Jharkhand, Ranchi 834205, India

<sup>b</sup> Indian Institute for Human Settlements, Bengaluru 560080, India

## ABSTRACT

The study encompasses spatio-temporal land use/ land cover (LULC) monitoring (1989–2014) and urban growth modelling (1994–2024) of Delhi, India to deduce the past and future urban growth paradigm and its influence on varied LULC classes integrating geospatial techniques and Cellular Automata (CA). The study focused on scrutinising the reliability of the CA algorithm to function independently for urban growth modelling, provided with strong model calibration. For this purpose, satellite data of six stages of time at equal intervals along with the population density, distance to CBD and roads, and terrain slope are used. The satellite-based LULC during 1989–2014 exhibited 457 km<sup>2</sup> of net urban growth (275% change), cloned by the simulated LULC with net increase 448 km<sup>2</sup> (270% change). The spatial variation analysis using the principal component analysis (PCA) technique exhibit high similarity in classification ranging from 72% to 88%. The statistical accuracy between the satellite-based and simulated built-up extent of 2014 resulted in the overall accuracy 95.62% of the confusion matrix, and the area under the receiver operating characteristic (ROC) curve as 0.928—indication high model accuracy. The projected LULC exhibit that the urban area will increase to 708 km<sup>2</sup> and 787 km<sup>2</sup>, primarily in western and eastern parts during 2019 and 2024 respectively. The rapid urban growth will replace and transform others LULC (net loss 138 km<sup>2</sup>) followed by vegetation cover (net loss 26 km<sup>2</sup>) during 2014–24. This rapid urban growth is detrimental to the habitat and may trigger critical risks to urban geo-environment and ecosystem in Delhi. Therefore, the study necessitates towards decentralization of urban functions and restoration of varied LULC in order to regulate the future urban growth patterns for sustainable development. The GDAL and NumPy libraries in Python 3.4 were efficient in spatial modelling and statistical calculations.

## 1. Introduction

Hybrid models of CA (Cellular Automata) such as CA-MC (Markov Chain) models, CA-logistic regression (LR) models, and CA-MC-LR dominate existing geospatial and related literature (Arsanjani, Kainz, & Mousivand, 2011; Jokar Arsanjani, Helbich, Kainz, & Darvishi Bolorani, 2013; Mondal, Sharma, Garg, & Kappas, 2016; Munshi, Zuidgeest, Brussel, & van Maarseveen, 2014; Mustafa et al., 2018; Siddiqui et al., 2017); the identity of the CA model to produce convincing results autonomously has faded over time. This study analyses the spatio-temporal land use/land cover (LULC) dynamics in recent decades to model urban growth using the CA algorithm for Delhi, India. The paper scrutinises the ability of the CA algorithm to replicate real-world urban growth process and project future growth. Many researchers have affirmed the reliability of the CA model, but the focus on appropriate model calibration with equidistant temporal data remain scarce (Jat, Choudhary, & Saxena, 2017; Rafiee, Mahiny, Khorasani, Darvishsefat, & Danekar, 2009). For this purpose, the LULC for six different years—1989, 1994, 1999, 2004, 2009 & 2014—has been analysed in the present study.

In addition, the LULC data along with other growth driving

parameters such as proximity to roads and CBD (central business district), topography, population statistics, areas with growth restrictions, etc. were considered to project built-up extent for forthcoming years. The future built-up projection was useful to extrapolate the imminent influence of rapid urbanisation in Delhi on the environment, which could aid in framing sustainable measures. The study also reports the accuracy and reliability of the CA algorithm in modelling urban growth.

Urbanisation is a global phenomenon, having varied rates and trends across geographical regions (Lal, Kumar, & Kumar, 2017). The physical and urban forms leading to unplanned and unsustainable patterns of urban growth characterises the growth of urban areas (Kumar & Pandey, 2017). The physical and morphological conditions, economic state, population growth, political situation, policies, and social behaviour varies across regions that makes the pattern of urban growth unpredictable (Thapa & Murayama, 2010). A majority of Indian cities witnessed dramatic growth, degrading the environment and the ecosystem on a large scale (Diksha & Kumar, 2017; Kumar & Pandey, 2016; McMichael, 2000; Peng, Chen, & Cheng, 1997). Modelling the urban growth is necessary for quantitative assessment of the growth patterns to bring down the future effects of urbanisation on the environment and aid in policymaking. Previous studies reported the

\* Corresponding author.

E-mail addresses: [pratyush@iihs.ac.in](mailto:pratyush@iihs.ac.in) (P. Tripathy), [amit.kumar@cuja.ac.in](mailto:amit.kumar@cuja.ac.in), [amit.iirs@gmail.com](mailto:amit.iirs@gmail.com) (A. Kumar).



# Synthesis, Characterization and Catalytic Application of Starch Supported Cuprous Iodide Nanoparticles

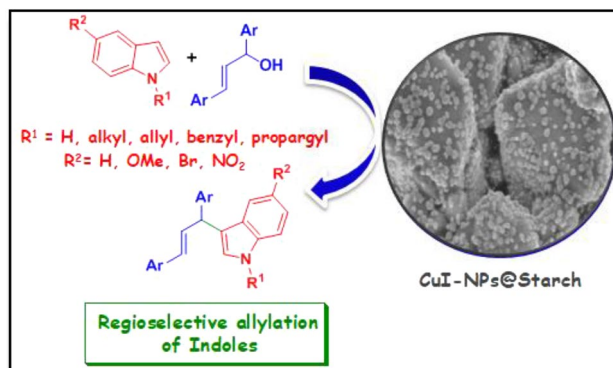
Sadhucharan Mallick<sup>1</sup> · Priyabrata Mukhi<sup>2</sup> · Poonam Kumari<sup>3</sup> · Kumari Reshmi Mahato<sup>3</sup> · Suryadev Kumar Verma<sup>3</sup> · Debjit Das<sup>4</sup>

Received: 17 February 2019 / Accepted: 19 July 2019 / Published online: 29 July 2019  
© Springer Science+Business Media, LLC, part of Springer Nature 2019

## Abstract

The starch supported cuprous iodide nanoparticles (CuI-NPs@Starch) were synthesized in aqueous medium and characterized by transmission electron microscopy, scanning electron microscopy, X-ray powder diffraction, energy-dispersive X-ray spectroscopy and atomic absorption spectra analysis. The newly synthesized CuI NPs on starch have been demonstrated first time as an efficient catalyst for the regioselective 3-allylation reaction of *N*-substituted indoles as well as ring-substituted indoles using various allyl alcohols under moisture and air insensitive conditions.

## Graphic Abstract



**Keywords** Nanocatalysis · CuI NPs · Allylation · Indole · Allylic alcohol

**Electronic supplementary material** The online version of this article (<https://doi.org/10.1007/s10562-019-02909-1>) contains supplementary material, which is available to authorized users.

✉ Debjit Das  
debjitochem@gmail.com

- 1 Department of Chemistry, Indira Gandhi National Tribal University, Amarkantak, India
- 2 School of Basic Sciences, Indian Institute of Technology, Bhubaneswar, India
- 3 Centre for Applied Chemistry, Central University of Jharkhand, Ranchi, India
- 4 Department of Chemistry, Triveni Devi Bhalotia College, Raniganj, India

## 1 Introduction

In recent years, nanocatalysis has become an emerging field of science with the benefits of excellent activity, selectivity and productivity [1–5]. The nanoscale size, shape and exceptionally large surface area to volume ratio of nanocatalysts impart distinct catalytic properties, which differentiates them from the bulk materials [1–10]. Among the various metallic nanoparticles, copper-based nanoparticles are comparatively inexpensive, environment-friendly and easily available. As a consequence, they have received tremendous attention in the field of organic transformation and fine chemical synthesis [6–10]. In this regard, cuprous iodide nanoparticles



# Chronic lead (Pb) exposure results in diminished hemocyte count and increased susceptibility to bacterial infection in *Drosophila melanogaster*



Kumari Pragati Nanda, Chandani Kumari, Madhavi Dubey, Hena Firdaus\*

Department of Life Sciences, Central University of Jharkhand, Ratu-Lohardaga Road, Brambe, Ranchi, 835205, Jharkhand, India

## HIGHLIGHTS

- *MtnB* helps in Pb scavenging in *Drosophila*.
- Pb exposure reduces immunity required to ward off *B. subtilis* infection.
- Pb decreases plasmacyte and crystal cell number in *Drosophila*.
- Lowered phenoloxidase pathway of immunity observed in Pb fed animals.

## ARTICLE INFO

### Article history:

Received 20 May 2019

Received in revised form

9 July 2019

Accepted 10 July 2019

Available online 11 July 2019

Handling Editor: Prof Willie Peijnenburg

### Keywords:

Heavy metal  
Immunotoxicity  
Hemocyte  
Phenoloxidase  
Metallothionein

## ABSTRACT

Heavy metal Pb is a common toxic pollutant present in our environment adversely affecting health of the living organisms. Recent studies suggest positive correlation between heavy metal exposure and immune dysfunction and present work utilizes *Drosophila* to address this issue in relation to Pb exposure. *In-vivo* Pb toxicity was established by dietary intake where essential parameters like development and life span were found to be hampered and augmented upon *metallothionein B (mtnB)* downregulation hinting towards potential role of *mtnB* in Pb detoxification. Further response of *Drosophila* to *B. subtilis* bacterial infection was monitored by carrying out oral infections. Pb fed flies showed increased susceptibility to infection as compared to their controls. Since *Drosophila* hemocytes play dual role as immune cells, we checked for the total hemocyte count and found significant decrease in hemocyte numbers in Pb fed larvae. Both crystal cells and plasmacytes, the two major hemocytes in third instar larval hemolymph were reduced. However we did not find any visible morphological changes in Giemsa stained hemocytes. Crystal cells are crucial for synthesis and release of phenoloxidase (PO), an enzyme required for melanin clot synthesis and deposition. PO activity assessed from total hemolymph protein isolates was found to be substantially decreased in Pb raised animals. Results were also confirmed by spot test and native gel activity assay of PO. Overall our results suggest immunotoxic effect of Pb through decrease in hemocyte count including crystal cell which in turn leads to decreased PO activity and increased susceptibility to *B. subtilis*.

© 2019 Elsevier Ltd. All rights reserved.

## 1. Introduction

Heavy metals are natural components of our biosphere. They constitute elements with metallic properties distributed in d, f and p block of periodic table. Though, their presence is very essential for the existence of life but, its excess inside our body can pose serious

life threatening health issues (Wu et al., 2016). However, some heavy metals are considered to be nonessential for living entities and Pb is one such undesirable heavy metal used since prehistoric times by humans causing worldwide adulteration (Hejna et al., 2018; Jaishankar et al., 2014). Pb along with other heavy metals disperses in natural environment through various anthropogenic activities and enters our system through dermal contacts, breathing of contaminated dust particles and ingestion of Pb polluted food, water and plants which bioaccumulate metals (Tchounwou et al., 2012; Wani et al., 2015).

\* Corresponding author.

E-mail address: [hena.firdaus@cuja.ac.in](mailto:hena.firdaus@cuja.ac.in) (H. Firdaus).



Contents lists available at ScienceDirect

## Economic Analysis and Policy

journal homepage: [www.elsevier.com/locate/eap](http://www.elsevier.com/locate/eap)

Full length article

## Foreign aid and growth nexus: Empirical evidence from India and Sri Lanka

Narayan Sethi<sup>a,\*</sup>, Padmaja Bhujabal<sup>a</sup>, Aurolipsa Das<sup>a</sup>, Sanhita Sucharita<sup>b</sup><sup>a</sup> Department of Humanities and Social Sciences, National Institute of Technology (NIT) Rourkela, Odisha, India<sup>b</sup> Department of Economics, School of Social Sciences Central University of Jharkhand, Ranchi, India

## ARTICLE INFO

## Article history:

Received 17 December 2018  
 Received in revised form 2 May 2019  
 Accepted 6 July 2019  
 Available online 9 July 2019

## JEL classification:

I22  
 O47  
 F4  
 F62

## Keywords:

Foreign aid  
 Economic growth  
 Granger Causality test  
 VAR modelling

## ABSTRACT

This paper examines the relationship between foreign aid and economic growth for India and Sri Lanka using annual time series data from 1960–61 to 2014–15. This study uses various time series techniques such as Johansen–Juselius test, Granger causality test and VAR modelling to find out the short-run and long-run equilibrium dynamics among the variables under consideration. The empirical results confirm that long-run relationship exists among foreign aid inflows, economic growth, trade, inflation, domestic investment and financial development in India. There also exists a uni-directional causality among the variables for the same. However, in Sri Lanka, foreign aid does not have a significant impact on growth, both in the long-run and short-run. The governments of the respective countries are thus required to make efforts in employing proper monetary and fiscal policies in order to stabilize the domestic economic cycle as well as external economic transformation in accordance with the impact of foreign aid on economic growth in each of them.

© 2019 Economic Society of Australia, Queensland. Published by Elsevier B.V. All rights reserved.

## 1. Introduction

The Organization for Economic Cooperation and Development (OECD) defines Official Development Assistance (ODA) as “government aid designed to promote the economic development and welfare of developing countries. Aid may be provided bilaterally, from donor to recipient, or channelled through a multilateral development agency such as the United Nations or the World Bank. Aid includes grants, “soft” loans (where the grant element is at least 25% of the total) and the provision of technical assistance”. ODA may be disbursed under different heads namely, social (which includes education, health, water supply, sanitation and social infrastructure), economic (transport and communications, energy, banking, business and other services) and production (agriculture, forestry and fishing, industry, mining and construction and trade and tourism). Further, aid may be targeted at multiple sectors or may be given on humanitarian grounds.

Few of the alternative views on the effectiveness of aid are as listed: (a) aid has decreasing returns, (b) aid effectiveness is influenced by external and climatic conditions, (c) aid effectiveness is influenced by political conditions, and (d) aid effectiveness depends on institutional quality (Feeny and McGillivray, 2008). Aid effectiveness primarily depends on a sound monetary, fiscal and trade policy (Burnside and Dollar, 2000), climatic conditions (Dalgaard et al., 2004) and institutional and political factors (Tang and Bundhoo, 2017).

\* Corresponding author.

E-mail addresses: [nsethinarayan@gmail.com](mailto:nsethinarayan@gmail.com) (N. Sethi), [padmaja.1806@gmail.com](mailto:padmaja.1806@gmail.com) (P. Bhujabal), [aurolipsa12@gmail.com](mailto:aurolipsa12@gmail.com) (A. Das), [Sanhita.sucharita@gmail.com](mailto:Sanhita.sucharita@gmail.com) (S. Sucharita).



## A breakthrough column study for removal of malachite green using coco-peat

Roshni Kumari and Soumen Dey

Centre for Applied Chemistry, Central University of Jharkhand, Ranchi, India

### ABSTRACT

A continuous adsorption study in a fixed bed column using coco-peat (CP) as an adsorbent was carried out for the removal of toxic malachite green (MG) from contaminated water. Fixed bed column studies were carried out to check field application viability. Various parameters like particle size, pH, concentration, dose and interference were exercised to optimize dye removal. Data obtained from breakthrough column studies were evaluated using Thomas and BDST model. Thomas rate constants  $K_t$  ( $0.22 \text{ ml min}^{-1} \text{ mg}^{-1}$ ) and adsorption capacity  $q_0$  ( $181.04 \text{ mg g}^{-1}$ ) were estimated and found to favor efficiency of CP. Thomas model was tested with several parameters like flow rate, concentration, and bed depth. Upon increase in input dye concentration, flow rate and bed height, adsorption coefficients increased. According to BDST model, maximum dye uptake of  $468.26 \text{ mg/l}$  was obtained with an input dye concentration of  $5 \text{ mg/l}$ . HYBRID and MPSD error functions were tested and found that Thomas model fits best. Dilute hydrochloric acid was found best for desorption. Real wastewater from textile industry was analyzed and confirmed the prospect of large-scale industrial application. In conclusion, coco-peat can be used as a promising bio-sorbent in column bed for scavenging of MG from contaminated water.

### KEYWORDS

Malachite green; coco-peat; breakthrough curves; Thomas model; BDST model; MPSD; HYBRID

### Introduction

Dyes are used in several commercial sectors including textile, paper, pulp, food, and pharmaceutical industries as coloring agent (Mittal *et al.* 2010; Yadav *et al.* 2012). Wastewater from these industries contains toxic dyes like Congo red (Han *et al.* 2008), methylene blue (Han *et al.* 2009), malachite green (Das *et al.* 2016), Novacrone golden yellow (Nawaz *et al.* 2014), etc. in high concentration. These wastewater offer a serious threat to humanity and aquatic life because of toxicity laden with them in the form of dyes broadly cationic dyes. Numerous conventional methods such as oxidation, coagulation, precipitation, ozonation, and adsorption were employed for treatment of these wastewater (Gong *et al.* 2005). Among these methods, adsorption is one such which had been proved to be highly efficient and simple due to easy implementation and availability of a large number of adsorbents (Salleh *et al.* 2011; Zhang *et al.* 2013). In recent years, use of naturally available biomass under the name of biosorbents has gained popularity due to low cost and no pretreatment expenses (Jain *et al.* 2003; Kaur and Gupta 2010). Biosorbents include a wide variety of living and non living biomass like agricultural waste including peanut husk (Sadaf and Bhatti 2014), pineapple leaf powder (Das *et al.* 2016), orange bagasse (Fiorentin *et al.* 2015), sugarcane bagasse (Noreen and Bhatti 2016), tea waste (Foroughi-Dahr *et al.* 2015), rice husk (Han *et al.* 2007), phoenix tree leaf powder (Han *et al.* 2009), eucalyptus bark (Srivastava and Rupainwar 2009), jujube seeds (Somasekhara

Reddy *et al.* 2012), date palm (Ahmed *et al.* 2012), dead fungi and fresh water algae (Padmesh *et al.* 2005; Gupta *et al.* 2010), etc. Coco-peat is one such highly efficient biomass which was used for the present study for the removal of toxic malachite green from aqueous solution. Coco peat finds its use in biofilters, roofing materials and serves as medium for crop production. MG is a cationic triphenylmethane dye widely used in coloring of cotton, woolen and silk fabrics, as well as bioinsecticide. Its high toxicity and carcinogenicity had attracted a concern for its removal from wastewater. Batch adsorption results of MG on CP showed high efficiency of the biosorbent. The adsorption kinetics followed pseudo 1st order with maximum correlation coefficient and thermodynamic parameters suggested the process to be spontaneous and endothermic in nature (Vijayaraghavan *et al.* 2016). Most of the research is confined to batch studies only. There is a need to understand the adsorption pattern in column mode so that field applicability can be suggested. This encouraged the use of the biomass in fixed column bed for the removal of MG.

The aim of the present work is to capitalize a naturally available plant by-product into technology-oriented processing for waste water treatment. It enables to systematically elaborate the practical work to field application. Column studies were performed to analyze the effects of adsorption parameters on industrial scale. The objectives included the investigation of the effects of flow rate, bed depth, dye concentration, and input pH on the biosorption of MG by column bed of CP (Aksu *et al.* 2007; Ahmad and Hameed



## UP-SCALING PADDY YIELD AT SATELLITE-FOOTPRINT SCALE USING SATELLITE DATA IN CONJUNCTION WITH CCE DATA IN SAHIBGANJ DISTRICT, JHARKHAND

Bikash Ranjan Parida<sup>1,\*</sup>, Avinash Kumar Ranjan<sup>1</sup>

<sup>1</sup> Department of Land Resource Management, School of Natural Resource Management, Central University of Jharkhand, Brambe-835205, Jharkhand, India - bikashrp@gmail.com

Commission III, WG III/10

**KEYWORDS:** Yield prediction, Remote sensing, NDVI, EVI, AquaCrop model, CCE data

### ABSTRACT:

Agriculture plays a vital role in the economy of India as almost half of the workforce dependent on agriculture and allied activities. Rice is an important staple food and provides nutritious need for the billions of population. Mapping the spatial distribution of paddy and predicting yields at district level aggregation are crucial for food security measures. This study has utilized the time-series MODIS-based Normalized Difference Vegetation Index (NDVI) and Enhanced Vegetation Index (EVI) data in conjunction with CCE data to derive a statistical model for up-scaling paddy yield at satellite-footprint scale over Sahibganj district in Kharif (monsoon) season 2017. The CCE data were collected from ten random paddy plots. In addition, Area, Production, and Yield (APY) data were collected during harvesting period by interacting with eighty farmers belong to eight villages. The AquaCrop model was also used to simulate the paddy yield for Kharif season. The key results showed that based on the farmers-based yield data, paddy yield was observed as ~3200 kg/hectare, whereas, NDVI and EVI-based yield models based on satellite data showed about 2,960 and 3,530 kg/hectare, respectively. Moreover, multi-regression-based yield model showed the mean yield of 3,070 kg/hectare. With respect to farmers-level yield data, the relative deviation (RD) of yield based on NDVI data was -7.5% (underestimation), while EVI was 10.31% (overestimation). The multi-regression-based yield model and AquaCrop model were underestimated by -4.06 and -10.16%, respectively. Thus, it can be inferred that the multi-regression-based yield was close to farmers-based survey yields. It can be concluded that the satellite databased yield prediction can be reliable with  $\pm 10\%$  of RD. Nevertheless, remote sensing technology can be beneficial over traditional survey method as the satellite-based methods are cost-effective, robust, reliable, and time-saving than the traditional methods.

### 1. INTRODUCTION

Agriculture plays a vital role in the economy of India as almost half of the workforce dependent on agriculture and contributes nearly 18% to the national GDP. Rice (*Oryza Sativa*) has a significant role by providing the nutritious requirement to 1.3 billion of the Indian population. Yield prediction before harvesting using remotely sensed satellite imagery and crop models are significant steps to make a key decision on food storage, procurement, public distribution, export-import (EXIM), and national food security.

Remote Sensing (RS) techniques and crop growth simulation models have been provided a dynamic and robust way to monitor the agriculture system in the current decades. These methods are cost-effective, accurate and reliable; require less manpower and time, as compared to traditional survey methods. In the contemporary world, remotely sensed information collected from various satellite sensors (multi-spectral, hyperspectral, synthetic aperture radar) have facilitated the development of modern agriculture systems by providing a wide range of spatial data to monitor crops and to predict crop yields (Ranjan and Parida 2019; Mondal et al. 2018; Panigrahy et al. 2010). Over the years, Remote Sensing (RS) sensors have been improved the quality of data by enhancing the spatial, temporal, spectral, and radiometric resolutions. Consequently, these RS data have been utilized to extend the accuracy of crop

acreage estimation as well as yield forecasting owing to synoptic coverage, a wide range of multi-temporal and multi-spectral data.

In this regard, several studies have accounted that RS satellite data have the potential for crop growth monitoring, acreage estimation, and yield prediction, as the spectral response of crops were strongly associated with crop canopy cover and biophysical parameters (Schgal et al. 2002; Patel et al. 2006). On account of yield prediction, numerous studies have recognized a virtuous correlation between the satellite-derived Vegetation Indices (VIs) and crop yields (Nuasra et al. 2012; Son et al. 2014).

Nevertheless, crop simulation models have been frequently used across the world to monitor and simulate the crop yield. Many crop simulation models viz. AquaCrop, DSSAT, InfoCrop etc. have been extensively used in diverse climatic condition to monitor and predict the various crop yield at regional to a national scale (Greaves and Wang 2016; Aggarwal et al. 2006). Crop simulation models are also a robust and dynamic way to monitor and estimate the crop yield at various scale in diverse climatic and geographic condition. As simulation, models require a smaller number of input parameters to calibrate the models. Thereby, crop simulation models are also very cost-effective, timesaving, robust and reliable over the traditional crop survey methods.

\* Corresponding author



## Research Article

# Equation of States and Charmonium Suppression in Heavy-Ion Collisions

Indrani Nilima and Vineet Kumar Agotiya 

Department of Physics, Central University of Jharkhand Ranchi, 835 205, India

Correspondence should be addressed to Vineet Kumar Agotiya; agotiya81@gmail.com

Received 7 December 2018; Revised 11 March 2019; Accepted 5 May 2019; Published 6 August 2019

Academic Editor: Theocharis Kosmas

Copyright © 2019 Indrani Nilima and Vineet Kumar Agotiya. This is an open access article distributed under the Creative Commons Attribution License, which permits unrestricted use, distribution, and reproduction in any medium, provided the original work is properly cited. The publication of this article was funded by SCOAP<sup>3</sup>.

The present article is the follow-up of our work Bottomonium suppression in quasi-particle model, where we have extended the study for charmonium states using quasi-particle model in terms of quasi-gluons and quasi quarks/antiquarks as an equation of state. By employing medium modification to a heavy quark potential thermodynamic observables, *viz.*, pressure, energy density, speed of sound, etc. have been calculated which nicely fit with the lattice equation of state for gluon, massless, and as well *massive* flavored plasma. For obtaining the thermodynamic observables we employed the debye mass in the quasi particle picture. We extended the quasi-particle model to calculate charmonium suppression in an expanding, dissipative strongly interacting QGP medium (SIQGP). We obtained the suppression pattern for charmonium states with respect to the number of participants at mid-rapidity and compared it with the experimental data (CMS JHEP) and (CMS PAS) at LHC energy (Pb+Pb collisions,  $\sqrt{s_{NN}} = 2.76$  TeV).

## 1. Introduction

The primary goal of heavy-ion experiment at the RHIC and the LHC is to search a new state of matter, *i.e.*, the Quark Gluon Plasma. To study the properties of the Quark Gluon Plasma (QGP) heavy quarks are considered to be a suitable tool. Initially, the heavy quarks can be calculated in pQCD, which are produced in primary hard N N collisions [1]. The charmonia is a bound states of charm (*c*) and anticharm ( $\bar{c}$ ), which is an extremely broad and interesting field of investigation [2]. Charmonium states can have smaller sizes than hadrons (down to a few tenths of a fm) and large binding energies ( $> 500$  MeV) [3]. In ultrarelativistic heavy-ion collisions, it has been realized that early ideas associating with charmonium suppression with the deconfinement transition [4] are less direct than originally hoped for [5–8].

At sufficiently large energy densities, lattice QCD calculations predict that hadronic matter undergoes a phase transition of deconfined quarks and gluons, called Quark Gluon Plasma (QGP). In order to reveal the existence and to analyze the properties of this phase transition several researches in this direction have been done. In the high-energy heavy-ion collision field, the study of charmonium production and

suppression is the most interesting investigations, since the charmonium yield would be suppressed in the presence of a QGP due to color Debye screening [4].

In heavy-ion collisions, charmonium suppression study has been carried out first at the Super Proton Synchrotron (SPS) by the NA38 [9–11] and NA60 [12] and then at the Relativistic Heavy-Ion Collider (RHIC) by the PHENIX experiment at  $\sqrt{s_{NN}} = 200$  GeV [13]. The suppression is defined by the ratio of the yield measured in heavy-ion collisions and a reference, called the nuclear modification factor  $R_{AA}$  [14] and it is considered as a suitable probe to identify the nature of the matter created in heavy-ion collisions. At high temperature, Quantum Chromodynamics (QCD) is believed to be in Quark Gluon Plasma (QGP) phase, which is not an ideal gas of quarks and gluons, but rather a liquid having very low shear viscosity to entropy density ( $\eta/s$ ) ratio [15–20].

This strongly suggests that QGP may lie in the nonperturbative domain of QCD which is very hard to address both analytically and computationally. Similar conclusion about QGP and perfect fluidity of QGP have been reached from recent lattice studies and from the AdS/CFT studies [20], spectral functions and transport coefficients in lattice



## Dependency of incomplete fusion on target deformation

Pankaj K Giri<sup>a</sup>, D Singh<sup>a\*</sup>, Sneha B Linda<sup>a</sup>, Amritraj Mahato<sup>a</sup>, Harish Kumar<sup>b</sup>, Suhail A Tali<sup>b</sup>, M Afzal Ansari<sup>b</sup>, R Kumar<sup>c</sup>, R P Singh<sup>c</sup> & S Muralithar<sup>c</sup>

<sup>a</sup>Department of Physics, Central University of Jharkhand, Ranchi 835 205, India

<sup>b</sup>Department of Physics, Aligarh Muslim University, Aligarh 202 002, India

<sup>c</sup>Inter University Accelerator Centre, Aruna Asaf Ali Marg, New Delhi 110 067, India

Received 8 April 2019

Excitation functions for the evaporation residues  $^{161,159,158}\text{Er}$  ( $xn$ ),  $^{161-159}\text{Ho}$  ( $pxn$ ),  $^{157,155}\text{Dy}$  ( $\alpha xn$ ) and  $^{155}\text{Tb}$  ( $\alpha pxn$ ) populated via complete and/or incomplete fusion in system  $^{16}\text{O} + ^{148}\text{Nd}$  system at low projectile energies  $\approx 3-7$  MeV/A have been measured. In these measurements recoil catcher activation technique followed by offline  $\gamma$ -ray spectrometry has been used. The total measured excitation functions of the evaporation residues  $^{161,159,158}\text{Er}$  ( $xn$ ) and  $^{161-159}\text{Ho}$  ( $pxn$ ) produced through  $xn$  and  $pxn$  channels are found to be well reproduced with the total PACE-4 predictions after subtraction of precursor contributions. A significant enhancement in the total measured excitation functions over their total theoretical predictions for the evaporation residues  $^{157,155}\text{Dy}$  ( $\alpha xn$ ) and  $^{155}\text{Tb}$  ( $\alpha pxn$ ) produced in  $\alpha$ -emitting channels has been observed. This enhancement is attributed due to the presence of break-up of the incident projectile  $^{16}\text{O}$  into  $\alpha$  clusters (i.e., break-up of  $^{16}\text{O}$  into  $^{12}\text{C} + \alpha$ ) and incomplete fusion of projectile  $^{16}\text{O}$  with target  $^{148}\text{Nd}$  at these low energies. A comparison of the present data with earlier measurements indicates that the ICF probability depends on Coulomb factor ( $Z_P Z_T$ ) along with target deformation ( $\beta_2^T$ ). However, more systematic study on same Z spherical and deformed targets with same projectile at low energy is required to understand the role of target deformation on incomplete fusion dynamics.

**Keywords:** Complete and incomplete fusion, Offline  $\gamma$ -ray spectrometry, Stacked foil activation technique, Excitation functions, Target deformation

### 1 Introduction

Comprehensive studies on heavy ion induced reaction have shown that the complete fusion (CF) and incomplete fusion (ICF) processes are the dominant modes at energy below 10 MeV/A and above the Coulomb barrier<sup>1-4</sup>. In the interaction of projectile with target, CF occurs when the projectile completely fuses with the target nucleus, forming a highly excited compound nucleus and it decays through the low energy light nuclear particles and/or  $\gamma$ -rays. However, the projectile may also breaks-up into its fragments and one of the fragment fuses with target while remnant behaves as spectator. This process is known as ICF. The first experimental evidence of ICF was given by Britt and Quinton<sup>5</sup>. Major advancement on the study of ICF dynamics took place after the pioneering work of Inamura *et al.*<sup>6</sup>. They observed the break-up of projectile like  $^{12}\text{C}$ ,  $^{14}\text{N}$  and  $^{16}\text{O}$  into  $\alpha$ -particles using particle-gamma coincidence technique. Various efforts have been made to probe the dependence of ICF on different

entrance channel parameters<sup>7-9</sup>. Studies done by some investigators show that the ICF dynamics depends on Coulomb factor ( $Z_P Z_T$ )<sup>10,11</sup> and deformation of target ( $\beta_2^T$ )<sup>12,13</sup>. However, no definite conclusion has been established yet regarding the dependence of ICF on these parameters.

Several investigators have proposed the theoretical models to explain the ICF dynamics. The Sumrule model of Wilczynski *et al.*<sup>14</sup>. The break-up fusion (BUF) model of Udagawa and Tamura<sup>15</sup>, promptly emitted particle (PEP) model<sup>16</sup>, hot spot model<sup>17</sup> and multistep direct reaction model<sup>18</sup> are some of the widely used models. These existing models can satisfactorily predict the measured ICF data at energy above 10 MeV/A. However, the non availability of any theoretical model below this energy makes the study of ICF dynamics still an active area of investigation.

There are some experimental techniques to probe the CF and ICF dynamics (i) excitation function (EFs), (ii) forward recoil range distributions (RRDs) (iii) forward angular distributions (FADs) (iv) kinetic and velocity spectra and (v) spin distribution (SDs)

\*Corresponding author (E-mail: dsinghcuj@gmail.com)

## Pre-equilibrium particle emission due to heavy and light ion interactions

D Singh<sup>a\*</sup>, Sneha B Linda<sup>a</sup>, Pankaj K Giri<sup>a</sup>, Amritraj Mahato<sup>a</sup>, Utkarsh<sup>a</sup>, Pramod K Shrotriya<sup>b</sup>, A K Mishra<sup>c</sup> & M Afzal Ansari<sup>d</sup>

<sup>a</sup>Department of Physics, Central University of Jharkhand, Ranchi 835 205, India

<sup>b</sup>KSRMV Inter College, Atrauli, Aligarh 202 280, India

<sup>c</sup>Department of Applied Science (Physics), SATI, Vidisha 464 001, India

<sup>d</sup>Department of Physics, Aligarh Muslim University, Aligarh, 202 002, India

*Received 8 April 2019*

To understand the mechanism of pre-equilibrium particle emission using light and heavy ion beams with different targets at energy above the Coulomb barrier, a study has been done. The cross-sections for twelve systems  ${}^4\text{He} + {}^{59}\text{Co}$ ,  ${}^4\text{He} + {}^{124}\text{Sn}$ ,  ${}^4\text{He} + {}^{165}\text{Ho}$ ,  ${}^{12}\text{C} + {}^{59}\text{Co}$ ,  ${}^{12}\text{C} + {}^{124}\text{Sn}$ ,  ${}^{12}\text{C} + {}^{165}\text{Ho}$ ,  ${}^{16}\text{O} + {}^{59}\text{Co}$ ,  ${}^{16}\text{O} + {}^{124}\text{Sn}$ ,  ${}^{16}\text{O} + {}^{165}\text{Ho}$ ,  ${}^{19}\text{F} + {}^{59}\text{Co}$ ,  ${}^{19}\text{F} + {}^{124}\text{Sn}$  and  ${}^{19}\text{F} + {}^{165}\text{Ho}$  have been calculated using the statistical model code ALICE-91. Significant pre-equilibrium particle emission contribution has been obtained for lighter systems at higher projectile energy. It has also been found that the pre-equilibrium particle emission affects predominantly over the equilibrated compound nucleus emissions at high projectile energies. Pre-equilibrium fraction ( $F_{\text{PEQ}}$ ) has been deduced from the excitation function data for different systems at different projectile energies. The present results indicate that the probability of pre-equilibrium particle emission depends not only on a single entrance channel parameter, but it also depends on various entrance channel parameters, namely: projectile energy, mass of the projectile, mass of the target and entrance-channel mass asymmetry. The present analysis of the data also suggests that the pre-equilibrium particle emission contributes significantly at higher projectile energy for lighter mass projectile and target.

**Keywords:** Pre-equilibrium emission, Excitation functions, Pre-equilibrium fraction, Mass, Asymmetry, ALICE-91

### 1 Introduction

Great effort has been employed in the study of light and heavy ion induced reactions in the field of nuclear physics. The pre equilibrium (PE) particle emission process has been found to affect the dynamics of heavy ion induced reactions at high energies  $>10$  MeV/nucleon<sup>1</sup>. The contribution of PE reactions can be obtained by comparing the measured excitation functions (EFs) and theoretical predictions of statistical model codes. The PE and the compound nucleus (CN) emission reactions have been studied by several researchers in past few decades<sup>2-7</sup>. The energy spectrum of charged particles emitted during a nuclear reaction, at a particular angle and high energies several discrete peaks are observed. Some of these peaks are well resolved. At low energy side a broad Maxwellian distribution followed by a continuum has been found. The curve shows that the reaction has taken place in several steps, which indicates that the particles are emitted from the equilibrated nucleus. The isolated peaks at higher energy side may be

attributed to the direct reactions without the formation of compound nucleus (CN). The explanation of the continuum may be attributed to some intermediate processes called pre-equilibrium particle emission (PE) process<sup>8,9</sup>. It may be assumed that the pre-equilibrium particle emission proceeds through two body residual interactions inside the compound system. The pre-equilibrium particle emission may be considered as a bridge between two extreme reaction mechanisms. The pre-equilibrium particle emission mechanism is characterized by slowly descending tails of excitation functions, forward peaked angular distribution of emitted particles and relatively large number of higher energy particles than predicted by the compound nucleus mechanism. The first successful theory of such process was the exciton model. This model gives the energy distribution of the emitted particles and the angle-integrated cross-section of all the reactions. This semi-classical model also predicts the main features of the angular distributions of emitted particles. At very high energy the reaction may be studied using Monte Carlo simulation method. Presence of PE emissions at HI

\*Corresponding author (E-mail: dsinghcuj@gmail.com)

## Role of alpha cluster over non alpha cluster projectile in low energy incomplete fusion reaction dynamics

Suhail A Tali<sup>a\*</sup>, Harish Kumar<sup>a</sup>, M Afzal Ansari<sup>a†</sup>, Asif Ali<sup>a</sup>, D Singh<sup>b</sup>, Rahbar Ali<sup>c</sup>, Pankaj K Giri<sup>b</sup>, Sneha B Linda<sup>b</sup>, R Kumar<sup>d</sup>, Siddharth Parashari<sup>a</sup>, R P Singh<sup>d</sup> & S Muralithar<sup>d</sup>

<sup>a</sup>Department of Physics, Aligarh Muslim University, Aligarh 202 002, India

<sup>b</sup>Department of Physics, Central University of Jharkhand, Ranchi 835 205, India

<sup>c</sup>Department of Physics, G F (PG) College, Shahjhanpur 242 001, India

<sup>d</sup>Inter University Accelerator Centre, New Delhi 110 067, India

*Received 8 April 2019*

Continuous efforts are being made to comprehend the process of low energy incomplete fusion (ICF) reaction dynamics. The lack of proper theoretical model below 8 MeV/nucleon, which could reproduce the experimentally measured ICF data satisfactorily, makes it the topic of great interest. Another important motivation is to look for some systematic dependence of ICF on various entrance channel parameters. Keeping the aforementioned aspects into consideration, the experiment has been performed using <sup>12</sup>C ion beam on <sup>165</sup>Ho target by employing the stacked foil activation technique. The experimentally measured cross sections of the populated evaporation residues have been measured and compared with the complete fusion code PACE4. It has been observed that the measured cross sections for evaporation residues populated via xn and pxn emission channels are well reproduced by PACE4 code. However, in the  $\alpha$ -emission channels (observed in the projectile break-up), the significant enhancement in the measured cross sections over PACE4 predictions is observed which is accredited to ICF process. In the present work, ICF dependence on the target deformation and the combined parameter  $\mu * Z_p Z_T * (1 - \beta_2)$  has been studied. The ICF fraction has also been found sensitive to projectile  $Q_\alpha$ -value.

**Keywords:** Complete and incomplete fusion, Incomplete fusion fraction, Target deformation, Projectile  $Q_\alpha$  value

### 1 Introduction

The study of heavy ion (HI) fusion reactions is of great interest for both theoretical and experimental nuclear physicists. Depending upon the mass and energy of the interacting nuclei, such reactions may lead to the formation of super-heavy elements. The study of such nuclear reactions may also provide explicitly some important information related to nuclear astrophysics. In the energy region of  $\approx 4$ -7 MeV/nucleon, various processes can take place for tightly bound projectile induced reactions with heavy mass targets<sup>1</sup>. The incident projectile may completely fuse with the target nucleus known as direct complete fusion (DCF). There is also a probability that projectile may break-up into fragments in the vicinity of target nuclear field and all the fragments may fuse with the target nucleus sequentially, known as sequential complete fusion (SCF). The third process is that one of the break-up fragments may fuse with the target nucleus known as break-up or incomplete

fusion (ICF). The unfused fragment in incomplete fusion moves in the forward direction as a spectator with almost the incident beam velocity<sup>2-4</sup>. There is also a probability that none of the break-up fragments may fuse with the target nucleus, which is known as non capture break-up (NCBU) process. Figure 1 shows these different reaction processes that may take place with <sup>12</sup>C as projectile. Experimentally the SCF cannot be distinguished from the DCF<sup>5</sup> hence, CF cross section is the sum of SCF and DCF.

Many efforts are being made to comprehend the phenomenon of complete and incomplete fusion nuclear reaction dynamics. The current interest is to understand the dependence of incomplete fusion on (a) incident projectile energy, (b) projectile-target mass asymmetry, (c) coulomb effect, (d) target deformation, (e) projectile structure and to search some new entrance channel parameters on which incomplete fusion process may depend. Further, the lack of proper theoretical model, which could reproduce the experimentally measured incomplete fusion reaction cross sections appropriately, is also a

\*Corresponding author (E-mail: amusuhailtali@gmail.com)

# Fusion incompleteness in $^{14}\text{N} + ^{169}\text{Tm}$ system: Measurement of recoil range distributions

S Kumar<sup>a</sup>, Pankaj K Giri<sup>b</sup> & R Kumar<sup>a\*</sup>

<sup>a</sup>Nuclear Physics Group, Inter-University Accelerator Centre, New Delhi 110 067, India

<sup>b</sup>Centre for Applied Physics, Central University of Jharkhand, Ranchi 835 205, India

Received 8 April 2019

To understand the incomplete fusion reaction dynamics and its dependency on various entrance channel parameters, an experiment using the forward recoil range technique was performed for the  $^{14}\text{N} + ^{169}\text{Tm}$  system at projectile energy  $\approx 83$  MeV. The recoil-catcher activation technique followed by off-line  $\gamma$ -spectrometry was employed. Experimentally measured forward recoil range distributions of evaporation residues indicates the occurrence of incomplete fusion channels in addition to complete fusion. Full and partial linear momentum transfer components have been observed. The experimentally measured ranges of the evaporation residues formed due to the transfer of complete and/or partial momentum by projectile in the thin Al catchers were compared with the SRIM code. The observed incomplete fusion events can be explained on the basis of the breakup of the projectile viz.  $^{14}\text{N} \rightarrow ^8\text{Be}$  and/or  $^4\text{He}$ , where  $^8\text{Be}$  and/or  $^4\text{He}$  fuses with  $^{169}\text{Tm}$  target and transfers the partial linear momentum to the target nucleus. The present data clearly indicates that the evaporation residues were not only populated through complete fusion, but incomplete fusion also plays an important role at low projectile energy.

**Keywords:** Recoil range distribution, Complete and incomplete fusion dynamics, Heavy ion collision, Catcher stack foil activation technique, Off-line gamma spectroscopy

## 1 Introduction

Heavy-ion (HI) induced fusion reactions are a direct and known method to study the properties of nuclei. A complete understanding of reaction mechanism in HI-induced reaction has always been an interesting area of research. In last few years, incomplete fusion (ICF) in addition to complete fusion (CF) has emerged in HI-induced reactions above the Coulomb barrier having projectile laboratory energy ( $E_{\text{lab}}$ ) around 4–7 MeV/nucleon<sup>1-4</sup>. In CF reactions, complete amalgamation of projectile with the target nucleus occurs, while in the case of ICF reactions partial fusion of projectile takes place<sup>4</sup>. The highly excited composite system formed via complete and/or partial fusion of the projectile de-excites by evaporating low energy nucleons followed by the decay of  $\gamma$ -rays. The ICF reactions were first observed by Britt and Quinton during the experimental studies of heavy ion ( $^{12}\text{C}$ ,  $^{14}\text{N}$ ,  $^{16}\text{O}$ ) induced reactions with targets  $^{197}\text{Au}$  and  $^{209}\text{Bi}$  at projectile energy  $\approx 7 - 10$  MeV/nucleon<sup>5</sup>. Later, Inamura *et al.*<sup>6</sup> performed a series of experiments using particle- $\gamma$ -coincidence technique. In these

experiments, they observed the spin distribution of evaporation residues (ERs) populated through ICF process behave differently from those populated through CF process.

To understand ICF reaction dynamics, a variety of dynamical models have been proposed viz. Breakup fusion (BUF)<sup>7</sup>, Sum rule<sup>8</sup>, promptly emitted particle model (PEP)<sup>9</sup> etc. However, most of the acceptable descriptions are based on the BUF and sum rule model. In the BUF model, Udagawa and Tamura *et al.*<sup>7</sup> suggested ICF as a two step process, according to which the incident projectile breaks up into its fragments in the vicinity of the target nucleus. One of the fragments may fuse with the target nucleus to form an incompletely fused composite system, and the remnant moves at forward angle with nearly projectile velocity. Contrary to this, Wilczynski *et al.*<sup>8</sup> in their sum rule model describe CF and ICF process on the basis of input angular momentum of the projectile ( $\ell$ -values). For the lower values,  $\ell \leq \ell_{\text{crit}}$ , the CF process is dominant, while for  $\ell \geq \ell_{\text{crit}}$ , the ICF process also comes in to the picture. In the case of  $\ell \geq \ell_{\text{crit}}$ , fusion pocket in potential energy curve is not sufficient enough to capture the entire projectile until a part of the projectile is released to provide sustainable input angular

\*Corresponding author (E-mail: rakuiiac@gmail.com)

**Development and optimization of nanoemulsion based gel for enhanced transdermal delivery of nitrendipine using box-behnken statistical design**

Abhishek sharma<sup>a\*</sup>, A.P. Singh<sup>b</sup>, S.L. Harikumar<sup>c</sup>

<sup>a</sup> *Research scholar, I.K. Gujral Punjab Technical University, Jalandhar, Punjab, India*

<sup>b</sup> *Research Innovation and consultancy, I.K. Gujral Punjab Technical University, Jalandhar, Punjab, India*

<sup>c</sup> *Central university of Jharkhand, Ranchi, India*

To whom correspondence should be addressed: Abhishek sharma\*, Department of Pharmaceutics, I.K. Gujral Punjab Technical University, Jalandhar-Kapurthala Highway, VPO-Ibban, Kapurthala-144603, Punjab, India. Email id- abhideeps21@gmail.com, Tel.: 9418859600

**Development and optimization of nanoemulsion based gel for enhanced transdermal delivery of nitrendipine using box-behnken statistical design**

**ABSTRACT**

**Objective:** The purpose of present research was to develop and statistically optimize nitrendipine nanoemulsion gel for transdermal delivery using box-behnken statistical design.

**Method:** The nanoemulsion formulations bearing nitrendipine were prepared by application of ternary phase diagram and spontaneous emulsification method. Box-behnken design was employed for the optimization of nitrendipine loaded nanoemulsion. The independent variables were oil, surfactant and co-surfactant while globule size, drug content and zeta potential were dependent variables. The optimized nanoemulsion formulation was incorporated into gel and evaluated for *in-vitro* release, *ex-vivo* permeation studies, confocal laser scanning microscopy, skin irritation and histopathological studies.

**Results:** The optimized formulation through box-behnken statistical design showed globule size of  $20.43 \pm 1.50$  nm, drug content of  $97.05 \pm 1.77$  % and zeta potential of  $-15.45 \pm 0.35$  mV. The *ex-vivo* study confirmed the enhanced delivery of nitrendipine from nanoemulsion gel than compare to drug solution by virtue of better permeation and solubility. Nanoemulsion gel was proved significantly superior by confocal laser scanning microscopy for satisfactory permeation and distribution of gel, deep into the rat skin. The optimized gel was found with no allergic dermal effects and was proved safe by histopathological studies for transdermal application.

**Conclusions:** Results reveals that developed nitrendipine nanoemulsion gel overcomes the limitation of low penetration and accentuate permeation through albino Wistar rat skin. It was



## Signature of incomplete fusion reaction in $^{20}\text{Ne} + ^{159}\text{Tb}$ system: Entrance channel parameters effect

Rahbar Ali<sup>a\*</sup>, D Singh<sup>b</sup>, Harish Kumar<sup>c</sup>, Suhail A Tali<sup>c</sup>, M Afzal Ansari<sup>c</sup> & M H Rashid<sup>d</sup>

<sup>a</sup>Department of Physics, G F (PG) College, Shahjahanpur 242 001, India

<sup>b</sup>Department of Physics, Central University of Jharkhand, Ranchi 835 205, India

<sup>c</sup>Department of Physics, Aligarh Muslim University, Aligarh 202 002, India

<sup>d</sup>Variable Energy Cyclotron Centre, 1/AF, Bidhan Nagar, Kolkata 700 064, India

Received 8 April 2019

More complex and interesting phenomenon of incomplete fusion (ICF) reactions induced by  $^{20}\text{Ne}$  on  $^{159}\text{Tb}$  have been measured at several beam energies range of 4.3 - 8.2 MeV/A by using catcher foil technique followed by the gamma-ray spectrometry. The cumulative cross-sections of evaporation residues produced in above reaction have been measured and deduced independent cross-sections have been compared with statistical model based computer code PACE-2. The complete fusion (CF) channels pxn agrees well with PACE-2 predictions after the subtraction of precursor contribution. The alpha emission products show higher cross-section than that predicted by the complete fusion product, which is attributed to the presence of incomplete fusion of projectile with target at lower energies. This enhancement in the measured cross-section is attributed to the fact that these residues are formed not only by complete fusion but also through the ICF of  $^{20}\text{Ne}$  into  $\alpha$  clusters, i.e.,  $^{20}\text{Ne}$  into  $^{16}\text{O} + \alpha$  and/or  $^{12}\text{C} + 2\alpha$  etc. For the better understanding of ICF, the incomplete fusion fraction has also been deduced and its sensitivity with various channel parameters like projectile energy, entrance channel mass-asymmetry,  $\alpha$ -Q value, Coulomb effect ( $Z_p Z_T$ ), deformation parameter ( $\beta_2$ ) have been observed.

**Keywords:** Complete and incomplete fusion reactions, Excitation function measurements, Mass-asymmetry, Projectile structure effect,  $\alpha$ -Q-value systematic

### 1 Introduction

In the last couple of years, study of the heavy ion induced reaction has raised the new interest especially about the complete fusion (CF) and incomplete fusion (ICF) at energies near the vicinity of coulomb barrier<sup>1-4</sup>. For energy of the projectile increases to well above the coulomb barrier, CF and ICF are dominant modes of the reaction. At large value of impact parameter, ions elastically or inelastically are scattered by the coulomb field. If impact parameter is progressively reduced, direct reaction takes place associated few nucleon transfers from projectile to target and vice versa. Moreover, impact parameter is further reduced, CF and ICF are the dominant modes of the reaction mechanism. It has been observed that at energies above the Coulomb barrier<sup>5</sup>, CF and ICF are considered as the dominant reaction mechanisms. In the CF-reaction, nuclear field is too strong to hold all the nucleonic degree of the freedom with target nucleus, forms the excited composite system, which

statistically decays by particle and/ or gamma emission. However in case of ICF, nuclear field is no longer hold to involve all the nucleonic degree of freedom of projectile and supposed to be break up into the fragments (for e.g.,  $^{20}\text{Ne}$  is break-up into  $^{16}\text{O}$  and  $\alpha$ -particle;  $^8\text{Be}$  and  $^{12}\text{C}$  etc.) and one of the fragments fuses with the target nucleus while remnant part of the projectile moves as a spectator in the forward direction. This outgoing particle is called projectile like fragments (PLFs). The PLFs were first observed by Britt and Quinton<sup>6</sup> as the breakup of projectile like,  $^{12}\text{C}$ ,  $^{14}\text{N}$  and  $^{16}\text{O}$  in an interaction of projectile with the surface of target nucleus. More experimental evidence for ICF was found by Inamura *et al.*<sup>7</sup> by measurement of forward peaked alpha particles in coincidence with prompt gamma rays. The study of entrance channel mass-asymmetry dependence of ICF by measuring the velocity spectra of residues in different mass-asymmetric systems were done by Morgenstern *et al.*<sup>8,9</sup> and Chakrabarty *et al.*<sup>4</sup>. Their study shows that more mass-asymmetric system has higher ICF contribution than that of

\*Corresponding author (E-mail: rahbara@gmail.com)

## Signature of incomplete fusion reaction in $^{20}\text{Ne} + ^{159}\text{Tb}$ system: Entrance channel parameters effect

Rahbar Ali<sup>a\*</sup>, D Singh<sup>b</sup>, Harish Kumar<sup>c</sup>, Suhail A Tali<sup>c</sup>, M Afzal Ansari<sup>c</sup> & M H Rashid<sup>d</sup>

<sup>a</sup>Department of Physics, G F (PG) College, Shahjahanpur 242 001, India

<sup>b</sup>Department of Physics, Central University of Jharkhand, Ranchi 835 205, India

<sup>c</sup>Department of Physics, Aligarh Muslim University, Aligarh 202 002, India

<sup>d</sup>Variable Energy Cyclotron Centre, 1/AF, Bidhan Nagar, Kolkata 700 064, India

Received 8 April 2019

More complex and interesting phenomenon of incomplete fusion (ICF) reactions induced by  $^{20}\text{Ne}$  on  $^{159}\text{Tb}$  have been measured at several beam energies range of 4.3 - 8.2 MeV/A by using catcher foil technique followed by the gamma-ray spectrometry. The cumulative cross-sections of evaporation residues produced in above reaction have been measured and deduced independent cross-sections have been compared with statistical model based computer code PACE-2. The complete fusion (CF) channels pxn agrees well with PACE-2 predictions after the subtraction of precursor contribution. The alpha emission products show higher cross-section than that predicted by the complete fusion product, which is attributed to the presence of incomplete fusion of projectile with target at lower energies. This enhancement in the measured cross-section is attributed to the fact that these residues are formed not only by complete fusion but also through the ICF of  $^{20}\text{Ne}$  into  $\alpha$  clusters, i.e.,  $^{20}\text{Ne}$  into  $^{16}\text{O} + \alpha$  and/or  $^{12}\text{C} + 2\alpha$  etc. For the better understanding of ICF, the incomplete fusion fraction has also been deduced and its sensitivity with various channel parameters like projectile energy, entrance channel mass-asymmetry,  $\alpha$ -Q value, Coulomb effect ( $Z_p Z_T$ ), deformation parameter ( $\beta_2$ ) have been observed.

**Keywords:** Complete and incomplete fusion reactions, Excitation function measurements, Mass-asymmetry, Projectile structure effect,  $\alpha$ -Q-value systematic

### 1 Introduction

In the last couple of years, study of the heavy ion induced reaction has raised the new interest especially about the complete fusion (CF) and incomplete fusion (ICF) at energies near the vicinity of coulomb barrier<sup>1-4</sup>. For energy of the projectile increases to well above the coulomb barrier, CF and ICF are dominant modes of the reaction. At large value of impact parameter, ions elastically or inelastically are scattered by the coulomb field. If impact parameter is progressively reduced, direct reaction takes place associated few nucleon transfers from projectile to target and vice versa. Moreover, impact parameter is further reduced, CF and ICF are the dominant modes of the reaction mechanism. It has been observed that at energies above the Coulomb barrier<sup>5</sup>, CF and ICF are considered as the dominant reaction mechanisms. In the CF-reaction, nuclear field is too strong to hold all the nucleonic degree of the freedom with target nucleus, forms the excited composite system, which

statistically decays by particle and/ or gamma emission. However in case of ICF, nuclear field is no longer hold to involve all the nucleonic degree of freedom of projectile and supposed to be break up into the fragments (for e.g.,  $^{20}\text{Ne}$  is break-up into  $^{16}\text{O}$  and  $\alpha$ -particle;  $^8\text{Be}$  and  $^{12}\text{C}$  etc.) and one of the fragments fuses with the target nucleus while remnant part of the projectile moves as a spectator in the forward direction. This outgoing particle is called projectile like fragments (PLFs). The PLFs were first observed by Britt and Quinton<sup>6</sup> as the breakup of projectile like,  $^{12}\text{C}$ ,  $^{14}\text{N}$  and  $^{16}\text{O}$  in an interaction of projectile with the surface of target nucleus. More experimental evidence for ICF was found by Inamura *et al.*<sup>7</sup> by measurement of forward peaked alpha particles in coincidence with prompt gamma rays. The study of entrance channel mass-asymmetry dependence of ICF by measuring the velocity spectra of residues in different mass-asymmetric systems were done by Morgenstern *et al.*<sup>8,9</sup> and Chakrabarty *et al.*<sup>4</sup>. Their study shows that more mass-asymmetric system has higher ICF contribution than that of

\*Corresponding author (E-mail: rahbara@gmail.com)

## Study of break-up fusion process from forward recoil range distribution measurement

Harish Kumar<sup>a\*</sup>, Suhail A Tali<sup>a</sup>, M Afzal Ansari<sup>a</sup>, Rahbar Ali<sup>b</sup>, D Singh<sup>c</sup>, Naseef M P N<sup>a</sup>, R Kumar<sup>d</sup>,  
K S Golda<sup>d</sup>, R P Singh<sup>d</sup> & S Muralithar<sup>d</sup>

<sup>a</sup>Department of Physics, Aligarh Muslim University, Aligarh 202 002, India

<sup>b</sup>Department of Physics, Gandhi Faiz-E-Aam College, Shahajhanpur 242 001, India

<sup>c</sup>Department of Physics, Central University of Jharkhand, Ranchi 835 205, India

<sup>d</sup>Nuclear Physics Group, Inter University Accelerator Centre, New Delhi 110 067, India

*Received 8 April 2019*

In the present work, the break-up fusion or incomplete fusion (ICF) process has been studied from the forward recoil range distribution measurement for  $^{16}\text{O} + ^{175}\text{Lu}$  system at  $\approx 96$  MeV energy. The measured forward recoil range distributions are analyzed in the framework of code SRIM. The present analysis shows clearly the role of linear momentum transfer and also the break-up of projectile  $^{16}\text{O}$  into its fragments ( $^{12}\text{C} + ^4\text{He}$  and/or  $^8\text{Be} + ^8\text{Be}$ ). Any systematic trend is not observed with the target deformation parameter ( $\beta_2$ ) dependent study of ICF. It is observed that projectile structure also affects the ICF dynamics. The projectile  $\alpha$ -Q-value is found to be a suitable parameter which explains effectively the observed projectile structure effect on ICF.

**Keywords:** Incomplete fusion, Activation technique, Linear momentum transfer, Target deformation, Projectile  $\alpha$ -Q-value

### 1 Introduction

The projectile break-up or incomplete fusion (ICF) reaction dynamics has been a subject of experimental and theoretical interest in heavy-ion (HI) induced reactions. In last few years, considerable experimental efforts are made to understand and explore the ICF process at energies above the Coulomb barrier and well beyond it<sup>1-3</sup>. Different fusion processes may take place in the collisions of heavy ions (HIs) at these energies. The direct complete fusion (DCF) is one of the possible reaction modes, where the projectile fuses entirely with the target nucleus. In addition to this the projectile may also break-up into its fragments near the target nuclear field. The sequential complete fusion (SCF) may take place, when all the fragments fuse with the target one after the other. On the other hand, the fusion of only one fragment with the target, leads to the ICF process and in case of non capture break-up process, both the break-up fragments may escape without getting fused with the target nucleus. Moreover, in ICF process, the projectile partially fuses with the target nucleus as compared to the CF process, leading to the formation of incompletely fused composite (IFC)

system with less mass, excitation energy and charge. Owing to the partial linear momentum transfer (LMT), the ICF products traverse the shorter path in the stopping medium than that of CF products. Britt and Quinton<sup>4</sup> first time pointed out the experimental features of ICF in the break-up of projectiles like  $^{12}\text{C}$ ,  $^{14}\text{N}$ , and  $^{16}\text{O}$  into  $\alpha$ -clusters. The additional but concrete information for the ICF was provided by Inamura *et al*<sup>5</sup>. The CF and the ICF processes are also categorized on the basis of imparted angular momentum ( $\ell$ ) into the system. The ICF process is assumed to exist only for  $\ell$  values greater than critical angular momentum values ( $\ell_{crit}$ ). A substantial contribution of ICF below  $\ell_{crit}$  has also been observed in recent studies<sup>6-9</sup>. Apart from this, the effect of projectile structure on the ICF process has also been observed<sup>10</sup>. However, several theoretical models<sup>11-13</sup> have been proposed to explain the ICF process but none of them is available to reproduce the experimental ICF data satisfactorily below 10 MeV/nucleon energies, which makes the ICF study still a relevant problem. The mass transferred from projectile to the target also adds the complexity in the study of ICF.

\*Corresponding author (E-mail: amu.harish@gmail.com)

## Incomplete momentum transfer in $^{16}\text{O} + ^{148}\text{Nd}$ system [at energy $\approx 5.8$ MeV/nucleon]

Pankaj K Giri<sup>a</sup>, Amritraj Mahato<sup>a</sup>, D Singh<sup>a\*</sup>, Sneha B Linda<sup>a</sup>, Harish Kumar<sup>b</sup>, Suhail A Tali<sup>b</sup>, R Ali<sup>c</sup>, N P M Sathik<sup>d</sup>, M Afzal Ansari<sup>b</sup>, R Kumar<sup>e</sup>, S Muralithar<sup>e</sup> & R P Singh<sup>e</sup>

<sup>a</sup>Department of Physics, Central University of Jharkhand, Ranchi 835 205, India

<sup>b</sup>Department of Physics, Aligarh Muslim University, Aligarh 202 002, India

<sup>c</sup>Department of Physics, G F (P G) College, Shahjahanpur 242 001, India

<sup>d</sup>Department of Physics, Jamal Mohammed College, Tiruchirappalli 620 020, India

<sup>e</sup>Inter University Accelerator Centre, Aruna Asaf Ali Marg, New Delhi 110 067, India

Received 3 July 2019

Measurements of the forward recoil ranges of the evaporation residues  $^{159,158}\text{Er}$  (xn),  $^{160g,159}\text{Ho}$  (pxn),  $^{157,155}\text{Dy}$  ( $\alpha$ xn) and  $^{155}\text{Tb}$  ( $\alpha$ pxn) formed in the interaction of  $^{16}\text{O}$  with  $^{148}\text{Nd}$  at energy  $\approx 5.8$  MeV/nucleon have been done. Measured forward recoil range distributions of these evaporation residues show population of several incomplete fusion channels in addition to complete fusion. The entire and incomplete linear momentum transfers inferred from these recoil range distributions have been used to identify the evaporation residues populated through complete and incomplete fusion dynamics. The forward recoil range distributions of evaporation residues populated via  $\alpha$ -emission channels show two composite peaks, one associated with complete fusion and other peak corresponds to the incomplete fusion. Further, the relative contributions of CF and/or ICF components have also been separated out from the present measurements. The contribution of ICF channels has been found to be  $\approx 9\%$  of total fusion. The present results clearly indicate the presence of break-up of the projectile  $^{16}\text{O}$  into  $^{12}\text{C} + \alpha$  at low projectile energy.

**Keywords:** Complete and incomplete fusion, Composite system, Offline  $\gamma$ -ray spectrometry, Recoil catcher activation technique, Recoil range distributions

### 1 Introduction

The dominant modes of heavy ion interactions are compound nucleus (CN) and direct reactions at projectile energies close to Coulomb barrier. The probability of formation of compound nucleus gets hindered with increasing the projectile energy and incomplete fusion (ICF) starts dominating with complete fusion (CF). In ICF reactions, only a part of the projectile fuses with the target while the remaining part moves at forward angles with approximately same velocity of projectile. A schematic diagram of CF and ICF reactions is shown in Fig. 1. These reactions were first observed experimentally by Britt and Quinton<sup>1</sup> and Galin *et al.*<sup>2</sup>. Later on, remarkable studies based on particle-gamma coincidence technique by Inamura *et al.*<sup>3</sup> contributed a lot to understand the dynamics of ICF reactions. Various dynamical models have been proposed to explain the mechanism of ICF reactions.

In the sum rule model of Wilczynski *et al.*<sup>4</sup>, ICF is considered as arising from peripheral collisions in the angular momenta range just above the critical angular momentum ( $\ell_{crit}$ ) for CF. Udagawa & Tamura<sup>5</sup> explained ICF as breakup of the projectile followed by fusion of one of the fragments with the target. The promptly emitted particle (PEP) model<sup>6</sup>, hot spot model<sup>7</sup>, multistep direct reaction model<sup>8</sup>, etc., are also some of the widely used theoretical models. All these models have been used to reproduce the experimental data at energy above 10 MeV/nucleon. There are many important aspects of ICF reactions at low projectile energy that should be clarified such as, how the ICF dynamics depends on various entrance channel parameters and the angular momenta involved in these reactions. Morgenstern *et al.*<sup>9</sup> have reported that ICF is more dominant for more mass asymmetric system at same relative velocity. Several investigators have made efforts to understand the role

\*Corresponding author (E-mail: dsinghcuj@gmail.com)

## Study of incomplete fusion dynamics on various entrance channel parameters

Sneha B Linda<sup>a</sup>, Pankaj K Giri<sup>a</sup>, D Singh<sup>a\*</sup>, Amritraj Mahato<sup>a</sup>, Harish Kumar<sup>b</sup>, Suhail A Tali<sup>b</sup>, M Afzal Ansari<sup>b</sup>,  
R Kumar<sup>c</sup>, S Muralithar<sup>c</sup> & R P Singh<sup>c</sup>

<sup>a</sup>Department of Physics, Central University of Jharkhand, Ranchi 835 205, India

<sup>b</sup>Department of Physics, Aligarh Muslim University, Aligarh 202 002, India

<sup>c</sup>Inter University Accelerator Centre, Aruna Asaf Ali Marg, New Delhi 110 067, India

Received 8 April 2019

The present work has been carried out to understand the dynamics of incomplete fusion reactions and its dependency on various entrance channel parameters at low projectile energy. The excitation functions of evaporation residues  $^{137,135,133}\text{Ce}$  ( $xn$ ),  $^{133}\text{La}$  ( $pxn$ ),  $^{133m,131m,129}\text{Ba}$  ( $\alpha xn$ ),  $^{135m,132}\text{Cs}$  ( $\alpha pxn$ ),  $^{131m}\text{Xe}$  ( $2\alpha xn$ ) and  $^{131}\text{I}$  ( $2\alpha pxn$ ) have been measured for the system  $^{16}\text{O} + ^{124}\text{Sn}$  at projectile energy  $\approx 3-7$  MeV/nucleon. The analysis of measured excitation functions have been done within the framework of statistical model code PACE-4. The incomplete fusion fraction ( $F_{\text{ICF}}$ ) has been deduced from present measurements for the study of systematics. Two new combined parameters  $\left(\frac{1-\beta_2}{Z_p Z_T}\right)$  and  $\left(\frac{1-\beta_2}{\mu_{EC}^{AS}}\right)$  have been introduced as a combination of the entrance

channel parameters mass-asymmetry ( $\mu_{EC}^{AS}$ ), coulomb factor ( $Z_p Z_T$ ) and deformation parameter ( $\beta_2$ ) of target. The present study shows that incomplete fusion fraction decreases independently for different projectiles with increase in these parameters. These combined parameters can explain the characteristics of incomplete fusion dynamics more clearly as compared to individual entrance channel parameters at these energies. These present results suggest that the incomplete fusion dynamics can be better explained by combined effects of entrance channel parameters than that of their individual effects.

**Keywords:** Heavy ion induced reactions, Complete and incomplete fusion, Excitation functions, Stacked foil activation technique, Incomplete fusion fraction

### 1 Introduction

The study of heavy ion (HI) induced reactions has been a topic of growing interest for researchers with the availability of heavy ion accelerator facilities. The complete (CF) and incomplete fusion (ICF) are the two dominant reaction modes of heavy ion collisions at projectile energy above the coulomb barrier<sup>1,4</sup>. The ICF reactions were first observed experimentally by Britt & Quinton<sup>5</sup> in their pioneering work. Later on Inamura *et al.*<sup>6</sup> provided the remarkable information of ICF dynamics by the measurement employing charged particle- $\gamma$  coincidence technique. Semiclassically, the CF and ICF processes in HIs interaction can be categorized on the basis of different values of driving input angular momenta ( $\ell$ ) imparted in the system. According to the sharp cutoff approximation<sup>7,8</sup>, the driving input angular momentum " $\ell$ " is distributed in the range  $0 \leq \ell \leq \ell_{crit}$  in the CF process. However, for the projectile incident on target with relatively higher value of energy and impact parameter, only a part of the projectile fuses with the target nucleus and

remnant projectile behaves as a spectator, wherein an incompletely fused composite system may be formed and ICF process may take place. In ICF process, the involvement of driving input angular momentum  $\ell$  is relatively larger than that of CF process. At this stage if the driving input angular momentum exceeds the critical limit ( $\ell_{crit}$ ) for CF i.e.,  $\ell > \ell_{crit}$ , no fusion can occur unless a part of the projectile is emitted to release excess driving input angular momentum. In recent years, several investigators have studied the dependence of ICF dynamics on various entrance channel parameters<sup>9-11</sup>. Their study shows that the ICF dynamics depends on various entrance channel parameters. Apart from experimental studies, various theoretical models have been proposed to explain ICF dynamics *viz.* SUMRULE<sup>12</sup>, Break-up fusion (BUF)<sup>13</sup>, Promptly emitted particles (PEPs)<sup>14</sup>, Hot spot<sup>15</sup>, Fermi-jet<sup>16</sup>, Exciton model<sup>17</sup> etc. These theoretical models have been used to fit the experimental data of ICF at projectile energy above 10 MeV/nucleon. However, as such no model exists to reproduce the experimental data at projectile energy below 7 MeV/nucleon.

\*Corresponding author (E-mail: dsinghcuj@gmail.com)

# On the fate of quarkonia in quark gluon plasma medium within a Quasi-particle model

Vineet Kumar Agotiya\* & Indrani Nilima

Department of Physics, Central University of Jharkhand, Ranchi 835 205, India

*Received 8 April 2019*

We work on equations of state for hot QCD obtained from a hard thermal loop expression for the gluon self-energy, by employing the quasi-parton equilibrium distribution functions. The method involves mapping the interaction part of the equation of state to an effective fugacity of otherwise non-interacting quasi-gluons. Using the quasi-gluon distribution function, we have studied the dissociation of heavy Quarkonium in hot QCD medium by investigating the medium modification to a heavy quark potential. Employing the in-medium (corrected) potential while considering the anisotropy (both oblate and prolate cases) in the medium, the thermal widths and the binding energies of the heavy quarkonia states (s-wave charmonia and s-wave bottomonia specifically, for radial quantum numbers  $n=1$  and  $2$ ) have been determined. In the present article, we shall consider an anisotropic QGP medium which is described in terms of quasi-particle degree of freedom based on a recent proposed quasi-particle model for hot QCD equation of state. The presence of anisotropy makes the real-part of the potential stronger but the imaginary-part is weakened slightly. However, since the medium corrections to the imaginary-part is a small perturbation to the vacuum part, overall the anisotropy makes the dissociation temperatures higher, compared to isotropic medium.

**Keywords:** Debye mass, Quasi-parton, Effective fugacity, Momentum anisotropy, Decay width, Heavy quarkonia, Inter-quark potential

## 1 Introduction

In the era of the relativistic heavy ion collider at Brookhaven and the large hadron collider at CERN the theoretical understanding of in-medium modifications of QCD bound states is expected to progress significantly. In this paper we focus on the properties of bound states of heavy quarks (quarkonia) in anisotropic plasma.

Following our recent work on dissociation of heavy quarkonia, within quasi-particle approach, for the isotropic medium in earlier study<sup>1</sup>, the present analysis accommodates the presence of local momentum anisotropy to estimate the dissociation temperature of heavy quarkonia. While considering the momentum anisotropy, both the oblate and the prolate situation have been taken into account and compared with the isotropic one. The motivation to incorporate the anisotropy in the study of quarkonia suppression comes from the fact that, the QGP produced in heavy ion (off-central) collisions does not possess isotropy. Instead, the momentum anisotropy is present in all the stages of the heavy-ion collisions, and hence, the inclusion of the anisotropy is inevitable. There are many articles present<sup>2,3</sup>, where

the impact of the anisotropy in various observables of QGP has been investigated. In most of these studies, the ideal Bose/Fermi distributions<sup>4</sup>, have been considered in a combination to define the distribution function in isotropic medium.

Here, we attempt to assess the properties of quarkonium states in a QCD plasma which exhibits an anisotropy in momentum space. Such anisotropy may arise due to a locally anisotropic hydrodynamic expansion of a plasma with non-vanishing shear viscosity. It leads to an angular dependence of the  $Q\bar{Q}$  potential<sup>3</sup>.

The effects of anisotropy will modify the in-medium potential and, in turn, significantly revise the values of dissociation temperature. In the oblate case, the dissociation temperature has observed to be higher than the isotropic case. While in the prolate case, it is observed to be the least among the three cases. The tightly bound ground state has higher binding energies and is expected to melt later than the excited state and hence, they must have a sequential suppression pattern with temperature. The order observed in the present analysis supports the above fact as,  $Y'$  ( $2s$ -state of  $b\bar{b}$ ), has been suppressed at smaller temperature than the  $Y$  ( $1s$ -state of  $b\bar{b}$ ), for all

\*Corresponding author (E-mail: agotiya81@gmail.com)



## Low energy ion beam study on Co/CoO thin films

Deepak Kumar & A S Bhattacharyya\*

Department of Nano Science and Technology, Central University of Jharkhand, Brambe 835 205, India

Computer simulation using SRIM software has been done for ion beam irradiation of different metal ions on Co/CoO thin film which is an FM/AFM system. The films have been experimentally deposited by magnetron sputtering and subjected to low energy ion beams (LEIB) of different energies and fluences. The variation of Si ion energy led to different ion distribution profiles which could be correlated with the morphological changes like dewetting occurring at the surface. Such phenomenon is potentially important for making spintronic devices in future.

**Keywords:** Low energy ion beam (LEIB), FM/AFM system, SRIM, Dewetting

### 1 Introduction

Ion beam irradiation is an effective means of studying the morphological changes occurring in thin films. Surface energy changes as well as displacement of atoms due to localized heating can bring about interesting phenomena which can lead to possible patterning and device fabrication in the future. Film thickness and temperature affect the Co nanoparticles size and uniformity formed by dewetting. Co films have been found to undergo dewetting on annealing. These Magnetic metal nanoparticle arrays are used in magnetic recording and carbon or semiconductor nanotubes. Other means of obtaining patterned nanoparticle arrays are by lithography, spin-coating, droplet drying, dip-coating, or LB methods<sup>1,2</sup>.

### 2 Experimental Details

Co/CoO thin films were deposited by magnetron sputtering. Thickness of each film was 25 nm. The films were then irradiated with Si and Ar ions at different fluences and energies. Scanning electron microscopy (SEM) and magnetic force microscopy (MFM) measurements were performed to study the changes in morphology and magnetic structure that occurred with the irradiation while SQUID and PPMS measurements were performed to study temperature and magnetic field dependence of dc magnetization.

### 3 Results and Discussion

Due to Si ion irradiation at 50 keV on the Co/CoO sample, the phenomenon of ion-beam-induced

dewetting occurred. Due to larger surface free energy of Co compared to CoO, globule-like structures, as shown in the SEM image Fig. 1, have formed. This phenomenon resulted in the loss of connectivity between the different regions and as a result the ferromagnetic property got lost and the Co clusters act as separate entities with no interaction between each other. The phenomenon known as ion-beam-induced dewetting. Superparamagnetism was observed for Co/CoO films, which were irradiated with 200 keV Ar ions at a fluence of  $10^{15}$  ions/cm<sup>2</sup>. Blocking temperature around 300 K was obtained from the measured ZFC-FC magnetization<sup>3,4</sup>.

Simulation studies using SRIM was done with Si (27.977 amu) ions of 40 keV energy irradiated on Co/CoO bilayers of thickness 100 Å each as shown in

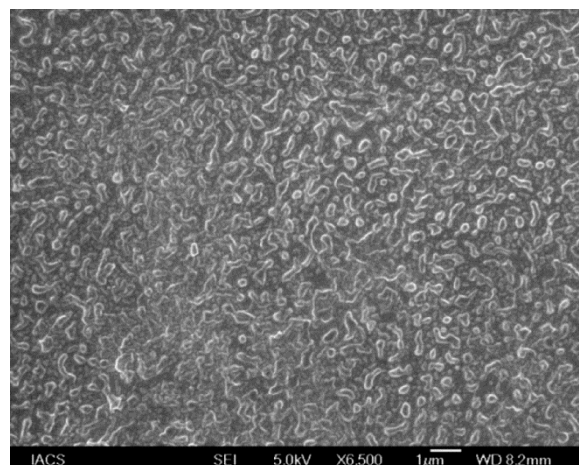


Fig. 1 – SEM image of ion beam induced dewetting caused by Si ions on Co/CoO bilayer<sup>4</sup>.

\*Corresponding author (E-mail: arnab.bhattacharya@cuja.ac.in)

## Pre-equilibrium particle emission in alpha induced reactions

D Singh<sup>a\*</sup>, Aditya Maurya<sup>a</sup>, Pankaj K Giri<sup>a</sup>, Amritraj Mahato<sup>a</sup>, Sneha B Linda<sup>a</sup>, Pramod K Shrotriya<sup>b</sup> & M Afzal Ansari<sup>c</sup>

<sup>a</sup>Department of Physics, Central University of Jharkhand, Ranchi 835 205, India

<sup>b</sup>KSRMV Inter College, Atrauli, Aligarh 202 280, India

<sup>c</sup>Department of Physics, Aligarh Muslim University, Aligarh 202 002, India

Received 3 July 2019

Study of the mechanism of pre-equilibrium particle emission in alpha particle induced reactions has been done in the present work. The cross-sections for systems  $\alpha + {}^{144}\text{Sm}$  and  $\alpha + {}^{154}\text{Sm}$  have been calculated using the statistical model code ALICE-91. Significant pre-equilibrium particle emission contribution has been obtained for these systems at higher projectile energy. At higher projectile energies, the pre-equilibrium particle emission has been found to affect predominantly over the equilibrated compound nucleus emissions. The contribution of pre-equilibrium particle emission is found larger for  $\alpha + {}^{144}\text{Sm}$  system than that of  $\alpha + {}^{154}\text{Sm}$  system. The present results indicate that the systems having spherical targets have more contribution of pre-equilibrium particle emission than that of systems with deformed targets. These results suggest that the shape of target (spherical or deformed) also affect the dynamics of pre-equilibrium particle emission at energy above the fusion barrier.

**Keywords:** Pre-equilibrium emission, Excitation functions, Pre-equilibrium fraction, Mass asymmetry, ALICE-91

### 1 Introduction

Efforts have been made to study the light and heavy ion induced reactions in the field of nuclear physics. At projectile energies of few tens of MeV,  $\alpha$ -induced reactions are generally considered to proceed through equilibrium (EQ) as well as pre-equilibrium (PE) emission of particles<sup>1</sup>. The relative contributions of these processes depend on the projectile energy and the entrance channel of the system. The contribution of PE reactions can be obtained by comparing the measured excitation functions (EFs) and theoretical predictions of statistical model codes. The PE and the compound nucleus (CN) emission reactions have been studied by several researchers in past few decades<sup>2-7</sup>. The PE emission probably arises from the collisions between individual nucleons of the target and projectile. The energy spectra of charged particles emitted in a nuclear reaction show several discrete peaks at a particular angle and high energies. Some of these peaks are well resolved. At low energy side a broad Maxwellian distribution followed by a continuum has also been observed. The Maxwellian distribution curve indicates that the particles are emitted from the equilibrated nucleus. The isolated peaks at higher energy region may be attributed to the direct reactions. The explanation of the continuum may be

attributed to some intermediate process called pre-equilibrium particle emission (PE) process<sup>8,9</sup>. It may be assumed that the pre-equilibrium particle emission proceeds through two body residual interactions inside the compound system. The pre-equilibrium particle emission may be considered as a bridge between two extreme reaction mechanisms. The pre-equilibrium particle emission process is characterized by (i) slowly descending tails of excitation functions, (ii) forward peaked angular distribution of emitted particles and (iii) relatively large number of higher energy particles than predicted by the compound nucleus mechanism. The first successful theory of such process was the exciton model. This model gives the energy distribution of the emitted particles and the angle-integrated cross-section of all the reactions. This semi-classical model also predicts the main features of the angular distributions of emitted particles. At very high energy the reaction may be studied using Monte Carlo simulation method. Presence of PE emissions at HI projectile energy slightly above the Coulomb barrier has also been noticed<sup>10</sup>. Recently, it has been observed that pre-equilibrium particle emission process may cause the emission of nuclear cluster or even fission also at moderate excitation energies<sup>11</sup>.

In the present work, statistical model code<sup>12</sup> ALICE-91 has been used to calculate the excitation functions for light ion induced reactions at energy

\*Corresponding author (E-mail: dsinghcuj@gmail.com)

## Fabrication and characterization of enriched $^{154,144}\text{Sm}$ and $^{142,148}\text{Nd}$ targets on Al-backing for nuclear physics experiments at IUAC, New Delhi, India

Pankaj K Giri<sup>a</sup>, Amritraj Mahato<sup>a</sup>, D Singh<sup>a,\*</sup>, Sneha B Linda<sup>a</sup>, Abhilash S R<sup>b</sup>, Nabendu K Deb<sup>c</sup>, G R Umaphathy<sup>b</sup>, S Ojha<sup>b</sup>, D Kabiraj<sup>b</sup> & S Chopra<sup>b</sup>

<sup>a</sup>Department of Physics, Central University of Jharkhand, Ranchi 835 205, India

<sup>b</sup>Inter University Accelerator Centre, Aruna Asaf Ali Marg, New Delhi 110 067, India

<sup>c</sup>Department of Physics, Gauhati University, Jalukbari, Guwahati 781 014, India

*Received 3 July 2019*

The enriched targets of stable isotopes  $^{154,144}\text{Sm}$  and  $^{142,148}\text{Nd}$  have been fabricated for the measurements of excitation functions and recoil range distributions studies using different heavy ion projectile at IUAC, New Delhi. These targets have been fabricated by electron gun evaporation on Al backing. A very thin capping has been applied to prevent material from getting oxidized and eventual deterioration of material itself. The enriched  $^{154,144}\text{Sm}$  and  $^{142,148}\text{Nd}$  samples have been capped by carbon and aluminium, respectively. These samples of multiple thicknesses have been prepared using a high vacuum evaporation chamber facility. The thickness and uniformity of the different samples have been measured by Rutherford backscattering spectrometry (RBS) and energy dispersive x-ray spectroscopy (EDXS). These measurements also confirm that there are no unwanted impurities in the prepared targets. Large number of sandwiched targets, more than 30, of  $^{144,154}\text{Sm}$  and  $^{142,148}\text{Nd}$  isotopes have been successfully fabricated in a single evaporation. In the present study, the sandwiched targets have been fabricated using high vacuum evaporation technique. This technique is a very useful and cost efficient method to prepare large number of thin isotopic enriched targets having oxidizing property for experimental nuclear physics.

**Keywords:** Vacuum evaporation, Thin film, Oxidized target fabrication, Rutherford backscatterings pectrometry, Energy dispersive x-ray spectroscopy

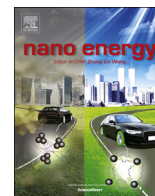
### 1 Introduction

It has been possible to study the nuclear structure and nuclear reaction dynamics in heavy ion interaction with the advancement of modern accelerators. Several modes of nuclear reactions are possible in heavy ion collisions at energy above the coulomb barrier. The complete fusion (CF) and incomplete fusion (ICF) reactions are the two dominate modes of reaction at these energies<sup>1</sup>. The first experimental evidence of ICF reactions in the break-up of the projectile at beam energy  $\sim 10.5$  MeV/nucleon was reported by Britt & Quinton<sup>2</sup>. The CF and ICF processes can be classified on the basis of driving input angular momenta ( $\ell$ ) involved during interaction of projectile with target. In the sharp cut-off approximation<sup>3</sup>, the driving input angular momentum " $\ell$ " is imparted in the range  $0 \leq \ell \leq \ell_{\text{crit}}$  for CF process. In this process, the attractive nuclear potential overcomes the repulsive Coulomb and centrifugal potentials in central and near-central collisions. As a result, at relatively lower values of energy and impact parameter, the projectile

completely fuses with the target and forms a fully equilibrated compound nucleus (CN). This CN nucleus may decay by emitting light particles. However, when projectile collide with target at relatively higher value of energy and impact parameter, the repulsive centrifugal potential increases. Hence, the attractive nuclear potential is unable to capture the entire projectile. In this condition, only a part of the projectile fuses with the target nucleus and remnant behaves as a spectator. This process is termed as incomplete fusion (ICF) or breakup fusion (BUF). It is not well established how different entrance channel parameters affect the ICF dynamics at intermediate energies. As such, this phenomenon is still an active area of investigation.

A series of experiments has been planned to perform EFs and FRRDs measurements using the alpha and non-alpha clusters ion-beam with enriched  $^{154,144}\text{Sm}$  and  $^{142,148}\text{Nd}$  targets. These studies will provide some definite conclusions about the role of various entrance channel parameters namely; mass-asymmetry of the system, coulomb factor ( $Z_P Z_T$ ), target deformation etc. on ICF dynamics. Thin targets

\*Corresponding author (E-mail: dsinghcuj@gmail.com)



Full paper

## Power-generating footwear based on a triboelectric-electromagnetic-piezoelectric hybrid nanogenerator

C. Rodrigues<sup>a,1</sup>, A. Gomes<sup>a,1</sup>, A. Ghosh<sup>a,b</sup>, A. Pereira<sup>a</sup>, J. Ventura<sup>a,\*</sup><sup>a</sup> IFIMUP-IN and Department of Physics and Astronomy, Faculty of Sciences, University of Porto, Porto, Portugal<sup>b</sup> Department of Physics, Central University of Jharkhand, Ranchi, Jharkhand, 835205, India

## ARTICLE INFO

## Keywords:

Hybridized nanogenerator  
 Triboelectric nanogenerator  
 Energy harvesting  
 Footwear & wearables

## ABSTRACT

Triboelectric nanogenerators (TENGs) are the most viable solution to harvest energy from low-frequency mechanical motions. Here, a triboelectric nanogenerator, an electromagnetic generator (EMG) and a piezoelectric nanogenerator (PENG) were hybridized and implemented inside a shoe sole to harvest energy from human walking. To optimize the TENG, we developed and studied three different structures (parallel, arched and zigzag triboelectric plates) based on the contact-separation mode and suitable to be assembled in footwear. The parallel-plate structure generated the largest electrical outputs, so that the distance between triboelectric layers and the number of tribo-pair in this configuration were also optimized. This resulted in a significant increase on the output performance of the TENG and enabled the charging of different capacitors. To further enhance energy generation properties, and through an effective conjugation of triboelectrification, electromagnetic induction and piezoelectricity, we fabricated a hybridized nanogenerator that increased 20% the charging capacity of the TENG system alone. This optimized device opens new horizons for ways to produce and store wasted energy and, in a near future, to power wireless sensors or electronic gadgets.

## 1. Introduction

There is an increasing need to monitor in real-time health or well-being parameters such as heart rate, burned calories, walked steps, blood pressure, time spent exercising or athletic performance [1–7]. To suit such demands, wearable and portable electronic devices are being developed and have attracted a large amount of attention in recent years [8–13]. However, as the number of portable and wearable electronics increases, so does the need for new and independent power sources that allow a continuous operation of these small devices. In fact, present developments in electronics are making devices increasingly smaller and operating at ultra-low power consumption, opening the possibility to power them by energy harvested from our living environment [1,13,14].

Thus, new technologies in the field of nanoenergy and energy harvesting are being researched as sustainable self-sufficient micro/nano-power sources. Various approaches for harvesting mechanical energy have been demonstrated based, for example, on piezoelectric [4,15–19], electromagnetic [20–24] and electrostatic [15,16] effects. A novel solution appeared in 2012 with the development of the first triboelectric nanogenerator (TENG) [2,25–28]. A TENG is an energy

harvesting device that converts external mechanical energy into electricity by a conjunction of contact electrification and electrostatic induction [8,12,29–32]. Contact electrification is a process that generates a charge distribution at the interface of materials that come into contact, and electrostatic induction is the main mechanism that converts mechanical energy into electricity [26,33–35]. This novel type of nanogenerators brings together high performance, efficiency, versatility, scalability, applicability and environmental friendliness [1,2,9,25,27,34,36]. In recent years, it was demonstrated that TENGs can be integrated in clothes and/or footwear and thus harvest energy from human body movements [5,8,14,22,29,37–39]. Bai et al. integrated a flexible multilayered TENG onto a shoe pad [40], while a power-generating shoe insole TENG with a multilayered zigzag-shaped structure was developed by Zhu et al. [25]. Recently, Liu et al. developed a triboelectric-electromagnetic hybrid nanogenerator that charged a 1000  $\mu\text{F}$  capacitor to 5.09 V after 100 cycles of vibration [14]. However, the optimization of the TENG configuration and corresponding hybridization for footwear applications still remains to be performed.

Here, we developed a triboelectric-electromagnetic-piezoelectric hybrid nanogenerator that can harvest energy through human walking, and that was integrated in a shoe insole. Due to its flexibility, this

\* Corresponding author.

E-mail address: [joventur@fc.up.pt](mailto:joventur@fc.up.pt) (J. Ventura).<sup>1</sup> These authors contributed equally to this work.



## Technical note

## Novel approach to recover rare earth metals (REMs) from Indian coal bottom ash



Archana Kumari<sup>a,b</sup>, Rukshana Parween<sup>c</sup>, Sanchita Chakravarty<sup>a</sup>, Kavita Parmar<sup>c</sup>,  
Devendra Deo Pathak<sup>b</sup>, Jae-chun Lee<sup>d</sup>, Manis Kumar Jha<sup>a,\*</sup>

<sup>a</sup> Metal Extraction and Recycling Division, CSIR- National Metallurgical Laboratory, Jamshedpur 831 007, India

<sup>b</sup> Department of Applied Chemistry, Indian Institute of Technology (ISM), Dhanbad 826 004, India

<sup>c</sup> Department of Environmental Sciences, Central University of Jharkhand, Ranchi 835 205, India

<sup>d</sup> Mineral Resources Research Division, Korea Institute of Geosciences & Mineral Resources (KIGAM), South Korea

## ARTICLE INFO

## Keywords:

Coal  
Coal bottom ash (CBA)  
Rare earth metals (REMs)  
Leaching  
Precipitation

## ABSTRACT

CSIR-National Metallurgical Laboratory (CSIR-NML), India dealing with coal characterization, has recently made sincere efforts to develop a process to recover REMs from Indian coal bottom ash (CBA) using hydrometallurgical route. The developed process consists of REMs leaching from CBA followed by solvent extraction and selective precipitation. After the selection of suitable leachant, bench scale studies were performed to optimize various process parameters viz. concentration of leachant, mixing time, temperature and pulp density. Maximum dissolution of REMs were achieved using 4 mol/L HCl at 90 °C for 2 h and pulp density 50 g/L. Unused acid present in the leach liquor was further extracted and subsequently processed for selective precipitation of REMs at pH 1.67. A novel process flow-sheet is proposed for the effective recovery of highly pure REMs salt. Developed process at laboratory scale has potential to be commercialized after scale-up and feasibility studies.

## 1. Introduction

Coal is a traditional fuel used for power production in developing as well as developed countries such as USA, Australia, China, India, etc. (Seredin et al., 2013). Significant amount of coal is also used in pyrometallurgical process for manufacturing iron and steel (Dai and Finkelman, 2018). Consequently, huge amount of coal bottom ash (CBA) and fly ash are being generated annually. In India, total amount of coal fly ash generated and utilized in the year 2016 and 2017 was reported to be 169.25 and 107.09 million tons, respectively ([http://www.cea.nic.in/reports/others/thermal/tcd/flyash\\_201617.pdf](http://www.cea.nic.in/reports/others/thermal/tcd/flyash_201617.pdf), n.d.). But recently, coal by-products have gathered much attention as an economic source of rare earth metals (REMs).

Worldwide utilization of REMs in highly advanced areas viz. permanent magnets, catalytic converters, batteries, etc. is consistently increasing their demand in the international market (Hower et al., 2016; Ponou et al., 2016). Moreover, exhaustion of primary ores, absence of adequate substitutes and the susceptibility of the market to supply shocks due to China's dominance in global production, has led to a scarcity of REMs around the world. Thus, to cope up with the supply and demand gap of REMs, new sources are being explored to ensure the adequate supply of REMs for future use (Dai & Finkelman, 2018; Hower

et al., 2016; Ponou et al., 2016; Peiro & Mendez, 2013). In this connection, coal by-products have emerged to be a promising alternative containing significant amount of REMs. In many coal samples, REMs concentration is reported to be equal to or higher than their average concentration available in the earth's crust (Seredin & Finkelman, 2008). REMs concentration is reported to vary between 270 and 1480 ppm in coal ash (Das et al., 2018). This divergence in REMs content might be due to improper sample collection, differences in coal geochemistry or changes in the analytical methods being utilized (Kertis & Yudovich, 2009). CBA can also serve to be a good option for REMs recovery as it is reported to contain on an average 900 ppm of light REMs and 110 ppm of heavy REMs (Hower et al., 2013).

Most of the work done reports the analytical studies to detect the presence of REMs in natural ores, minerals, solid, etc. However, a review was also made to analyze the concentration of REMs in power plant burning variety of coal samples (Hower et al., 2013). Laser-induced breakdown spectroscopy was used to detect the presence of lanthanide and actinide elements in the coal ash sample collected from 'powder river basin' (Phuoc et al., 2016). Quantitative determination of REMs in low-ash Appalachian coal was performed and found that 25% of REMs present in the feed coal was associated with the organic matter (Lin et al., 2017). Laboratory scale experiments were conducted to

\* Corresponding author.

E-mail addresses: [jclee@kigam.re.kr](mailto:jclee@kigam.re.kr) (J.-c. Lee), [mkjha@nmlindia.org](mailto:mkjha@nmlindia.org) (M.K. Jha).

<https://doi.org/10.1016/j.hydromet.2019.04.024>

Received 20 August 2018; Received in revised form 15 April 2019; Accepted 21 April 2019

Available online 22 April 2019

0304-386X/ © 2019 Elsevier B.V. All rights reserved.

# A spiral shaped regenerative microfluidic fuel cell with Ni-C based porous electrodes

Ravi Kumar Arun<sup>1</sup>  | Anjali<sup>1,2</sup> | Moumita Sardar<sup>1</sup> | Preeti Singh<sup>1,3</sup> | Bishnu Mohan Jha<sup>2</sup>  | Nripen Chanda<sup>1,3</sup>

<sup>1</sup>Material Processing and Microsystems Laboratory CSIR-Central Mechanical Engineering Research Institute, Durgapur, West Bengal, India

<sup>2</sup>Department of Energy Engineering, Central University of Jharkhand, Brambe, India

<sup>3</sup>Academy of Scientific and Innovative Research(AcSIR), New Delhi, India

## Correspondence

Ravi Kumar Arun, Material Processing and Microsystems Laboratory, CSIR-Central Mechanical Engineering Research Institute, Durgapur, West Bengal 713209, India.

Email: rarun2001@gmail.com

## Funding information

Council of Scientific and Industrial Research (CSIR); DST-Science and Engineering Research Board; Fast-Track Translational (FTT) Project, Grant/Award Number: MLP-211012; DST-SERB Project, Grant/Award Number: GAP-221112; Director, CSIR-CMERI, Durgapur

## Summary

Microchannel geometry, electrode surface area, and better fuel utilization are important aspects of the performance of a microfluidic fuel cell (MFC). In this communication, a membraneless spiral-shaped MFC fabricated with Ni as anode and C as a cathode supported over a porous filter paper substrate is presented. Vanadium oxychloride and dilute sulfuric acid solutions are used as fuel and electrolyte, respectively, in this fuel cell system. The device generates a maximum open-circuit voltage of  $\sim 1.2$  V, while the maximum energy density and current density generated from the fuel cell are  $\sim 10$  mW cm<sup>-2</sup> and  $\sim 51$  mA cm<sup>-2</sup>, respectively. The cumulative energy density generated from the device after five cycles are measured as  $\sim 200$  mW after regeneration of the fuel by applying external voltage. The spiral design of the fuel cell enables improved fuel utilization, rapid diffusive transport of ions, and in-situ regeneration of the fuel. The present self-standing spiral-shaped MFC will eliminate the challenges associated with two inlet membrane-less fuel cells and has the potential to scale up for commercial application in portable energy generation.

## KEYWORDS

energy generation, open circuit voltage, porous electrodes, spiral microfluidic fuel cell, vanadium oxychloride

## 1 | INTRODUCTION

Microfluidic-based systems have taken the lead toward the development of alternative sources for on-board energy conversion and harvesting.<sup>1</sup> Such fuel cells offer a unique advantage to generate energy by electrochemical redox reactions without the use of a physical membrane to transfer protons between the two reactants, i.e. fuel and oxidant.<sup>2</sup>

Typically, a membrane-less micro fuel cell (MFC) is equipped with a microchannel with two inlets for co-flowing of fuel and oxidant in a laminar fashion with an interface between them. This arrangement facilitates the proton transfer and simultaneously experiences redox reactions on electrodes surfaces and generate energy.<sup>3</sup>

Membraneless MFCs demonstrated in the past used various types of fuels and oxidants in microchannels.<sup>1</sup> The optimization of the channel geometry at miniaturized scale was achieved by fabrication of the channel on polydimethylsiloxane (PDMS), poly (methyl

Ravi Kumar Arun and Anjali contributed equally.



## Synthesis of porous iron – zirconium mixed oxide fabricated ethylene diamine composite for removal of cationic dye

Roshni Kumari, Soumen Dey\*

Centre for Applied Chemistry, Central University of Jharkhand, Ranchi-835205, Jharkhand, India, Tel. +91 9661399711; emails: soumen.dey@cuja.ac.in, soumdey@gmail.com (S. Dey), roshnikumari311@gmail.com (R. Kumari)

Received 23 September 2018; Accepted 4 April 2019

### ABSTRACT

Synthesis of iron-zirconium binary oxide fabricated ethylene diamine (IZBO-en) composite involved two step synthesis including mixed binary oxide synthesis followed by synthesis of binary oxide-ethylene diamine composite. Mixed binary oxide was synthesized by co-precipitation method using ammonia as neutralizing agent. Binary oxide based ethylene diamine composite was synthesized using sodium dodecyl sulfate and potassium persulfate as reagents in reaction. Yield of product was 88%. Characterization of the material was done using Fourier-transform infrared spectroscopy, scanning electron microscopy, and Brunauer–Emmett–Teller analysis. Surface area was found to be  $54.74 \text{ m}^2 \text{ g}^{-1}$ . The synthesized material was efficient for removal of cationic dye methylene blue which is known for its toxicological effects. Adsorption parameters like contact time, dose, interference and pH were studied. Maximum adsorption capacity was found to be  $242.79 \text{ mg g}^{-1}$ . Kinetic data suggested the mechanism of adsorption follows pseudo-second-order rate ( $R^2 = 0.998$ ) with a rate constant of  $2.788 \text{ mg g}^{-1} \text{ min}^{-1}$  and follows Langmuir adsorption isotherm model ( $R^2 = 0.987$ ). Thermodynamic study revealed the process to be spontaneous and feasible with large negative free energy ( $\Delta G = -9.54 \text{ kJ mol}^{-1}$ ). Column study shows a removal of  $600 \text{ ml } 2 \text{ mg L}^{-1}$  with  $1 \text{ g}$  material. Desorption was achieved with 79% regeneration in acidic medium. Real wastewater from nearby textile industry was tested and found to get decolourized with the material. In conclusion, IZBO-en can be efficiently used in detoxification of cationic dyes.

*Keywords:* Binary oxide; Ethylene diamine; SEM; Adsorption; Kinetics

### 1. Introduction

The rapid growth of population coupled with increased industrialization leads to scarcity of pure water [1]. Water contamination with organic compounds and heavy metals is becoming a serious health concern. Dyes are used in wide variety of important industries, including but not limited to: textiles, paper, pigment, paint, plastic, leather, food and beverages, cosmetic and pharmaceuticals [2]. Dyes are large complex aromatic compounds which are non-biodegradable and have carcinogenic effect [3]. Besides its detrimental effect to mankind, dyes impose serious threat

to biological processes inside water bodies as the colour of dyes prevents penetration of sunlight [4]. Hence there is a need for removal of toxicity from wastewater. Large number of treatment methods used widely for removal of toxicity [5–10]. Adsorption has proved to be of uttermost importance in recent years for wastewater treatment because of easy implementation, cost-effectiveness and simple procedures [11–15]. A wide variety of adsorbents like metal oxides [16], activated carbon [17,18], biomass [19,20], polymer, nano-silicates, nanoferrites, resins etc. were extensively used [21–27]. Polymer-based adsorbents are used worldwide for remediation of wastewater due to their high stability,

\* Corresponding author.



# A transition metal free expedient approach for the C=C bond cleavage of arylidene Meldrum's acid and malononitrile derivatives



Muthiah Suresh, Anusueya Kumari, Raj Bahadur Singh\*

Department of Chemistry, Central University of Jharkhand, Brambe, Ranchi, 835 205, India

## ARTICLE INFO

### Article history:

Received 4 July 2019

Received in revised form

16 August 2019

Accepted 29 August 2019

Available online 4 September 2019

### Keywords:

Arylidene Meldrum's acid

Arylidinemalononitrile

Oxidative C=C bond cleavage

PIDA

Oxone

## ABSTRACT

A transition metal free expedient approach for the C=C bond cleavage of electron deficient alkenes such as arylidene Meldrum's acid and malononitrile derivatives are discussed. The C=C bond of these compound were cleaved to benzoic acid in good yield at high temperature. Most importantly, with oxone in CH<sub>3</sub>CN/H<sub>2</sub>O at 45 °C or *m*-CPBA in DCM or NaClO<sub>2</sub> in THF/H<sub>2</sub>O or PIDA in THF at room temperature furnished benzaldehyde derivatives selectively in excellent yields.

© 2019 Elsevier Ltd. All rights reserved.

## 1. Introduction

Structurally diverse alkenes from natural products have been considered to be a suitable source for the synthesis of complex molecules [1]. Transforming the alkenes to carbonyls or carboxylic compounds via oxidative cleavage have greatly received the attention of chemists for their extensive application in organic chemistry [2]. Normally, the oxidative cleavage of the C=C bond is instigated by transition metal and non-metal oxidants and helps to incorporate the oxo group [3]. However, the formation of toxic by-products restricts the usage of metal oxidants. Response to such a problem is abetted to develop various sustainable approaches for cleaving the electron-rich C=C bond [4]. In 2010, Vinod et al. reported the facile approach to cleave a C=C bond of electron rich as well as electron deficient olefins by using the water-soluble in-situ generated hypervalent iodine reagent. Moorthy et al. reported the oxone mediated oxidative cleavage of various electron deficient olefins to afford the corresponding benzoic acids [5]. Like electron rich olefins, electron deficient olefins such as arylidene Meldrum's acid, malononitrile, diethyl malonate derivatives have been used in the synthesis of various synthetically important molecular scaffolds [6]. In 2001, Tsuno et al. reported that epoxidation of arylidenene

Meldrum's acid can be obtained with H<sub>2</sub>O<sub>2</sub> [7]. Similarly, McQuaid et al. showed that epoxidation of various conjugated diester can be achieved with iodosylbenzene [8]. Notably, no oxidative cleavage product of these molecules were observed. However, Caliskan et al. reported (Scheme 1) the Mn(OAc)<sub>3</sub> and Cu(OAc)<sub>2</sub> mediated unusual transformation of Meldrum's acid derivative as well as diethylmalonate derivative of naphthaldehyde to 1-naphthaldehyde [9]. In our previous report, we used the oxone for the epoxidation of styrene derivative and obtained it in good yield [10]. In turn, we attempted to the epoxidation of arylidene Meldrum's acid derivative with oxone at room temperature. Surprisingly, we found that the starting material was consumed in short time and provided selectively aldehyde as a major product. These results intrigued us to investigate oxidative cleavage reaction of electron deficient olefins of arylidene Meldrum's acid, malononitrile derivatives by using various water-soluble and insoluble oxidants [11]. Unlike styrene or cinnamates, arylidene Meldrum's acid, malononitrile and diethylmalonate derivatives exhibit highly reactive benzylic carbon which is inclined to act as a strong Michael acceptor [6]. Hence, cleaving such C=C bond needed mild conditions to selectively afford the corresponding aldehyde. Herein, mild and efficient methods for the oxidative cleavage of the electron deficient C=C bond of arylidene Meldrum's acid, malononitrile derivatives with oxidants Oxone or *m*-CPBA or NaClO<sub>2</sub> or PIDA are demonstrated.

\* Corresponding author. ,

E-mail addresses: [rajbahadur.iitb@gmail.com](mailto:rajbahadur.iitb@gmail.com), [raj.singh@cuja.ac.in](mailto:raj.singh@cuja.ac.in) (R.B. Singh).



# Differential responses of growth, photosynthesis, oxidative stress, metals accumulation and *NRAMP* genes in contrasting *Ricinus communis* genotypes under arsenic stress

Rajani Singh<sup>1</sup> · Ambuj Bhushan Jha<sup>2</sup> · Amarendra Narayan Misra<sup>1,3</sup> · Pallavi Sharma<sup>1</sup>

Received: 22 January 2019 / Accepted: 16 August 2019 / Published online: 28 August 2019  
© Springer-Verlag GmbH Germany, part of Springer Nature 2019

## Abstract

Effect of arsenate [As(V)] on biomass, photosynthetic rate, stomatal conductance, transpiration, oxidative stress, accumulation of As, Fe, Zn, Cu and Mn and expression of *NRAMP* genes was investigated in As(V) tolerant and sensitive genotypes of bioenergy crop *Ricinus communis*. As(V) treatments (100 and 200  $\mu$ M) led to significant reduction in root and leaf biomass, photosynthetic rate, stomatal conductance and transpiration in GCH 2 and GCH 4 genotypes but no significant change or increase was observed in WM and DCH 177 genotypes. No significant difference was observed in hydrogen peroxide content and lipid peroxidation in As(V)-treated tolerant genotypes compared to control, whereas these parameters enhanced significantly in As(V)-treated sensitive genotypes. GCH 2 accumulated around two times As in leaves and showed significant reduction in concentration of Zn and Mn in the leaves and roots due to 200  $\mu$ M As(V) treatment compared to WM. *NRAMP* genes are critical for uptake and distribution of essential divalent metal cations, photosynthesis and controlled production of reactive oxygen species in plants. *RcNRAMP2*, *RcNRAMP3* and *RcNRAMP5* genes showed differential expression in response to 200  $\mu$ M As(V) in GCH 2 and WM suggesting that *NRAMP* genes are associated with differential responses of WM and GCH 2 genotypes to As(V) stress.

**Keywords** *Ricinus communis* · *NRAMP* · Photosynthesis · Lipid peroxidation · Hydrogen peroxide

## Introduction

Arsenic (As), a highly toxic metalloid, is ranked as the 20th most abundant element of the Earth's crust. Although naturally present in small concentration, weathering and erosion of As-containing rocks, human activities viz. industrial waste discharge, coal combustion, mining and smelting of As-bearing ore and use of As-contaminated water for irrigation have aggravated As contamination of the soil (Masscheleyn et al. 1991; Marin et al. 1993). Plants absorb As from high As-containing soil through the roots.

From the roots, As is transported to above ground parts and can enter the food chain causing health problems to humans and animals. It is known for its severe toxic effect on all organisms and has been listed as class I carcinogen by the International Agency of Research on Cancer (IARC 1979). High amount of As deleteriously interferes with various key metabolic processes in plants resulting in poor growth, reduced yield and often death of plant (Meharg and Hartley-Whitaker 2002; Tu and Ma 2002; Gupta et al. 2009; Sharma et al. 2014).

Photosynthetic systems are highly damaged by high As concentrations (Mahdich et al. 2013; Zu et al. 2016). The effect of several abiotic stresses on photosynthetic process is linked with excessive reactive oxygen species (ROS) production (Gill and Tuteja 2010; Sharma et al. 2012). On the electron acceptor side of photosystem II (PSII), leakage of electron to molecular oxygen leads to superoxide anion production which dismutates to hydrogen peroxide ( $H_2O_2$ ) (Schröder and Åkerlund 1990).  $H_2O_2$  is then reduced to hydroxyl radical ( $OH\cdot$ ) by the non-heme iron (Pospíšil et al. 2004). On the electron donor side of PSII,  $H_2O_2$  is produced due to incomplete oxidation of water which is then reduced to hydroxyl radical by manganese (Pospíšil 2009). Release of excessive ROS in plant tissues leads

Responsible editor: Gangrong Shi

✉ Pallavi Sharma  
pallavi.sharma@cuja.ac.in

<sup>1</sup> Department of Life Sciences, Central University of Jharkhand, Brambe, Ranchi, Jharkhand 835205, India

<sup>2</sup> Crop Development Centre, Department of Plant Sciences, University of Saskatchewan, 51 Campus Drive, Saskatoon, SK S7N 5A8, Canada

<sup>3</sup> Khallikote Cluster University, Berhampur, Odisha 760001, India



# Ecological and human health risk assessment of heavy metal contamination in road dust in the National Capital Territory (NCT) of Delhi, India

Sayantee Roy<sup>1</sup> · Sanjay Kumar Gupta<sup>1</sup> · Jai Prakash<sup>1</sup> · Gazala Habib<sup>1</sup> · Kuldeep Baudh<sup>2</sup> · Mahmoud Nasr<sup>3</sup>

Received: 10 May 2019 / Accepted: 14 August 2019 / Published online: 22 August 2019  
© Springer-Verlag GmbH Germany, part of Springer Nature 2019

## Abstract

The present study was carried out to determine the contamination levels of heavy metals in road dust of the National Capital Territory of Delhi (NCT), India and its consequent effect on human and environment. The levels of heavy metals (Pb, Zn, Cu, Cr, Ni, Mn, and Fe) in 9 districts (Z1–Z9) of NCT were monitored and the corresponding human health risk was estimated. District-wise evaluation of heavy metal pollution in the road dust was performed. The mean concentrations of Pb, Zn, Cu, Ni, Cr, Mn, and Fe in the road dust samples over the study area were  $164.2 \pm 53.2$ ,  $200.7 \pm 45.3$ ,  $99.9 \pm 64.8$ ,  $24.7 \pm 5.7$ ,  $57.7 \pm 25.9$ ,  $241.4 \pm 39.8$ , and  $11113.9 \pm 1669.7$  mg kg<sup>-1</sup>, respectively. PLI showed a high pollution load in the monitored nine locations, indicating an alarming condition and the urgent need for immediate remedial actions. Ecological risk assessment depicted that a 74% risk was attributed to Pb. Hazard quotient (HQ) values indicated that ingestion was the major pathway of road dust heavy metal exposure to human beings. Hazard index values showed that there was no probable non-carcinogenic risk of the heavy metals present in the road dust of the area. Children were found vulnerable to the risks of road dust metals. The findings of this study showed the alarming status of heavy metal contamination to road dust in NCT and the associated risk to human health.

**Keywords** Road dust · Heavy metal · Health risk · Ecological risk · Delhi NCR

## Introduction

In India, the rapid growth in urbanization and industrialization has increased the risk of pollution in road areas due to dust particles (Amato et al. 2010; Shi et al. 2010). Dust is a solid particulate matter that can adsorb heavy metals and a diverse range of contaminants from various anthropogenic and natural

sources (Žibret et al. 2013; Moreno et al. 2013). Further, the particles either accumulate on roadsides and outdoor ground surfaces or re-suspend in air under certain dynamic conditions (Yongming et al. 2006). Moreover, dust particles containing multiple organic and inorganic pollutants can transfer from road traffic to the residential areas, and they can cause atmospheric pollution (Chabukdhara and Nema 2013). For instance, Aryal et al. (2007) reported that heavy metals including Zn, Mn, Co, Ni, and Cu could be released via road dust to the underlying soil, leading to the contamination of groundwater through seepage. These actions disrupt the natural biogeochemical cycle of the ecosystem and cause substantial risks to human health (Faiz et al. 2009; Shi et al. 2010). Accordingly, the composition, quantity, distribution pattern, and source identification of road-deposited sediments should be comprehensively assessed to provide an accurate indication of urban environmental conditions (Liu et al. 2014; Ali et al. 2017).

Various anthropogenic sources have been recognized to contribute to the occurrence of heavy metals in roadside soil and street dust. These sources include vehicular emissions from traffic (Atiemo et al. 2012; Zhang et al. 2012), tire-

---

Responsible editor: Philippe Garrigues

---

**Electronic supplementary material** The online version of this article (<https://doi.org/10.1007/s11356-019-06216-5>) contains supplementary material, which is available to authorized users.

---


✉ Sanjay Kumar Gupta  
sanjuenv@gmail.com

<sup>1</sup> Environmental Engineering, Department of Civil Engineering, Indian Institute of Technology Delhi, New Delhi, India

<sup>2</sup> Centre for Environmental Sciences, Central University of Jharkhand, Ranchi, India

<sup>3</sup> Sanitary Engineering Department, Faculty of Engineering, Alexandria University, Alexandria 21544, Egypt

## Systematic study of the break-up fusion process in the $^{12}\text{C} + ^{165}\text{Ho}$ system and interplay of entrance channel parameters

Suhail A. Tali <sup>1,\*</sup>, Harish Kumar,<sup>1</sup> M. Afzal Ansari,<sup>1,†</sup> Asif Ali,<sup>1</sup> D. Singh,<sup>2</sup> Rahbar Ali,<sup>3</sup> Pankaj K. Giri,<sup>2</sup> Sneha B. Linda,<sup>2</sup> R. Kumar,<sup>4</sup> Siddharth Parashari,<sup>1</sup> S. Muralithar,<sup>4</sup> and R. P. Singh<sup>4</sup>

<sup>1</sup>*Department of Physics, Aligarh Muslim University, Aligarh-202002, India*

<sup>2</sup>*Centre for Applied Physics, Central University of Jharkhand, Ranchi-835205, India*

<sup>3</sup>*Department of Physics, G.F. (P.G.) College Shahjahanpur-242001, India*

<sup>4</sup>*Inter-University Accelerator Centre, New Delhi-110067, India*



(Received 28 January 2019; revised manuscript received 21 June 2019; published 22 August 2019)

To understand the low-energy incomplete fusion (ICF) reaction dynamics, the excitation function measurements of  $^{12}\text{C} + ^{165}\text{Ho}$  system has been performed in the energy region of  $\approx 4\text{--}7$  MeV/nucleon, by employing the stacked foil activation technique. The cross sections of the measured evaporation residues are compared with the theoretical predictions of statistical model code PACE4, which takes into account only the complete fusion (CF) reaction cross section. It is observed that residues populated via xn and pxn channels are in good agreement with the PACE4 predictions, implying that these residues are populated via CF process. However, in the case of  $\alpha$ -emission channels a significant enhancement from the PACE4 predictions is observed even after the deduction of precursor contribution, which is accredited to ICF process. The projectile break-up probability is found to increase with increment in the incident projectile energy. Further, the dependence of incomplete fusion dynamics on entrance channel parameters like mass asymmetry, Coulomb effect ( $Z_p Z_T$ ), and projectile  $Q_\alpha$  value is systematically studied. The present results reveal that a single entrance channel parameter does not oversee the ICF reaction dynamics but have varying contributions depending upon the projectile-target combination. Moreover, the effect of projectile break-up on complete fusion cross section at energies above the Coulomb barrier is also studied. The suppression in fusion cross section is observed when compared with the universal fusion function.

DOI: [10.1103/PhysRevC.100.024622](https://doi.org/10.1103/PhysRevC.100.024622)

### I. INTRODUCTION

Fusion reactions induced by heavy ions (HIs) play an utmost role in nuclear physics, as they enable us to study the properties of super-heavy nuclei near and away from the stability line. At projectile energies above the Coulomb barrier, complete fusion (CF) and incomplete fusion (ICF) are the two most dominant reaction modes [1–3]. Study of such fusion reactions has remained the subject of great interest for both theoretical and experimental nuclear physicists over the past two decades. In the case of CF, the incident projectile completely fuses with the target nucleus and leads to the formation of highly excited compound nucleus (CN), which de-excites via emission of light nuclear particles and  $\gamma$  rays. In ICF (also known as break-up fusion process), the incident projectile breaks in the vicinity of target nuclear field, one of the fragment fuses with the target nucleus giving rise to a composite system of low mass, excitation energy, charge, and momentum transfer. The excited composite system also de-excites via emission of light nuclear particles and  $\gamma$  rays. The unfused fragment moves as a spectator in the forward direction, with nearly the projectile velocity and have no impact

on the way the reaction proceeds [4,5]. Semiclassically, the CF and ICF phenomenon in heavy-ion (HI) interactions can be explained on the basis of driving input angular momentum ( $\ell$ ) imparted into the system [2,3,6]. For the values, with  $\ell < \ell_{\text{crit}}$ , there is a pocket in an effective potential energy curve, (the attractive nuclear potential dominates the sum of repulsive Coulomb and centrifugal potential) hence the incident projectile is completely assimilated by the target nucleus-CF. However as the energy of incident projectile increases  $\ell > \ell_{\text{crit}}$ , the fusion pocket in the effective potential energy curve subsequently vanishes, hence to provide the sustainable amount of input  $\ell$ , the incident projectile breaks into clusters, leading to the fusion of one of the fragment with the target nucleus-ICF [1–3]. Some studies have also reported the existence of ICF well below the  $\ell_{\text{crit}}$  [7–10]. To understand the phenomenon of ICF reaction dynamics various theoretical models have been put forth, but none of them is able to reproduce satisfactorily the experimentally measured ICF data below 8 MeV/nucleon [3,5,7], this has revived the interest in exploring the low-energy ICF reaction dynamics. The another unresolved question which is also of large interest is to understand the systematic dependence of ICF on various entrance channel parameters such as projectile energy, mass asymmetry, Coulomb effect ( $Z_p Z_T$ ), projectile structure, and input  $\ell$  values. In the present work, with an incentive to comprehend the systematic dependence of ICF on

\* amusuhailtali@gmail.com

† drmafzalansari@yahoo.com



## Systematic study of low-energy incomplete-fusion dynamics in the $^{16}\text{O} + ^{148}\text{Nd}$ system: Role of target deformation

Pankaj K. Giri,<sup>1</sup> D. Singh,<sup>1,\*</sup> Amritraj Mahato,<sup>1</sup> Sneha B. Linda,<sup>1</sup> Harish Kumar,<sup>2</sup> Suhail A. Tali,<sup>2</sup> Siddharth Parasari,<sup>2</sup> Asif Ali,<sup>2</sup> M. Afzal Ansari,<sup>2</sup> Rakesh Dubey,<sup>3</sup> R. Kumar,<sup>3</sup> S. Muralithar,<sup>3</sup> and R. P. Singh<sup>3</sup>

<sup>1</sup>*Department of Physics, Central University of Jharkhand, Ranchi 835 205, India*

<sup>2</sup>*Department of Physics, Aligarh Muslim University, Aligarh 202 002, India*

<sup>3</sup>*NP-Group, Inter-University Accelerator Centre, New Delhi 110 067, India*



(Received 27 January 2019; revised manuscript received 20 June 2019; published 22 August 2019)

A study of low-energy incomplete fusion was done by the measurements of excitation functions of evaporation residues produced in the  $^{16}\text{O} + ^{148}\text{Nd}$  system at energies  $\approx 4\text{--}7$  MeV/nucleon. The stacked foil activation technique using offline  $\gamma$ -ray spectrometry was employed. Significant enhancements were found in the measured cross sections from the theoretical predictions of PACE-4 for the evaporation residues populated through  $\alpha$ -emission channels. This enhancement is attributed to incomplete fusion (ICF) of  $^{16}\text{O}$  with  $^{148}\text{Nd}$ . The comparison of present work with literature data shows that the ICF probability increases exponentially with existing entrance channel parameters. The dependence of ICF dynamics on target deformation was investigated using deformation parameter ( $\beta_2^T$ ), deformation length ( $\beta_2^T R^T$ ) and neutron excess ( $N - Z$ )<sup>T</sup> of the target. The present analysis indicates that the ICF fraction rises exponentially with  $\beta_2^T$ ,  $\beta_2^T R^T$ , and  $(N - Z)^T$ . These results show that the ICF fraction follows a systematic exponential pattern rather than a simple linear growth with various entrance channel parameters reported in the literature. However, this study also suggests that the ICF dynamics is strongly influenced by the structure of projectile along with that of the target. Further, the role of deformation parameters on incomplete-fusion dynamics was also investigated through the method of universal fusion function. Analysis of the present data indicates that the experimental fusion functions are suppressed with different factors depending on deformation of the target nuclei. These suppressions are removed by including incomplete-fusion cross sections in the fusion function calculations. The average value of experimental fusion functions deviates from the universal fusion function for deformed targets. However, the average value of the total fusion function for deformed targets shifts towards the average value of the universal fusion function. The present study shows that the effect of target deformation plays an important role in affecting the ICF dynamics, along with various entrance channel parameters for different systems.

DOI: [10.1103/PhysRevC.100.024621](https://doi.org/10.1103/PhysRevC.100.024621)

### I. INTRODUCTION

Heavy-ion induced reactions at energies above the Coulomb barrier have been a subject of growing interest to nuclear physicists. It has been observed that complete fusion (CF) and incomplete fusion (ICF) are the dominant modes in heavy-ion interaction at energies above the Coulomb barrier [1–4]. The first experimental evidence of ICF was observed by Britt and Quinton [5]. However, major advancement on the study of ICF took place after the study of Inamura *et al.* [6], which provided significant information about ICF dynamics from  $\gamma$ -ray multiplicity measurements. Further, the dependence of localization of the entrance channel angular momentum ( $\ell$ ) window on deformation of the target was summarized by Gerschel [7]. Studies of ICF dynamics by the measurement of excitation functions (EFs) of the evaporation residues (ERs) have been done by several investigators [8–10].

Morgenstern *et al.* [11] observed that a more mass-asymmetric system has relatively higher ICF contribution than that of a less mass-asymmetric system at the same relative velocity. Further, systematic studies [12–14] on the dependence of ICF on various entrance channel parameters, namely, entrance channel mass-asymmetry ( $\mu_{EC}^{AS}$ ),  $\alpha$ - $Q$  value,  $Z_P Z_T$ , etc., have also been done. These studies show that a single entrance channel parameter is not able to explain completely the measured yields of the incomplete-fusion dynamics at low energy. Recently, Singh *et al.* [15] revealed that the ICF dynamics also depend on deformation of the target, according to the measurement of spin distributions of ERs using the particle- $\gamma$  coincidence technique. Various theoretical models have been proposed to explain the characteristics of ICF dynamics. Udagawa and Tamura [16] proposed the breakup fusion (BUF) model to explain the kinetic energy spectra and angular distributions of emitted particles. The sum-rule model was given by Wilczynski *et al.* [17], based on a generalized concept of the critical angular momentum for complete fusion (CF). Other theoretical models, e.g., the promptly emitted particles (PEP) model [18], the hot spot model [19], etc., were also

\*Corresponding author: dsinghcuj@gmail.com, dsinghiuac@gmail.com





# Kharif crop characterization using combination of SAR and MSI Optical Sentinel Satellite datasets

ABHINAV VERMA<sup>1</sup>, AMIT KUMAR<sup>2</sup> and KANHAIYA LAL<sup>2,\*</sup> 

<sup>1</sup>Indian Institute of Remote Sensing, ISRO, Dehradun, India.

<sup>2</sup>Department of Geoinformatics, School of Natural Resource Management, Central University of Jharkhand, Ranchi 835 205, India.

\*Corresponding author. e-mail: jnu.kanhaiya@gmail.com kanhaiya.lal@cuja.ac.in

MS received 7 February 2019; revised 7 June 2019; accepted 15 July 2019; published online 24 August 2019

In the present study, the differences in the *kharif* crop reflectance at varied wavelength regions and temporal SAR backscatter (at VV and VH polarizations) during different crop stages were analyzed to classify crop types in parts of Ranchi district, East India using random forest classifier. The spectral signature of crops was generated during various growth stages using temporal Sentinel-2 MSI (optical) satellite images. The temporal backscatter profile that depends on the geometric and dielectric properties of crops were studied using Sentinel-1 SAR data. The spectral profile exhibited distinctive reflectance at the NIR (0.842  $\mu\text{m}$ ) and SWIR (1.610  $\mu\text{m}$ ) wavelength regions for paddy (*Oryza sativa*;  $\sim 0.25$  at NIR,  $\sim 0.27$  at SWIR), maize (*Zea mays*;  $\sim 0.24$  at NIR,  $\sim 0.29$  at SWIR) and finger millet (*Eleusine coracana*,  $\sim 0.26$  NIR,  $\sim 0.31$  at SWIR) during pre-sowing season (mid-June). Similar variations in crop's reflectance at their different growth stages (vegetative to harvesting) were observed at various wavelength ranges. Further, the variations in the backscatter coefficient of different crops were observed at various growth stages depending upon the differences in sowing–harvesting periods, field conditions, geometry, and water presence in the crop field, etc. The Sentinel-1 SAR based study indicated difference in the backscatter of crops (i.e.,  $\sim -18.5$  dB (VH) and  $\sim -10$  dB (VV) for paddy,  $\sim -14$  dB (VH) and  $\sim -7.5$  dB (VV) for maize,  $\sim -14.5$  dB and  $\sim -8$  dB (VV) for finger millet) during late-July (transplantation for paddy; early vegetative for maize and finger millet). These variations in the reflectance and backscatter values during various stages were used to deduce the best combination of the optical and SAR layers in order to classify each crop precisely. The GLCM texture analysis was performed on SAR for better classification of crop fields with higher accuracies. The SAR-MSI based *kharif* crop assessment (2017) indicated that the total cropped area under paddy, maize and finger millet was 24,544.55, 1468.28 and 632.48 ha, respectively. The result was validated with ground observations, which indicated an overall accuracy of 83.87% and kappa coefficient of 0.78. The high temporal, spatial spectral agility of Sentinel satellite are highly suitable for *kharif* crop monitoring. The study signifies the role of combined SAR–MSI technology for accurate mapping and monitoring of *kharif* crops.

**Keywords.** Crop monitoring; crop spectral profile; random forest classification; SAR texture; SAR–MSI image fusion.

## 1. Introduction

*Kharif* (referred as monsoon crops) is the prime crop growing season in India. The *kharif* crops, viz., *Oryza sativa* (paddy), *Zea mays* (maize), *Sorghum*

(jowar), *Pennisetum glaucum* (bajra), *Cajanus cajan* (tur), *Vigna radiata* (moong), *Vigna mungo* (urad), *Gossypium* (cotton), *Corchorus capsularis* (jute), *Eleusine coracana* (finger millet) are grown with the onset of monsoon from July to November.



# Role of biomass supply chain management in sustainable bioenergy production

Dipesh Kumar and Bhaskar Singh

Centre For Environmental Sciences, Central University of Jharkhand, Ranchi-835205

## ABSTRACT

The demand for bioenergy (biofuels, heat and electricity) is increasing steadily around the globe. Major policy-related interventions for adoption and promotion of bioenergy have also been realized by several countries over the past few decades. The biomass supply chain incorporates several components of bioenergy production, which in turn consist of several activities for which different alternative methods are available. Different components of the biomass supply chain include production of bioenergy feedstock (biomass), logistics of biomass, conversion of biomass to bioenergy, and distribution of bioenergy or bioenergy carriers for end use. The single largest limiting factor for the production of bioenergy is the unavailability of biomass. Dedicated, fast-growing and high-biomass-producing plantations on non-arable land and utilization of agro-industrial waste materials can overcome this problem. Holistic integration of different components of the biomass supply chain and activities involved therein along with judicious design are likely to enhance the quantum of energy return, improve the greenhouse gas balance and reduce the water footprint of the bioenergy production facility. Additionally, the emerging yet promising concept of lignocellulosic and algal biorefinery would require a careful and prudent design of the biomass supply chain to achieve one of the most attractive characteristic of bioenergy: environmental sustainability.

## ARTICLE HISTORY

Received 28 April 2017  
Accepted 11 July 2017

## KEYWORDS

Bioenergy; biomass supply chain; environmental sustainability

## Introduction

The world is going through a period of transition from fossil forms of energy to other forms of energy in order to overcome the limitations and shortcomings of fossil fuel consumption [1]. While not rapid, the trend is nevertheless persistent, and non-fossil forms of energy will eventually dominate the world's energy mix [2]. Among the alternatives energy derived from biomass is gaining popularity around the globe as bioenergy is a renewable, carbon-neutral and non-toxic form of energy that can be locally produced and thus also promotes energy security [3]. Bioenergy refers to energy (heat) or energy carriers (biofuels) derived from biomass. Unlike fossil energy, bioenergy is derived from biomass of recent origin and thus is renewable on a human timescale [4]. Biomass has remained an important source of primary energy (particularly in the developing world) especially in the form of dung cake, firewood, leaves, etc., largely for cooking purposes. With increasing concerns and awareness about the health impacts of noxious emissions from domestic biomass burning for cooking, and increasing coverage of cooking gas, this share of bioenergy is slowly decreasing. On the other hand the demand for biomass for the production of industrial heat, electricity and energy carriers (biofuels) is increasing steadily. Bioenergy can be considered carbon neutral as plants

photosynthetically fix atmospheric carbon for producing biomass which, when used as bioenergy, releases the carbon backbone of the biomass in the form of CO<sub>2</sub> to the atmosphere without causing any net emission of carbon dioxide [5]. However, the overall greenhouse gas (GHG) balance of bioenergy production depends on a multitude of factors which cannot be ignored. Chemical energy locked up in the biomass can be released directly from the biomass matrix upon combustion (for the production of heat and electricity) or can be transformed into energy carriers (biofuels) for different utility purposes [6]. Biofuels are solid (bio-coal), liquid (biodiesel, bioethanol, bio-oil, etc.) and gaseous fuels (biogas, syngas, etc.) derived from biomass via different biomass processing techniques [7]. In the past few years several countries have introduced policies to incorporate bioenergy in their energy mix [8]. Since there are other competing demands for biomass, ensuring abundant availability of cheap biomass as bioenergy feedstock can be problematic. Utilization of first-generation feedstocks for bioenergy production is not feasible for some countries as it might lead to a food versus fuel conflict. First-generation feedstocks are suitable only when their production is in excess of demand (as in the case of sugarcane-derived ethanol in Brazil and soybean-derived biodiesel in the US) [9]. This has led to the development of second-generation



## Eucalyptus leaf powder as an efficient scavenger for Congo red from water: Comprehensive batch and column investigation

Roshni Kumari<sup>a</sup>, Jhilirani Mohanta<sup>a</sup>, Banashree Dey<sup>b</sup>, and Soumen Dey<sup>a</sup>

<sup>a</sup>Department of Chemistry, Central University of Jharkhand, Ranchi, India; <sup>b</sup>Department of Chemistry, The Graduate School College for Women, Jamshedpur, India

### ABSTRACT

Abundantly available Eucalyptus leaf (*Eucalyptus globulus*) was investigated as promising bio-sorbent for removal of Congo red by batch and column method. Material was characterized by proximate analysis, SEM-EDS, FT-IR, BET, XRD, and chemical analysis. Physico-chemical parameters like contact time, dose, and pH were optimized. Maximum adsorption capacity is 29.68 mg/g. Adsorption follows intraparticle diffusion kinetics ( $K = 0.211 \text{ mg/g/min}^{0.5}$ ,  $R^2 = 0.996$ ) and Freundlich isotherm model ( $R^2 = 0.996$ ). Thermodynamic study revealed a spontaneous and feasible process ( $\Delta G = -13.06 \text{ kJ/mol}$ ). Regeneration (82%) with dilute alkali enables multicycle use. Column breakthrough follows Thomas and BDST model. Cost-benefit analysis suggests economically sustainable material for dye decolorization.

### ARTICLE HISTORY

Received 27 May 2019  
Accepted 17 September 2019

### KEYWORDS



Adsorption; Congo red; *Eucalyptus* leaves; kinetics; regeneration; throughput volume

### Introduction


Water pollution is one of the major problems to be dealt with. Dyes toxicity in water bodies is caused due to disposal of industrial effluents, sewage discharges, and agricultural runoff, which imposes the necessity of various treatment methods.<sup>[1,2]</sup> Toxic dyes include a wide variety of organic compounds namely diazo dyes, basic, anionic, or neutral dyes. It acts as mutagen and induces somnolence (affects clotting), skin, and eye irritant with other respiratory and gastrointestinal problems. Use of low-cost and easily available adsorbents was established.<sup>[3,4]</sup> Bio-sorbents can be agricultural waste or nonliving biomass.<sup>[5]</sup> These include waste banana pith, hazelnuts, etc.<sup>[6,7]</sup> Removal of Congo red (CR) dye from water by adsorption onto the activated carbon prepared from coir pith was reported.<sup>[8]</sup> Conventional and cost-effective adsorbents were used nowadays.<sup>[9]</sup> Bio-sorption involves the partial interaction to inactive materials that might be gained from agricultural or industrial or marine and microbial material, etc.<sup>[10,11]</sup> Mostly agricultural waste like rice husk, raw pine, eucalyptus bark, jujube seeds, chemically treated eucalyptus leaves, etc. were seen to be effective.<sup>[12–17]</sup> Bio-sorption is one of the best alternative method for the removal of organic pollutants like dyes to treat the effluents from industries.<sup>[18,19]</sup> It is economically viable also.<sup>[20]</sup> A number of processes

were used to remove toxicity of dyes from waste water.<sup>[21]</sup> Adsorption proved to be one of the cheapest and suitable method for wastewater treatment.<sup>[22]</sup> So, efforts were made to remove various dyes like malachite green, CR, methylene blue, rhodamine B etc. from water resources.<sup>[23,24]</sup> CR is a bright red neutral dye, easily miscible in water solutions and is carcinogenic in nature.<sup>[25]</sup> This led to the search of a cheap and versatile bio-sorbent for removal of CR dye, the present work aimed to test the bio-sorption potential of Eucalyptus leaf (EL) powder for removal of toxic CR dye in both batch column mode. Also, the batch and column bio-sorption data were justified using various kinetic and isotherm models. There were very few literature citations to evaluate the adsorption efficiency of Eucalyptus tree-based biomass. Removal of CR as well as its regeneration has been reported using activated carbon.<sup>[26]</sup> The use of ELs as adsorbent for copper (II) ion removal was reported.<sup>[27]</sup> The study showed uptake capacity of 1.92 mg/g with Langmuir model as the best fitted isotherm model. Removal of zinc (II) ion by EL biomass was reported. The study showed maximum uptake capacity of 23.5 mg/g with Langmuir and Pseudo second-order models as the best fitted isotherm and kinetic models, respectively.<sup>[28]</sup>

Hence, best efforts were made to evaluate the efficiency of EL powder as biomass for removal of CR

**CONTACT** Soumen Dey  [soumen.dey@cuja.ac.in](mailto:soumen.dey@cuja.ac.in)  Department of Chemistry, The Graduate School College for Women, Jamshedpur, India

Color versions of one or more of the figures in the article can be found online at [www.tandfonline.com/LSST](http://www.tandfonline.com/LSST).

 Supplementary details of this article can be accessed [here](#).

# Probing incomplete fusion dynamics and role of the projectile deformation in the $^{19}\text{F} + ^{154}\text{Sm}$ system

D. Singh<sup>1,a</sup>, Pankaj K. Giri<sup>1</sup>, Amritraj Mahato<sup>1</sup>, Sneha B. Linda<sup>1</sup>, R. Tripathi<sup>2</sup>, Harish Kumar<sup>3</sup>, M. Afzal Ansari<sup>3</sup>, N.P.M. Sathik<sup>4</sup>, Rahbar Ali<sup>5</sup>, R. Kumar<sup>6</sup>, S. Muralithar<sup>6</sup>, and R.P. Singh<sup>6</sup>

<sup>1</sup> Department of Physics, Central University of Jharkhand, Ranchi - 835 205, India

<sup>2</sup> Radio-chemistry Division, Bhabha Atomic Research Centre, Mumbai - 400 085, India

<sup>3</sup> Department of Physics, Aligarh Muslim University, Aligarh - 202 002, India

<sup>4</sup> Department of Physics, Jamal Mohamed College, Tiruchirappalli - 620 020, India

<sup>5</sup> Department of Physics, G.F. (P.G.), College, Shahjahanpur - 242 001, India

<sup>6</sup> Nuclear Physics Group, Inter-University Accelerator Centre, Aruna Asaf Ali Marg, New Delhi - 110 067, India

Received: 4 May 2019 / Revised: 9 August 2019

Published online: 27 September 2019

© Società Italiana di Fisica / Springer-Verlag GmbH Germany, part of Springer Nature, 2019

Communicated by R.V.F. Janssens

**Abstract.** Transition intensity distributions for evaporation residues  $^{169-166}\text{Lu}(\text{xn})$ ,  $^{168,167}\text{Yb}(\text{pxn})$ ,  $^{168,165,164}\text{Tm}(\alpha\text{xn})$ ,  $^{165}\text{Er}(\alpha\text{p3n})$ ,  $^{162}\text{Ho}(2\alpha\text{3n})$  and  $^{163-160}\text{Dy}(2\alpha\text{pxn})$  populated through complete and incomplete fusion in the  $^{19}\text{F} + ^{154}\text{Sm}$  system have been measured. The feeding intensity patterns of incomplete fusion channels are found to have a narrow range feeding only for high spin states, while complete fusion channels are strongly fed over a broad spin range and widely populated. A comparative study of present measurements shows the effect of projectile deformation along with entrance channel mass asymmetry. Further, comparison of present results with the literature suggests that the mean input angular momentum values are relatively larger in the collision of a deformed projectile with a deformed target than that in the collision of a spherical projectile with a deformed target at the same relative velocity of incident projectile. However, ICF dynamics has also been found to be influenced by relative orientations (*i.e.* tip-tip or side-side) of the interacting partners. It means that there is more involvement of peripheral collisions between the deformed-deformed nuclei. The present analysis also shows that there is a projectile dependence on ICF dynamics, which would require more investigation. Present results of mean input angular momenta for different evaporation residues highlight the role of projectile deformation and orientations of interacting nuclei in the dynamics of incomplete fusion as well as complete fusion.

## 1 Introduction

The study of complete fusion (CF) and incomplete fusion (ICF) reactions using heavy ions (HIs) has been a topic of resurgent interest at energies above the Coulomb barrier [1–7]. Several reaction channels may open in the interaction of a heavy ion with the target. Britt and Quinton [8] reported the first experimental evidence of ICF contribution in the break-up of the incident projectiles. After that, a similar study was also carried out by Galin *et al.* [9]. However, a major advancement in the study of ICF dynamics took place after the exclusive measurement of charged particle- $\gamma$  coincidence by Inamura *et al.* [10]. Siwek-Wilczynska *et al.* [11, 12] provided a classical picture of HI interaction to understand the ICF dynamics. Zolowaski *et al.* [13] and Yamada *et al.* [14] pointed out that

the projectile like fragments (PLFs) are emitted in the interaction of projectile with target using charged particle ( $Z = 1, 2$ ) coincidence with prompt  $\gamma$ -rays. Semi classical theory of HI interaction categorizes the CF and ICF processes on the basis of driving input angular momentum ( $\ell$ ) imparted in the system. According to the sharp cut-off approximation [15–17], the CF process lies in the range of driving input angular momentum  $0 \leq \ell \leq \ell_{crit}$ , while the dominant contribution from ICF comes from the range  $\ell_{crit} \leq \ell \leq \ell_{max}$ . Here,  $\ell_{crit}$  is the critical angular momentum for CF and  $\ell_{max}$  is the maximum angular momentum of the system at a particular projectile energy. In the case of CF, the attractive nuclear potential overcomes the repulsive Coulomb and centrifugal potentials in central collisions. Consequently, at a small value of impact parameter and relatively lower value of projectile energy, the incident projectile completely fuses with the target nucleus, forming an excited compound system which

<sup>a</sup> e-mail: dsinghcuj@gmail.com



< Back to results | 1 of 1

Download Print Save to PDF Save to list Create bibliography

Oriental Anthropologist • Volume 19, Issue 2, Pages 240 - 256 • December 2019

Document type

Article

Source type

Journal

ISSN

0972558X

DOI

10.1177/0972558X19858550

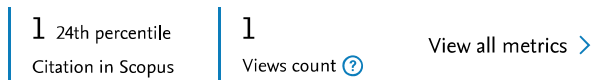
View more

# Gender, Resource Management, and Social Unrest: An Ethnographic Case Study

Nayak, Anindita

Save all to author list

Centre for Indigenous Culture Studies (CICS), Central University of Jharkhand, Jharkhand, Ranchi, India



Full text options Export

Abstract

Author keywords

Sustainable Development Goals

SciVal Topics

Metrics

## Abstract

This paper aims at locating the relationship between gender and resource management, especially the indigenous knowledge system of women for natural resource management of the Kondh tribe of Nayagarh district, Odisha. The Kondh live within the forest and they are highly dependent on forest for maintaining their livelihood. Specifically, women, who take family and community responsibilities, usually go through a continuous struggle from inside the family, as well as from the outside. Further, this study explains the case of the community's role in maintaining the forest through social unrest. This work further intends to study how government policies, particularly forest policy, affect indigenous Kondh, when the destruction of natural resources has been increasing, and how women raise voices to sustain their environment. © 2019 Oriental Institute of Cultural and Social Research and SAGE Publications.

## Author keywords

community; conservation; forest resources; Gender; management; protection

## Cited by 1 document

Integrating traditional ecological knowledge into US public land management: Knowledge gaps and research priorities

Souther, S. , Colombo, S. , Lyndon, N.N. (2023) *Frontiers in Ecology and Evolution*

View details of this citation

Inform me when this document is cited in Scopus:

Set citation alert >

## Related documents

Gendering resource rights and democratic citizenship

Vasan, S. (2007) *Indian Journal of Gender Studies*

F G Bailey's bisipara revisited

Otten, T. , Simpson, E. (2016) *Economic and Political Weekly*

Times of trouble for christians in muslim and hindu societies of South Asia

Pfeffer, G. (2014) *Constructing Indian Christianities: Culture, Conversion and Caste*

View all related documents based on references

Find more related documents in Scopus based on:

Author > Keywords >







# Process optimization of biodiesel production catalyzed by CaO nanocatalyst using response surface methodology

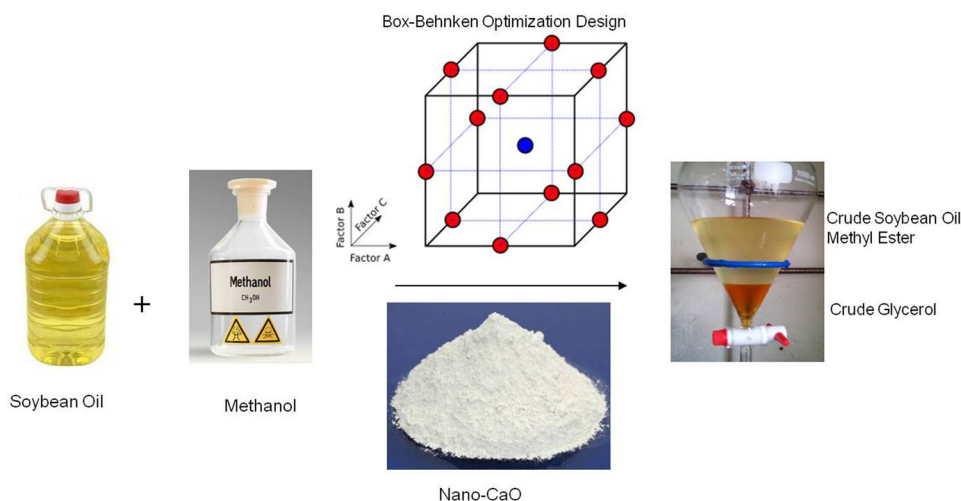
Priyanka Bharti<sup>1</sup> · Bhaskar Singh<sup>1</sup> · R. K. Dey<sup>2</sup>

Received: 2 May 2019 / Accepted: 18 September 2019 / Published online: 24 September 2019  
© The Author(s) 2019

## Abstract

Uses of nanocatalysts have become more useful in optimizing catalytic reactions. They are known to enhance the rate of reaction by offering a greater number of active sites by possessing a high surface-to-volume ratio. In the present work, calcium oxide nanocatalysts were synthesized through the sol–gel method. The particle size of the nanocatalyst prepared ranged up to 8 nm. Soybean oil was used as the raw material for the synthesis of biodiesel. The synthesized nano-CaO was characterized through scanning electron microscopy (SEM), transmission electron microscopy (TEM), X-ray diffraction (XRD), Fourier transform infrared spectroscopy (FTIR) and BET (Brunauer–Emmett–Teller). Average BET surface area analysis of the nanocatalyst was calculated to be 67.781 m<sup>2</sup>/g and pore diameter was 3.302 nm. Nano-CaO catalyst was used to synthesize biodiesel and optimize the reaction variables through optimization processes to achieve a high yield of biodiesel. The reaction variables that were optimized were catalyst amount, oil to methanol molar ratio and reaction temperature. Upon optimization, the conversion of biodiesel was found to be 97.61%. The optimized value of the reaction variables was: catalyst amount of 3.675 wt% with respect to oil, molar ratio (alcohol to oil) of 11:1, and reaction temperature of 60 °C for 2 h.

## Graphic abstract



**Keywords** Biodiesel · Calcium oxide (CaO) · Nanocatalyst · Response surface methodology

✉ Bhaskar Singh  
bhaskar.singh@uj.ac.in

✉ R. K. Dey  
rkdey@rediffmail.com

Extended author information available on the last page of the article

## Introduction

Renewable energy has attracted the interest of researchers worldwide owing to diminishing fossil fuel reserves and environmental concerns [1]. Biodiesel composed of fatty







# Coastal Social Vulnerability and Risk Analysis for Cyclone Hazard Along the Andhra Pradesh, East Coast of India

K. K. Basheer Ahammed<sup>1</sup> · Arvind Chandra Pandey<sup>1</sup>

Received: 13 June 2019 / Accepted: 21 August 2019 / Published online: 12 September 2019  
© The Author's 2019, corrected publication 2019

## Abstract

People around the world are prone to frequent and intensive hazards due to the global climate change scenario and human interventions. Particularly, the coastal communities are always prone to various long-term coastal hazards like sea-level rise, shoreline changes, and short-term hazards like tsunami cyclone and storm surge. Coastal Andhra Pradesh state is consisting of 9 district and 670 villages and also having 3.43 Million Population (69.3%). Andhra Pradesh has a vast 972 km long coastline and total coastal area spread over 92,906 km<sup>2</sup> comprising the nine coastal districts. Andhra Pradesh state is prone to various natural hazards, especially cyclone and associated storm surges. There is an extreme loss of life and damage to properties caused by these cyclones. During the past 40 years Andhra Pradesh coast experienced more than 62 cyclones including depression, cyclone surge, and severe cyclone surges. Among these cyclones, there were 32 cyclones which affected the Krishna–Godavari region, comprising four districts, namely East Godavari, West Godavari, Krishna, and Guntur. Therefore, these four districts have been considered for this social vulnerability study to identify the cyclone vulnerable villages. Geospatial applications are used in this study for spatial and non-spatial data processing and spatial analysis. The study indicated that half of the study area (3121.07 km<sup>2</sup>) lying moderately risk zone and around 7% of the study area observed high vulnerability. This study revealed that the use of geospatial application is most reliable and cost-effective approach for vulnerability and risk mapping and analysis. The result obtained from the present study may serve the baseline information for disaster management planning in the area.

**Keywords** Climate change · Natural hazard · Tropical cyclone · Vulnerability · Risk · GIS

## Küsten Soziale Anfälligkeit und Risikoanalyse für Zyklon Gefahr entlang der Andhra Pradesh, Ostküste von India

### Zusammenfassung

Menschen auf der ganzen Welt anfällig aufgrund des globalen Klimawandels und menschlicher Eingriffe häufigen und intensiven Gefahren ausgesetzt. Insbesondere die Küstengemeinden sind immer verschiedenen langfristigen Küstengefahren ausgesetzt, z. B. dem Anstieg des Meeresspiegels, Änderungen der Küstenlinie und kurzfristigen Gefahren wie Tsunami-Wirbelstürmen und Sturmfluten. Der Küstenstaat Andhra Pradesh besteht aus 9 Distrikten und 670 Dörfern und hat 3.43 Millionen Einwohner (69.3%). Andhra Pradesh hat eine 972 km lange Küste und eine GesamtküsteKüstengebietfläche von 92,906 km<sup>2</sup>, die die neun Küstenbezirke umfasst. Der Bundesstaat Andhra Pradesh ist verschiedenen Naturgefahren ausgesetzt, insbesondere dem Wirbelsturm und den damit verbundenen Sturmfluten. Durch diese Zyklone kommt es zu extremen Lebens- und Sachschäden. In den letzten 40 Jahren erlebte die Küste von Andhra Pradesh mehr als 62 Wirbelstürme, darunter

---

✉ Arvind Chandra Pandey  
arvindchandrap@yahoo.com

K. K. Basheer Ahammed  
basheer.kk@yahoo.com

<sup>1</sup> Department of Geoinformatics, Central University of Jharkhand, Ranchi 835 205, India

## ASSESSING HUMAN AND CARBON FOOTPRINT OF RANCHI URBAN ENVIRONMENT USING REMOTE SENSING TECHNOLOGY

Amit Kumar<sup>1\*</sup> and Ashwani Kumar<sup>2</sup>

<sup>1</sup>Department for Land Resource Management, School of Natural Resource Management, Central University of Jharkhand, Ranchi 835205, India

<sup>2</sup>Faculty of Planning, Centre for Environmental Planning and Technology University, Ahmedabad 380009, India

Received 23 January 2019; received in revised form 06 October 2019; accepted 12 October 2019

### Abstract:

In the present study, the total carbon emission of rapidly growing Ranchi Urban Agglomeration (RUA) was estimated in geospatial environment considering certain factors. The carbon emission estimation is based on the increase in human as well as vehicular population and loss of vegetation cover employing standardized conversion factors. The rapid built-up expansion (180%) and human population growth (223%) during 1975-2010 led to innumerable socio-economic and environmental impacts including deterioration of urban ecosystem. The built-up expansion as observed through satellite images reflects degradation in the natural ecosystem primarily apparent on forest ecosystem in RUA. The study reveals that after reorganization of Ranchi as state capital (post 2000), the carbon emission was more prevalent as compared to the earlier periods. The estimates of carbon stock (terrestrial carbon) represents that the vegetation cover, attributed as the major source of carbon sink, was lost and leads to emission of total 2.44 metric tonnes of carbon during 1975-2010. The vehicular based carbon emission estimation exhibits high level of carbon emission in RUA (198,038,728 metric tonnes) during the year 2010. The population distribution pattern in wards of Ranchi Municipal Corporation revealed that the wards located in the selected city core northern, north-eastern, eastern and south-western parts emitted than the mean city carbon emission (>38,500 metric tonnes) as compared to the wards located in central, north-eastern, south-western and south-western parts (>60,000 metric tonnes). The study suggests towards urgent imposition of regulations for rapid land use transformation together with preservation and growth of carbon sink locations of RUA.

**Keywords:** Carbon footprint; Urban growth; Urban traffic; Geoinformatics

© 2019 Journal of Urban and Environmental Engineering (JUEE). All rights reserved.

\* Correspondence to: Amit Kumar. E-mail: [amit.iirs@gmail.com](mailto:amit.iirs@gmail.com)



# Assessment of Water Supply–Demand Using Water Evaluation and Planning (WEAP) Model for Ur River Watershed, Madhya Pradesh, India

Sunny Agarwal<sup>1</sup> · Jyoti P. Patil<sup>2</sup> · V. C. Goyal<sup>3</sup> · Ajai Singh<sup>4</sup>

Received: 5 April 2017 / Accepted: 10 October 2018 / Published online: 24 October 2018  
© The Institution of Engineers (India) 2018

**Abstract** Many watersheds experience scarcity of water for agricultural and domestic use for most part of the year. Ur river watershed in Tikamgarh district of Madhya Pradesh, India, falls under a drought prone region of India. Water allocation and management are essential for sustainable agriculture for this region. Water Evaluation and Planning system (WEAP)-based decision support system can prove to be an effective tool for water allocation, supply and demand analysis. In the present study, spatially distributed model by using WEAP-MABIA method has been developed for analysis and simulation of agricultural water demands in the Ur river watershed. WEAP-MABIA method uses dual crop coefficient approach which helps in computing the separate soil evaporation and transpiration under various water availability situations. Year 2012–2013 is used as base year for customizing WEAP model for 8 subwatersheds. The model was calibrated

using PEST tool, available in WEAP. The calibrated model was used for estimating future water demands and unmet demands by using future climate series, from 2015 to 2030, of IPCC scenario- RCP 4.5 of GFDL-ESM2M model. As per GFDLESM2M model (RCP4.5) predictions, rainfall is going to greatly vary in the coming years. The years 2020–2021 and 2028–2029 may experience very dry climatic conditions with 500 mm or less annual rainfall, while 2017–2018, 2023–2024 and 2025–2026 may experience heavy showers (1200 mm). Straight effects of this rainfall pattern could be seen in future water availability for agriculture and resultant crop yield. A high unmet demand exists in the case of agriculture since the first priority for water supply is meant to be for domestic purpose. Area under agriculture in Ur river watershed is large, while respective water supply is low. This gap puts an extra pressure on water resources leading to over extraction of groundwater and related problems. Looking at this scenario, water allocation requires great attention to narrow down the gap between existing demands and water supply. Since area under agriculture is large, water-efficient crops should be more emphasized. Also, efficient agricultural practices and rain water harvesting should be promoted in the study area. Since the watershed falls in semiarid condition and river flows are seasonal, different stress/deficit irrigation scenarios can be built using customized WEAP model to get higher yield.

✉ Ajai Singh  
ajai.singh@cej.ac.in  
Sunny Agarwal  
sunny.agarwal@cej.ac.in  
Jyoti P. Patil  
jyotipp2003@gmail.com  
V. C. Goyal  
vcgoyal@yahoo.com

- <sup>1</sup> Department of Civil Engineering, K.L. Education Foundation, Vaddeswaram, Guntur, Andhra Pradesh 522502, India
- <sup>2</sup> National Institute of Hydrology, New Delhi 110002, India
- <sup>3</sup> Head of RMO Division, National Institute of Hydrology, Roorkee, Uttarakhand 247667, India
- <sup>4</sup> Department of Water Engineering and Management, Central University of Jharkhand, Ranchi 835205, India

**Keywords** WEAP · MABIA · Ur river · Water allocation · Bundelkhand

OPEN

# TNF- $\alpha$ promoter polymorphisms (G-238A and G-308A) are associated with susceptibility to Systemic Lupus Erythematosus (SLE) and *P. falciparum* malaria: a study in malaria endemic area

Harishankar Mahto<sup>1,2</sup>, Rina Tripathy<sup>3</sup>, Biswa Ranjan Meher<sup>4</sup>, Birendra K. Prusty<sup>5</sup>, Meenakshi Sharma<sup>2</sup>, Divya Deogharia<sup>2</sup>, Anjana Kumari Saha<sup>2</sup>, Aditya K. Panda<sup>1,2</sup> & Bidyut K. Das<sup>6</sup>

Tumor necrosis factor- $\alpha$  (TNF- $\alpha$ ) is a proinflammatory cytokine associated with autoimmune and infectious diseases. Importance of TNF- $\alpha$  in *P. falciparum* malaria and systemic lupus erythematosus (SLE) have been demonstrated. However, association of functional promoter variants with SLE and malaria is lacking in malaria endemic population. A total of 204 female SLE patients and 224 age and sex matched healthy controls were enrolled in the study. Three hundred fourteen *P. falciparum* infected patients with different clinical phenotypes were included. TNF- $\alpha$  polymorphisms (G-238A & G-308A) were genotyped by PCR-RFLP. Plasma levels of TNF- $\alpha$  was quantified by ELISA. Heterozygous mutants and minor alleles of TNF- $\alpha$  (G-238A and G-308A) polymorphisms were significantly higher in SLE patients compared to healthy controls and associated with development of lupus nephritis. In addition, both promoter variants were associated with severe *P. falciparum* malaria. SLE patients demonstrated higher levels of plasma TNF- $\alpha$  compared to healthy controls. TNF- $\alpha$  (G-238A and G-308A) variants were associated with higher plasma TNF- $\alpha$ . In conclusion, TNF- $\alpha$  (G-238A & G-308A) variants are associated with higher plasma TNF- $\alpha$  levels in SLE patients residing in malaria endemic areas and could be a contributing factor in the development of SLE and susceptibility to severe *P. falciparum* malaria.

Tumor necrosis factor-alpha (TNF- $\alpha$ ) is a pro-inflammatory cytokine produced by wide range of cells such as macrophages, B cells, T cells and mast cells<sup>1</sup>. TNF- $\alpha$  is primarily produced as a trans-membrane protein that gets released from the membrane by a metalloprotease- TNF alpha converting enzyme (TACE), to form soluble 17 kDa protein<sup>2</sup>. TNF- $\alpha$  is a pleiotropic cytokine with wide range of biological functions: it can initiate host defense against infectious diseases and along with it involved in toxicity and inflammatory processes<sup>1</sup>. TNF- $\alpha$  exerts its biological effect through specialized types of receptors viz. TNF receptor 1 (TNFR-1) and TNFR-2<sup>3</sup>. Expression of TNF receptors is tissue specific. TNFR1 is normally observed in most tissues but TNFR2 is restricted to cells of the immune system<sup>3</sup>. TNF- $\alpha$  has both a beneficial and deleterious role and it has been linked with infectious diseases and autoimmune disorders<sup>4-7</sup>. The TNF- $\alpha$  gene is located in short arm of chromosome 6 at position 21.3 and spans about 12 kilobase (kb) length<sup>8</sup>. Till date, 43 single nucleotide polymorphisms (SNPs) at promoter

<sup>1</sup>Department of Bioscience and Bioinformatics, Khallikote University, GMax Building, Konisi, Berhampur, 761008, Odisha, India. <sup>2</sup>Centre for Life Sciences, Central University of Jharkhand, Brambe, Ranchi, 835205, Jharkhand, India.

<sup>3</sup>Department of Biochemistry, S.C.B. Medical College, Cuttack, 753007, Odisha, India. <sup>4</sup>Computational Biology and Bioinformatics Laboratory, Department of Botany, Berhampur University, Berhampur, Odisha, 760007, India.

<sup>5</sup>Infectious Disease Biology Group, Institute of Life Sciences, Bhubaneswar, Odisha, India. <sup>6</sup>Department of Medicine, S.C.B. Medical College, Cuttack, 753007, Odisha, India. Correspondence and requests for materials should be addressed to A.K.P. (email: [adityarmrc@gmail.com](mailto:adityarmrc@gmail.com)) or B.K.D. (email: [bidyutdas@hotmail.com](mailto:bidyutdas@hotmail.com))

**Investigation of breakup fusion in  $^{16}\text{O} + ^{124}\text{Sn}$  system and its correlation with various entrance channel parameters**D. Singh<sup>†</sup>, Sneha B. Linda, Pankaj K. Giri, Amritraj Mahato*Department of Physics,  
Central University of Jharkhand,  
Ranchi-835 205, India*<sup>†</sup>e-mail: [dsinghcuj@gmail.com](mailto:dsinghcuj@gmail.com)

Harish Kumar, Suhail A. Tali, M. Afzal Ansari,

*Department of Physics,  
Aligarh Muslim University,  
Aligarh-202 002, India*

R. Kumar, S. Muralithar and R. P. Singh

*Inter-University Accelerator Centre,  
Aruna Asaf Ali Marg, New Delhi 110 067, India*

Forward recoil range distribution of evaporation residues populated through complete and incomplete fusion dynamics in  $^{16}\text{O} + ^{124}\text{Sn}$  system have been measured. Different full and partial linear momentum transfer components have been observed. The results indicate the occurrence of incomplete fusion involving break-up of  $^{16}\text{O}$  into  $^4\text{He} + ^{12}\text{C}$  and  $^8\text{Be} + ^8\text{Be}$ . However, the present data shows that the ERs are populated through both complete and incomplete fusion. **A systematic study was performed which shows that the ICF fraction rises exponentially with the established entrance channel parameters and their various combinations. Moreover, these present results clearly show that  $Z_p Z_T \mu_{EC}^{AS}$  is able to explain the ICF dynamics more conclusively than combined parameter  $Z_p Z_T \beta_2$  for the systems having spherical or slightly deformed target. Further, the dependence of ICF dynamics on target structure has also been studied through a new parameter  $N/Z$  of the target. The parameter  $N/Z$  is directly associated with the target structure and has been found more effective and sensitive than existing parameters to investigate the target structure effect on ICF dynamics. Thus, the present observations suggest that  $N/Z$  ratio of the target should also be considered as an important entrance channel parameter which strongly affects the ICF dynamics.**

**Keywords:** Heavy Ion Collisions, Complete and Incomplete fusion, Forward Recoil Range Distributions, Recoil-catcher Activation Technique

**1. Introduction**

The study of complete (CF) and incomplete fusion (ICF) reactions induced by heavy ion (HI) has been a topic of resurgent interest at low projectile energy above the Coulomb barrier<sup>1-4</sup>. The probability of breakup fusion (ICF) was first observed by Britt and Quinton<sup>5</sup> using the experimental technique. However, the advances in the study of ICF reactions took place after spin distribution measurements of ERs using particle- $\gamma$  coincidence technique<sup>6</sup> for the identification of CF and ICF channels. The study of ICF reactions has also been done by measuring the forward peaked  $\alpha$ -particles in the energy spectra and angular distribution of  $\alpha$ -particles<sup>7</sup>. Evidences for ICF process are also found from time-of-flight measurements<sup>8</sup> of evaporation residues (ERs). The ICF reaction dynamics have also been studied<sup>9</sup> using loosely bound projectiles at beam energies below 10 MeV/nucleon. The analysis of measured EFs data<sup>10-13</sup> shows that ICF process has a substantial contribution to the reaction cross-sections. Morgenstern et al.<sup>14</sup> studied the entrance channel mass-asymmetry dependence of ICF by the measurement of the velocity spectra of heavy ERs in different mass-asymmetric systems. Studies have been done using measured EFs data<sup>15,16</sup> to observe the effect of Coulomb factor ( $Z_p Z_T$ ) on ICF dynamics. Further, more systematic studies<sup>17,18</sup> have also been done to investigate the effect of various entrance channel parameters namely; mass-asymmetry,  $\alpha$ - $Q$ -value,  $Z_p Z_T$  and others on ICF dynamics. These studies show that a single entrance channel parameter is not able to explain completely yields of the low energy ICF contribution. The measurements<sup>19-21</sup> show that there are significant changes in the spin distributions and





# Crop insurance model to consolidate academia-industry cooperation: a case study over Assam, India

Subhro Banerjee<sup>1</sup> · A. C. Pandey<sup>1</sup>

Received: 3 June 2019 / Revised: 15 September 2019 / Accepted: 17 September 2019  
© Korean Spatial Information Society 2019

**Abstract** Agriculture is one of the deciding factors of Indian economy, contributing almost 17% of the total GDP. Every year, crops are lost due to natural disasters. This academic research may provide a solution for a long-standing problem in the industry. Crop insurance is one of the most effective ways to not only compensate loss, but also to increase poor farmers' resilience. Remote sensing has huge potential in the crop insurance market; it can be exploited for vulnerability mapping, damage assessment, risk mapping, and various other aspects. The purpose of this study was to present a method for evaluating crop vulnerability over an area using remote sensing and Geographic Information System (GIS), followed by an assessment of crops damaged due to flood. For application purposes, a crop risk map was prepared from a GIS model for the determination of crop insurance parameters. The study area selected (i.e., the Morigaon and Nagaon districts of Assam) is very much flood-prone. The districts have almost 50% agricultural land of the total land cover, thus making the crops very vulnerable to recurrent flooding. For this study, assessment of damage to crops due to flood was performed for a full year, followed by crop risk map generation from the GIS model. The results revealed that 345 km<sup>2</sup> of land was inundated by flood in August 2016. Due to the flooding, 1435.08 km<sup>2</sup> of agricultural land bearing crops was damaged at different levels. The crop

risk map depicts 103.33 km<sup>2</sup> of cropland at high risk due to flood.

**Keywords** Crop damage · Crop insurance · Crop vulnerability · Flood inundation · Remote sensing and GIS in agriculture

## 1 Introduction

Agriculture is an important part of India's economy. At present India is among the top two farm producers in the world, providing approximately 52% of the total job prospects in India and 17% of the total GDP of the Indian economy [1]. The agricultural sector of India has occupied almost 60.4% of India's geographical area showing significant growth from 58.8% in the year 1961 to 60.4% in the year 2015 (World Bank, Agricultural land [% of land area]) [2].

India had a total land cover of 1,797,210 km<sup>2</sup> of agriculture in 2015 (World Bank, Agricultural land, km<sup>2</sup>) [3] which increased over the years since 1961 (1,749,520 km<sup>2</sup>). Most Indians are directly or indirectly dependent on agriculture, with some are being directly attached to farming and others being involved in business with the agricultural goods and to boost the agriculture of India and provide maximum food security, the government needs to provide support in the form of land, bank loans and machinery for the small and big farmers. With such support we can expect some improvement in Indian economy [4]. The government can also help boost the agricultural sector by providing crop insurance.

Crop insurance [5]: Refers to insurance for farmers and crop producers against loss of crops due to natural

✉ A. C. Pandey  
arvindchandrap@yahoo.com

Subhro Banerjee  
subhro.pikubanerjee@gmail.com

<sup>1</sup> Department of Geoinformatics, Central University of Jharkhand, Ranchi, Jharkhand 835205, India





# Predictions and Strategies Learned from Machine Learning to Develop High-Performing Perovskite Solar Cells

Jinxin Li, Basudev Pradhan, Surya Gaur, and Jayan Thomas\*

Perovskite solar cells (PSCs) have recently received considerable attention due to the high energy conversion efficiency achieved within a few years of their inception. However, a machine learning (ML) approach to guide the development of high-performing PSCs is still lacking. In this paper ML is used to optimize material composition, develop design strategies, and predict the performance of PSCs. The ML models are developed using 333 data points selected from about 2000 peer reviewed publications. These models guide the design of new perovskite materials and the development of high-performing solar cells. Based on ML guidance, new perovskite compositions are experimentally synthesized to test the practicability of the model. The ML model also shows its ability to predict underlying physical phenomena as well as the performance of PSCs. The PSC model matches well with the theoretical prediction by the Shockley and Queisser limit, which is almost impossible for a human to find from an ensemble of data points. Moreover, strategies for developing high-performing PSCs with different bandgaps are also derived from the model. These findings show that ML is very promising not only for predicting the performance, but also for providing a deeper understanding of the physical phenomena associated with the PSCs.

## 1. Introduction

PSCs have recently taken the center stage for photovoltaic research as a viable clean and renewable energy source due to their low cost, light weight, flexibility, and large area processability with improved cell efficiency.<sup>[1–4]</sup> The power conversion efficiency (PCE) of a single junction PSC has risen from 3.8% to 24.2%<sup>[5–9]</sup> in just a little more than a decade since its inception. This is due to its high optical absorption characteristics, charge transport with long diffusion lengths, new perovskite material design, and optimization of device architecture. The achievement of high-performing PSCs is often based on a trial-and-error method, which includes material synthesis and development, film property optimization, and new device fabrication techniques. It takes a long time to optimize device performance, which requires major recourses like time, materials, equipment, and manpower. Several significant attempts have been made to rationalize the design

of new materials by theoretical simulation using density functional theory (DFT).<sup>[10,11]</sup> Most of the simulation methods are only useful for a few material systems and cannot be used for the chemical space where a large number of materials are present. Although hundreds of new perovskite materials have been developed with different bandgaps, and PSC devices have been fabricated in different device architectures with different hole transporting layers (HTL) and electron transport layers (ETL), the analysis of these results using ML has not been performed collectively and systematically. Such ML is beneficial for investigating the underlying mechanism and easing the experimental hurdles to synthesize perovskite materials in order to develop highly efficient and stable solar cells.


In general, there are two kinds of PSC architecture: regular (n–i–p) and inverted (p–i–n).<sup>[12]</sup> Although the structures are different, they follow the common energy conversion processes: i) photon absorption, exciton generation, and exciton dissociation in the perovskite layer, ii) electron and hole transport through ETL and HTL, and iii) a collection of charges at the respective metal/metal oxide electrodes. The device performances depend on optical and electrical properties of the perovskite materials such as bandgap, exciton binding energy, carrier mobility, crystallinity of materials, grain size, the highest occupied molecular orbital (HOMO), and lowest unoccupied molecular orbital

J. Li  
CREOL, The College of Optics and Photonics  
University of Central Florida  
Orlando, FL 32816, USA

Dr. B. Pradhan<sup>[†]</sup>  
NanoScience Technology Center  
University of Central Florida  
Orlando, FL 32826, USA

S. Gaur  
Department of Computer Science  
University of Central Florida  
Orlando, FL 31816, USA

Prof. J. Thomas  
NanoScience Technology Center  
CREOL, The College of Optics and Photonics  
Department of Materials Science and Engineering  
University of Central Florida  
Orlando, FL 32816, USA  
E-mail: Jayan.Thomas@ucf.edu

 The ORCID identification number(s) for the author(s) of this article can be found under <https://doi.org/10.1002/aenm.201901891>.

<sup>[†]</sup>Present address: Centre of Excellence in Green and Efficient Energy Technology & Department of Energy Engineering, Central University of Jharkhand, Brambe, Ranchi, Jharkhand 835 205, India

DOI: 10.1002/aenm.201901891



## Review

# Algal biorefinery: An integrated approach for sustainable biodiesel production

Dipesh Kumar, Bhaskar Singh \*

Department of Environmental Sciences, Central University of Jharkhand, Ranchi, Jharkhand, 835 205, India



## ARTICLE INFO

## Keywords:

Microalgae  
Biorefinery  
Biodiesel  
Techno-economic assessment  
Environmental sustainability

## ABSTRACT

Numerous studies on the techno-economic and life cycle assessment of microalgal biodiesel production are available in the literature, and an overwhelming majority of such studies suggest that the standalone production of biodiesel is currently unviable. The production of microalgal biomass using the currently available technologies costs approximately  $\$4.92 \text{ kg}^{-1}$ , which is unacceptably high for biodiesel production. The challenges lie in high biomass production cost and unfavorable energetic balance and significant process, and engineering advancements are desirable before mass-scale production of algal oil and biodiesel at a cost-competitive price is realized. On the other hand, various high-value products sourced from microalgae are already commercialized. The biomass production cost of  $\$4.92 \text{ kg}^{-1}$  is more than acceptable if such products are also derived which, according to some estimates, may command a price as high as  $\$123 \text{ kg}^{-1}$  biomass. It is expected that with process modifications and engineering advancements, the biomass production cost can be brought down to as low as  $\$0.50 \text{ kg}^{-1}$ . Moreover, coupling phycoremediation of pollution loads in waste streams to microalgal biomass production offers economic (up to  $\$170 \text{ t}^{-1}$  biomass produced) and environmental gains (90% reduction in water footprint, improved GHG balance, and a substantial reduction in external input of fertilizers). Such approaches are more likely to translate into an economically appealing and environmentally desirable business model. The current study is an attempt to analyze some of the recent research investigations addressing the concept of a microalgal biorefinery for the production of biodiesel.

## 1. Introduction

Energy is a vital input for growth and sustenance of our socio-economic structure. The demand for energy is growing steadily in line with population growth, economic development, and urbanization. Critical dependence on traditional forms of energy (fossil fuels) is unsustainable in the long run from environmental as well as economic point of view [1]. The value of energy return on energy investment (EROI) for the extraction of oil and gas is now on a declining path [2]. Furthermore, fossil fuels have historically remained to be one of the most significant sources of greenhouse gases (GHGs) and environmental pollution [2]. These concerns, along with several other direct and indirect impacts associated with the extraction and combustion of fossil fuels, have spurred tremendous interest in the development and utilization of alternative forms of energy [3].

Along with solar and wind energy, bioenergy is at the forefront of scientific and policy attention as it offers several clear-cut advantages over traditional and new forms of energy. Bioenergy is energy derived

from living/recently living biomass in the form of heat, electricity, and energy carriers (biofuels) [4]. The potential of bioenergy in meeting energy security and environmental sustainability is tremendous, and it has been highlighted by several researchers [5,6]. Gauging the attractiveness of bioenergy several nations across the globe have introduced ambitious legislation mandates for incorporating bioenergy in the national energy mix [7]. Although the mass-scale production potential of bioenergy is tremendous, the economics and sustainability of such large-scale systems are repeatedly being questioned. It is primarily attributed to the following; low EROI, the high cost of biomass production, direct and indirect emission of GHGs, and the requirement of space, freshwater, and nutrients [8].

The concept of the biorefinery is akin to petroleum refineries in which a variety of products are derived from biomass feedstocks [9]. Biorefinery integrates different components of biomass, conversion routes, and equipment to produce energy, feed, chemicals, and nutraceuticals. International Energy Agency's bioenergy task document No. 42 defines biorefinery as "the sustainable processing of biomass into a

\* Corresponding author.

E-mail address: [bhaskar.singh@cuja.ac.in](mailto:bhaskar.singh@cuja.ac.in) (B. Singh).

# Performance Limitation of Si Nanowire Solar Cells: Effects of Nanowire Length and Surface Defects

Deepika Bora<sup>1,3,b)</sup>, Shrestha Bhattacharya<sup>2,3,c)</sup>, Nitin Kumar<sup>3,4,d)</sup>, Aishik Basu Mallick<sup>2,3,e)</sup>, Avritti Srivastava<sup>3,4,f)</sup>, Mrinal Dutta<sup>3,a)</sup>, Sanjay K. Srivastava<sup>3,4,g)</sup>, P. Prathap<sup>3,4,h)</sup> and C.M.S. Rauthan<sup>3,i)</sup>

<sup>1</sup>Amity Institute of Applied Science, Amity University, Noida, India

<sup>2</sup>Department of Energy Engineering, Central University of Jharkhand, Jharkhand-835205, India

<sup>3</sup>PV Metrology Group, Advanced Materials Devices and Metrology Division, CSIR-National Physical Laboratory (NPL), New Delhi-110012, India

<sup>4</sup>Academy of Scientific and Innovative Research, CSIR-NPL Campus, New Delhi-110012, India.

<sup>a)</sup>Corresponding author: [sspmd.iacs@gmail.com](mailto:sspmd.iacs@gmail.com), [duttamrinal1081@gmail.com](mailto:duttamrinal1081@gmail.com)

<sup>b)</sup>[deepika.bora.56@gmail.com](mailto:deepika.bora.56@gmail.com), <sup>c)</sup>[shrestha.bhattacharya@cuja.ac.in](mailto:shrestha.bhattacharya@cuja.ac.in), <sup>d)</sup>[nitinphykumar@gmail.com](mailto:nitinphykumar@gmail.com),

<sup>e)</sup>[abmallick6206@gmail.com](mailto:abmallick6206@gmail.com), <sup>f)</sup>[avrittisrivastava@gmail.com](mailto:avrittisrivastava@gmail.com), <sup>g)</sup>[srivassk@nplindia.org](mailto:srivassk@nplindia.org), <sup>h)</sup>[pathiprathap@gmail.com](mailto:pathiprathap@gmail.com), <sup>i)</sup>[cms.rauthan@nplindia.org](mailto:cms.rauthan@nplindia.org)

**Abstract.** In Si nanowire (SiNW) solar cells enhanced light confinement property in addition to decoupling of charge carrier collection and light absorption directions plays a significant role to resolve the drawbacks of bulk Si solar cells. In this report we have studied the dependence of the photovoltaic properties of Si NW array solar cells on the SiNW length and enhanced surface defect states as a result of enhanced surface area of the NWs. The SiNW arrays have been fabricated using metal catalyzed electroless etching (MCEE) technique. p-n junction has been produced by spin-on-dopant technique followed by thermal diffusion process. Front and rear electrodes have been deposited by e-beam evaporation techniques. SiNW lengths have been controlled from ~ 320 nm to 6.4  $\mu$ m by controlling the parameters of MCEE technique. Photovoltaic properties of the solar cells have been characterized by measuring quantum efficiency and photocurrent density vs. voltage characteristics. Morphological studies have been carried out by using scanning electron microscopy. Reduction in light trapping capability comes at the benefit of reduced surface defects. The reduction of surface defects has been proved to be more advantageous in comparison to the decrement of light trapping capability. The major contribution to the changes in cell efficiency comes from the enhancement of short circuit current density with a very weak dependence on open circuit voltage. This work is beneficial for the production of commercial Si solar cells where SiNW arrays could be used as an antireflection coating instead of using separate antireflection layers. Thus could reduce the production cost.

## INTRODUCTION

Silicon nanowires (SiNWs) have attracted global attention as a promising material to achieve high efficiency at low cost due to their unique structural, optical, and electrical properties [1, 2]. As Si has low absorption in the visible and near infrared region of the solar spectrum, so efficient commercial Si solar cells to fully absorb incident sunlight need relatively large amounts of high-purity solar-grade Si. In this decade, worldwide effort has been started to address this problem by fabricating SiNW based solar cells. Due to light-trapping within the NW arrays these cells exhibit a higher absorbance per unit thickness compare to commercial Si solar cells and thus open a path to avoid the need of extra antireflection coating layer that could lower the production cost [3].

There are several processes like CVD, molecular beam epitaxy, reactive ion etching in addition to lithography, metal catalyzed electroless etching (MCEE) technique etc. which are used to fabricate SiNWs [4]. Among these MCEE technique is only simple and low-cost while others are costly and time consuming. By MCEE technique

# Relativistic charged spheres: compact stars, compactness and stable configurations

J. Kumar,<sup>a</sup> S.K. Maurya,<sup>b,1</sup> A.K. Prasad<sup>a</sup> and Ayan Banerjee<sup>c</sup>

<sup>a</sup>Department of Applied Mathematics, Central University of Jharkhand, Ranchi-835205, India

<sup>b</sup>Department of Mathematical and Physical Sciences, College of Arts and Science, University of Nizwa, Nizwa, Sultanate of Oman

<sup>c</sup>Astrophysics and Cosmology Research Unit, University of KwaZulu Natal, Private Bag X54001, Durban 4000, South Africa

E-mail: [jitendark@gmail.com](mailto:jitendark@gmail.com), [sunil@unizwa.edu.om](mailto:sunil@unizwa.edu.om), [amitkarun5@gmail.com](mailto:amitkarun5@gmail.com), [ayan-7575@yahoo.co.in](mailto:ayan-7575@yahoo.co.in)

Received November 9, 2018

Revised August 4, 2019

Accepted October 18, 2019

Published November 5, 2019

**Abstract.** This paper aims to explore a class of static stellar equilibrium configuration of relativistic charged spheres made of a charged perfect fluid. For solving the Einstein-Maxwell field equations, we consider a particularized metric potential, Buchdahl ansatz [60] and then by using a simple transformation. The study is developed by matching the interior region with Riessner-Nordström metric as an exterior solution. The matter content the charged sphere satisfies all the energy conditions and hydrostatic equilibrium equation, i.e. the modified Tolman-Oppenheimer-Volkoff (TOV) equation for the charged case is maintained. In addition to this, we also discuss some important properties of the charged sphere such as total electric charge, mass-radius relation, surface redshift, and the speed of sound. Obtained solutions are presented by the graphical representation that provides strong evidence for a more realistic and viable stellar structure. Obtained results are compared with analogue objects with similar mass and radii, such as SAX J1808.4-3658, 4U 1538-52, PSR J1903+327, Vela X-1, and 4U1608-52. It is also noted that the Buchdahl ansatz for a given transformation provides a physically viable solution only for the charged case when  $0 < K < 1$ , where density and pressure are maximum at the center and monotonically decreasing towards the boundary. Obtained results are also quite important both from theoretical and astrophysical scale to analyze other compact objects such as white dwarfs, neutron stars, boson stars, and quark stars.

**Keywords:** first stars, neutron stars, stars, white and brown dwarfs

**ArXiv ePrint:** [1804.01779](https://arxiv.org/abs/1804.01779)

<sup>1</sup>Corresponding author.



# Optimization of Dielectric Properties of PVDF–CFO Nanocomposites

Sweety Supriya,<sup>1</sup> Lawrence Kumar,<sup>2</sup> Manoranjan Kar<sup>1</sup>

<sup>1</sup>Department of Physics, Indian Institute of Technology Patna, Bihta, Patna, 801103, India

<sup>2</sup>Department of Nanotechnology, Central University of Jharkhand Ranchi, Ranchi, Jharkhand, 835205, India

**Incorporation of different types of nanofillers in the PVDF poly(vinylidene difluoride) matrix exhibits promising dielectric, magnetic, piezo, pyro, and ferroelectric properties for various applications. Hence a novel nanocomposite has been developed by using PVDF and cobalt ferrite (CFO) (CoFe<sub>2</sub>O<sub>4</sub>) with different particle size of CFO for dielectric applications. The nanocomposite has been characterized by the X-ray diffraction pattern, atomic force microscopy, transmission electron microscopy, fourier transform infrared spectroscopy, field emission-scanning electron microscopy, and dielectric measurements. The space charge effect at the PVDF and CFO interfaces offers the interfacial polarization in nanocomposite, which contribute to tune the dielectric response of nanocomposite along with low dielectric loss. The filler size has been optimized to have better formation of polar  $\beta$  phase in PVDF along with high dielectric properties. The dielectric constant in nanocomposite has increased three times compare to that of PVDF. The  $20 \pm 1$  nm size (CFO) filler in PVDF matrix exhibits optimized dielectric properties. POLYM. COMPOS., 2018. © 2018 Society of Plastics Engineers**

## INTRODUCTION

In order to enhance the performance of the dielectric material, that is, to have an improved capacitive effect of the ferrite and polymer based nanocomposite films have grabbed the researchers' attention in the recent years. The nanocomposite films having good flexibility, strength, and compactness can be used to make portable and durable devices [1]. To fulfill these requirements, PVDF (poly [vinylidene difluoride]) polymer has been utilized because of its unique properties like thermal stability, good chemical resistance and extraordinary pyroelectric and piezoelectric properties, flexibility, high dielectric breakdown field, and so forth. [1,2]. PVDF is a semicrystalline polymer that is, both crystalline and amorphous phases are present in the bulk PVDF. PVDF consists of carbon as the backbone,

hydrogen and fluorine as substituent, which is depicted in the Fig. 1a and b for  $\alpha$  and  $\beta$  phases of PVDF, respectively. It has four unique crystalline phases called  $\alpha$  (in *trans-gauche twist conformation TGTG'*),  $\beta$  (in all *trans* planar zigzag conformation *TTTT*),  $\gamma$  (three *trans* linked to a *gauche* conformation *TTTGTG'*, in an intermediate conformation of the PVDF  $\alpha$  and  $\beta$  phases), and  $\delta$  (a polar version of the  $\alpha$  phase) [2]. Percentages of individual phases present in PVDF depend on the processing conditions, chain conformation and molecular packing [2]. Among all the crystalline phases,  $\alpha$  (paraelectric) and  $\beta$  (ferroelectric) phases are most significant.  $\alpha$  is the non polar phase and rest are polar phases, among which  $\beta$  phase exhibits very strong polarization. The dielectric, piezoelectric, and ferroelectric properties of PVDF lies in these phases, but especially polar  $\beta$  phase is responsible for high dielectric properties of PVDF. This is due to its polarized structure of all-*trans* planar zigzag conformation between positive hydrogen ion and negative fluorine ion. The total potential energy due to intramolecular and intermolecular interaction of the  $\beta$  phase of PVDF is higher than that of  $\alpha$  and  $\gamma$  phases of PVDF [3]. The  $\alpha$ -phase has *trans gauche* (TGTG) bond conformation obtained generally by solvent cast method. In this phase, hydrogen and fluorine are at  $\pm 60^\circ$  to each other and connected to carbon atom shown in the Fig. 1a [2]. The  $\beta$ -phase has all *trans* (TTT) bond conformation with hydrogen and fluorine atoms are on opposite side (at  $180^\circ$ ) and forms the net non zero dipole moment [1,2] as shown in Fig. 1b [2]. The polar  $\beta$  phase, intensively contribute to dipole formation and enhance the dielectric properties and hence the capacitive performance for versatile application in electronic industry. However, the properties of PVDF need to be improved for the industrial needs [4]. And that requires to fabricate PVDF based nanocomposites with better dielectric properties compared with PVDF without losing its mechanical strength and other physical properties. Nanocomposites are opted for better tunability of the physical properties for nano scale portable devices as today's requirement. For this, one can deal in order to have nano sized core within the shell of

Correspondence to: M. Kar; e-mail: mano@iitp.ac.in


DOI 10.1002/pc.24840

Published online in Wiley Online Library (wileyonlinelibrary.com).

© 2018 Society of Plastics Engineers



## Examination of break-up fusion in the $^{16}\text{O} + ^{148}\text{Nd}$ system through measurements of forward recoil range distributions and angular distributions

Pankaj K. Giri <sup>1</sup>, Amritraj Mahato,<sup>1</sup> D. Singh,<sup>1,\*</sup> Sneha B. Linda,<sup>1</sup> Harish Kumar,<sup>2</sup> Suhail A. Tali,<sup>2</sup> M. Afzal Ansari,<sup>2</sup> R. Kumar,<sup>3</sup> S. Muralithar,<sup>3</sup> and R. P. Singh<sup>3</sup>

<sup>1</sup>*Department of Physics, Central University of Jharkhand, Ranchi 835 205, India*

<sup>2</sup>*Department of Physics, Aligarh Muslim University, Aligarh 202 002, India*

<sup>3</sup>*Inter University Accelerator Centre, Aruna Asaf Ali Marg, New Delhi 110 067, India*



(Received 7 August 2019; revised manuscript received 25 September 2019; published 11 November 2019)

The forward recoil range distributions and angular distributions of several evaporation residues produced via complete and incomplete fusion (ICF) dynamics in  $^{16}\text{O} + ^{148}\text{Nd}$  system at energy  $\approx 6$  MeV/nucleon were measured. The measured forward recoil range distributions of various reaction products show the presence of incomplete fusion components apart from complete fusion. Full and partial linear momentum transfer components of reaction products were found in the interaction of  $^{16}\text{O}$  with  $^{148}\text{Nd}$ . These results were also confirmed by the measurements of angular distributions of evaporation residues. The measured angular distributions of the evaporation residues populated through complete and incomplete fusion channels were found to be distinctly different. The evaporation residues populated via complete fusion channels were trapped in the narrow angular zone as compared to incomplete fusion channels. A systematic study of the dependence of incomplete fusion dynamics on well-known entrance channel parameters shows that the incomplete fusion fraction grows exponentially with mass asymmetry ( $\mu_{EC}^{AS}$ ), Coulomb factor ( $Z_P Z_T$ ) and  $\alpha$ - $Q$  value of the projectile. The present observations suggest an exponential rise of ICF fraction with entrance channel parameters in contrast with the linear pattern reported in some earlier measurements. Further, the correlation of incomplete fusion fraction with the structure of target (T) was investigated employing four different parameters viz. deformation parameter ( $\beta_2^T$ ), interaction radius ( $R^T$ ), deformation length ( $\beta_2^T R^T$ ) and excess of neutrons ( $N - Z$ )<sup>T</sup> in the target. In the present study, the ICF fraction was found to rise exponentially with these parameters, independently for different projectiles. The three parameters  $\beta_2^T$ ,  $\beta_2^T R^T$ , and ( $N - Z$ )<sup>T</sup> were found more sensitive and effective to investigate the entire picture about the influence of projectile and target deformation along with their relative orientations on incomplete fusion dynamics at low projectile energy. Moreover, the interaction radius of target ( $R^T$ ) is suitable to explain the characteristics of ICF dynamics in the spherical-spherical collisions. These present results show that incomplete fusion dynamics is strongly affected by the structure of projectile along with the target.

DOI: [10.1103/PhysRevC.100.054604](https://doi.org/10.1103/PhysRevC.100.054604)

### I. INTRODUCTION

The study of the break-up of the projectile and incomplete fusion induced by heavy ions (HI) at low projectile energy has been a topic of special interest in nuclear physics [1–4]. It is a well-known fact that the complete fusion (CF) and incomplete fusion (ICF) are the most dominant modes of reaction in heavy-ion interactions at energy above the Coulomb barrier. As the incident projectile energy increases, the unambiguous reaction processes are the formation of the compound nucleus followed by the fusion of entire projectile with the target nucleus and decay of an excited compound nucleus. In this CF reaction, all nucleonic degrees of freedom are involved. However, for the projectile incident on target with relatively higher energy and impact parameter, the repulsive centrifugal potential increases. Hence, the dominance of attractive nuclear potential ceases to capture the entire projectile by the

target. Therefore, only a part of the projectile fuses with the target nucleus and the remnant behaves as a spectator, wherein an incompletely fused composite system may be formed and the ICF (break-up fusion) process may take place [5]. The probability of ICF reaction was experimentally observed for the first time [6] in the production of forward-peaked fast  $\alpha$  particles in the break-up of the projectiles  $^{16}\text{O}$ ,  $^{14}\text{N}$ , and  $^{12}\text{C}$  at energy  $\approx 10.5$  MeV/nucleon. However, the advances in the study of ICF dynamics took place after the measurements of transition intensity distributions (spin distribution) of evaporation residues (ERs) using particle  $\gamma$ -coincidence technique [7]. Evidence for the ICF process was also found by measuring the forward-peaked  $\alpha$  particles in the kinetic energy spectra and angular distribution of  $\alpha$  particles [8] and from time-of-flight measurements [9] of ERs. The analysis of measured excitation functions (EFs) data [10–12] shows that the ICF process has a substantial contribution to the reaction cross sections.

Several theoretical models were proposed to explain the ICF dynamics, such as break-up fusion (BUF) model [13],

\*Corresponding author: [dsinghcuji@gmail.com](mailto:dsinghcuji@gmail.com)





## Pea (*Pisum sativum* L.) peel waste carbon loaded with zirconium: study of kinetics, thermodynamics and mechanism of fluoride adsorption

S. K. Swain<sup>a</sup>, Simpi Bhawna Patel<sup>b</sup>, Amulya Prasad Panda<sup>a</sup>, Tanushree Patnaik<sup>c</sup>, and R. K. Dey<sup>b</sup>

<sup>a</sup>Central Instrumentation Facility, Birla Institute of Technology, Ranchi, India; <sup>b</sup>Centre for Applied Chemistry, Central University of Jharkhand, Ranchi, India; <sup>c</sup>Department of Chemistry, Stewart Science College, Cuttack, India

### ABSTRACT

Pea peel waste carbon loaded with zirconium is used as an engineered biochar material for adsorption of fluoride from aqueous solution. The prepared adsorbent was characterized and the material degradation kinetics were studied using thermogravimetric analysis. Adsorption kinetics follow both pseudo-second order and intra-particle diffusion model. Optimization of algorithm yielded Freundlich isotherm as the best fitting equation. Increment in solution temperature thermodynamically favors fluoride adsorption. Fluoride adsorption remains unaffected in presence of specific co-ions. Adsorbed fluoride could be successfully leached using 0.001 N NaOH and reusability of the material was tested up to tenth cycle of continuous operation.

### ARTICLE HISTORY

Received 17 January 2018  
Accepted 29 October 2018

### KEYWORDS





Pea peel; bio-sorbent;  
zirconium; fluoride;  
adsorption

### Introduction


Availability of safe drinking water is an utmost priority around the world due to limited drinking water resources.<sup>[1]</sup> Presence of excess fluoride in drinking water has been a concern for long time, therefore, requires an urgent and sustainable solution.<sup>[2]</sup> Technologically, conventional methods like adsorption/ion-exchange and coagulation processes are quite simple and hence find extensive use in developing countries like India for the purpose of defluoridation of drinking water in fluoride endemic areas.<sup>[3]</sup> However, use of such method also risks generation of secondary pollutants. Hence, in search of environmentally amenable, cost effective and efficient adsorbents, use of biowaste materials presents an alternate viable option.

Biochar, a pyrogenic carbon material, is generated by combustion of biomass under limited oxygen condition.<sup>[4]</sup> Engineering biochar represents materials which is prepared through pyrolysis of pretreated biomass feed stocks.<sup>[5]</sup> Such kind of material also possesses high surface area and pore volume as required for good adsorption characteristics. Pea peel waste, obtained from outer cover of *Pisum sativum* L., is a widely available lingo-cellulosic biomass. Various organic materials such as holocellulose and lignin are major constituents of oven dried pea peel waste.<sup>[6]</sup> Use of

pea peel waste for adsorption of methylene blue,<sup>[7]</sup> amaranth dye,<sup>[8]</sup> and heavy metals<sup>[9]</sup> has also been reported previously. Adsorption characteristics of pea peel waste are essential due to its heterogeneous pore structure. The surface characteristics of the material favor electrostatic interactions with ions in solution which facilitates the adsorption process. Thus, the macropore surface structure of green pea peel facilitates faster uptake of dye from solution in comparison to commercial activated carbon.<sup>[7,8]</sup> The proximate as well as ultimate analysis of green pea peels shows that the dried material contains approximately 0.60% of fixed carbon with porosity 61% indicating characteristics of carbonaceous materials.<sup>[10]</sup> Evaluation of surface charge of green pea peel material indicates that the material can be used suitably for removal of both cationic as well as anionic kind of impurities from solution.<sup>[10]</sup> In addition, the presence of functional groups such as carboxylic acid also makes the material most suitable for metal adsorption. The thermogravimetric (TG) properties of the green pea peel were studied up to 400°C where the material loss within 150–400°C was attributed to the decomposition of cellulose and hemicellulose.<sup>[10]</sup> Material weight loss was found to be very less beyond 400°C which could be attributed to the presence of more stable fixed carbon at higher temperature.

**CONTACT** R. K. Dey  [rkdey@rediffmail.com](mailto:rkdey@rediffmail.com)  Central Instrumentation Facility, Birla Institute of Technology, Ranchi, India; S. K. Swain  [sanjayarkl@gmail.com](mailto:sanjayarkl@gmail.com)  
 Centre for Applied Chemistry, Central University of Jharkhand, Ranchi, India

Color versions of one or more of the figures in the article can be found online at [www.tandfonline.com/lsst](http://www.tandfonline.com/lsst).

 Supplemental data for this article can be accessed [here](#).

## Implementing an object-based multi-index protocol for mapping surface glacier facies from Chandra-Bhaga basin, Himalaya

Shridhar Digambar Jawak<sup>1,2</sup>, Sagar Filipe Wankhede<sup>2,3,4\*</sup>, Alvarinho Joaozinho Luis<sup>2</sup>, Prashant Hemendra Pandit<sup>5</sup>, Shubhang Kumar<sup>6</sup>

<sup>1</sup>*Svalbard Integrated Arctic Earth Observing System (SIOS), SIOS Knowledge Centre, Svalbard Science Park, N-9171, Longyearbyen, Svalbard, Norway*

<sup>2</sup>*Earth System Science Organization (ESSO), National Centre for Polar and Ocean Research (NCPOR), Ministry of Earth Sciences (MoES), Govt. of India, Headland Sada, Goa 403804, India*

<sup>3</sup>*Department of Civil Engineering, Manipal Institute of Technology, Manipal Academy of Higher Education, Manipal, Karnataka 576104, India*

<sup>4</sup>*Department of Marine Geology, Mangalore University, Mangalagangothri, Karnataka 574199, India*

<sup>5</sup>*National Bureau of Soil Survey and Land Use planning (NBSS & LUP) - Indian Agriculture Research Institute (IARI), New Delhi 110012, India*

<sup>6</sup>*Centre for Land Resource Management, Central University of Jharkhand, Ranchi 835205, India*

### Abstract

Surface glacier facies are superficial expressions of a glacier that are distinguishable based on differing spectral and structural characteristics according to their age and inter-mixed impurities. Increasing bodies of literature suggest that the varying properties of surface glacier facies differentially influence the melt of the glacier, thus affecting the mass balance. Incorporating these variations into distributed mass balance modelling can improve the perceived accuracy of these models. However, detecting and subsequently mapping these facies with a high degree of accuracy is a necessary precursor to such complex modelling. The variations in the reflectance spectra of various glacier facies permit multiband imagery to exploit band ratios for their effective extraction. However, coarse and medium spatial resolution multispectral imagery can delimit the efficacy of band ratioing by muddling the minor spatial and spectral variations of a glacier. Very high-resolution imagery, on the other hand, creates distortions in the conventionally obtained information extracted through pixel-based classification. Therefore, robust and adaptable methods coupled with higher resolution data products are necessary to effectively map glacier facies. This study endeavours to identify and isolate glacier facies on two unnamed glaciers in the Chandra-Bhaga basin, Himalayas, using an established object-based multi-index protocol. Exploiting the very high resolution offered by WorldView-2 and its eight spectral bands, this study implements customized spectral index ratios via an object-based environment. Pixel-based supervised classification is also performed using three popular classifiers to comparatively gauge the classification accuracies. The object-based multi-index protocol delivered the highest

---

Received May 27, 2019, accepted December 30, 2019.

\*Corresponding author: S. F. Wankhede <swankhede436@gmail.com>

*Acknowledgements:* The authors thank Dr. Gangadhara Bhat, Chairman, Dept. of Geoinformatics, Mangalore University, and Dr. M. Ravichandran, Director ESSO-NCPOR for their motivation and support.

# Effect of Annealing Temperature on Morphology and Magnetic Properties of Cobalt Ferrite Nanofibers

Suman Kumari<sup>1</sup>, Lagen Kumar Pradhan<sup>1</sup>, Lawrence Kumar<sup>2</sup>, Murli Kumar Manglam<sup>1</sup>, and Manoranjan Kar<sup>1\*</sup>

<sup>1</sup> Department of Physics, Indian Institute of Technology Patna, Bihta, Patna-801106, Bihar, India

<sup>2</sup> Department of Nanoscience and Technology, Central University of Jharkhand, Ranchi-835205, Jharkhand, India

E-mail: mano@iitp.ac.in

Received xxxxxx

Accepted for publication xxxxxx

Published xxxxxx

## Abstract

Magnetic nanofibers of cobalt ferrite (CFO) have been prepared by the electrospinning technique using the solution of cobalt nitrate and iron nitrate mixed with a supporting media polyvinylpyrrolidone. A high voltage (~9 kV) has been applied to overcome the surface tension of the polymer solution. The as-spun nanofibers are annealed at three different temperatures (i.e. 600°C, 800°C, and 1000°C) to study the effect of annealing temperature on the growth of CFO and magnetic properties of nanofibers. X-ray diffraction (XRD) pattern reveals the formation of inverse spinel cobalt ferrite phase. The monotonous increase of the crystallite size of nanofiber from 26nm (at 600°C) to 45nm (at 1000°C) with the increase of annealing temperature has been observed from the XRD pattern. The Field Emission Scanning Electron Microscopy (FE-SEM) micrograph confirms the formation of nanofibers. The effect of annealing temperature on magnetocrystalline anisotropy constant, saturation magnetization ( $M_s$ ), morphology, porosity, grain size of the CFO nanofibers has been explained. It is interesting to note that the magnetocrystalline anisotropy constant of CFO nanofibers increases with the decrease in temperature.

Keywords: Nanofiber, Magnetocrystalline anisotropy constant, Electrospinning technique

## 1. Introduction

Ferrites are one of the magnetic materials, which is known for their spontaneous magnetization. It is widely used for industrial applications [1]. The development of new and cost-effective techniques for ferrite nanostructures is of great scientific interest. One-dimensional magnetic material (nanorods and nanofibers) has attracted attention of scientific communities for their technical applications, especially in nanotechnology [2,3]. These nanostructured materials are also useful inactive components such as ultrahigh-density data storage devices, sensors and spintronic related devices [4]. Cobalt ferrite ( $\text{CoFe}_2\text{O}_4$ ), better known as CFO, possesses high magneto-crystalline anisotropy energy with positive anisotropy constant [5]. It exhibits cubic inverse spinel ferrite structure and belongs to  $\text{AB}_2\text{O}_4$  group. The symmetry of cubic structure has multiple easy directions. It

has six easy directions along the cubic edges of the crystal and four hard directions along the body diagonals, which are represented as  $\langle 100 \rangle$  and  $\langle 111 \rangle$ , respectively. There are 12 saddle points across the face diagonals of spinel ferrite [6]. The large magnetic anisotropy energy of cobalt ferrite is due to the presence of  $\text{Co}^{2+}$  ions on the B-site of the spinel cobalt ferrite. The crystal field of spinel ferrite has not been able to quench the orbital magnetic moment. Therefore, the large magneto-crystalline anisotropy energy is observed due to presence of strong L-S coupling [7]. The magnetic properties of material strongly depend on the interaction between A and B sites of cation distribution in cubic spinel ferrite. It also depends upon the lattice parameter, crystallite size, bond angle, and bond length. The cation migration between octahedral and tetrahedral sites in spinel ferrites depends upon the preparation technique and annealing condition [8]. The above parameters can be tuned by using different synthesis methods and experimental conditions [9].



ELSEVIER

Contents lists available at ScienceDirect

## Seminars in Cancer Biology

journal homepage: [www.elsevier.com/locate/semcancer](http://www.elsevier.com/locate/semcancer)

## Review

## Glycogen synthase kinases: Moonlighting proteins with theranostic potential in cancer

Siddavaram Nagini<sup>a,\*</sup>, Josephraj Sophia<sup>a</sup>, Rajakishore Mishra<sup>b</sup><sup>a</sup> Department of Biochemistry and Biotechnology, Faculty of Science, Annamalai University, Annamalaiagar 608 002, Tamil Nadu, India<sup>b</sup> Centre for Life Sciences, School of Natural Sciences, Central University of Jharkhand, Ratu-Lohardaga Road, Brambe, Ranchi 835205, Jharkhand, India

## ARTICLE INFO

## Keywords:

Cancer  
GSK-3  
MicroRNA  
Moonlighting proteins  
Oncogenic signalling  
Targeted therapy

## ABSTRACT

Glycogen synthase kinase-3 (GSK-3), a serine/threonine kinase is an archetypal multifunctional moonlighting protein involved in diverse cellular processes including metabolism, insulin signaling, proliferation, differentiation, apoptosis, neuronal function and embryonic development. The two known isoforms, GSK-3 $\alpha$  and GSK-3 $\beta$  that undergo activation/inactivation by post-translational, site-specific phosphorylation incorporate a vast number of substrates in their repertoire. Dysregulation of GSK-3 has been linked to diverse disease entities including cancer. The role of GSK-3 in cancer is paradoxical and enigmatic. The enzyme functions as a tumour promoter or suppressor based on the context, cell type and phosphorylation status. GSK-3 is the central hub that orchestrates signals from the Wnt/ $\beta$ -catenin, PI3K/PTEN/Akt/mTOR, Ras/Raf/MEK/ERK, hedgehog, Notch and TP53 pathways to elicit regulatory influences on cancer initiation, epithelial-mesenchymal transition, and resistance to therapy. As a direct target of several microRNAs, GSK-3 influences hallmark attributes of cancer, cancer stemness and treatment resistance. There is overwhelming evidence to indicate that GSK-3 is aberrantly regulated in different cancer types. Consequently, GSK-3 has emerged as a potential therapeutic target in cancer. A plethora of natural and synthetic GSK-3 modulators have been discovered and the number of patents published for GSK-3 inhibitors has also been steadily increasing in recent years. This review focuses on the intricate interactions between GSK-3 and oncogenic signalling circuits as well as the feasibility of targeting GSK-3 for the treatment of cancer.

## 1. Introduction

Glycogen synthase kinase 3 (GSK-3), a family of proteins with two known members, GSK-3 $\alpha$  and GSK-3 $\beta$  are enzymes that belong to the serine/threonine group of protein kinases. GSK-3, first isolated from rat skeletal muscle was identified as a kinase that phosphorylates and inactivates glycogen synthase, the last enzyme in glycogen biosynthesis [1]. Over the years, dysregulation of GSK-3 has been linked to diverse disease entities including diabetes, atherosclerosis, neurodegenerative disorders and a wide range of malignant tumours [2,3]. GSK-3 is recognised to play a paradoxical role in cancer. The enzyme functions as a tumour promoter or suppressor based on the context, cell type and

phosphorylation status [4–6].

Accumulating evidence has provided proof-of-concept that targeting GSK-3 is a promising strategy for treating malignant tumours [7,8]. Aberrant GSK-3 $\beta$  expression has also been implicated in resistance to radiation and chemotherapy [9]. This review summarizes the physiological functions, activation/inactivation of GSK-3, and the complex role of GSK-3 in cancer hallmarks. The major focus of this review is on the intricate interactions between GSK-3 and oncogenic signalling circuits and microRNAs as well as the potential of GSK-3 for the therapeutic intervention of cancer.

**Abbreviations:** 6 BIO, 6-bromindirubine-3'-monoxime; ADMET, absorption, distribution, metabolism, elimination and toxicity; AMPK, 5'-adenosine monophosphate-activated protein kinase; APC, adenomatous polyposis coli; CDK, cyclin-dependent kinase; CK1, casein kinase-1; CSCs, cancer stem cells; Doc, docetaxel; EGF, epidermal growth factor; EMT, epithelial-mesenchymal transition; ERK, extracellular regulated kinase; GADD45, growth arrest and DNA damage 45; GBM, glioblastoma multiforme; GSCs, glioblastoma stem-like cells; GSK-3, glycogen synthase kinase-3; Hh, hedgehog; IRS-1, insulin receptor substrate-1; IRS-2, insulin receptor substrate-2; JNK, c-jun N-terminal kinase; MAPK, mitogen-activated kinase; MMP, matrix metalloproteinase; mTOR, mammalian target of rapamycin; NF- $\kappa$ B, nuclear factor-kappaB; NICD, notch intracellular domain; p70S6K, p70 ribosomal S6 kinase; p90RSK, p90 ribosomal S6 kinase; PDGF, platelet-derived growth factor; PI3K, phosphatidylinositol 3-kinase; PKA, protein kinase A; PKB, protein kinase B; PP, protein phosphatase; PTEN, phosphatase and tensin homolog; PYK2, proline-rich tyrosine kinase 2; SMO, smoothened; SUFU, suppressor of fused; TCF/LEF, T-cell factor/lymphoid enhancer factor; TDZD, thiazolidinone; TLR, toll-like receptor; TNF- $\alpha$ , tumour necrosis factor-alpha

\* Corresponding author.

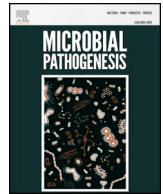
E-mail address: [nagini.s.1602@annamalaiuniversity.ac.in](mailto:nagini.s.1602@annamalaiuniversity.ac.in) (S. Nagini).<https://doi.org/10.1016/j.semcan.2017.12.010>Received 4 July 2017; Received in revised form 23 October 2017; Accepted 28 December 2017  
1044-579X/© 2017 Published by Elsevier Ltd.



ELSEVIER

Contents lists available at ScienceDirect

## Microbial Pathogenesis

journal homepage: [www.elsevier.com/locate/micpath](http://www.elsevier.com/locate/micpath)

## A trial sequential meta-analysis of *IFN- $\gamma$* +874 A > T (rs2430561) gene polymorphism and extrapulmonary tuberculosis risk

Raju K. Mandal<sup>a</sup>, Mohd Wahid<sup>a</sup>, Arshad Jawed<sup>a</sup>, Sajad A. Dar<sup>a</sup>, Aditya K. Panda<sup>b</sup>,  
Naseem Akhter<sup>c</sup>, Mohtashim Lohani<sup>d</sup>, B.N. Mishra<sup>e</sup>, Saif Khan<sup>f</sup>, Mohammed Y. Areeshi<sup>a</sup>,  
Shafiul Haque<sup>a,\*</sup>

<sup>a</sup> Research and Scientific Studies Unit, College of Nursing & Allied Health Sciences, Jazan University, Jazan, 45142, Saudi Arabia

<sup>b</sup> Centre for Life Sciences, Central University of Jharkhand, Ranchi, 835205, Jharkhand, India

<sup>c</sup> Department of Laboratory Medicine, Faculty of Applied Medical Sciences, Albaha University, Albaha, 65431, Saudi Arabia

<sup>d</sup> Department of Emergency Medical Services, College of Applied Medical Sciences, Jazan University, Jazan, 45142, Saudi Arabia

<sup>e</sup> Department of Biotechnology, Institute of Engineering & Technology, Lucknow, 226021, Uttar Pradesh, India

<sup>f</sup> Department of Basic Sciences, College of Dentistry, University of Ha'il, Hail, 2440, Saudi Arabia

## ARTICLE INFO

## Keywords:

Meta-analysis

*IFN- $\gamma$* 

Pulmonary tuberculosis

Polymorphism

Genetic model

## ABSTRACT

Interferon- $\gamma$  (*IFN- $\gamma$* ) plays a crucial role in immunological responses against *Mycobacterium tuberculosis* (*M.tb*) infection. The polymorphism at +874 A > T (rs2430561) influences the levels of *IFN- $\gamma$* , which may further influence the susceptibility to extrapulmonary tuberculosis (EPTB). This polymorphism has been investigated with respect to EPTB occurrence in different populations and provided contradictory and conflicting results. This study was performed to meta-statistically analyze the data and draw a more accurate conclusion regarding the association of *IFN- $\gamma$*  +874 A > T gene polymorphism and EPTB susceptibility. A quantitative synthesis was executed for the pertinent studies retrieved from online web-databases viz. Google Scholar, PubMed/Medline and EMBASE. The pooled odds ratios (ORs) and confidence intervals (95% CIs) were estimated for all the genetic models by meta-analysis. A total of eight studies were retrieved which included 762 confirmed EPTB cases and 1341 controls. The meta-analysis results revealed reduced association of EPTB in allelic contrast (T vs. A:  $p = 0.001$ ; OR = 0.668, 95% CI = 0.524 to 0.850), homozygous (TT vs. AA:  $p = 0.017$ ; OR = 0.450, 95% CI = 0.234 to 0.868), heterozygous (AT vs. AA:  $p = 0.004$ ; OR = 0.574, 95% CI = 0.395 to 0.835), dominant (TT + AT vs. AA:  $p = 0.003$ ; OR = 0.536, 95% CI = 0.354 to 0.810) and recessive (TT vs. AA + AT:  $p = 0.039$ ; OR = 0.662, 95% CI = 0.448 to 0.980) genetic models. Furthermore, re-sampling statistics also revealed reduced risk of EPTB in overall population and Asian subgroup. This meta-analysis concluded that *IFN- $\gamma$*  +874 A > T gene polymorphism is meaningfully related with the reduced EPTB risk in overall and Asian population, and further necessitates larger studies to be conducted on this topic in other races.

### 1. Introduction

Tuberculosis (TB) is a well-known airborne disease, caused by the pathogen *Mycobacterium tuberculosis* (*M.tb*). This disease is one of the most frequently occurring infectious diseases haunting the human race for long. It is accountable for high morbidity and mortality rate worldwide. Many effective treatment strategies have been adopted to curb this dreaded disease all over the world. But the incidences of TB cases are increasing by leaps and bounds [1]. Among all the studies conducted in the past for all type of TB cases, it was found that almost 20% cases are of extrapulmonary tuberculosis (EPTB). The reports

indicate that despite one-third population being infected with *M.tb*, only 5–10% develops actual clinical tuberculosis in their entire lifetime [2]. The identification of these high-risk, above stated, individuals would be of great help to reduce the menace of TB disease in the community.

Different agents like etiology, environment and the host immune responses interact and plays an important role in spreading and controlling TB [3]. The most important role is played by the host genetic factors in the development of TB and drug response following infection with *M.tb* [4]. The broad spectrum clinical manifestations of *M.tb* infection is managed basically by the combined effects of both the innate

\* Corresponding author.

E-mail address: [shafiul.haque@hotmail.com](mailto:shafiul.haque@hotmail.com) (S. Haque).

<https://doi.org/10.1016/j.micpath.2018.12.050>

Received 6 July 2018; Received in revised form 14 December 2018; Accepted 15 December 2018

Available online 27 February 2019

0882-4010/ © 2019 Elsevier Ltd. All rights reserved.





## EPS bound flavins driven mediated electron transfer in thermophilic *Geobacillus* sp.



Dummi Mahadevan Gurumurthy<sup>a,\*\*</sup>, Ram Naresh Bharagava<sup>b</sup>, Ashok Kumar<sup>c</sup>, Bhaskar Singh<sup>d</sup>, Muhammad Ashfaq<sup>e</sup>, Ganesh Dattatraya Saratale<sup>f</sup>, Sikandar I. Mulla<sup>g,\*</sup>

<sup>a</sup> Department of Biotechnology, G.M. Institute of Technology, Davangere, 577006, India

<sup>b</sup> Department of Microbiology (DM), School for Environmental Sciences (SES), Babasaheb Bhimrao Ambedkar University (A Central University), Vidya Vihar, Raebareilly Road, Lucknow 226 025, Uttar Pradesh, India

<sup>c</sup> Department of Biotechnology and Bioinformatics, Jaypee University of Information Technology, Waknaghat, Solan, Himachal Pradesh, 173234, India

<sup>d</sup> Department of Environmental Sciences, Central University of Jharkhand, Ranchi, 835205, Jharkhand, India

<sup>e</sup> Department of Chemistry, University of Gujrat, Gujrat, 50700, Pakistan

<sup>f</sup> Department of Food Science and Biotechnology, Dongguk University-Seoul, Ilsandong-gu, Goyang-si, Gyeonggi-do, 10326, Republic of Korea

<sup>g</sup> Department of Biochemistry, School of Applied Sciences, REVA University, Bangalore, 560 064, Karnataka State, India

### ARTICLE INFO

#### Keywords:

Extracellular polysaccharide  
Extracellular electron transfer  
Riboflavin  
Thermophiles

### ABSTRACT

Through extracellular electron transfer (EET), bacteria are capable of transforming different insoluble materials of geochemical interest into energy-rich molecules for their growth. For this process, bacteria have been depending directly or indirectly on molecules synthesized within the cells or by various synthetics as mediators. Herein, we studied the in-situ change in electrochemistry and supporting components for EET in the extracellular polysaccharide (EPS) producing biofilm of thermophilic *Geobacillus* sp. The CV and DPV results revealed that the intact biofilm of bacteria was not able to generate any potential at 25 °C /- ≤ 50 °C. However, at 55 °C (optimal condition), the potential occurred drastically after the EPS production by bacteria. HPLC and MALDI-TOF results revealed that the presence of Flavins, which can be adsorbed to the electrodes from the cell surface. Moreover, the temperature-dependent EPS production and originally conceived ability of flavins to act as electron shuttles suggest that not much complexity in bacteria with minerals. Additionally, the electrochemical potential was severely affected upon removal of EPS/flavin moiety from the intact biofilm, revealed the necessity of EPS bound flavins in transferring the electrons across its thick cell walls. This paradigm shift to electrogenic nature of *Geobacillus* sp. biofilm will become evident in the adaptation of other microbes during mineral respiration in extreme environments.

### 1. Introduction

Flavins, an active redox compounds, have been reported to participate in extracellular electron transfer (EET) by bacteria (Marsili et al., 2008; von Canstein et al., 2008; Masuda et al., 2010; Kotloski and Gralnick, 2013; Engel et al., 2019). Although, flavins are produced endogenously by bacteria (Yatsyshyn et al., 2009), and are located at a specific locus in its genome (Light et al., 2018). These are required to cross and interact with the transmembrane barriers for energy derivations (Covington et al., 2010; Babanova et al., 2017). Despite, behaves distinctly in the electrochemical environment, the flavins precursors are essential for biogeochemistry (Shi et al., 2013), minerals (von Canstein et al., 2008), and electrode respiration (Yang et al., 2012). Till date,

many reports available exclusive for *Shewanella* spp. (Marsili et al., 2008; von Canstein et al., 2008; Kotloski and Gralnick, 2013), and *Geobacter* spp. (Reguera et al., 2005; Okamoto et al., 2014), which is inherited the EET research. Although, many other bacteria have been characterized for EET activity so far (Pham et al., 2008; Yang et al., 2012; Dopson et al., 2016), however, the arguments unlikely differed on the gram (+) profile of the bacteria. These bacteria are widespread and are likely to execute in a different EET mechanism. Until recently, there are several studies are documented the EET mechanism in these type of bacteria (Marshall and May, 2009; Wrighton et al., 2011; Wu et al., 2014; Tokunou et al., 2016; Pankratova et al., 2019). Furthermore, their presence in the electrochemical system was extensively documented previously (Logan, 2009; Marshall and May, 2009; Dopson

\* Corresponding author at: Department of Biochemistry, School of Applied Sciences, REVA University, Bangalore, India.

\*\* Corresponding author at: Department of Biotechnology, GM Institute of Technology, Davangere, Karnataka, India.

E-mail addresses: [drgurumurthydm@gmit.ac.in](mailto:drgurumurthydm@gmit.ac.in) (D.M. Gurumurthy), [sikandar.mulla@gmail.com](mailto:sikandar.mulla@gmail.com) (S.I. Mulla).



# SPATIO-TEMPORAL EVALUATION OF LONG-TERM EARTHQUAKE EVENTS AND ITS CONTRIBUTION IN GENESIS OF *TSUNAMI* IN THE INDIAN OCEAN

A. A. Khan<sup>1</sup>, A. Kumar<sup>1,2\*</sup>, P. Lal<sup>1</sup>

<sup>1</sup>Department of Geoinformatics, Central University of Jharkhand, Ranchi, India - imashif17@gmail.com, preet.lal@cuja.ac.in  
<sup>2</sup>IUCN Commission of Ecosystem Management - amit.kumar@cuja.ac.in, amit.iirs@gmail.com

Commission V, WG V/7 & Commission IV, WG IV/6

**KEY WORDS:** Earthquake, *Tsunami*, GIS, Remote Sensing, Hypocentre, Disaster Management

## ABSTRACT:

A very high magnitude earthquake (9.1 MW) triggered a devastating *Tsunami* in the Indian Ocean on 26<sup>th</sup> December 2004. The epicentre was located at 3.3° N, 95.8° E with a focal depth of ~ 30 km. The impacts of *Tsunami* were felt as far away in Somalia, Tanzania and Kenya along the east coast of Africa. Considering the role of earthquake, in the present study the spatio-temporal analysis of long term (1901 to 2019) earthquake events was performed, which recorded by USGS to understand the genesis of *Tsunami* (2004) in the Indian Ocean. The study exhibited that the maximum frequency of earthquake was observed between the ranges of 4 MW to 6 MW on the Richter scale during 2001 – 2010. There was only one earthquake event >8 MW on the Richter scale (26<sup>th</sup> December 2004 having depth 30 Km) in the Indian Ocean recorded during 1901 - 2019. The study exhibited that the maximum earthquake was observed between 30-40 km below the surface, and primarily of moderate to low magnitudes. The proximity analysis along the major fault line indicates that the maximum earthquakes were in the buffer of 200 km from fault line in Bay of Bengal. The decadal variation of earthquake exhibits that the maximum number of earthquake events (8427 events) were triggered during the year 2001-2010, whereas during the year 2004, the total 902 earthquake events >4 MW was recorded. The study indicates that the earthquakes >7 MW (on Richter scale) and depth below 30 km (shallow earthquake) are primarily responsible to major *Tsunami* events in the Indian Ocean. The very high magnitude (>9 MW on the Richter scale) and shallow depth (~ 30 km) are the major cause of 2004 *Tsunami* and its high level of damage. There were very low frequency (10 – 15 events) of earthquake occurred having magnitude >7 and depth < 30 km.

## 1. INTRODUCTION

*Tsunami*, often incorrectly called tidal waves, is a series of waves with a long wavelength and period (time between crests) (Mathur and Udani, 2015). Since 1750, the Indian Ocean has not experienced a natural disaster of such magnitude, with enormous consequences for the region's environment (Sirikulchayanon et al., 2008). On 26<sup>th</sup> December 2004, an earthquake of 9.1 MW occurred at 0:58:53 GMT in Indian Ocean. The epicentre of earthquake was located at 3.3 N, 95.8 E with a focal depth of approximately 30 km (Lavigne et al., 2013), which triggered a massive *Tsunami* in the coastal areas of Indian Ocean. Around 280,000 people were killed in South Asia, Southeast Asia, and East Africa (Lavigne et al., 2013). The vertical offset of the ocean floor by 7 to 10 meters on 26<sup>th</sup> December 2004, Sumatra earthquake displaced massive volumes of water, resulting in a destructive *Tsunami*. Because of the north-south direction of the fault line, the *Tsunami* was the strongest in the east-west direction. The wave height in deep water (open ocean) was measured through satellites to be approximately 60 cm, while traveling at a speed of 500 to 800 km/hr. The velocity decreased to only tens of kilometres per hour in shallow water near the shoreline, depending on the local bathymetry. This, however, resulted in large and destructive waves that reached run-up heights of 20 to 30 meters in Banda Aceh (Saatcioglu et al., 2005). The distribution of aftershocks (U.S. Geological Survey<sup>1</sup>) suggests that the rupture extended over a distance of 1500 km (measured parallel to the arc), but seismic inversions for this event are non-unique and cannot resolve many details of slip, especially along the northern portion of the rupture (Ammon et al. 2005). Furthermore, considering that slip north of ~9°N appears to have generated little or no seismic radiation (Lay et al. 2005; Ammon et al. 2005), seismic inversions will only provide a minimum constraint on the extent and amount of slip, and geodetic

inversions will be required to provide a maximum (and perhaps more accurate) constraint. However, inversions of the sparse geodetic data that were available prior to this study provided only limited constraints on the amount and distribution of slip (Subarya et al. 2006). Since as per current research knowledge there is no established methods to detect the tsunami being generated due to earthquake or landslide. The phenomenon of tsunami is mainly generated undersea disturbance due to earthquake or landslide or activity near the coast or in the ocean and displace few kilometres to >1000 km apart from epicentre. The earthquakes mainly occurs in the region having a high tectonic subduction zones along with tectonic plate boundaries and high seismicity in a regions, caused due to collision of tectonic plates. When a disturbance happens the ocean, the ocean floor rise or falls and effects on water above it and as the water moves up and down, seeking to regain its balance, a tsunami is born. (Borrero, 2005; Kanamori and Kikuchi, 1993; Pelayo and Wiens, 1990; Tsuboi, 2000).

The earthquake of 26<sup>th</sup> December 2004 occurred due to slip on the subduction interface between the Indo- Australian plate and the Burma microplate below Andaman and Nicobar Islands and Aceh province, Sumatra. The Indian plate has been moving north-east at a rate of approximately 60 mm/year, subduction under the overriding Burma microplate. The epicentre of the quake was about 155 km west of Sumatra and about 255 km south-east of Banda Aceh, Indonesia (Saatcioglu et al., 2005). Along the Java Trench to the southeast of Sumatra, the Australian plate subducts beneath the Sunda Shelf in a direction nearly orthogonal to the trench and at a rate of about 63 mm/year. (Bock, 2003; Michel et al., 2001). Along Sumatra the direction of convergence becomes increasingly oblique towards the north-west and the relative plate slip is partitioned into nearly perpendicular thrusting at the trench and trench-parallel, right-lateral slip at the Sumatran fault (SF) (Fitch, 1972). The strength of a *Tsunami* depends upon the magnitude of earthquakes occur in the Ocean. There are a number

<sup>1</sup> <http://neic.usgs.gov/neis/poster/2004/20041226.html>

\* Corresponding author

## SAR – OPTICAL REMOTE SENSING BASED FOREST COVER AND GREENNESS ESTIMATION OVER INDIA

P. Lal<sup>1</sup>, A. K. Dubey<sup>2</sup>, A. Kumar<sup>1,3</sup>, P. Kumar<sup>2</sup>,\* C. S. Dwivedi<sup>1</sup>

<sup>1</sup>Department of Geoinformatics, Central University of Jharkhand, Ranchi, India; preet.lal@cuja.ac.in

<sup>2</sup>Department of Earth and Environmental Sciences, Indian Institute of Science Education and Research Bhopal, India; adityadubey@iiserb.ac.in, kumar@iiserb.ac.in

<sup>3</sup>IUCN Commission of Ecosystem Management; amit.kumar@cuja.ac.in

Commission V, WG V/7 & Commission IV, WG IV/6

**KEYWORDS:** ALOS PALSAR MOSIAC, Browning, Greening, LAI, SAR, Vegetation cover

### ABSTRACT:

Indian natural forest has a high ecological significance as it holds much biodiversity and is primarily affected due to deforestation. The present study exhibits the forest cover change on Global Forest Non-Forest (FNF) data for India and greenness trend using MOD15A2H LAI product, which is the best product available till date. JAXA uses of SAR datasets for forest classification based on FAO definitions. Later, Forest Survey of India (FSI) used different definitions for forest classification from FAO and was to compare with JAXA based forest cover. The global FNF study exhibited that total forest cover was reduced from 568249 Km<sup>2</sup> to 534958 Km<sup>2</sup> during 2007-17 in India. The significant loss of forest cover (33291.59 Km<sup>2</sup>; by -5.85% change) was primarily evident in Eastern Himalayas followed by Western Himalayas. Whereas forest cover increase was observed in Eastern and the Western Ghats from 2007 to 2017. The state of forest report by FSI states an increase in the forest cover from 690889 Km<sup>2</sup> to 708273 Km<sup>2</sup> during 2007-17 by 2.51%. The difference in forest cover as estimated by JAXA global FNF datasets and FSI report is attributed to differences in forest cover mapping definitions by both the agencies and use of varied datasets (SAR datasets by JAXA and optical datasets by FSI). It is to note that SAR is highly sensitive to forest cover and vegetation's as compare to optical datasets. Recent satellite-based (2000 – 2018) LAI product reveals the increase in leaf area of vegetation during 2000-18. It may be attributed to proper human land use management and implications of green revolutions in the region. The greening in India is most evident from the croplands with insignificant contribution from forest cover.

### 1. INTRODUCTION

Forest is the most essential and critical element of earth's surface, and its dynamics on the landscape are driven by both human activities and natural processes (Morales-Diaz et al. 2019; Tucker and Richards 1989). The green leaves of vegetation play a crucial role in maintaining terrestrial carbon balance and also supports climatic systems as it amalgamates sugar from water (H<sub>2</sub>O) and CO<sub>2</sub>, using the energy that leads to cooling of the surface by transpiring a large amount of water (Chen et al., 2019; Piao et al., 2003). The growth of vegetation in an ecosystem can be strongly influenced by climate change and human activity (Cavicchioli et al., 2019; Chu et al., 2019; Liu et al., 2019). Long-time change in greenness of vegetation are driven by multiple factors such as biogeochemical drivers i.e., fertilization effects of eCO<sub>2</sub>, regional change of climatic factors as temperature, precipitation and radiation and varying rate of Nitrogen deposition or cycle change and land-use effects i.e., change in land use/ land cover (LULC) due to land management intensity, including use for fertilizers, irrigation, deforestation and grazing) (Wang et al., 2014). So, it is crucial to monitor vegetation changes because spatiotemporal changes can alter the structure and function of landscapes, subsequently influencing ecology and biodiversity and became an important issue in global biodiversity change (Li et al., 2012; Peng et al., 2012, 2011; Steidinger et al., 2019).

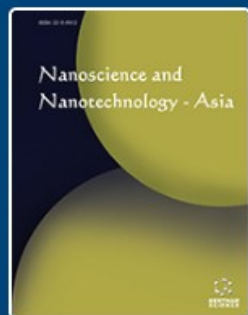
Greenness on earth's surface can be monitored through various developed indices like Normalized Differential Vegetation Index (NDVI), Leaf Area Index (LAI). Enhanced Vegetation Index (EVI) and many more used by several researchers (Chu et al., 2019; Rani et al., 2018). LAI (one half the total green leaf area per unit horizontal ground surface) can be more efficient

to monitor the greenness because it is one of the main driving forces of net primary production, water and nutrient use, and carbon balance and important structural property of vegetation (Bréda, 2008; Fang and Liang, 2014).

Remote sensing is a beneficial technique for studying various earth observations on regional to a global scale. Optical remote sensing (ORS) data are widely used for the vegetation mapping by using a near-infrared and red band as it useful for vegetation mapping. As per current research knowledge, very less study has applied microwave remote sensing (MRS) datasets for vegetation mapping due to the requirement of robust hardware for processing. Major advantages of MRS over ORS is that it has day and night capabilities and penetration of cloud cover and can provide an image at any time (Woodhouse, 2005). There are various spectral bands at which SAR data is being captured. X-band is useful for various surface deformation and movement tracking activities (Lal et al., 2018), C-band is used for both ground surface deformation and vegetation studies, L-bands are used for vegetation studies primarily because of its higher penetration depth (Antropov et al., 2017; Kumar et al., 2019; Plank et al., 2017). By increasing the wavelength in SAR datasets, vegetation type classification accuracy will increase because of its penetration depth. Mapping a vast region with optical datasets leads to inaccuracies due to cloud cover data and have to be replaced with another time periods datasets, whereas by SAR datasets researchers can overcome these problems accuracies will be more.

With continuous availability of satellite-based datasets, the efforts to accurately classify forest types have increased over the year to correctly capture the real dynamism of any ecological landforms/landscapes. The ambiguity in management approaches for forest conservation raises the need to develop

\* Corresponding author



## Nanoscience & Nanotechnology-Asia

[Editor-in-Chief >>](#)

ISSN (Print): 2210-6812

ISSN (Online): 2210-6820

[Back](#)[Journal ▾](#)[Subscribe](#)[Review Article](#)

# Implications of Metal Nanoparticles on Aquatic Fauna: A Review

**Author(s):** Kamlesh Kumari, Prashant Singh\*, Kuldeep Bauddh\*, Sweta, Sadhucharan Mallick and Ramesh Chandra

Volume 9, Issue 1, 2019

Page: [30 - 43]

Pages: 14

DOI: [10.2174/2210681208666171205101112](https://doi.org/10.2174/2210681208666171205101112)

Price: \$65

**Purchase  
PDF**



[< Back to results](#) | 1 of 1[Download](#) [Print](#) [Save to PDF](#) [Save to list](#) [Create bibliography](#)**Nonlinear Optics Quantum Optics** • Volume 51, Issue 3-4, Pages 237 - 249 • 2019**Document type**

Article

**Source type**

Journal

**ISSN**

15430537

[View more](#)

# Wavelength filter based on photonic crystal resonant cavity

Kumar, Alok; Medhekar, Sarang

[Save all to author list](#)<sup>a</sup> Department of Physics, Central University of Jharkhand, Ranchi, 835205, Jharkhand, India1 28th percentile  
Citation in Scopus0.10  
FWCI 10  
Views count [View all metrics](#) [Full text options](#) [Export](#) [Abstract](#)[Author keywords](#)[Indexed keywords](#)[SciVal Topics](#)[Metrics](#)[Funding details](#)**Abstract**

An optical wavelength filter employing a resonant cavity (RC) in 2-D photonic crystal (2DPC) is proposed in this paper. Photonic band gap (PBG) of the considered structure (wavelength filter) is calculated by Plane Wave Expansion (PWE) method and the simulation results of light propagation in the proposed wavelength filter are obtained using Two Dimensional Finite Difference Time Domain (2DFDTD) method. The effect of changing (i) radius of defect rods of RC (ii) refractive index of defect rods of RC (iii) refractive index of rods of the whole structure (iv) radius of the coupling rods (v) radius of the central rod of RC on resonant wavelength (and hence, filtered wavelength of the wavelength filter) is investigated. The results of the investigations give an intuitive idea of manipulating the resonant wavelength to a desired value. Further, It is found in our investigations that sharp wavelength filtering is possible with transmission efficiency as high as 90%. A scheme to realize wavelength demultiplexer is also given at the end. © 2019 Old City Publishing, Inc.

**Author keywords**

Photonic crystals; Resonant cavity

**Cited by 1 document**

Design of two-dimensional photonic crystal based optical NOT gate using square photonic crystal cavity

Saxena, P. , Kumar, A. , Gautam, G.

*(2021) 2021 IEEE International Conference on Technology, Research, and Innovation for Betterment of Society, TRIBES 2021*[View details of this citation](#)

Inform me when this document is cited in Scopus:

[Set citation alert >](#)**Related documents**

All-optical NOT and AND gates based on 2D nonlinear photonic crystal ring resonant cavity

Kumar, A. , Gupta, M.M. , Medhekar, S. *(2018) Optik*

All optical NOT and NOR gates using interference in the structures based on 2D linear photonic crystal ring resonator

Kumar, A. , Medhekar, S. *(2019) Optik*

Optical add-drop filter based on square ring resonator consisting of octagon shape core

Sharma, P. , Gupta, M.M. , Ghosh, N. *(2021) 2021 IEEE International Conference on Technology, Research, and Innovation for Betterment of Society, TRIBES 2021*[View all related documents based on references](#)

Find more related documents in Scopus based on:

[Authors](#) > [Keywords](#) >



# Shoreline morphology changes along the Eastern Coast of India, Andhra Pradesh by using geospatial technology

K. K. Basheer Ahammed<sup>1</sup> · Arvind Chandra Pandey<sup>1</sup>

Received: 11 May 2018 / Revised: 4 September 2018 / Accepted: 9 September 2018 / Published online: 25 October 2018  
© Springer Nature B.V. 2018

## Abstract

Shoreline changes on account of global climate change and sea level rise is one of the major problems along the coastlines in different continents of the world. This study was carried out along the coastlines of Andhra Pradesh state in India using multi-temporal satellite images from 1973 to 2015 period. Long-term coastal erosion and accretion rate over a period of 42 years has calculated using Digital Shoreline Analysis System and prepared shoreline maps by using GIS-Software. End point rate (EPR) statistical method is applied to estimate the shoreline change rate. Various coastal parameters like sea level rise, geomorphology, elevation and coastal slope were used to find out the interactive relationship between the physical parameters and shoreline changes in the area. The study revealed that the coastal changes are more dominant in Krishna and Godavari Deltaic plain. The average erosion and accretion rate observed in the Krishna Godavari delta was 10.63 and 17.29 m per year respectively. The study indicated that, climatic changes and fluvial process are playing key role in changing shoreline positions. The study exhibited that elevation and slope are played intense role in the shoreline positional change. The present study demonstrates that combined use of satellite imagery and EPR statistical method as an accurate and reliable method for shoreline change analysis.

**Keywords** Shoreline change · Digital shoreline analysis system · EPR · GIS

## Introduction

Tremendous population and developmental process have been building in the coastal regions for the last 40 years (Kumar et al. 2010). More than 50 percentages of the world's population lives within the 60 km of a shoreline (United Nations Environment Programme (UNEP) 2007; Kumar et al. 2010). Urbanization and the fast developments of coastal cities exhibited dominant population trends over the last few decades, leading to the development of mega cities in all coastal regions across the world. In 1950 there were only two mega cities in the world (New York and London), whereas there were 20 M cities

in 1990 (Nicholls 1995; Basheer Ahammed et al. 2016). The average population density in the coastal zone was 77/km<sup>2</sup> in 1990 and 87/km<sup>2</sup> in 2000, and a projected 99/km<sup>2</sup> in 2010 (UNEP 2007; Chandrasekar et al. 2013). The scenario of people living in the coastal regions compared with available coastal lands further indicates that the people have tendency to live in coastal areas than inland.

The coastal environment is dynamic due to constantly changing types of interactions among the ocean, atmosphere, land and people (Nicholls et al. 2007). Coastlines are not static entities but fluctuate at a short-term seasonal level as well as a longer-term climatic-change level. However, much development in the littoral zone occurs with the intention of 'stabilizing the shoreline', creating a conflict between human use and the coastline's natural processes. The dynamic systems found on the coast are under increasing pressure by anthropogenic development (Nicholls et al. 2007). Developmental pressures within the coastal zone are clearly set to increase as its population rises. It is estimated that by 2050, 91% of the world's coast will be impacted by development (Nellemann and Hain 2008). Pressure is not

---

✉ Arvind Chandra Pandey  
arvindchandrap@yahoo.com

K. K. Basheer Ahammed  
basheer.kk@yahoo.com

<sup>1</sup> Department of Land Resource Management, Central University of Jharkhand, Brambe, Ranchi, India

# On Semilocal convergence of Two step Kurchatov method

Himanshu Kumar\* and P.K. Parida<sup>†</sup>

Centre for Applied Mathematics, Central University of Jharkhand, Ranchi-835205, India

Received 09 Sep 2016, Revised 31 Aug 2017, Accepted 25 Nov 2017

---

## Abstract

In this article we present a new semilocal convergence analysis for the two step Kurchatov method by using recurrence relations under Lipschitz type conditions on first order divided difference operator. The main advantage of this iterative method is that it does not require to evaluate any Fréchet derivative but it includes extra parameters in the first order divided difference in order to ensure a good approximation to the first derivative in each iteration. The detailed study of the domain of parameters of the method has been carried out and the applicability of the proposed convergence analysis is illustrated by solving some numerical examples. It has been concluded that the present method converges more rapidly than the one step Kurchatov method and two step Secant method.

*MSC:* 65H10, 65J15.

*Keywords:* Nonlinear equations, Kurchatov's method, Semilocal convergence, Recurrence relations, Domain of parameters.

---

\*E-mail: himanshu.kumar.01@cej.ac.in

<sup>†</sup>Corresponding author: E-mail: pkparida@cej.ac.in, Phone No: +91 6531292531



## Mitigation effect of exogenous nitric oxide (NO) on some metabolic compounds of maize seedling grown under salt stress

Amal A Mohamed<sup>1,2</sup>, Ekhlaque A Khan<sup>3,4</sup> and Amarendra N Misra<sup>2,5</sup>

<sup>1</sup>Chemistry Dept., University College of Al Leith- Umm Al-Qura University, Saudi Arabia

<sup>2</sup>Plant Biochemistry Dept., National Research Centre (NRC), Dokki, Giza, Egypt

<sup>3</sup>Centre for Life Sciences, Central University of Jharkhand, Ratu-Lohardaga Road, Brambe-835205, Ranchi, India

<sup>4</sup>Department of Biotechnology, Ch. Bansi Lal University, Bhiwani-1270221, Haryana, India.

<sup>5</sup>Khallote University, Berhampur-760001, Odisha, India.

Email : [amin\\_amal@yahoo.com](mailto:amin_amal@yahoo.com)

**Abstract** . Salt stress is considered as a major limiting factor for plant growth and crop productivity. The present study was conducted to investigate whether using nitric oxide (NO) molecule could alleviate the adverse effects of salt stress in maize (*Zea mays* L.) seedling. Sodium nitroprusside (SNP) was used at 60  $\mu$ M concentration, as NO donor in the nutrient solution of maize seedlings grown with three concentrations of NaCl (0.0, 150 and 200 mM). Leaf samples were collected on the 7th and 15th day after NaCl treatment. Chlorophyll contents and lipid peroxidation gave different values under salt stress. The NO treated seedling showed high content of proline, phenolic and flavonoid. Nitric oxide induced an increase in antioxidant enzymes including peroxidase (POD) and catalase (CAT) activities. These data indicated that the exogenous NO application is useful way to mitigate the salinity-induced oxidative stress in maize seedling.

**Keywords:** Antioxidant enzymes, proline, malondialdehyde, salt stress, signaling messenger

### Introduction:

Salt stress as a major adverse factor can lower leaf water potential, leading to reduced turgor and some other responses, and ultimately decrease crop productivity in arid regions. When a plant is exposed to high salinity stress, its major processes such as photosynthesis, protein synthesis, and lipid metabolism are adversely affected. High concentrations of salts lead to damage at the molecular level, arrested growth, and even death (**Implay, 2003**). Under salinity conditions, tolerant plants typically maintain low sodium (Na) in the cytosol of cells (**Jeschke, 1984**). The control of Na<sup>+</sup> movement across the plasma-membrane and tonoplast to maintain a low Na<sup>+</sup> concentration in the cytosol is a key factor to the cell adaptation to salt stress (**James et al., 2011**). Another common biochemical change occurring when plants are exposed to salt stress is the accumulation of reactive oxygen species (ROS), which unbalances the cellular redox in favor of oxidized forms, thereby creating oxidative stress that can damage DNA, inactivate enzymes and cause lipid peroxidation (**Manaa et al., 2013**). The





# Comparative evaluation of conceptual and physical rainfall–runoff models

R. K. Jaiswal<sup>1</sup> · Sohrat Ali<sup>2</sup> · Birendra Bharti<sup>2</sup>

Received: 24 April 2019 / Accepted: 12 December 2019 / Published online: 3 January 2020  
© The Author(s) 2020

## Abstract

The design of water resource structures needs long-term runoff data which is always a problem in developing countries due to the involvement of huge cost of operation and maintenance of gauge discharge sites. Hydrological modelling provides a solution to this problem by developing relationship between different hydrological processes. In the past, several models have been propagated to model runoff using simple empirical relationships between rainfall and runoff to complex physical model using spatially distributed information and time series data of climatic variables. In the present study, an attempt has been made to compare two conceptual models including TANK and Australian water balance model (AWBM) and a physically distributed but lumped on HRUs scale SWAT model for Tandula basin of Chhattisgarh (India). The daily data of reservoirs levels, evaporation, seepage and releases were used in a water balance model to compute runoff from the catchment for the period of 24 years from 1991 to 2014. The rainfall runoff library (RRL) tool was used to set up TANK model and AWBM using auto and genetic algorithm, respectively, and SWAT model with SWATCUP application using sequential uncertainty fitting as optimization techniques. Several tests for goodness of fit have been applied to compare the performance of conceptual and semi-distributed physical models. The analysis suggested that TANK model of RRL performed most appropriately among all the models applied in the analysis; however, SWAT model having spatial and climatic data can be used for impact assessment of change due to climate and land use in the basin.

**Keywords** Rainfall runoff model · Optimization · Water balance · Conceptual model · Physical model

## Introduction

The rainfall–runoff modelling is an important and useful tool for hydrological research, water engineering and environment application. The runoff computation from ungauged or poorly gauged catchments is a serious challenge in developing countries like India where higher operation and maintenance cost differed gauging on small and medium rivers. The knowledge-based or data-driven hydrological models were developed and used by researchers to extend runoff records and address modelling issues (Kar et al. 2015, 2017). The hydrological model can be classified into three broad groups, namely metric, physical and conceptual models (Beck et al.

1990). The rainfall–runoff relationships in metric models are essentially based on observations and without characterizing different processes involved in the hydrologic system (Kokkonen and Jakeman 2001). The linearity assumption-based unit hydrograph theory (Sherman 1932), catchment characteristics-based rational formula for peak runoff given by JM Thomas (1822–1892) and reproduced by Loague (2010), Strange tables, etc., are some of the examples of metric modelling. The metric models are observation-based models developed using observed runoff and catchment characteristics without considering much of hydrological processes. The physical models represent different hydrological processes through mass, momentum and energy conservation equations. The physical models may be capable of considering the spatial variability of land use, slope, soil and climate to deal with the hydrological processes within the watershed semi- or fully distributed in nature.

The conceptual models are hydrological models that use simplified mathematical conceptualization of a system with the help of a number of interconnected storages used to

✉ R. K. Jaiswal  
rkjaiswal.nih@gmail.com

<sup>1</sup> CIHRC, National Institute of Hydrology, WALMI Campus, Bhopal, M.P., India

<sup>2</sup> Centre for Water Engineering and Management, Central University of Jharkhand, Ranchi, Jharkhand, India



# Graphene-supported TiO<sub>2</sub>: study of promotion of charge carrier in photocatalytic water splitting and methylene blue dye degradation

Neha Singh<sup>1</sup> · Soumita Jana<sup>2</sup> · Gajendra Prasad Singh<sup>2</sup> · R. K. Dey<sup>1</sup>

Received: 13 August 2019 / Revised: 17 January 2020 / Accepted: 20 January 2020 / Published online: 24 January 2020  
© Springer Nature Switzerland AG 2020

## Abstract

Hydrogen from water provides safe and alternative route for sustainable energy production. The present investigation reports the photocatalytic water splitting using rGO–TiO<sub>2</sub> which efficiently promotes the conversion of solar energy to chemical energy through charge promotion activity. The catalyst was prepared by hydrothermal decomposition process and further characterized for its structural morphology, crystal structure, and photocatalytic properties. Incorporation of GO in the hybrid material found to shrink the band gap of the samples from 3.12 to 2.99 eV. Further, promotion of charge separation is confirmed from the quenching of the emission spectra of the material. The hybrid material with proportionate increment in GO content enhances the H<sub>2</sub> production up to five times higher than pristine TiO<sub>2</sub> material. The catalytic material with 1 wt% GO loading shows decay of methylene blue (MB) dye in aqueous solution at 0.07622 mmol/min. The hybrid material (rGO–TiO<sub>2</sub>) found to inhibit recombination center of electron-hole pairs successfully, thus facilitating overall photocatalytic properties of the material for diversified applications.

**Keywords** Graphene · TiO<sub>2</sub> · Hydrogen · Methylene blue · Photocatalyst

## 1 Introduction

Designing a new type of photocatalytic material often require successful inhibition of electron-hole pairs' recombination process [1]. Generally, in a single-component photocatalytic material, the quick recombination of the photo-generated charge carriers significantly reduces the conversion efficiency of solar energy into hydrogen energy [2–4]. Increase in conversion efficiency of such kind of catalyst often requires prolongation of lifetime of charge carrier as well as enhancement

of charge transfer rate. In this aspect, combination of two dissimilar materials (composite) involving doping/deposition of transition metal, noble metals, or mixing of other semiconductors or supported by any other conducting material such as carbon nanotubes, graphene, and other conducting polymers are immensely useful for fabrication of new photocatalytic materials with improved properties [5–11]. Such kind of structure is commonly known as heterostructure configuration. Heterostructured photocatalytic materials could satisfy both kinetic and thermodynamic stability in addition to providing favorable energy levels for enhancement of redox ability towards charge transfer processes. Absorption of light by heterostructured materials could provide suitable band gap required for improvement of process efficiency.

Graphene–metal oxide composite material possesses good photocatalytic activities in comparison with unadulterated metal oxide. It is mainly due to the unique chemical and physical properties of the material [12, 13]. Combination of graphene oxide with semiconductor photocatalysts such as g-C<sub>3</sub>N<sub>4</sub>/graphene [14], CdS/graphene [15], and ZnO/graphene [16] could enhance photocatalytic performance by transferring photo-excited electrons from semiconductor surface to graphene oxide sheet, thus delaying the recombination

**Electronic supplementary material** The online version of this article (<https://doi.org/10.1007/s42114-020-00140-w>) contains supplementary material, which is available to authorized users.

✉ Gajendra Prasad Singh  
gpsinghcuj@gmail.com; gajendra.singh@cuj.ac.in

✉ R. K. Dey  
rkdey@rediffmail.com; ratan.dey@cuj.ac.in

<sup>1</sup> Department of Chemistry, Central University of Jharkhand, 835 205, Ranchi, Jharkhand, India

<sup>2</sup> Department of Nanoscience and Technology, Central University of Jharkhand, 835 205, Ranchi, Jharkhand, India



Contents lists available at ScienceDirect

Optik

journal homepage: [www.elsevier.com/locate/ijleo](http://www.elsevier.com/locate/ijleo)

Original research article

# A simplified simulation model of silicon photovoltaic modules for performance evaluation at different operating conditions



Durgesh Kumar<sup>a</sup>, Pritish Mishra<sup>a</sup>, Ashutosh Ranjan<sup>a</sup>, Dharmendra Kumar Dheer<sup>b</sup>,  
Lawrence Kumar<sup>a,\*</sup>

<sup>a</sup> Department of Nanoscience and Technology, Central University of Jharkhand, Brambe, Ranchi, 835205 India

<sup>b</sup> Department of Electrical Engineering, National Institute of Technology Patna, Patna, 800005 India

## ARTICLE INFO

### Keywords:

Photovoltaic module  
Partial shading  
Simulink  
Shunt resistance and series resistance  
MATLAB/Simulink

## ABSTRACT

We report here a simplified and improved technique for modeling and simulation for the Photovoltaic module using MATLAB/Simulink environment. Parameters of the equivalent-circuit model are obtained using the iterative algorithm by adjusting the output characteristics curve. The present work evaluates the current-voltage (I-V) and power-voltage (P-V) characteristics under different ambient conditions employing a single-diode model. The module performance is significantly affected by solar irradiance, ambient temperature and partial shading. This report aims to perform the detailed analysis of partial shading effect on module performance, which is considered as important real-time problem. The proposed simulation technique provides an accurate and reliable method to extract different sources of resistance, such as series and shunt resistance in the PV module. A MSX60 photovoltaic module is used as a reference for the present study. The characteristic curves of the simulated model are in good agreement with the available experimental data. The developed simulation model could also be extended for performance assessment of other photovoltaic modules and in the design of efficient power converters.

## 1. Introduction

Photovoltaic modules are the semiconductor device, which converts a portion of light energy into electrical energy. The fundamental building block of the photovoltaic module is Photovoltaic Cell, which are grouped together to form a Photovoltaic (PV) module to generate significant amount of power. To evaluate the dynamic behavior of the PV module at different environmental condition, it is imperative to establish precise equivalent model for simulation purposes. In practice, there are two major equivalent circuit models for describing the non-linear output characteristic curve of PV cell. These are classified as Single diode model (SDM) and double diode model (DDM). Generally, single diode model is extensively used in practice in comparison to the double diode model. Although double diode model shows high level of accuracy, but at the same time, it includes too many parameters making it complex for mathematical computation and algorithm development, which makes single diode model a convenient choice for modeling of the PV cell [1,2]. The accurate modeling of PV module requires a range of parameters that could be extracted using the mathematical analysis of the photovoltaic cell equivalent model [3,4]. In the field of the photovoltaic research, the modeling and simulation of PV cell has been reported using different simulation tools [5–14]. Among these, MATLAB/Simulink has been extensively used by different groups for developing the simulation models of the PV module [5,6,11]. In this work, a simulation model

\* Corresponding author.

E-mail addresses: [lawrencecej@gmail.com](mailto:lawrencecej@gmail.com), [lawrence.kumar@cej.ac.in](mailto:lawrence.kumar@cej.ac.in) (L. Kumar).

<https://doi.org/10.1016/j.ijleo.2020.164228>

Received 29 November 2019; Received in revised form 9 January 2020; Accepted 13 January 2020  
0030-4026/© 2020 Elsevier GmbH. All rights reserved.



# Fertilizer management through coated urea to mitigate greenhouse gas (N<sub>2</sub>O) emission and improve soil quality in agroclimatic zone of Northeast India

Nirmali Bordoloi<sup>1</sup> · Kushal Kumar Baruah<sup>2</sup> · Barbie Hazarika<sup>3</sup>

Received: 29 March 2019 / Accepted: 29 December 2019 / Published online: 24 January 2020  
© Springer-Verlag GmbH Germany, part of Springer Nature 2020

## Abstract

Agricultural soils are an important source of greenhouse gas nitrous oxide (N<sub>2</sub>O) emission. The comprehensive effects of nitrogen fertilizer management on N<sub>2</sub>O emission from paddy fields of India have not been evaluated under field conditions. A 2-year field study was conducted to evaluate the effect of different nitrogen fertilizers, namely, conventional fertilizer (NPK), starch-coated urea (SCU), neem-coated urea (NCU), and normal urea alone (NUA) on soil quality, grain yield, and N<sub>2</sub>O emission from rice field. Gas samples were collected from the field at weekly intervals by static chamber technique and analyzed in a gas chromatograph. During the crop-growing season, the application of NPK resulted in the highest cumulative N<sub>2</sub>O emission (2.49 kg N<sub>2</sub>O–N ha<sup>-1</sup>) followed by NUA (2.34 kg N<sub>2</sub>O–N ha<sup>-1</sup>), NCU (2.20 kg N<sub>2</sub>O–N ha<sup>-1</sup>), and SCU (1.97 kg N<sub>2</sub>O–N ha<sup>-1</sup>). As against the application of conventional fertilizer (NPK), the application of SCU and NCU reduced the total N<sub>2</sub>O emission by 21% and 12%, respectively ( $p < 0.05$ ), during the rice-growing period. The results indicate a good correlation of N<sub>2</sub>O emissions with soil organic carbon, soil mineral nitrogen, and urease activity ( $p < 0.05$ ) at different stages of crop growth. Application of SCU significantly increased the rice grain productivity by 12%, 10%, and 3% over NPK (control), NCU, and NUA respectively without affecting the soil quality and nutrient status. The use of SCU improved the nitrogen use efficiency (NUE) and was the effective substitute for conventional fertilizer in terms of reducing N<sub>2</sub>O emissions from tropical rice paddy.

**Keywords** Nitrous oxide · Starch-coated urea · Soil urease activity · Nitrogen use efficiency

## Introduction

Nitrous oxide (N<sub>2</sub>O) is a potent greenhouse gas, responsible for the destruction of the stratospheric ozone (O<sub>3</sub>) layer (Ravishankara et al. 2009). It also contributes to rising

atmospheric temperature and global climate change. Among the greenhouse gases, N<sub>2</sub>O contributes to 8% of the radiative forcing at the global scale (Henault et al. 2012). Although N<sub>2</sub>O alone accounts for around 0.03% of the total GHG emissions, it nearly has a 298-fold greater potential for global warming effects than that of CO<sub>2</sub> in a time horizon of 100 years (Thomson et al. 2012; IPCC 2013). The concentration of atmospheric N<sub>2</sub>O has increased from the pre-industrial value of 270 ppb to the pre-industrial value of 319 ppb in 2005 and 324 ppb in 2011 (IPCC 2013).

Agricultural soils are responsible for more than one third of N<sub>2</sub>O emission and have contributed approximately 4.1 Tg N<sub>2</sub>O–N year<sup>-1</sup> or 66% of total gross anthropogenic emissions (UNEP 2013). Rice fields contribute approximately 11% of global agricultural N<sub>2</sub>O emissions (Wang et al. 2011; Hussain et al. 2015). Application of synthetic nitrogen (N) fertilizer in rice fields is a common practice of the farmers. This is likely to contribute to increase global warming through enhanced emission of N<sub>2</sub>O into the atmosphere (Trinh et al. 2016). The application of N to soils stimulates N<sub>2</sub>O production by way

Responsible editor: Philippe Garrigues

**Electronic supplementary material** The online version of this article (<https://doi.org/10.1007/s11356-019-07571-z>) contains supplementary material, which is available to authorized users.

✉ Kushal Kumar Baruah  
kkbaruah14@gmail.com; kkbaruah@tezu.ernet.in

<sup>1</sup> Department of Environmental Sciences, Central University of Jharkhand, Ranchi, Jharkhand 835205, India

<sup>2</sup> Department of Environmental Science, Tezpur University, Tezpur, Assam 784028, India

<sup>3</sup> Department of Chemical Engineering, Centre of Environment, Indian Institute of Technology Guwahati, Guwahati, Assam 781039, India

# Determinants of Seasonal Migration of Jharkhand: An Empirical Investigation

Sanhita Sucharita<sup>1</sup>  | Lisma Rout<sup>2</sup>

<sup>1</sup>Department of Business Administration, Central University of Jharkhand, Ranchi, India

<sup>2</sup>Department of Humanities and Social Sciences, Central University of Jharkhand, Ranchi, India

## Correspondence

Sanhita Sucharita, Assistant Professor in Economics, Department of Business Administration, Central University of Jharkhand, Ranchi, Barmbe Campus, Ranchi-835205, Jharkhand, India.  
Email: sanhita.sucharita@gmail.com

In Jharkhand, migration from rural to urban areas accounted for more than half of seasonal migration flows. In terms of spatial movements, rural–urban migration dominates migration for economic reasons. In Jharkhand seasonal migration is high and it is very high among the socio-economically deprived and marginal groups. This paper examines the association between seasonal migration and its determining factors, particularly socio-economic status; it observes that there is a significant negative association between economic status and temporary migration. Socio-economically deprived and marginal groups such as ST, SC, Muslim, household from lower Monthly Per Capita Expenditure quintile and household having lower land holding have a greater propensity to migrate seasonally, which also reflects its distress-driven nature. The study has found no significant effects of educational attainment on the propensity to migrate. Our results have numerous potential policy implications, including the design of typical social; security schemes for Jharkhand.

## JEL CLASSIFICATION

O15; Q15; O1

## 1 | INTRODUCTION

Seasonal migration is irreversibly part of the lives and livelihoods of many of the poorest sections of India. Seasonal migration is growing substantially in India (Rogaly, 1998; Deshingkar and Start 2003; Deshingkar et al. 2008 and Keshari and Bhagat, 2012; Nayyar and Kim, 2018). In India inter-state migration is from the poorer eastern states to western and northern developed states (Rogaly, 1998 and Deshinger, 2006). The stock of “interstate” migrants is negatively correlated with per capita state NSDP. It suggests that poorer states are more likely to have individuals migrating to other states (Nayyar and Kim, 2018) This paper studies the causes of internal seasonal migration in Jharkhand, a state which has second highest percentage (36.96%) of population below the poverty line in comparison to other states, which is much higher than national average (21.92%) (planning commission report, 2013). Jharkhand has seen a sharp decline in poverty in the past decade. Despite this, poverty in the state is among the highest in the country after Chhattisgarh. Significant share of SCs and ST population in the total population is a constraint to the Jharkhand economy. There are striking differences across social groups in Jharkhand. The

Scheduled Tribes stand out for chronic poverty (India states brief-Jharkhand, World Bank, 2016). Apart from General category households, there is poor access to basic services for most households in Jharkhand in comparison to the rest of the country (Jharkhand Social Inclusion Group brief, World Bank, 2016). Overall job creation in the state lags behind the expansion of the working age population (Jharkhand- Jobs brief, World Bank 2016). Jharkhand has been observed with highest level of food insecurity (MSSRF, Food Insecurity Atlas of Urban India, 2002). Jharkhand is ranked sixteenth among seventeen states with the ISHI score of 28.6 (India State Hunger Index 2009, IFPRI). Jharkhand faces food shortage at the end of winter and the starvation phase starts from mid of summer (June) and in many cases continues till the end of October. Seasonal migration is one of the most common coping livelihood strategy adopted by the rural poor to adapt to seasonal food insecurity. Despite a number of studies based on the field surveys of individual researchers, there is dearth of literature that covers a large population and presents a generalized analysis of seasonal migration in Jharkhand (see Table 1). Therefore, there is a need to use large scale survey data to be able to generalize the findings on



## MATERIALS SCIENCE

# Ultrasensitive and ultrathin phototransistors and photonic synapses using perovskite quantum dots grown from graphene lattice

Basudev Pradhan<sup>1\*†</sup>, Sonali Das<sup>1†</sup>, Jinxin Li<sup>2</sup>, Farzana Chowdhury<sup>1</sup>, Jayesh Cherusseri<sup>1</sup>, Deepak Pandey<sup>3</sup>, Durjoy Dev<sup>1,4</sup>, Adithi Krishnaprasad<sup>1,4</sup>, Elizabeth Barrios<sup>1,3</sup>, Andrew Towers<sup>1,5</sup>, Andre Gesquiere<sup>1,2,5</sup>, Laurene Tetard<sup>1,3,4</sup>, Tania Roy<sup>1,3‡</sup>, Jayan Thomas<sup>1,2,3‡</sup>

Copyright © 2020  
The Authors, some  
rights reserved;  
exclusive licensee  
American Association  
for the Advancement  
of Science. No claim to  
original U.S. Government  
Works. Distributed  
under a Creative  
Commons Attribution  
NonCommercial  
License 4.0 (CC BY-NC).

Organic-inorganic halide perovskite quantum dots (PQDs) constitute an attractive class of materials for many optoelectronic applications. However, their charge transport properties are inferior to materials like graphene. On the other hand, the charge generation efficiency of graphene is too low to be used in many optoelectronic applications. Here, we demonstrate the development of ultrathin phototransistors and photonic synapses using a graphene-PQD (G-PQD) superstructure prepared by growing PQDs directly from a graphene lattice. We show that the G-PQDs superstructure synchronizes efficient charge generation and transport on a single platform. G-PQD phototransistors exhibit excellent responsivity of  $1.4 \times 10^8 \text{ AW}^{-1}$  and specific detectivity of  $4.72 \times 10^{15}$  Jones at 430 nm. Moreover, the light-assisted memory effect of these superstructures enables photonic synaptic behavior, where neuromorphic computing is demonstrated by facial recognition with the assistance of machine learning. We anticipate that the G-PQD superstructures will bolster new directions in the development of highly efficient optoelectronic devices.

## INTRODUCTION

Graphene emerged as the dream material for electronic and optoelectronic applications due to its broad spectral bandwidth, excellent carrier transport properties with very high mobility (electron mobility,  $>15,000 \text{ cm}^2 \cdot \text{V}^{-1} \cdot \text{s}^{-1}$ ), and exceptional stability in ambient conditions and outstanding flexibility (1, 2). A plethora of composites and devices have been developed for applications in energy harvesting and storage, photodetectors, and transistors (3). However, a single layer of graphene absorbs only 2.3% of incident visible light (4). Moreover, to date, the responsivity of graphene photodetectors has been limited to about  $10^{-2} \text{ A W}^{-1}$ . These limitations critically impede the use of graphene in optoelectronic and photonic devices (4). On the other hand, organic-inorganic halide perovskite quantum dots (PQDs) have risen as attractive materials for optoelectronic devices due to their bandgap tunability across the visible spectrum, high photoluminescence (PL) quantum yield, narrow emission spectrum, and high extinction coefficients (5). A major drawback is their inferior charge transport compared with graphene.

To improve the performance of graphene-based phototransistors, various approaches such as PQDs in the form of bilayers (6) or heterostructures (7) have been pursued. A phototransistor composed of a two-dimensional (2D) perovskite thin film deposited on graphene by spin coating exhibited responsivity  $\sim 10^5 \text{ A W}^{-1}$  at 530 nm (7). Pan *et al.*

(6) has also demonstrated photoresponsivity of  $1.15 \times 10^5 \text{ A W}^{-1}$  at 520 nm using spin-coated formamidinium lead halide PQDs on a graphene layer. Presently, most of the PQD films prepared as the active layer of phototransistors by various deposition techniques have a minimum thickness of at least 100 nm. The highest photoresponsivity reported for a graphene-based phototransistor is  $10^7 \text{ A W}^{-1}$ , measured with an infrared phototransistor prepared by spin coating lead sulfide (PbS) quantum dots (QDs) on chemical vapor deposition-grown graphene (8). Growing PQDs from a graphene lattice to enhance charge transfers between the two moieties constitutes an entirely new direction for electronic and optoelectronic device applications.

Here, we demonstrate that the strong photogeneration efficiency of methylammonium lead bromide PQDs can be exploited by growing PQDs from the lattice of a single-layer graphene by a defect-mediated process. The rationale for designing this hybrid superstructure stems from the ability of PQDs to absorb light and generate charge carriers. The charges generated are transferred to graphene, which transports the carriers across the active layer of the device. Through the implementation of this thin superstructure in a phototransistor geometry, we produce a photoresponsivity of  $1.4 \times 10^8 \text{ A W}^{-1}$  at 430 nm and a specific detectivity ( $D^*$ ) of  $4.72 \times 10^{15}$  Jones, which is, by far, the best responsivity and detectivity across similar devices reported to date. This is promising for the development of highly efficient optoelectronic materials for high-speed communications, sensing, ultrasensitive cameras, and high-resolution imaging and displays (9). In addition, we find the graphene-PQD (G-PQD) superstructure to behave as a photonic synapse with low energy consumption of 36.75 pJ per spike that mimics crucial characteristics of its biological equivalent, with unique optical potentiation and electrical habituation function. This is critical for pattern recognition. This enables the building of a hardware unit for the neuromorphic architecture to mimic the human brain functionalities, which is critical for applications such as pattern recognition.

<sup>1</sup>NanoScience Technology Center, University of Central Florida, Orlando, FL 32826, USA. <sup>2</sup>CREOL, The College of Optics and Photonics, University of Central Florida, Orlando, FL 32816, USA. <sup>3</sup>Department of Materials Science and Engineering, University of Central Florida, Orlando, FL 32816, USA. <sup>4</sup>Department of Physics, University of Central Florida, Orlando, FL 32816, USA. <sup>5</sup>Department of Chemistry, University of Central Florida, Orlando, FL 32816, USA.


\*Present address: Centre of Excellence in Green and Efficient Energy Technology, Department of Energy Engineering, Central University of Jharkhand, Brambe, Ranchi, Jharkhand 835205, India.

†These authors contributed equally to this work.

‡Corresponding author. Email: jayan.thomas@ucf.edu (J.T.); tania.roy@ucf.edu (T.R.)



# The major lightning regions and associated casualties over India

Pramod Kumar Yadava<sup>1</sup> · Manish Soni<sup>2</sup> · Sunita Verma<sup>1,3</sup> · Harshbardhan Kumar<sup>1</sup> · Ajay Sharma<sup>4</sup> · Swagata Payra<sup>2</sup> 

Received: 21 August 2019 / Accepted: 1 February 2020 / Published online: 12 February 2020  
© Springer Nature B.V. 2020

## Abstract

Lightning, a climate-related highly localized natural phenomenon, claims lives and damage properties. These losses could only be reduced by the identification of active seasons and regions of lightning. The present study identifies and correlates the lightning-prone regions with the number of casualties reported over India at the state/union territory level. The seasonal and monthly composite satellite data of Lightning Imaging Sensor for the duration of 16 years (1998–2013) have been analyzed in this study for the identification of the major lightning-prone seasons and regions over India. The casualties due to lightning have also been estimated using data from Accidental Deaths and Suicides in India, National Crime Record Bureau report of India. The spatial distribution analysis reveals that lightning occurs mostly in hilly regions over India throughout the year (26 flash/sq. km/yr) and, however, causes lesser casualties because of the sparse population over the hilly terrain. The seasonal analysis reveals the most lightning phenomena occur during the pre-monsoon period (40–45 flash/sq. km/yr) over the northeast region of India. During the winter period, the lightning dominates over the northern parts of India such as Jammu and Kashmir. The state-wise casualties' study reveals that maximum casualties are reported in Madhya Pradesh (313 deaths), Maharashtra (281 deaths) and Orissa (255 deaths) on an average per annum. The favorable climatic conditions, such as availability of moisture content, unstable atmosphere and strong convection, cause severe cases of lightning over the regions of Orissa and Maharashtra.

**Keywords** Lightning flash count · Lightning hazards · TRMM/LIS · FRD · Casualty

---

✉ Swagata Payra  
spayra@gmail.com

<sup>1</sup> Institute of Environment and Sustainable Development, Banaras Hindu University, Varanasi 221005, India

<sup>2</sup> Department of Physics, Birla Institute of Technology Mesra, Extension Centre Jaipur, 27 Malviya Industrial Area, Jaipur 302017, India

<sup>3</sup> DST-Mahamana Centre of Excellence in Climate Change Research, Banaras Hindu University, Varanasi, India

<sup>4</sup> Department of Geoinformatics, Central University of Jharkhand, Ranchi 835205, India



ELSEVIER

Contents lists available at ScienceDirect

Fuel

journal homepage: [www.elsevier.com/locate/fuel](http://www.elsevier.com/locate/fuel)

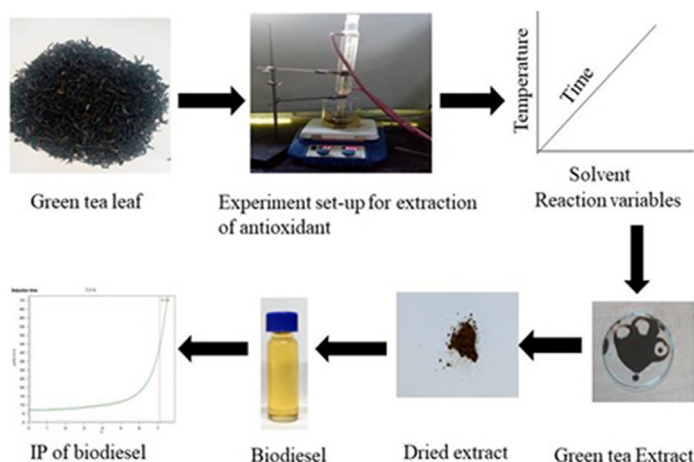
Full Length Article

## Green tea (*Camellia assamica*) extract as an antioxidant additive to enhance the oxidation stability of biodiesel synthesized from waste cooking oil

Rupam Bharti, Bhaskar Singh\*

Department of Environmental Sciences, Central University of Jharkhand, Ranchi 835205, India

## GRAPHICAL ABSTRACT



## ARTICLE INFO

## Keywords:

Green tea leaves  
Oxidation stability  
Phenolic compound  
Biodiesel  
Waste cooking oil

## ABSTRACT

Green tea (*Camellia assamica*) leaves extract as an antioxidant additive and its influence on the oxidation stability of biodiesel produced from waste cooking oil (WCO) has been studied. *Camellia assamica* extract can be used as an eco-friendly and non-toxic alternative of synthetic antioxidants used to enhance the oxidation stability of biodiesel. The extraction of antioxidants was performed in an oil bath at 60 °C for 4 h using ethanol as a solvent. Folin-Ciocalteu assay was used to determine the total phenolic content (TPC) of green tea extract spectrophotometrically. Calibration was done using Gallic acid at a concentration of 10–50 ppm in methanol. The calibration curve was used to obtain the concentration of phenolic compounds present in green tea extract. The extract yield was found to be 0.3 g g<sup>-1</sup> dry green tea leaves. The TPC in the extract was found to be 173.16 mg GAE g<sup>-1</sup> biomass. A 1000 ppm concentration of green tea extract in biodiesel was capable of enhancing the induction period (IP) of biodiesel from 2.88 h to 7.11 h, which met the American (ASTM D67451) and European (EN 14214) standard specification for oxidation stability of biodiesel. Hence, *Camellia assamica* can be used as a natural antioxidant for enhancing biodiesel stability in place of synthetic antioxidants derived from non-renewable resources.

\* Corresponding author.

E-mail address: [bhaskar.singh@cuja.ac.in](mailto:bhaskar.singh@cuja.ac.in) (B. Singh).<https://doi.org/10.1016/j.fuel.2019.116658>

Received 1 September 2019; Received in revised form 19 October 2019; Accepted 12 November 2019

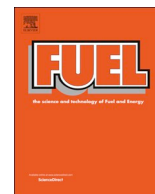
0016-2361/ © 2019 Elsevier Ltd. All rights reserved.



ELSEVIER

Contents lists available at ScienceDirect

Fuel

journal homepage: [www.elsevier.com/locate/fuel](http://www.elsevier.com/locate/fuel)

Full Length Article

## Effect of winterization and plant phenolic-additives on the cold-flow properties and oxidative stability of Karanja biodiesel

Dipesh Kumar, Bhaskar Singh\*

Department of Environmental Sciences, Central University of Jharkhand, Ranchi 835 205, India

## ARTICLE INFO

## Keywords:

Biodiesel  
Oxidative stability  
Cloud point  
Pour point  
Winterization  
Natural antioxidant

## ABSTRACT

Poor stability and low-temperature operability are among the major hurdles in the commercialization of biodiesel. The presence of polyunsaturated fatty acid esters renders the fuel susceptible to oxidative attack while the long-chain saturated components limit its utility under low-temperature conditions. In this study, an attempt was made to improve these properties of Karanja biodiesel. Karanja biodiesel synthesized via a two-step alkali-catalyzed process exhibited poor stability and cold-flow properties. Karanja biodiesel was winterized to limit the content of long-chain saturates, and it had a favorable effect on the cloud and pour point of the fuel. Removal of long-chain saturated components led to an enrichment of the fuel in unsaturated fractions, and as a result, the stability of the fuel further deteriorated. For improving, the stability of the fuel *T. cordifolia* stem extract rich in phenolic constituents was added to winterized biodiesel. The combined treatment of winterization and phenolic-rich extract (1000 ppm) had a pronounced effect on fuel quality as it led to a reduction in the cloud (by 7 °C) and pour point (by 6 °C) and substantially improved the stability of the fuel under accelerated oxidative test conditions. The ASTM D6751, IS 15607, and EN 14214 specifications for the minimum induction period for blendstock biodiesel were satisfied. Thus, coupling the use of winterization and natural antioxidants offers novel opportunities in improving the fuel properties and acceptability of biodiesel in an efficient, economical, and environment-friendly manner.

### 1. Introduction

Biodiesel, as defined by the ASTM D6751, IS 15607 and EN 14214 is "a mixture of mono-alkyl (methyl) esters of long-chain fatty acids derived from vegetable oil or animal fat." However, several other oleaginous materials including single cell (microalgae and yeast) oil [1,2], municipal sludge [3], waste cooking oil [4], etc. have also been transesterified for the production of biodiesel [5]. The single most significant hindrance in the direct utility of vegetable oil (or other oleaginous matter) as an alternative fuel for compression ignition engine is its higher viscosity [6,7]. To circumvent the challenges arising from high viscosity of triglyceride-rich oleaginous matter, the utility of direct use and blending, microemulsion, pyrolysis, transesterification, and hydroprocessing have been reported [8,9]. Transesterification remains to be the most commonly adopted strategy for the purpose [10,11]. Hydroprocessing of oleaginous matter to renewable diesel (also termed as green diesel or hydroprocessed vegetable oil) is emerging as an attractive approach, but its overall feasibility is yet to be clearly understood [12,13]. Biodiesel is an attractive alternative fuel for climate change mitigation commitments and for meeting the ever-increasing

demand for fuel [14,15]. The past few decades have witnessed a surge in demand for biodiesel as several countries have incorporated policy mandates for biodiesel in transport energy mix [16,17].

Renewability, cleaner emission profile, biodegradability, miscibility in diesel, and comparable fuel properties are among the significant advantages of biodiesel [18]. Some of the properties of biodiesel, including its viscosity, density, cold flow properties, oxidative stability, cetane number, etc. are intricately related to the fatty acid profile of the feedstock [19]. The widespread acceptability of the fuel is limited by its poor stability and inferior performance under low-temperature conditions [20,21].

The saturated fractions of biodiesel have a favorable effect on its stability, but they (particularly the long-chain saturates) can potentially compromise the low-temperature performance (cold-flow properties; CFPs) of the fuel. Long-chain saturated esters have a very high melting point, and they tend to crystallize under conditions of low temperature [22]. The highest temperature at which these crystals are first detected under a strictly controlled cooling test is referred as the cloud point (CP), and if the temperature continues to fall beyond the CP the crystals continue to agglomerate and grow in size until a point is reached when

\* Corresponding author.

E-mail address: [bhaskar.singh@cuja.ac.in](mailto:bhaskar.singh@cuja.ac.in) (B. Singh).<https://doi.org/10.1016/j.fuel.2019.116631>

Received 25 June 2019; Received in revised form 7 November 2019; Accepted 9 November 2019

0016-2361/ © 2019 Elsevier Ltd. All rights reserved.



# Forest health estimation in Sholayar Reserve Forest, Kerala using AVIRIS-NG hyperspectral data

Shahbaz Ahmad<sup>1</sup> · Arvind Chandra Pandey<sup>1</sup> · Amit Kumar<sup>1</sup> ·  
Nikhil V. Lele<sup>2</sup> · Bimal K. Bhattacharya<sup>2</sup>

Received: 1 January 2019 / Revised: 2 March 2019 / Accepted: 5 March 2019  
© Korean Spatial Information Society 2019

**Abstract** The present study deals with analyzing forest health, its parameters, and suitability of hyperspectral data for vegetation health-related studies. Sholayar reserve forest in Kerala has a huge reserve of equatorial moist evergreen forest and demands preservation in every respect. Due to increased human interferences coupled with possible climate change, its health is undergoing a stage of deterioration. Stress levels in the canopy were assessed using a number of stress-related pigments. Detailed study of vegetation response to canopy leaf pigments have been carried out in the study. Airborne Visible Infrared Imaging Spectrometer Next Generation (AVIRIS-NG) data provides immense possibilities to study a number of stress-related pigments like anthocyanin, carotenoid, lignin, chlorophyll-a, b etc. Dominant species in these forests are *Holigarna arnottiana*, *Grevillea robusta*, *Grewia tiliifolia*, *Syzygium cumini*, *Alstonia Scholaris*, *Cinnamomum verum*, *Artocarpus heterophyllus*, *Bischofia javanica*, *Mangifera indica*, *Bombax ceiba*, *Anogeissus latifolia*, *Terminalia paniculata*

etc. Apart from luscious natural vegetation, plantation of teak (*Tectona Grandis*), rubber (*Hevea brasiliensis*), tea (*Camellia sinensis*), Coffee (*Coffea Arabica*), Palm-Oil tree (*Elaeis guineensis*) etc. also exists. Field data pertaining to one of the selected pigments was correlated with remotely sensed pigment estimates. Correlation of field measured chlorophyll concentration and EVI showed  $R^2 = 0.421$ . Similarly, the anthocyanin index showed a correlation of  $R^2 = 0.319$ . In the Sholayar Reserve Forest (493.0 km<sup>2</sup>) an area of 141.0 km<sup>2</sup> was found to be in a healthy state. Whereas about 218.0 km<sup>2</sup> of area exhibit moderately healthy condition and 77.0 km<sup>2</sup> area was in the least healthy state.

**Keywords** AVIRIS-NG · Forest health · Hyperspectral remote sensing · Leaf pigment · Vegetation indices · Sholayar Reserve Forest

## 1 Introduction

Due to the increased population, air pollution, development activities, climate change, etc. forest health is declining globally [1]. This demands an efficient forest monitoring systems to assess the changes undergoing in forest areas. Although widely used, the term “forest health” is vaguely defined in the literature, making its application in forest management cumbersome [2]. Health is related to the capacity of self-renewal of land and thus its conservation is an effort to understand and preserve this capacity [3]. Aerial sketch-mapping in which the damage due to insects are observed manually has been frequently used [4]. Healthy forests are required for aesthetical pleasure and a number of outdoor activities. Human intervention should

✉ Arvind Chandra Pandey  
arvindchandrap@yahoo.com

Shahbaz Ahmad  
shahbaz.ameen@gmail.com

Amit Kumar  
amit.iirs@gmail.com; amit.kumar@uj.ac.in

Nikhil V. Lele  
mail.nikhillele@gmail.com

Bimal K. Bhattacharya  
bkbhattacharya@sac.isro.gov.in

<sup>1</sup> Department of Geoinformatics, School of Natural Resource Management, Central University of Jharkhand, Ranchi 835205, India

<sup>2</sup> Space Application Centre, ISRO, Ahmedabad 380015, India





# MODIS based forest fire hotspot analysis and its relationship with climatic variables

Binita Kumari<sup>1</sup> · Arvind Chandra Pandey<sup>1</sup>

Received: 11 January 2019 / Revised: 22 May 2019 / Accepted: 29 May 2019  
© Korean Spatial Information Society 2019

**Abstract** Global warming caused an increase of forest fire events worldwide causing widespread forest degradation. Geospatial techniques aid in analysing climatic parameters to examine their relationship with forest fire. The research analyses time series forest fire events during 2001–2017 to deduce forest fire hotspots in PTR. MODIS forest fire spots was converted into points and hotspot analysis tool was used to map hotspot. The forest fire incidences were analysed with reference to climatic parameters viz. precipitation, solar radiation (SR), mean temperature and relative humidity (RH). The average RH was highest in May (0.69) and lowest in March (0.18), whereas high temperature with low RH was observed till the end of April. The SR was highest in April (27.24 MJ/m<sup>2</sup>) whereas lowest in May (15.68 MJ/m<sup>2</sup>). Satellite based land surface temperature (LST) was compared with fire spot and found that area having high temperature lies under high forest fire zone. The highest LST observed was 49.52 °C whereas the lowest was 29.40 °C. The study revealed that most forest fires occurred during March–April and total forest fire events was 1212. For accuracy assessment an analysis between fire pixels and post fire data from Landsat was shown, which showed that same areas were under forest fires during 2001–2017.

**Keywords** Forest fire · MODIS · Climatic parameters · LST · Fire frequency · Hotspot

## 1 Introduction

Climate and environmental variables (e.g., weather, soils, topography, and vegetation) of a region control the natural fire regimes [1]. Fire regimes like frequency, intensity, size, pattern, season, and severity are important factors in many ecosystems [2, 3]. Climate change of any region adversely affects the cultural, ecological and socio-economic condition of inhabitant tribal community [4] due to increase in intensity and frequency of forest fires. High temperatures and drought lead to extreme changes in the ecosystem which ultimately leads to forest habitat degradation. Rising temperatures, dry and scorching summers, and forest fires are expected to increase in frequency, intensity, and severity [5]. Tree mortality, droughts and vegetation stress are the factors responsible for long fire seasons [6] owing to increased fuel load [7], plant disease [8], insect outbreaks [9] and the spread of invasive species [10].

India is one of the mega-biodiversity countries which retain 173,000 forest villages largely occupied by ethnic communities whose lives fully revolve in and around forests for their livelihood [11]. Forest cover are deteriorating at an alarming rate to due to increasing population. Besides other factors, wildfires are the main factors for degradation of the forest cover of Jharkhand. Forest fire damages the regeneration of important tree species including Sal (*Shorea robusta*), which is a major species in Jharkhand [12].

The study of forest fire statistics for the generation of forest fire maps becomes essential when the historical

✉ Arvind Chandra Pandey  
arvindchandrap@yahoo.com

Binita Kumari  
binita.kumari@cuja.ac.in

<sup>1</sup> Department of Land Resource Management, School of Natural Resource Management, Central University of Jharkhand, Ranchi, Jharkhand, India



Cite this: *Energy Adv.*, 2022,  
1, 950

# Headway towards contemporary 2D MXene-based hybrid electrodes for alkali-ion batteries

Helen Treasa Mathew,<sup>a</sup> Kumar Abhisek,<sup>a</sup> Shashikant Shivaji Vhatkar<sup>a</sup> and Ramesh Oraon \*<sup>ab</sup>

Recent studies have revealed that the current consumption rate of fossil fuels may lead to their exhaustion in the coming years. Due to the depletion of non-renewable energy sources and the fitness of renewable energy sources, energy storage and management can be viewed as a prime requisite. The inception of advancements in energy storage techniques and rechargeable batteries has eased the problem to a certain extent. With highly exceptional properties such as inherent volumetric capacitance, outstanding conductivity, durability, low energy barriers for metal ion diffusion and the presence of surface functional groups, MXenes have entered the field of energy storage. MXenes are 2-D layers of transition metal carbides or nitrides, synthesized by the selective etching of aluminium from layered MAX phases. The large interlayer spaces for ion intercalation permits alkali ions in these layers, revealing unexpected properties that can be exploited for energy storage in alkali-ion batteries (AIBs) such as lithium/sodium/potassium/magnesium/calcium ion batteries. Electrochemical energy storage can also be visualised as a clean energy storage system. This review covers the synthesis of MXenes, their eminent properties and the fabrication of MXene-based nanomaterials and hybrids for electrochemical energy storage in various alkali-ion batteries. Finally, possible challenges are highlighted for the future exploration of the research possibilities.

Received 9th August 2022,  
Accepted 11th October 2022

DOI: 10.1039/d2ya00212d

rsc.li/energy-advances

## 1. Introduction

Sustainable energy utilisation is vital since the consumption of resources for our present needs should be established without compromising the needs of future generations. Maximising the efficiency of the energy storage devices and the subsequent

<sup>a</sup> Department of Nanoscience and Technology, Central University of Jharkhand, Ranchi, India. E-mail: ramesh.oraon@cuj.ac.in

<sup>b</sup> Department of Chemistry, Central University of Jharkhand, Ranchi, India



**Helen Treasa Mathew**

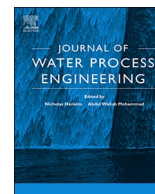
*Ms Helen Treasa Mathew received her bachelors' and masters' degree from Mahatma Gandhi University and Kannur University Kerala, India in 2018 and 2020, respectively. She has worked as project trainee in ESMB Division of CSIR-NPL, New Delhi. Currently, she is pursuing PhD from the Department of Nanoscience and Technology, Central University of Jharkhand, India. Her research interest is in the synthesis and modification of MXene-based hybrid materials for multifarious applications.*



**Kumar Abhisek**

*Mr Kumar Abhisek obtained his masters' degree from NIST, Berhampur, Odisha, India in 2020, and pursuing PhD in Department of Nanoscience and Technology, Central University of Jharkhand, India. He is currently working on the development of transition metal dichalcogenide-based multifunctional hybrid materials for environmental applications.*





## Efficient removal of arsenic using plastic waste char: Prevailing mechanism and sorption performance



Ekta Singh<sup>a,b</sup>, Aman Kumar<sup>a,b</sup>, Abhishek Khapre<sup>b,c</sup>, Purabi Saikia<sup>a</sup>, Sushil Kumar Shukla<sup>a</sup>, Sunil Kumar<sup>b,c,\*</sup>

<sup>a</sup> Central University of Jharkhand, Brambe, Ranchi, 835 205, India

<sup>b</sup> CSIR- National Environmental and Engineering Research Institute (CSIR-NEERI), Nagpur, 440 020, India

<sup>c</sup> The Academy of Scientific and Innovative Research (AcSIR), Ghaziabad, Uttar Pradesh, 201 002, India

### ARTICLE INFO

#### Keywords:

PE  
PET  
PVC  
Adsorption  
Langmuir isotherm

### ABSTRACT

The present study aimed to investigate the effects of low-cost plastic char synthesized from pyrolysis of waste Polyvinyl chloride (PVC), Polyethylene terephthalate (PET) and Polyethylene (PE) for adsorbing Arsenic (As). Adsorption of As under kinetic and equilibrium conditions was evaluated against changing pH (4–8), contact time (0–40 min) and a dose of char (0.5–1.5 g). The uptake capability was found to be in the range of 10.7–99.4 %. Amongst all the plastic chars used, PE and PVC mixed char showed the highest removal of As that ranged from 71.6–99.4%. Least amount of sorption was shown by PE and PET chars which was found to be in range of 12.4–32.5%. The optimum equilibrium time of 20 min with acidic medium (pH 6.0) at 1.5 g was the best-favored dose for 99.4 % adsorption of As. Pseudo-Second-Order rate effectively fitted well with removal kinetics, whereas Langmuir isotherm models fitted more accurately to the obtained results. The study concluded that plastic chars have a greater possibility to act as a promising sorbent for effective removal of As.

### 1. Introduction

Arsenic (As) is the twentieth most abundant element in the geosphere and fourteenth in seawater [1]. Its contamination in nature is turning out as one of the most serious issues in some places of the earth [2,3]. It is a strong cancer-causing agent, prompting skin, liver and various lung diseases [4,5]. It has been well-known to cause genotoxicity, cytotoxicity, skin sores and peripheral vascular sickness [6]. Various sources, comprising of man-made as well as natural sources, are continuously increasing the mean measure of As which was earlier evaluated to be 1.8 mg kg<sup>-1</sup> [7]. The removal of As from contaminated water sites is a challenge because of the varying arsenic speciation that depends directly on the solution pH [8]. In water bodies, arsenite and arsenate have been perceived as major lethal types of arsenic. Arsenite is 25–60 times more lethal than arsenate and has been accounted to be increasingly portable in the environment [9]. The concentration of As is very low to be considered as a causative factor for health issues and thus, its safe limit is exceptionally low in comparison to other lethal metals (10 µg L<sup>-1</sup>) as prescribed by the World Health Organization [10].

It is quite important for developing some efficient arsenic removal techniques from the contaminated sites. The major techniques for the

remediation of As predominantly include chemical oxidation, chemical coagulation-precipitation, adsorption, ion exchange, reverse osmosis, and membrane separation [7,8,11–14]. Membrane separation technique has been found effective in the removal of As in the developed countries but not in the developing countries [15]. This is mainly due to the increment in the unit cost (almost 10 times), which renders it to be unjustifiable for the smaller treatments [16]. Oxidation techniques demand high energy usage, which is not at all cost-effective and thus, it is also not feasible. Coagulation, along with filtration, is although economic but was found to often display lower efficiencies (< 90 %) [16]. Despite high As removal efficiencies shown by all these techniques, they are not preferred for higher supply systems due to the high capital and maintenance cost [17]. Amongst all the available techniques, adsorption has been considered as the most efficient strategy in the last few decades because of the involvement of low-cost during the entire process along with its efficient design and wide range of adsorbent choice [4,18,19]. Carbon materials have been considered as an optimal solid adsorbent due to the low cost in spite of some disadvantages like hygroscopicity and pore-blocking [20–22].

Because of the limitations of the available techniques, it was opined to use plastic chars for concurrent adsorption of As. Plastics have turned out as a disastrous issue to be managed and removed from the

\* Corresponding author at: CSIR- National Environmental and Engineering Research Institute (CSIR-NEERI), Nagpur, 440 020, India.

E-mail address: [s.kumar@neeri.res.in](mailto:s.kumar@neeri.res.in) (S. Kumar).

<https://doi.org/10.1016/j.jwpe.2019.101095>

Received 21 September 2019; Received in revised form 1 December 2019; Accepted 5 December 2019

2214-7144/ © 2019 Elsevier Ltd. All rights reserved.

# Sorption of Volatile Organic Compounds on Non-activated Biochar

Aman Kumar<sup>1,2</sup>, Ekta Singh<sup>1,2</sup>, Abhishek Khapre<sup>2,3</sup>, Nirmali Bordoloi<sup>1</sup>, Sunil Kumar<sup>2,3\*</sup>

<sup>1</sup>Central University of Jharkhand, Brambe, Ranchi, 835 205, India

<sup>2</sup>CSIR-National Environmental and Engineering Research Institute (CSIR-NEERI), Nagpur, 440 020, India

<sup>3</sup> The Academy of Scientific and Innovative Research, Ghaziabad (AcSIR), Ghaziabad, Uttar Pradesh, 201 002, India

\*Corresponding author's email: s\_kumar@neeri.res.in

## Abstract

This work dealt with the determination of the suitability of sorption of Volatile Organic Compounds (VOCs) on biochars prepared from neem, sugarcane and bamboo feedstocks. Six different VOCs namely benzene, toluene, methyl chloride, xylene, chloroform and carbon tetrachloride were used in a laboratory-scale set-up on non-activated biochars prepared via slow pyrolysis (350-550 °C). Although all the chars showed considerable sorption but amongst them N3 (neem-based biochar) showed the maximum removal efficiency (65.5 mg g<sup>-1</sup> for toluene). Variation in pyrolysis temperature and feedstock type showed significant change in the porosity and specific surface area of the biochar, which is favorable for VOC sorption efficiency. With higher surface area and contact time, the sorption capacity of char enhanced. However, the extent of sorption capacity of biochars differed with changing VOC type. Pseudo-Second-Order model fitted well with the results obtained from VOC sorption kinetics.

**Keywords:** Biochar, Pyrolysis, Pseudo- Second-Order, Sorption, Volatile Organic Compounds



# Development of observation-based parameterizations of standard deviations of wind velocity fluctuations over an Indian region

Piyush Srivastava<sup>1,2</sup> · Maithili Sharan<sup>1</sup> · Manoj Kumar<sup>3</sup>

Received: 22 April 2019 / Accepted: 11 September 2019 / Published online: 23 November 2019  
© Springer-Verlag GmbH Austria, part of Springer Nature 2019

## Abstract

The present study utilizes the turbulence observations over an Indian region, Ranchi, to study the diurnal and seasonal characteristics of mean and turbulent parameters in the atmospheric surface layer under different wind speed and stability regimes. Data for the year 2009 are chosen to compute mean and turbulent statistics using the eddy correlation technique and are studied within the framework of Monin–Obukhov similarity theory. The analysis of the observational behaviour of the standard deviation of wind velocity fluctuations ( $\sigma_i$ ,  $i = u, v, w$ ) normalized by friction velocity ( $u_*$ ) suggests that these parameters remain independent of stability of layer in near-neutral to moderately stable/unstable conditions. However, they are observed to increase following the classical 1/3 power law with increasing stability/instability in moderate to strong stable/unstable conditions. Further, an attempt has been made to develop possible parameterizations of these coefficients in terms of Monin–Obukhov stability parameter in low and moderate to strong wind regimes for four different seasons. The proposed observation-based functional forms the  $\sigma_i$  as functions of the stability exhibit different behaviours depending on the optimal values of unknown coefficients obtained for different seasons. However, within the limit of the uncertainty in the observed input parameters, the values of the season-dependent set of coefficients do not affect the overall statistical agreement between predicted and observed values of the normalized standard deviation of wind velocity fluctuations.

**Keywords** Atmospheric surface layer · Surface fluxes · Mean and turbulent characteristics · Monin–Obukhov similarity theory · Parameterization

## 1 Introduction

The turbulent structure of the atmospheric boundary layer is poorly described in low wind conditions. The complexity of the boundary layer grows with the weakening of the winds and the degree of atmospheric stability (Mahrt 1998, 2008; Luhar et al. 2009). The scarcity of data in low wind convective as well as very stable conditions over the tropical region has resulted in a limited understanding of turbulence structure in such types of atmospheric conditions (Gopalakrishnan et al.

1998; Aditi and Sharan 2007). The limited knowledge of the boundary layer characteristics and their representation in numerical models is a major contributing factor for relatively poor performance of almost all dispersion models under low wind and very stable/unstable conditions (Sharan et al. 1997; Kumar and Sharan 2010; Qian and Venkatram 2011). The diffusion of a pollutant released from emission sources is irregular and indefinite in weak and variable wind conditions (Sharan et al. 2012). Studies reported in the literature (Sharan et al. 1996; Anfossi et al. 2006; Luhar 2011) suggest that the operational dispersion models fail to predict the observed concentrations under low wind conditions due to inadequate understanding of turbulence and dispersion characteristics in these conditions. The dispersion of pollutants in the atmosphere is influenced by the standard deviation of wind velocity fluctuations ( $\sigma_u$ ,  $\sigma_v$  and  $\sigma_w$ ). These parameters provide useful information regarding the turbulent state of the atmospheric surface layer and are used as important inputs implicitly as well as explicitly to almost all dispersion models (Hanna et al. 1982; Sharan et al. 1997; Holmes and Morawska 2006; Luhar 2010; Kumar and Sharan 2010; Kumar and Goyal

✉ Piyush Srivastava  
piyoosh.iitr@gmail.com

<sup>1</sup> Centre for Atmospheric Sciences, Indian Institute of Technology, New Delhi, Delhi, India

<sup>2</sup> Present address: School of Earth and Environment, University of Leeds, Leeds, UK

<sup>3</sup> School of Natural Resource Management, Center for Environmental Sciences, Central University, Ranchi, Jharkhand, India



# One pot method to synthesize three-dimensional porous hydroxyapatite nanocomposite for bone tissue engineering

Chandrani Sarkar<sup>1,2,3</sup> · Kumar Anuvrat<sup>4</sup> · Subhadra Garai<sup>1</sup> · Sumanta Kumar Sahu<sup>2</sup> · Jui Chakraborty<sup>5</sup>

Published online: 18 September 2019  
© Springer Science+Business Media, LLC, part of Springer Nature 2019

## Abstract

A three-dimensional porous hydroxyapatite nanocomposite has been synthesized by a simple, less energy consuming and cost effective one-pot method. In this study, gelatin foam has been used as pore forming agent and incorporated in carboxymethyl cellulose-hydroxyapatite system in composite formation stage. A three-dimensional porous polymers-hydroxyapatite nanocomposite has been formed as a final product. The synthesized porous nanocomposite has been thoroughly characterized by different techniques. It was found that the nanocomposite is highly porous with almost 80% porosity, and has multi-scale pores from 2.5 to 900  $\mu\text{m}$  in size. Furthermore, the synthesized porous composite has compressive strength  $\sim 11.8 \pm 1.5$  MPa and modulus  $\sim 0.243 \pm 0.031$  GPa, in the range of cancellous bone. Moreover, the nanocomposite provides favorable environment to cells for proliferation, high alkaline phosphatase (ALP) activity and extracellular mineralization. In vitro degradation of synthesized nanocomposites was tested in simulated body fluid. Results ascertained that the synthesized porous hydroxyapatite nanocomposite would be a promising scaffold for bone tissue engineering.

**Keywords** Hydroxyapatite · Gelatin · Carboxymethyl cellulose · Nanocomposite · Scaffold

## 1 Introduction

The treatment of severely damaged bones with functional bone substitutes is a major concern for clinicians to get successful post-implantation outcomes. In this sense, three-dimensional synthetic bone grafts have received wide

attention in orthopedic applications [1]. However, the suitability and efficacy of these bone substitutes in bone tissue engineering mainly rely on their structural features such as the porosity, pore size and strength [2–5]. Hence, scaffold, a porous three-dimensional structure attracts the attention of many researchers because it helps in guiding and modulating the growth of cells through its porous structure. However, it requires an interconnected porous system with multi scale pores for nutrient flows, vascular ingrowth and bone tissue formation. Moreover, it needs to be biocompatible, biodegradable and bioresorbable [2–7]. So, a proper selection of materials is required. To date, several natural polymers such as collagen, alginate, cellulose, chitosan and gelatin are widely used due to their excellent biocompatibility, biodegradability and hydrophilicity [8–10]. Alternatively, ceramics basically calcium phosphates-based ceramics are also used because they possess high stiffness, biocompatibility and osteoconductivity [7, 11, 12]. Despite of their excellent properties, the use of such monolithic scaffolds is limited by significant drawbacks. Generally, the application of polymers is restricted due to their poor strength and high degradability, whereas, ceramics are commonly fragile in nature and processability is very poor. In this perspective, composite scaffolds are always a better option to mitigate

**Electronic supplementary material** The online version of this article (<https://doi.org/10.1007/s10934-019-00805-y>) contains supplementary material, which is available to authorized users.

✉ Chandrani Sarkar  
chandranisarkarjsr@gmail.com

- <sup>1</sup> Advanced Materials and Processes Division, CSIR-National Metallurgical Laboratory, Jamshedpur, Jharkhand 831007, India
- <sup>2</sup> Department of Applied Chemistry, Indian Institute of Technology (Indian School of Mines), Dhanbad, Jharkhand 826004, India
- <sup>3</sup> Department of Chemistry, Mahila College, Kolhan University, Chaibasa, Jharkhand 833201, India
- <sup>4</sup> Centre for Nanotechnology, Central University of Jharkhand, Ranchi, Jharkhand 835205, India
- <sup>5</sup> CSIR-Central Glass & Ceramic Research Institute, 196, Raja S.C. Mullick Road, Jadavpur, Kolkata 700 032, India





# Thermal degradation of eco-friendly alternative plastics: kinetics and thermodynamics analysis

Satyanarayan Patnaik<sup>1</sup> · Sachin Kumar<sup>2</sup> · Achyut K. Panda<sup>1</sup>

Received: 21 May 2019 / Accepted: 28 January 2020 / Published online: 17 February 2020  
© Springer-Verlag GmbH Germany, part of Springer Nature 2020

## Abstract

This work reports the thermal degradation behaviour, kinetics and thermodynamics of two different eco-friendly plastics, viz. non-woven plastic and corn starch-based biodegradable plastics, which are commonly used nowadays as an alternative to synthetic plastics. In this context, thermogravimetric analysis of plastic waste samples was carried out at wide range of heating rates of 10, 20, 40, 60, 80 and 100 °C/min in nitrogen atmosphere, and activation energy is determined by first-order model-fitting method while thermodynamic parameters are determined on the basis of Eyring theory of activated complex. The regression coefficient obtained from kinetic study of thermal degradation of these plastics best fits to the first-order kinetic equation. The kinetics and thermodynamic parameters obtained for both the plastics are found very close to each other. So, this study would help design more effective conversion system for the recycling of both the wastes together.

**Keywords** Non-woven plastics · Biodegradable plastics · Thermal degradation · Thermogravimetric analysis · Activation energy

## Introduction

The use of plastics is increasing tremendously around the world due to its compatible properties in diversified applications. The plastic used in majority of the applications has low life leading to generation of huge plastic waste huge littering on the outskirts of towns creating unhealthy conditions in and around human ecosystem. In addition, the unscientific dumping and unskilled processing and or recycling of such plastic wastes may led to fugitive and toxic emissions, infertile land due to its barrier properties, disrupt marine ecosystem and drain chocking problem. All these issues have become very acute and the government have imposed ban of plastic bags. Scientific breakthroughs have made it possible to provide some sustainable and green solution to this problem. The non-woven plastics

are one of such inventions that is being encouraged to be used as a substitute of ordinary plastic bags as they can be used number of times before they get worn out, and also, they are recyclable although not compostable. Other alternate be the use of compostable bioplastics derived from renewable sources, and biodegradable plastics made from traditional petrochemicals engineered to break down more quickly. These plastics upon biodegradation may not always produce harmless substance making them unsuitable for composting. Use of such alternate plastics for prolonged period also gathers plastic wastes and needs appropriate method to get rid of their harmful effects. Pyrolysis is reported to be the most suitable technique to manage plastics giving rise to fuel feedstock without any toxic emission and other by-products. The design of pyrolysis reactor requires input of kinetic and thermodynamic parameters and can be obtained from the prototype experiment carried out using thermogravimetric analysis. Literature reports the thermal degradation kinetics of different plastics such as polypropylene (PP), high density polyethylene (HDPE), low density polyethylene (LDPE), polystyrene (PS), acrylonitrile butadiene styrene (ABS), polyvinyl chloride (PVC) and polyethylene terephthalate(PET), and biomasses such as natural fibres, lignin, cellulose, sawdust, corn stover and non-edible oil seeds. The summary of few of the literatures are as

Responsible editor: Philippe Garrigues

✉ Achyut K. Panda  
achyut.panda@gmail.com

<sup>1</sup> Department of Chemistry, Veer Surendra Sai University of Technology, Burla, Odisha, India

<sup>2</sup> Department of Energy Engineering and Centre of Excellence in Green & Efficient Energy Technology (CoE-GEET), Central University of Jharkhand, Ranchi, Jharkhand 835205, India



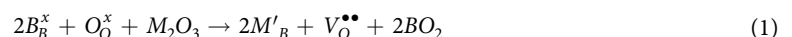
OPEN

# A Promising Proton Conducting Electrolyte $\text{BaZr}_{1-x}\text{Ho}_x\text{O}_{3-\delta}$ ( $0.05 \leq x \leq 0.20$ ) Ceramics for Intermediate Temperature Solid Oxide Fuel Cells

Deepash S. Saini<sup>1\*</sup>, Avijit Ghosh<sup>2</sup>, Shuvendu Tripathy<sup>3</sup>, Aparabal Kumar<sup>3</sup>, Sanjeev K. Sharma<sup>3</sup>, Nawnit Kumar<sup>4</sup>, Shubhankar Majumdar<sup>5</sup> & Debasis Bhattacharya<sup>3</sup>

In this study, the Ho-substituted  $\text{BaZrO}_3$  electrolyte ceramics ( $\text{BaZr}_{1-x}\text{Ho}_x\text{O}_{3-\delta}$ ,  $0.05 \leq x \leq 0.20$ ) were synthesized through a low-cost flash pyrolysis process followed by conventional sintering. The effects of Ho-substitution in  $\text{BaZrO}_3$  studied in terms of the structural phase relationship, microstructure and electrical conductivity to substantiate augmented total electrical conductivity for intermediate temperature solid oxide fuel cells (IT-SOFCs). The Rietveld refined X-ray diffraction (XRD) patterns revealed that pure phase with  $Pm\bar{3}m$  space group symmetry of cubic crystal system as originated in all samples sintered at  $1600^\circ\text{C}$  for 8 h. The Raman spectroscopic investigations also approved that Ho incorporation in  $\text{BaZrO}_3$  ceramics. Field Emission Scanning Microscopic (FESEM) study informed a mixture of fine and coarse grains in the fracture surface of Ho-substituted  $\text{BaZrO}_3$  sintered samples. The relative density and average grain size of samples were observed to decrease as per the addition of Ho-substitution in  $\text{BaZrO}_3$  ceramics. The electrical conductivity study was accomplished by Electrical Impedance Spectroscopy (EIS) under 3% humidified  $\text{O}_2$  atmosphere from  $300$  to  $800^\circ\text{C}$ . Furthermore, the total electrical conductivity of  $\text{BaZr}_{0.8}\text{Ho}_{0.2}\text{O}_{3-\delta}$  ceramic was found to be  $5.8 \times 10^{-3} \text{ S}\cdot\text{cm}^{-1}$  at  $600^\circ\text{C}$  under 3% humidified atmosphere, which may be a promising electrolyte for IT-SOFCs.

Recently, the proton conductive oxide ceramics have fascinated worldwide attention due to widespread applications in intermediate temperature solid oxide fuel cells (IT-SOFCs), hydrogen separation and electrolysis of steam, etc. In this context, the rare-earth cerates and zirconates with the perovskite-type  $\text{A(II)B(IV)O}_3$  crystallographic structure are the two foremost families of proton-conducting oxides for electrochemical applications<sup>1-4</sup>. Generally, in these categories of oxide materials, oxygen vacancies are increased by replacement of tetravalent cation B(IV) by trivalent cation M(III) as given in the Eq. (1) using Kröger-Vink notation.



In this case, an  $\text{H}_2\text{O}$  molecule from the vapor phase dissociates into hydroxide ( $\text{OH}^-$ ) ion and proton ( $\text{H}^+$ ) in these oxide materials. The hydroxide ( $\text{OH}^-$ ) ion fills up an oxygen vacancy, and proton ( $\text{H}^+$ ) forms a hydroxide ( $\text{OH}^-$ ) ion with oxygen lattice<sup>5-7</sup> according to the Eq. (2).



The protons are induced in these types of the perovskite oxides through oxygen vacancies due to replacement of tetravalent cation B(IV) by trivalent cation M(III). This proton conducts through hopping to the adjacent oxygen site and revolving around the oxygen that contribute to the protonic conductivity in the material<sup>6,7</sup>. Furthermore, trivalent cation M(III) substituted barium zirconates (i.e.  $\text{BaZr}_{1-x}\text{M}_x\text{O}_{3-\delta}$ ) are more chemically

<sup>1</sup>Department of Physics, Deen Dayal Upadhaya Gorakhpur University, Gorakhpur, 273009, India. <sup>2</sup>Department of Physics, Central University of Jharkhand, Ranchi, 835205, India. <sup>3</sup>Materials Science Centre, Indian Institute of Technology, Kharagpur, 721302, India. <sup>4</sup>Department of Physics, Malti Dhari College, Naubatpur, Patliputra University, Patna, 801109, India. <sup>5</sup>Department of Electronics and Communication Engineering, National Institute of Technology, Meghalaya, 793003, India. \*email: [dssainiddugu@gmail.com](mailto:dssainiddugu@gmail.com)



# India's contribution to mitigating the impacts of climate change through vegetation management

J. Dash<sup>1</sup> · M. D. Behera<sup>2</sup> · C. Jeganathan<sup>3</sup> · C. S. Jha<sup>4</sup> · S. Sharma<sup>5</sup> · R. Lucas<sup>6</sup> · A. A. Khuroo<sup>7</sup> · A. Harris<sup>8</sup> · P. M. Atkinson<sup>1,9</sup> · D. S. Boyd<sup>10</sup> · C. P. Singh<sup>11</sup> · M. P. Kale<sup>12</sup> · P. Kumar<sup>13</sup> · Soumit K. Behera<sup>14</sup> · V. S. Chitale<sup>2,15</sup> · S. Jayakumar<sup>16</sup> · L. K. Sharma<sup>3,17</sup> · A. C. Pandey<sup>3,18</sup> · K. Avishek<sup>3</sup> · P. C. Pandey<sup>2,19</sup> · S. N. Mohapatra<sup>20</sup> · S. K. Varshney<sup>21</sup>

Received: 12 December 2018 / Revised: 10 October 2019 / Accepted: 11 November 2019  
© International Society for Tropical Ecology 2020

## Abstract

The changes in natural ecosystems provide opportunity to increase vegetation carbon sink capacity and thereby contribute to mitigation of climate change impacts. The Indian tropics and the large ecological variation within the country afford the advantage of diverse niches and offer opportunities to reveal the role of biotic factors at different levels of organization from populations to ecosystems. The last 4 decades of research and development in the Indian space science community has been primarily application driven in response to the government space programme for national development. The expenditure in R&D over next 5 year suggest that scientific research is higher on the country's agenda. The Indo-UK Terrestrial Carbon Group (IUTCG) comprising both Indian and UK scientists, funded jointly by the Department of Science and Technology, India and the Department of Business, Innovation and Skills organised a workshop to explore ways in which Earth observation data can be effectively utilised in mitigating the impacts of climate change through vegetation management. Effective integration of field observations, collected through various monitoring networks, and satellite sensor data has been proposed to provide country-wide monitoring.

**Keywords** Carbon observation · Indian ecological observation network · Satellite remote sensing · Vegetation dynamics model

## Introduction

Across India, human-driven land use and climate changes are altering the structure, functioning and extent of ecosystems (Menon et al. 2002; Behera et al 2018) and, in-turn, these are affecting regional bio-geochemical feedbacks. This is evident from the fact that, there is an increase in the length of vegetation growing season (Menzel and Fabian 1999); in the Himalayas, vegetation is advancing to higher elevations and the overall productivity is increasing where conditions (e.g., soils, aspect) allow (Sharma and Roy 2007; Khuroo et al. 2011). Therefore, these changes in natural ecosystems also provide a potential opportunity to increase carbon sink capacity and thereby contribute to mitigating climate change impacts. Human-directed initiatives such as the National Mission for a Green India (Jha 2012) launched

by the Government of India is focusing on increasing forest density by decentralising forest management and interventions at a local scale; the mission has a target to increase carbon sequestration by 60 Mio. tonnes by 2020. There are also many areas that might potentially support vegetation into the future, particularly where elements of the original ecosystem remain (Chazdon 2008). In each case, a substantial, but as yet un-quantified amount of carbon can be sequestered annually (Lal 2002). In particular, the Indian tropics and the large ecological variation within the country provide the advantage of diverse niches and offer opportunities to elucidate comparative adaptation biology, including the role of biotic factors, at different levels of organization from population to ecosystems. For this reason, it is recommended that India puts in place a programme that allows actual and potential carbon sequestration to be quantified and monitored on a regular basis.

India has a strong network of scientific institutions located in various bio-geographical provinces and a dedicated Space Programme through the Indian Space Research Organisation

✉ M. D. Behera  
mdbehera@coral.iitkgp.ac.in

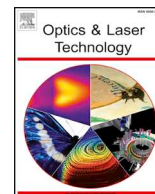
Extended author information available on the last page of the article



ELSEVIER

Contents lists available at ScienceDirect

## Optics and Laser Technology

journal homepage: [www.elsevier.com/locate/optlastec](http://www.elsevier.com/locate/optlastec)

Full length article

## All optical NOR and NAND gates using four circular cavities created in 2D nonlinear photonic crystal

Alok Kumar, Sarang Medhekar\*

Department of Physics, Central University of Jharkhand, Ranchi 835205, Jharkhand, India

## HIGHLIGHTS

- Novel photonic crystal NOR and NAND gates are presented.
- Low operating power, good contrast ratio and cascadeable.
- Unique in terms of bypass waveguides of the structures.

## ARTICLE INFO

## Keywords:

Photonic crystal  
All optical logic gate  
Circular cavities  
Kerr effect

## ABSTRACT

The paper presents novel 2D photonic crystal (PhC) structures comprising of four circular cavities (CCs) that mimic NOR and NAND gates. 2D Finite difference time domain (2DFDTD) method is used for simulation and analysis of optical behavior of the proposed structures considering perfectly matched layers (PML) around the simulation region. Photonic band gap (PBG) and projected band diagram are obtained using plane wave expansion (PWE) method. It is shown that both the structures function with optical inputs of same wavelength and intensity. The proposed NOR and NAND gates are having low operating powers and good contrast ratio. Being universal gates, NOR and NAND allows for Boolean completeness.

Implementation of bypass waveguides is a unique feature of the structures proposed in this paper. When the output is LOW, most of the optical power channelizes out of the structure through bypass waveguides, which otherwise, would go into the input ports affecting the input devices or would remain trapped inside the structure resulting in heating. This issue is not touched in the previous literature and in our opinion, being addressed for the first time.

## 1. Introduction

Theoretical modeling and fabrication of all optical devices based on photonic crystal (PhC) is of recent interest due to their (PhC's) unique properties [1]. PhC based optical devices have several advantages over conventional waveguide devices such as compactness and power consumption [2]. PhCs are periodic structures with a period of the order of optical wavelength [3,4]. Photonic bandgap (PBG) originates in PhCs due to periodic distribution of dielectric permittivity. It is the range of frequencies in which the electromagnetic waves propagation is forbidden regardless the wave vector and polarization state [5]. With introducing line and point defect, photonic waveguide and cavity are created in a PhC [6]. Numerous optical devices based on PhC are existing in the literature, such as the optical filter [7], de-multiplexer [8], logic gate [9,10], junction [11], decoder [12], S-R latch [13], and converter [14] etc.

Among various optical devices, optical logic gates play important role

in optical communication and computing system [15]. Various proposals for optical logic gates using linear and nonlinear PhCs are existing in the literature [16,17]. In linear PhCs, all optical logic is obtained using interference effect and thus, require small power [18]. However, desired interference effect requires precise control on phases of the optical inputs, which, in a complex circuitry is challenging and a major limitation in terms of practicability of such devices. Optical logic gates based on nonlinear PhCs, work on optical Kerr or Kerr like effects [19–23]. Such devices require higher operating powers for switching but the control on phase is not an issue and hence, are considered as potential candidates for future optical computing and communication systems. The quest is of their miniaturization and lowering of operating powers. Previously, different structures for obtaining optical logic gate based on Kerr effect have been reported. Man Mohan et al. [24] reported all optical NOT and AND gates using counter propagation beam in nonlinear Mach-Zehnder interferometer made of PhC waveguide which require operating power

\* Corresponding author.

E-mail addresses: [smedhekarbit@gmail.com](mailto:smedhekarbit@gmail.com), [sarang.medhekar@cuja.ac.in](mailto:sarang.medhekar@cuja.ac.in) (S. Medhekar).<https://doi.org/10.1016/j.optlastec.2019.105910>

Received 5 May 2019; Received in revised form 26 August 2019; Accepted 16 October 2019

0030-3992/ © 2019 Elsevier Ltd. All rights reserved.



# Synthesis of pH-moderated cobalt molybdate with bifunctional (photo catalyst and graphene-based supercapacitor) application

Biraj K. Satpathy<sup>1,2</sup> · Rasmita Barik<sup>1</sup> · Arun K. Padhy<sup>3</sup> · Mamata Mohapatra<sup>1</sup>

Received: 14 June 2019 / Revised: 24 October 2019 / Accepted: 4 November 2019 / Published online: 22 November 2019  
© Springer-Verlag GmbH Germany, part of Springer Nature 2019

## Abstract

The present manuscript deals with one photosynthesis of cobalt molybdate for multifunctional application as supercapacitor and photo catalyst. The cobalt molybdate is synthesized by various concentration of urea as precursor. Nanostructured transition metal has been synthesized by hydrothermal method from spent catalyst leach liquor. Different physico-chemical characterization techniques are obtained to illustrate the nanomaterials followed by X-ray diffraction, field-emission scanning electron microscopy, Fourier-transform infrared spectroscopy, Raman spectroscopy, and nitrogen adsorption–desorption isotherm for surface area analysis. Nanorod cobalt molybdate is proved as efficient photocatalyst for Rhodamine B dye under visible light irradiation, which possess a high degradation rate of 98% after 15 min. Electrochemically active cobalt molybdate shows high specific capacitance value of maximum specific capacitance of 175.34 F g<sup>-1</sup> at three-electrode system and 74.2 F g<sup>-1</sup> at two-electrode system. It also revealed excellent rate capability and superior cycling stability with long cycle life (92.7% retention in specific capacitance after 5000 cycles) along with high energy and power densities.

**Keywords** Cobalt Molybdate · Photo catalyst · Supercapacitor · Specific capacitance

---

**Electronic supplementary material** The online version of this article (<https://doi.org/10.1007/s11581-019-03339-0>) contains supplementary material, which is available to authorized users.

---

✉ Mamata Mohapatra  
mamata@immt.res.in

Biraj K. Satpathy  
rocky.biraj@gmail.com

Rasmita Barik  
rasmitabarikimmt@gmail.com

Arun K. Padhy  
arun.padhy@cuja.ac.in

<sup>1</sup> Department of Hydro & Electrometallurgy, CSIR-Institute of Minerals and Materials Technology, Bhubaneswar 751013, India

<sup>2</sup> School of Nanoscience and Technology, Indian Institute of Technology, Kharagpur, India

<sup>3</sup> Centre for Applied Chemistry, Central University of Jharkhand, Ranchi 835205, India

## Introduction

Over the years, transition metal molybdates (TMMs) due to their unique physical and electrochemical properties have gained an immense research interest as a potential candidate to meet the worldwide solution of energy storage and environmental pollution simultaneously [25]. Owing to the striking features of non-toxicity and high stability, molybdenum compounds have attracted a wide range of researchers for their versatility of their catalytic properties too making them a promising material for various applications including supercapacitors, materials, sensors, photocatalysis, and magnetism ([45, 15, 42]). A new insight into developing novel bifunctional materials over the past decades has consistently increased due to the vital requirements in certain specific areas. Still there are hardly any reports attributing to these sorts of bifunctional materials which have been rarely ever discovered both as an efficient photocatalyst and supercapacitor owing to the potential semiconductor materials with quality performance. So, the development of a novel



## Research Article

# Impact of 2014 Kashmir flood on land use/land cover transformation in Dal lake and its surroundings, Kashmir valley



Tauseef Ahmad<sup>1</sup>  · Arvind Chandra Pandey<sup>1</sup>  · Amit Kumar<sup>1</sup> 

Received: 17 December 2019 / Accepted: 5 March 2020 / Published online: 17 March 2020  
© Springer Nature Switzerland AG 2020

## Abstract

Kashmir Valley has witnessed a catastrophic flood in 2014, which led thousands of people homeless and devastated the agricultural lands. In the present study, the impact of 2014 flood occurred during the month of September was analysed in the vicinity of Dal lake using the pre- and post-flood periods satellite observations. The study exhibited an inundation of 42.50 km<sup>2</sup> area (52.47% of total area) during September 2014 flood period, which is primarily topographical low-lying area (i.e. below 1530 m). The land use/land cover (LULC) analysis during pre- and post-flood periods exhibited significant impact over the built-up land with 20.4% decrease in the built-up (from 25.44 to 20.25 km<sup>2</sup>), which was mostly evident in the western, southern and eastern parts of Dal lake. It has also severely affected the road network with inundation of 220.84 kms (55.62% of total road network). The road network in the lower elevation (< 1530 m) not only disrupted but also acted as a carrier for the flood water dispersal in the region. The long-term impact and recovery of flood inundation were assessed using spatio-temporal built-up growth during 2014, 2015 and 2018 within the flooded zone through geospatial overlay analysis. The flood (September 2014) affected a total 10.42 km<sup>2</sup> of built-up, wherein the built-up was reduced to 7.50 km<sup>2</sup>, due to the low-lying topography and nearest proximity to flow path of Jhelum river. Later, the built-up was increased to 9.60 km<sup>2</sup> within the flooded zone during 2018 primarily in the southern parts, representing the long-term recovery after the flood aftermath. Although the impact of flood (2014) was evident in both the flooded and non-flooded zones, the built-up growth was reduced significantly in the flooded zone (– 25.18% change) as compared to non-flooded zones (– 17.32% change). Also, the long-term recovery was comparatively higher in the non-flooded zone (31.84% growth) as compared to the flooded zone (28.03% growth). The study necessitates towards implication of effective urban planning method primarily along the major lakes in order to reduce the increasing impact of catastrophic flood.

**Keywords** Dal lake · Flood inundation · LULC · Built-up growth · Recovery

## 1 Introduction

The lakes in the world are facing the tremendous environmental problems due to combination of rapid urbanization and natural hazards [25, 55, 77]. The lakes contribute an important role in ecological balance as well as serve as a primary source for local economy, cultural heritage and socio-economic values. The major lakes of the world are affected by eutrophication affecting the lake ecosystem

[60]. There are several lakes (Dal, Anchar, Khanpur, Manasbal, Naranbagh, Pashkuri, Tilwan, Trigam, Waskur and Wular) located in Kashmir valley (Western Himalayas) at high altitude (1510–1600 m) [84]. The structural and functional process of these aquatic ecosystem has been the major attraction for the researchers [32, 33, 35, 75, 85]. Dal lake is multi-basined-shaped lake located in Srinagar city, Kashmir valley. It is one of the major sources of irrigation and economy including floating gardens for fresh

✉ Arvind Chandra Pandey, arvindchandrap@yahoo.com; Tauseef Ahmad, tauseef@live.in; tauseef@cuja.ac.in; Amit Kumar, amit.kumar@cuja.ac.in; amit.iirs@gmail.com | <sup>1</sup>Department of Geoinformatics, Central University of Jharkhand, Ranchi, India.







# Improved performance of cadmium sulfide-sensitized solar cells by interface engineering

Arup Mahapatra<sup>1,2</sup> · Prashant Kumar<sup>1</sup> · Basudev Pradhan<sup>1,2</sup>

Received: 14 November 2019 / Accepted: 27 February 2020 / Published online: 5 March 2020  
© Springer Science+Business Media, LLC, part of Springer Nature 2020

## Abstract

The solar cells have been fabricated using cadmium sulfide (CdS) as a sensitizer by the chemical bath deposition (CBD) technique on the mesoporous TiO<sub>2</sub> substrate. The different device configurations with titanium(IV) tetrachloride (TiCl<sub>4</sub>) treatment, TiO<sub>2</sub> compact layer, with mesoporous TiO<sub>2</sub> along with CdS sensitizer layer, were investigated. The CdS film morphology, optical properties, and crystalline structure of CdS film were studied. It was observed that TiCl<sub>4</sub> treatment helped in reducing the recombination at the interfaces between conducting glass and TiO<sub>2</sub> compact layer enabling higher carrier transport. Power conversion efficiency of 1.44% is achieved using a TiCl<sub>4</sub> treatment on TiO<sub>2</sub> compact layer with TiO<sub>2</sub> mesoporous/CdS device under illumination of 100 mW/cm<sup>2</sup>.

## 1 Introduction

A new era of photovoltaics research began with the advent of dye sensitization solar cells which have received significant attention due to their high efficiency and low production cost in 1991 [1]. These photo-electro-chemical devices use separate materials for light absorption and transport of carriers, unlike the traditional silicon-based solar cells. The carrier transport in dye-sensitized solar cells (DSSCs) is generally done by wide bandgap semiconductors such as TiO<sub>2</sub> and ZnO [2–5], and the absorption of light is done by dye or other sensitizers which absorbs the photon and goes into the excited state. In the order of femtoseconds, interfacial electron transfer occurs to the wide gap semiconductor. The ruthenium-based dyes are most common and very much successful as sensitizers in DSSCs [6, 7]; however, many narrow bandgap semiconductor quantum dots (QDs) such as CdS, CdTe, CdSe, Ag<sub>2</sub>S, and Bi<sub>2</sub>S<sub>3</sub> are the promising alternative sensitizers over the traditional dyes (as ruthenium dyes) in DSSCs due to their strong photoresponse in

the visible region, higher extinction coefficient, bandgap tunability, and solution processability [8–12]. However, the use of CdS as thin film absorber has been less studied. Among these direct bandgap, CdS can be an excellent candidate for many optoelectronics and photonics application. CdS nanocrystal (NC) has unique photo-physical, optical, and structural properties compared to bulk CdS and also bandgap can be tuned by changing the size of the particle. In DSSCs, it is important that the sensitizer molecule should be in close proximity with the photoanode to avoid recombination, so a mesoporous layer is always deposited and the sensitizer molecules need to be absorbed throughout the photoanode for the devices. Therefore, the deposition process also plays a key role in the processing of the devices. Lee and his group fabricated devices with vertically aligned ZnO along with CdS chemical bath deposition to achieve an efficiency of 0.54% [13]. Hossian et al. fabricated CdS-sensitized solar cell by ammonia-free chemical bath technique and achieved maximum 1.13% efficiency [14]. In another work, Lin et al. have reported 1.35% efficiency using combination of two techniques: self-assembled monolayer and chemical bath deposition for increasing the coverage ratio of CdS onto a mesoporous TiO<sub>2</sub> film [8]. Overall DSSC performance depends on both sensitizer and mesoporous TiO<sub>2</sub> layer but it has been observed that the weak interfacial bonding between TiO<sub>2</sub> and FTO limits the electron transfer between them which reduces the overall power conversion efficiency [15]. Kim et al. used sputtered TiO<sub>2</sub> as compact layer in CdS QD-sensitized solar cells to reduce the back

✉ Basudev Pradhan  
basudev.pradhan@cuja.ac.in

<sup>1</sup> New Generation Photovoltaics Research Laboratory, Department of Energy Engineering, Central University of Jharkhand, Brambe, Ranchi, Jharkhand 835205, India

<sup>2</sup> Centre of Excellence (CoE) in Green and Efficient Energy Technology (GEET), Central University of Jharkhand, Brambe, Ranchi, Jharkhand 835205, India





# Entrapment of enzyme in the presence of proline: effective approach to enhance activity and stability of horseradish peroxidase

Rajani Singh<sup>1</sup> · Ambuj Bhushan Jha<sup>2</sup> · Amarendra Narayan Misra<sup>1,3</sup> · Pallavi Sharma<sup>1</sup>

Received: 27 January 2019 / Accepted: 15 February 2020 / Published online: 4 March 2020  
© King Abdulaziz City for Science and Technology 2020

## Abstract

In this report, activity and stability of horseradish peroxidase (HRP) entrapped in polyacrylamide gel in the presence of proline (HEP) are compared with that of enzyme entrapped in absence of proline (HE). Within polyacrylamide (8%) beads, 80% entrapment yield for peroxidase was observed in the presence as well as absence of proline. The HEP (1.5 M proline) showed 170% higher activity compared to HE. HEP also showed significant increase in  $K_M$ ,  $V_{max}$  and  $K_{cat}$ . At 8th cycle of use, HEP retained 40% of its activity, whereas HE retained only 10% of activity. In addition, in comparison with HE, HEP showed increased storage stability and thermo-stability. HEP showed higher activity compared to HE over an extensive range of pH (4–8), temperature (30–80 °C) and inhibitors such as  $\text{NaN}_3$ ,  $\text{Cd}^{2+}$  and  $\text{Pb}^{2+}$ . Our results suggest that peroxidase entrapment in polyacrylamide gel in the presence of proline can be a useful approach for increasing activity and stability of horseradish peroxidase.

**Keywords** Immobilization · Peroxidase · Polyacrylamide gel · Proline

## Abbreviations

HE	Horseradish peroxidase enzyme entrapped in the absence of proline
HRP	Horseradish peroxidase enzyme
HEP	Horseradish peroxidase enzyme entrapped in polyacrylamide gel in the presence of proline
$K_{cat}$	Turnover number, a constant which depicts the rate of turnover of an enzyme–substrate complex into product
$K_M$	Michaelis constant, a constant which depicts substrate concentration that allows the enzyme to attain half $V_{max}$
$V_{max}$	Maximum rate of reaction, reaction rate when the enzyme is saturated with substrate

## Introduction

Peroxidases belong to oxido-reductase class of enzyme and catalyze the oxidation of various aromatic compounds. They have broad applications in many areas including chemical synthesis, diagnostic, medicine, pulp and paper industries, food processing industry and remediation of wastewaters (Agostini et al. 2002; Moreira et al. 2007; Bansal and Kanwar 2013; Chiong et al. 2014; Agarwal et al. 2018). Aromatic compounds including phenols, cresols, and chlorinated phenols are the major pollutants present in wastewaters of various industries including petroleum refining, coal conversion and pulp and paper industries (Mojiri et al. 2019). Removal of these pollutants from wastewaters is of prime importance due to their high toxic effect in living organisms. Over past decades, extensive research has been carried out for removal of contaminants from water. Application of enzymes has been found to be a potential method for successful removal of contaminants over conventional methods. Advantages of using enzymes for wastewater treatment are their ability to operate over a broad concentration range of substrate and requirement of low retention times (Karam and Nicell 1997; Unuofin et al. 2019). Peroxidase obtained from horseradish (HRP) is used for the laboratory-scale treatment of aqueous aromatic contaminants

✉ Pallavi Sharma  
pallavi.sharma@cuj.ac.in

<sup>1</sup> Department of Life Sciences, Central University of Jharkhand, Brambe, Ranchi 835205, India

<sup>2</sup> Crop Development Centre, Department of Plant Sciences, University of Saskatchewan, Saskatoon, SK S7N5A8, Canada

<sup>3</sup> Khallikote University, Berhampur, Odisha 761008, India

# Study of BDNF protein expression in type 2 diabetic model of zebrafish (*Danio rerio*)

Ranjan Shovit<sup>1,2\*</sup> and Sharma Praveen Kumar<sup>2</sup>

<sup>1</sup> Department of Zoology, Miranda House, University of Delhi, Delhi-110007, INDIA

<sup>2</sup> Department of Life Sciences, Central University of Jharkhand, Brambe, Ranchi-835205, Jharkhand, INDIA

\*shovitranjan@gmail.com, shovit.ranjan@mirandahouse.ac.in

## Abstract

Type 2 Diabetes (T2D), which causes hyperglycemia, also affects the central nervous system, leading to cognitive dysfunctions. Nowadays, zebrafish (*Danio rerio*) has emerged as a promising model organism for studying the neurobehavioral disorders like stress, anxiety and depression. The aim of this study was to determine the BDNF (Brain Derived Neurotrophic Factor) activity and protein expression levels in high sucrose induced hyperglycemic zebrafish. Hyperglycemia was induced in adult zebrafish by immersion in 83.25 mM sucrose solution for 14 days after performing the study for survival in sucrose solutions. The animals were divided into 2 groups in replicates: control and sucrose-treated hyperglycemic groups.

Afterwards, the BDNF activity and protein expression were determined from the samples isolated from whole brain of both the groups. Results showed that high-sucrose induced hyperglycemic group showed significantly reduced BDNF protein expression level as compared to control group. Overall, our results confirm that impaired glucose metabolism in the zebrafishes resulted in the decreased BDNF levels. This decreased BDNF level observed in T2D (other than cognitive disorders) can be possibly helpful for explaining the missing link in interplay of these diseases in future.

**Keywords:** Type 2 Diabetes, Hyperglycemia, Brain, BDNF, Zebrafish.

## Introduction

Type 2 Diabetes (T2D), a disease state recognized by impaired insulin sensitivity and hyperglycemia, is one of the world's leading causes of mortality and morbidity<sup>21,22</sup>. The increase in blood glucose levels i.e. hyperglycemia is also found to be associated with impaired cognitive abilities in humans<sup>3,24</sup>. Earlier studies have already shown the higher risk of any dementia (mostly Alzheimer's disease and vascular dementia) and major depression in individuals with T2D than normal ones<sup>2,6</sup>.

The use of zebrafish as a model organism to study vertebrate development has been in trend from long times in the past. However, from last few years, a drastic increase in the use of this model organism to study the wide range of human

dysfunctions has been observed<sup>1,10,15,16</sup>. It is because since many cellular processes have remained highly conserved throughout the vertebrate evolution<sup>4,5,9,15,25,26</sup>. The zebrafish is endowed with many advantages over previous other existing model organisms like its small size, high fecundity, short generation time, rapid development, less maintenance cost and production of transparent embryos through early adulthood (thus, making the study of developmental processes quite easier) and array of tools for gene manipulation. Furthermore, it also has a very similar genome structure to humans, thus helping in the studies of any human disorders easier.

BDNF (Brain Derived Neurotrophic Factor), a member of neurotrophic factor family plays important role in regulation of survival, growth and maintenance of neurons, thus also helping in certain cognitive abilities of organisms to function correctly<sup>11,27</sup>. The decreased BDNF levels are already shown in Alzheimer's disease, major depression and other Central Nervous System (CNS) disorders<sup>7,11,14</sup>. BDNF has also been found to be associated with the lowering of blood glucose levels in obese diabetic mice, thus showing its role in insulin sensitivity<sup>18,19,26</sup>. Moreover, BDNF also activates several signaling pathways, similar to as activated by insulin<sup>8</sup>.

The link between T2D and CNS disorders like stress, anxiety, depression and cognitive dysfunctions has not yet been understood clearly. So, in the present study, we have tried to check the BDNF activity and protein expression levels in hyperglycemic zebrafish to test the possibility that whether BDNF plays a role in glucose metabolism or not.

## Material and Methods

**Animals and Housing conditions:** The wild type adult zebrafish (*Danio rerio*) strain was purchased at their age of 6-8 months old from Fish Research Centre, Ranchi. The fishes were acclimatized for at least 1 week to the constant laboratory conditions in the stock water tanks before all experiments were conducted. All fishes were housed in the groups of 8-10 fishes per 10-litre tank. The fishes were maintained in filtered facility (biologically active) water with both room and water temperatures maintained at approximately 28°C.

Illumination was provided by ceiling and wall-mounted tube lights turned on at 9:00 hr. and off at 21:00 hr. (i.e. 12-12 hr light-dark cycle). Fish were fed twice daily Tetramin flakes food (3.5 mg/fish/day; Optimum company, Thailand). All fishes used in these experiments were experimentally naive and randomly chosen of both sexes from different clutches.



# *Hippophae rhamnoides* L. rhizobacteria exhibit diversified cellulase and pectinase activities

Pooja Bhadrecha<sup>1</sup> · Madhu Bala<sup>2,3</sup> · Yogender Pal Khalsa<sup>4</sup> · Anfal Arshi<sup>3</sup> · Joginder Singh<sup>5</sup> · Manoj Kumar<sup>6</sup>

Received: 19 August 2019/Revised: 2 January 2020/Accepted: 17 February 2020/Published online: 19 March 2020  
© Prof. H.S. Srivastava Foundation for Science and Society 2020

**Abstract** *Hippophae rhamnoides* L. provides an enormous range of medicinal and nutritional benefits. The significant abilities of this plant to survive in Himalayan high altitudes enticed our study to investigate its rhizosphere. Seventeen rhizobacterial strains were isolated from the rhizospheric soil and plant root nodules, belonging to genus *Frankia*, *Azorhizobium*, *Bacillus*, *Paenibacillus*, *Brevibacillus* and *Pseudomonas*, as identified by 16SrRNA sequencing. This varying bacterial population was further examined for the presence of root degrading enzymes pectinase and cellulase, which enable them to intrude the plant roots. Based on the growth and substrate utilization by these rhizobacteria on pectinase screening agar medium and Mandels and Reese agar medium, all the seventeen strains were

identified as pectinase and cellulase producing rhizobacteria. The quantitative analysis by DNS method demonstrated varying enzyme activities, spot-lighting the physiological variation in the microbiome. The divergence in the enzyme activities shown by all the strains was analysed statistically, using the software ASSISTAT.

**Keywords** *Hippophae rhamnoides* L. · Pectinase · Cellulase · Enzyme activity

## Abbreviations

PSAM	Pectinase screening agar medium
MRAM	Mandels and Reese agar medium
PGPR	Plant growth promoting rhizobacteria
IAA	Indole acetic acid
CLEA	Cross-linked enzyme aggregates
DNS	Di-nitrosalicylic acid

**Electronic supplementary material** The online version of this article (<https://doi.org/10.1007/s12298-020-00778-2>) contains supplementary material, which is available to authorized users.

✉ Joginder Singh  
joginder.15005@lpu.co.in

✉ Manoj Kumar  
manoj@cuja.ac.in; head.cls@cuja.ac.in

- <sup>1</sup> Department of Biotechnology, Mangalmai Group of Institutions, Greater Noida, UP, India
- <sup>2</sup> Institute of Nuclear Medicine and Allied Sciences, Defence Research and Development Organisation, New Delhi, India
- <sup>3</sup> Defence Institute of Bio-Energy Research (DIBER), DRDO, Haldwani, Uttarakhand, India
- <sup>4</sup> Department of Microbiology, South Campus, Delhi University, New Delhi, India
- <sup>5</sup> Department of Biotechnology, Lovely Professional University, Phagwara, Punjab, India
- <sup>6</sup> Life Science Department, Central University of Jharkhand, Brambe Campus, Ranchi, Jharkhand 834205, India

## Introduction

Microorganisms play vital roles in maintaining soil fertility and plant health. Plant growth promoting rhizobacteria (PGPR) benefit the host plants in different ways like indole acetic acid (IAA) production, phosphate solubilisation, HCN production, siderophore formation etc. (Santoyo et al. 2016). Several enzyme-producing bacteria can destroy oospores of phytopathogenic fungi and affect the spore germination and germ-tube elongation of phytopathogenic fungi. Therefore, they can also act as biofertilizers and increase the resistance to biotic and abiotic stress (Sharma et al. 2007). These rhizobacteria aid in plant growth and are often classified as extracellular-(ePGPR) and intracellular-(iPGPR). ePGPR reside in the rhizosphere, rhizoplane or in the spaces between the cells of root cortex, e.g.



# Synergetic use of in situ and hyperspectral data for mapping species diversity and above ground biomass in Shoolpaneshwar Wildlife Sanctuary, Gujarat

Ramandeep Kaur M. Malhi<sup>1</sup> · Akash Anand<sup>2</sup> · Ashwini N. Mudaliar<sup>3</sup> · Prem C. Pandey<sup>4</sup> · Prashant K. Srivastava<sup>1</sup> · G. Sandhya Kiran<sup>3</sup>

Received: 28 December 2018 / Revised: 13 September 2019 / Accepted: 3 November 2019  
© International Society for Tropical Ecology 2020

## Abstract

Biodiversity loss in tropical forests is rapidly increasing, which directly influence the biomass and productivity of an ecosystem. In situ methods for species diversity assessment and biomass in synergy with hyperspectral data can adeptly serve this purpose and hence adopted in this study. Quadrat sampling was carried out in Shoolpaneshwar Wildlife Sanctuary (SWS), Gujarat, which was used to compute Shannon–Weiner Diversity Index ( $H'$ ). Above ground biomass (AGB) was calculated measuring the Height and Diameter at Breast Height (DBH) of different trees in the sampling plots. Four spectral indices, namely Normalized Difference Vegetation Index (NDVI), Enhanced Vegetation Index (EVI), Photochemical Reflectance Index (PRI), and Structure Insensitive Pigment Index (SIPI) were derived from the EO-1 Hyperion Data. Spearman and Pearson's correlation analysis was performed to examine the relationship between  $H'$ , AGB and spectral indices. The best fit model was developed by establishing a relationship between  $H'$  and AGB. Fifteen models were developed by performing multiple linear regression analysis using all possible combinations of spectral indices and  $H'$  and their validation was performed by relating observed  $H'$  with model predicted  $H'$ . Pearson's correlation relation showed that SIPI has the best relationship with the  $H'$ . Model 15 with a combination of NDVI, PRI and SIPI was determined as the best model for retrieving  $H'$  based on its statistics performance and hence was used for generating species diversity map of the study area. Power model showed the best relationship between AGB and  $H'$ , which was used for the development of AGB map.

**Keywords** Hyperion · Quadrat sampling · Spearman and pearson's correlation · Vegetation indices

## Introduction

Biodiversity loss impacts the biomass and primary productivity of ecosystems (Hector et al. 1999; Tilman et al. 2001, 2012). Several ecosystem studies have investigated the relationships between above ground biomass (AGB) and species diversity (Grime 1979; Huston 1997; Aarssen 2001; Grime 2002; Loreau et al. 2002; Li et al. 2018). Such studies highlighted the role of species diversity in monitoring the primary productivity and functioning of an ecosystem (Guo 2007). Declining biodiversity in the forests is occurring at an alarming rate, and thus, conservation and monitoring efforts are very imperative (Mulatu et al. 2017).

Traditional means of biodiversity assessment are based on in situ survey and measurement that determine diversity at different levels such as alpha (at the local level), beta (between dissimilar sites) and a combination of these two measures (Whittaker 1972; Foody and Cutler

✉ Prashant K. Srivastava  
prashant.just@gmail.com

<sup>1</sup> Institute of Environment and Sustainable Development, Banaras Hindu University, Varanasi 221005, Uttar Pradesh, India

<sup>2</sup> Centre for Land Resource Management, Central University of Jharkhand, Ranchi 835205, Jharkhand, India

<sup>3</sup> Department of Botany, Faculty of Science, The Maharaja Sayajirao University of Baroda, Vadodara 390002, Gujarat, India

<sup>4</sup> Center for Environmental Sciences and Engineering, School of Natural Sciences, Shiv Nadar University, Dadri 201314, India





# Multiple indices based drought analysis by using long term climatic variables over a part of Koel river basin, India

Stuti Chaudhary<sup>1</sup> · Arvind Chandra Pandey<sup>1</sup>

Received: 4 April 2019/Revised: 7 August 2019/Accepted: 9 August 2019  
© Korean Spatial Information Society 2019

**Abstract** The present study demonstrates changes in vegetation pattern and climatic variability in past years in the parts of Koel basin in Jharkhand state of India by considering the spatial climatic variability, NDVI anomaly and satellite based drought indices viz Vegetation Condition Index (VCI), Temperature Condition Index (TCI) and Vegetation Health Index (VHI). Least square statistical method has been used for assessment of long term climatic fluctuation of major four climatic parameters viz maximum temperature of summer season, minimum temperature of winter season, rainfall of monsoon season, and solar radiation of Rabi and kharif season. Analysis of climate extremes has been done for 26 locations in the study area and then interpolated spatially in Geographical Information System platform. Long term NDVI anomaly shows adverse effect of climate extreme in past 20 years in the study area. The climatic variability exhibits that average maximum temperature during 1979–2017 fluctuates with an increase of 0.50–0.81 °C contrary to a decrease of 0.32–0.15 °C in various parts of study area. Similarly rainfall fluctuates with a decrease of 26–90 mm contrary to an increase of 19–230 mm. Drought prone zones as delineated from spatial overlaying map of VCI, TCI and VHI indicated value from 23 to 55. Major part of the study area severely

affected by drought facing water scarcity and mediocre vegetation condition. These areas need proper planning and soil moisture management to overcome the recurrent drought conditions perceived in upcoming years.

**Keywords** Climatic parameters · NDVI anomaly · VCI · TCI · VHI · Agricultural drought · Koel river basin

## 1 Introduction

Global warming and climate change are the major issue in the current world face today. Variations in the climate change such as transformation in air temperature, relative humidity, rainfall and solar radiation are killed millions of living habitant throughout the world [1, 2]. Disaster like recurrent drought and flood are result of climatic change [3]. The studies reports that 0.1° C per decade increase in minimum and maximum temperature since 1950 which resulted in changes in agricultural pattern, reduction of water resources and rapid melting of glaciers [4–6]. The change and fluctuation of rainfall pattern in monsoon season and extended interval of monsoon failures hit drought condition in India and southeastern Asia in last few years [6]. The countrywide analysis of climatic parameter shows mean maximum temperature of India has ascended by 0.6 °C, and the mean minimum temperature has declined by 0.1 °C [7]. Along the Ganga basin of India decreasing trend of rainfall and increasing trend of maximum temperature has been analyzed by Kothyari and Singh [8]. Along plateau terrain area in Palamu and Garhwa district of Jharkhand facing severe water scarcity and recurrent drought condition [9]. Thus, detailed monitoring and assessment of climate change in part of study area requires to be evaluated for analyzing the impact on the

---

**Electronic supplementary material** The online version of this article (<https://doi.org/10.1007/s41324-019-00287-9>) contains supplementary material, which is available to authorized users.

---

✉ Arvind Chandra Pandey  
arvindchandrap@yahoo.com

Stuti Chaudhary  
stuti@cuja.ac.in

<sup>1</sup> Department of Geoinformatics, School of Natural Resource Management, Central University of Jharkhand, Brambe, India

## Super-Halley method under majorant conditions in Banach spaces

SHWET NISHA AND P. K. PARIDA  
*Department of Applied Mathematics,*  
*Central University of Jharkhand,*  
*Ranchi-835205, India.*

*shwetnisha1988@gmail.com, pkparida@cuja.ac.in*

### ABSTRACT

In this paper, we have studied local convergence of Super-Halley method in Banach spaces under the assumption of second order majorant conditions. This approach allows us to obtain generalization of earlier convergence analysis under majorizing sequences. Two important special cases of the convergence analysis based on the premises of Kantorovich and Smale type conditions have also been concluded. To show efficacy of our approach we have given three numerical examples.

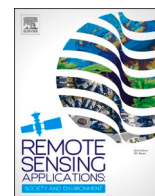
### RESUMEN

En este artículo, hemos estudiado la convergencia local del método Super-Halley en espacios de Banach, asumiendo condiciones mayorantes de segundo orden. Este punto de vista nos permite obtener generalizaciones de análisis de convergencia bajo sucesiones mayorantes obtenidos anteriormente. También se han concluido dos casos especiales del análisis de convergencia basados en las premisas de condiciones tipo Kantorovich y Smale. Para mostrar la eficacia de nuestro enfoque, damos tres ejemplos numéricos.

**Keywords and Phrases:** Nonlinear equations; Super-Halley method; Majorant conditions; Local Convergence; Semilocal Convergence; Smale-type conditions; Kantorovich-type conditions.

**2010 AMS Mathematics Subject Classification:** 65D10,65G99, 65K10,47H17,49M15, 47H99.





## Landsat-8 and Sentinel-2 based Forest fire burn area mapping using machine learning algorithms on GEE cloud platform over Uttarakhand, Western Himalaya

Somnath Bar<sup>\*</sup>, PhD Bikash Ranjan Parida, Assistant Professor, PhD Arvind Chandra Pandey, Professor

Department of Geoinformatics, School of Natural Resource Management, Central University of Jharkhand, Ranchi, 835205, India

### ARTICLE INFO

#### Keywords:

Forest fire  
Burn area  
Weka clustering  
CART  
RF  
SVM  
GEE

### ABSTRACT

The accurate quantitative and qualitative estimation of burn-area are crucial to analyze the impact of fire on forest. The medium resolution optical-satellite imagery of Landsat-8 and Sentinel-2 are employed covering the period 2016 to 2019 for forest fire patches identification on Google Earth Engine (GEE). The most indispensable season of Forest Fire (FF) is pre-monsoon in Uttarakhand, western Himalaya, India. Bi-temporal (pre and post fire) reflectance contrast of burn-sensitive spectral bands was used to compute differential spectral indices, namely, Normalized Burn Ratio (dNBR), Normalized Difference Vegetation Index (dNDVI), Normalized Difference Water Index (dNDWI), and Short-Wave Infrared (dSWIR). The differential spectral-indices composite is further used as an input to unsupervised Weka clustering algorithms for capturing the shape and pattern of fire patches. Sample training-data of burn and unburn classes were collected with reference to thermal and optical spectral principle. Classification Regression Tree (CART), Random Forest (RF), and Support Vector Machine (SVM) algorithms have been employed to identify FF. The key findings revealed that CART and RF algorithms displayed similar forest fire patches with an overall accuracy of 97–100%. The classification accuracy is slightly lower in SVM and its underestimating forest fire patches detections. Landsat-8 OLI derived burn area was fitted better with fire product of Climate Change Initiative (Fire-CCI of ESA) and MCD64A1 of MODIS burn area product with R-square of 0.71–0.93 and 0.62–0.91, respectively which attributed to better spectral bands of Landsat-8 than the Sentinel-2. However, Sentinel-2 bands have the potential to capture fire patches during post-fire events. This study has demonstrated the potential utilities of combined effort of unsupervised and supervised algorithms on Landsat-8 and Sentinel-2 on GEE to identify fire patches.

### 1. Introduction

Forest fire (FF) is one of significant increasing anthropogenic and natural disturbing phenomenon over the globe including the South East Asian (SEA) countries, which has substantial impact upon ecosystem, biodiversity as well as human health (Langmann et al., 2009). India has shown a higher increasing trend of forest fire in comparison to other SEA countries (Vadrevu et al., 2019). FF has emitted a large mixtures of trace gases and particulate matter (e. g. CO<sub>2</sub>, CO, CH<sub>4</sub>, NO<sub>x</sub>, SO<sub>x</sub>, VOC, C<sub>2</sub>H<sub>6</sub>, C<sub>2</sub>H<sub>4</sub>, C<sub>3</sub>H<sub>8</sub>, C<sub>3</sub>H<sub>6</sub>, PM<sub>2.5</sub>, PM<sub>10</sub>, etc.), which has a widespread impact upon chemical composition of atmosphere (Crutzen et al., 1979), atmospheric radiative forcing (Ramanathan et al., 2005), albedo by modifying the land cover type (Bowman et al., 2009), local and regional

weather, and climate (Langmann et al., 2009). Worldwide, biomass burning (BB) is accountable for 2 Petagram of carbon emission, which accounted for 20% of global carbon emissions (Giglio et al., 2013; Van Der Werf et al., 2010). So, quantitative and qualitative valuation of burn area is essential for its primary and secondary environmental and anthropogenic impact assessment in varying spatial and temporal resolutions (Lentile et al., 2006; Morgan et al., 2014). Specifically, FFs could be possible reasons of biodiversity losses, disruption of soil microbial process, and alteration of biogeochemical cycles (Bruun et al., 2009; Ojima et al., 1994), and transformation of landscape pattern (Baker and Bunyavejchewin, 2009).

In principle, FFs can be identified based on the spectral reflectance properties of healthy vegetation and burnt scar vegetation. Thermal

<sup>\*</sup> Corresponding author.

E-mail addresses: [bar.somnath@yahoo.in](mailto:bar.somnath@yahoo.in) (S. Bar), [bikashrp@gmail.com](mailto:bikashrp@gmail.com) (B.R. Parida).

<https://doi.org/10.1016/j.rsase.2020.100324>

Received 14 January 2020; Received in revised form 29 March 2020; Accepted 25 April 2020

Available online 1 May 2020

2352-9385/© 2020 Elsevier B.V. All rights reserved.



## Wild edible plants of Jharkhand and their utilitarian perspectives

R Kumar & P Saikia\*<sup>†</sup>

Department of Environmental Sciences, Central University of Jharkhand, Brambe, Ranchi 835 205, Jharkhand, India

E-mail: <sup>†</sup>purabi.saikia83@gmail.com

Received 24 April 2019; revised 19 December 2019

The wild edible plants (WEPs) form an important constituent of traditional diets of the tribal community of Jharkhand. Most of the rural populations residing in different parts of Jharkhand depend on plants and their parts to fulfil their daily needs and have developed unique knowledge about their utilization. The present study has been conducted to document the indigenous knowledge related to the diversity and uses of wild edible weeds in day to day life of tribal in Jharkhand. A total of 77 different herbs, shrubs, and small trees have been recorded belonging to 38 families of which 73 are edible either as a vegetable or as medicine or in both forms directly or after proper processing. The common wild edible herbs frequently distributed in the study area are *Hemidesmus indicus* R. Br. (51 quadrats out of 134) and *Cynodon dactylon* (L.) Pers. (47 quadrats out of 134). Similarly, the most frequent edible shrubs are *Clerodendrum viscosum* Vent., nom. superfl. (40), *Lantana camara* L. (35), *Croton oblongifolius* Roxb. (34) and *Flemingia strobilifera* (L.) R.Br. (20). The diversity of WEPs in Jharkhand has found to be depleted due to their over exploitation and unsustainable harvesting for foods, medicines as well as because of various other biotic interferences including grazing, herbivory and anthropogenic fire. Therefore, there is an urgent need to conserve these valuable Wild edible plants (WEPs) and use it in a sustainable manner to ensure future demand. Besides, further research is also warrant to explore the therapeutic potentials as well the nutritive values of WEPs, so that, it can give a scientific basis for the further development of herbal drugs and traditional foods.

**Keywords:** Edible plants, Jharkhand, Medicinal uses, Tribal population

**IPC Code:** Int. Cl.<sup>20</sup>: A23B 9/00, A61K 9/00, A61K 36/00

India is one of the 17 mega diversity nations with over 45,000 plant species representing about 7% of the world's flora. It holds the 10<sup>th</sup> position among the 25 most plant-rich countries of the world with 24.39% forests cover<sup>1</sup>. India has ca. 800 edible plant species that are grown in the wild and consume mainly by tribal populations<sup>2</sup>. Jharkhand is one of the biodiversity rich states of India with extensive forests resources (29.65% of the total geographic area) because of its origin, diverse physiographic and climatic conditions<sup>3</sup>. Besides, it is well known for its rich mineral resources with over 40% of the country's total mineral reserve. Wild plants and its parts are used by most of the rural Indian populations (ca. 85%) as traditional medicines, diet supplements, and for livelihood security, socio-economic upliftment<sup>4,5</sup>. Indigenous communities of both industrialized and developing countries use wild plants for various day to day activities and the mean use of wild plant is 120 species per community<sup>6</sup>. Wild plants are used in several ways from timbers, fuelwoods, foods, wild vegetables, spices, wild fruits, thatch, construction materials, and raw materials for

industries, and often as traditional medicines. WEPs are those naturally grown plants and their parts including roots, shoots, leafy greens, fleshy fruits, nuts, grains and seeds that can be used for food if gathered at the appropriate stage of growth<sup>7</sup>. It is commonly grown in forests, agriculture and non-agriculture fields as well as along the roadsides, drains and wastelands. WEPs can be classified on the basis of economic importance<sup>8,9</sup> or based on the utility of plants as a whole or any plant parts<sup>10</sup>. WEPs may be herbs, shrubs or trees and can be used directly or after cooking and processing. Forests of Jharkhand are mainly tropical deciduous type and highly species rich<sup>11</sup>. The state of Jharkhand has a large tribal population (26.3%) with a total of 32 tribes predominant in 17 districts out of the total 24<sup>1</sup>. Knowledge of harvest and preparation of WEPs is important<sup>12</sup> and the indigenous communities reside in different parts of Jharkhand have a rich knowledge of WEPs and have developed unique knowledge of their mode of utilization. The dependency on WEPs are quite high in Jharkhand as forests are considered as a high value commodity across the state. Most of the indigenous peoples' of Jharkhand are dependent on forests as well as on

\*Corresponding author



# Flood Inundation Mapping and Impact Assessment Using Multi-Temporal Optical and SAR Satellite Data: a Case Study of 2017 Flood in Darbhanga District, Bihar, India

Gaurav Tripathi<sup>1</sup> · Arvind Chandra Pandey<sup>1</sup> · Bikash Ranjan Parida<sup>1</sup> · Amit Kumar<sup>1</sup>

Received: 22 August 2019 / Accepted: 22 March 2020 /

Published online: 22 April 2020

© Springer Nature B.V. 2020

## Abstract

Flooding is a recurrent hazard in east Gangetic plains, largely on account of natural factors that pose risks to life and property. Bagmati and Burhi Gandak rivers draining parts of North Bihar causes substantial flooding owing to higher rainfall. This comprehensive study was carried out to map near real-time flood inundation using multi-temporal Sentinel-1A (SAR) and Moderate-resolution Imaging Spectroradiometer Near Real-Time (MODIS NRT) flood data (Optical and 3-day composite) over Darbhanga district of North Bihar during August and September 2017. Floodwater pixels were extracted using the binarization technique, wherein the threshold was applied as  $-22.5$ ,  $-23.4$ ,  $-23.8$  and  $-22.7$  over VH polarization image. The key results revealed that during peak flooding stage (23rd August), 13% of areas were submerged based on SAR data, whereas overestimation by  $>20\%$  was estimated using MODIS data. As shown in the composite flood inundated map, the inundated patches are quite similar in both the optical and SAR based data. Notably, there were higher flood patches observed in the central, northern, and western parts of the district due to the presence of more water channels in those regions. Our findings suggested that agriculture patches of  $\sim 392$  sq.km area were inundated due to flood followed by vegetation clutters (16.07 sq.km) and urban (8.46 sq.km). These results indicated the impact of floodwater on agriculture and urban patches. These findings are crucial for policymakers to assess flood impacts. It can be inferred that flood prognosis using SAR data will lead to spatial accuracy and can be improved when coupling with various hydro-meteorological parameters and hydrological models.

**Keywords** TRMM · SAR · Urban flood · Dual polarization · Threshold · MODIS NRT

---

✉ Arvind Chandra Pandey  
arvindchandrap@yahoo.com

# Evaluation of ANN, M5P, RBF, Reptree for Runoff and Sediment yield

Sanoj Kumar, Birendra Bharti, H.P. Singh

**Abstract:** There are many water resources problems are the nature of prediction and estimation of rainfall, runoff, contamination concentration and water stages etc. Solving these problems with the conventional techniques are computationally expensive and far from the real-life situation. It is most useful for watershed management. In the present study, runoff and sediment yield are evaluated respectively by different model on the Nagwan watershed. This watershed is located on the upper part of the Sewani River in Hazaribagh district of Jharkhand. The input parameters rainfall, temperature, relative humidity, wind velocity, dew point and output parameters are runoff, sediment yield. The monthly data from 1983 to 2006 are used for training and from 2007 to 2016 are used for testing. For the prediction of runoff and sediment yield different type of models are used i.e. ANN, M5P, RBF, Reptree. In the present study model evaluation criteria i.e. NSE, CC, RSR, Pbias, R<sup>2</sup> are calculated. The value of NSE,CC,RSR,PBIAS and R<sup>2</sup> of Runoff are found as 0.99, 0.98,0.30, 0.15, 0.99 during calibration and 0.98, 0.98, 0.45, 0.56, 0.98 during validation and the evaluation criteria of NSE,CC,RSR,PBIAS and R<sup>2</sup> of Sediment Yield are found as 0.99, 0.98, 0.46, 0.67, 0.99 during calibration and 0.98, 0.96, 0.58, 0.02, 0.98 during validation. In this study we found that predication of runoff and sediment yield value M5P model is the best model. Keywords: M5P, ANN, RBF, NSE, CC.

## 1 INTRODUCTION

The hydrological phenomena, the variation due to runoff and sediment yield in the catchment. A linear and non linear hydrological models have been developed in 1930 for explaining the processes of rainfall, runoff and sediment yield in the watershed and these very useful for the prediction. Many parameter s are required to process the hydrological model like surface roughness, watershed treatment, conservation practices, soil moisture variation, soil horizon, topographic data, watershed treatment, land uses, soil characteristics etc. For describing the hydrological model following assumption are made, 1) Uniform soil group 2) uniformly distributed over the catchment is sediment produced in the catchment 3) Slope approximations, etc. The assumptions are very useful for the development of classical model. Apart from that, ANN based approach method is very flexible for the determination of catchment characteristics. The artificial neural network (ANN) approach includes both linear and non linear concepts for the development of model. The ANN model minimises the error effectively. Kumar et al. (2002) investigated utility of ANN for the estimation of daily reference crop evapotranspiration and compared the performance with the conventional method (24). Kim et al. (2003) used ANN to forecast draught and the result indicates that the conjunctive Models significantly improve the ability of ANN to forecast the indexed regional draught (23). Jain et al. (2004) applied knowledge of ANN to analyze the soil water retention data (21).

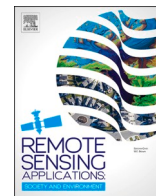
Kumar et al. (2005) used artificial neural networks (ANNs) in rainfall-runoff modelling has suggested certain issues that are still not addressed properly (33). Sarangi and Bhattacharya (2005) developed for the prediction of sediment yield were validated using the hydrographs and silt load data of 1995–1998 for the Banha watershed in the Upper Damodar Valley in Jharkhand state in India (32). Raghuvanshi et al. (2006) developed to predict both runoff and sediment yield on daily as well as weekly basis from simple information of rainfall and temperature (30). Upadhyay et al. (2009) predicted Runoff and sediment yield from an Indian watershed during the monsoon period were forecasted for different time periods (daily and weekly) using the back propagation artificial neural network (BPANN) modelling technique (4). Goyal (2014) predicted the sediment yield generated within a watershed is an important input in the water resources planning and management (29). The focus of present study is to evaluate the performance of ANN, M5P, RBF, Reptree for Runoff and Sediment yield in Nagwan watershed of the upper part of the Sewani river in Hazaribagh of Jharkhand.

## 2 STUDY AREA

The Nagwan watershed is located at the upper part of the Sewani river between 85.2500 to 85.4300 E longitudes and 23.9900 to 24.1200 N latitude within the Damodar-Barakar catchment in India. The watershed is just 7 km from the soil conservation department of D.V.C. at Hazaribagh, Jharkhand. The catchment is rectangular in shape with an area of 92.46 sq. km shown in figure 1. Geologically, the area is quite complex, having rocks of varying composition, the soils of the area are mainly of clay loam type. The maximum and the minimum elevations of the area are 637 m and 564 m, respectively from mean sea level. The catchment has very undulating and irregular slope varying from 1 to 25%. The area experiences sub-humid sub-tropical monsoon type of climate, characterized by hot summers (4000C) and mild winters (400C). The total annual precipitation of 1200 mm is distributed mainly between June to September. The mean monthly relative humidity varies from a minimum of 40% in the month of April to a maximum of 85% in the month of July.

• Sanoj Kumar, M.Tech. student, Department of Water Engineering and Management, Central University of Jharkhand, India-835205, Email [sanojkumar.cuj@gmail.com](mailto:sanojkumar.cuj@gmail.com) Correspondence Author: Birendra Bharti, Assistant professor, Department of Water Engineering and Management, Central University of Jharkhand, India-835205, Email: [birendrabharti@gmail.com](mailto:birendrabharti@gmail.com)

• H.P. Singh, Professor, Department of Water Engineering and Management, Central University of Jharkhand, India-835205, Email: [singh.harendra121@gmail.com](mailto:singh.harendra121@gmail.com)



# Estimating biochemical parameters of paddy using satellite and near-proximal sensor data in Sahibganj Province, Jharkhand (India)

Avinash Kumar Ranjan<sup>\*</sup>, Bikash Ranjan Parida

Department of Geoinformatics, School of Natural Resource Management, Central University of Jharkhand, Ranchi, 835205, Jharkhand, India

## ARTICLE INFO

### Keywords:

Chlorophyll content  
Crop nitrogen status (CNS)  
Near-proximal sensor (NPS)  
Remote sensing (RS)  
Vegetation indices (VIs)  
Root mean square error (RMSE)

## ABSTRACT

Rice is one of the most important crops in India, and chlorophyll (Chl) and nitrogen (N) content of leaf serve as a significant indicator for monitoring crop status and precision farming. These biochemical parameters can be obtained from remote sensing data, but can have limitation on the precision of these parameters. In this aspect, near-proximal optical sensors placed in contact with the crop and can provide a rapid assessment of Chl content and N status. So, in this study, both satellite data and proximal sensors were used to estimate Chl content and N status of paddy in Sahibganj district in the state of Jharkhand (India). The key findings showed that multiple regression (MR) based models comprising RVI, NDVI, and EVI were more competent to estimate the Chl content and crop nitrogen status (CNS) with r-value of 0.72 and 0.77, respectively. Notably, the ratio vegetation index (RVI) based model was also promising with r-value of 0.69 and 0.74 for Chl and CNS estimation, respectively. It was noticed that the empirically derived Chl content and N status of paddy were in general hyped than the satellite-based estimates as represented by the root mean square error (RMSE) and mean absolute deviation (MAD).

## 1. Introduction

Rice (*Oryza Sativa*) has a prodigious role as a staple food and providing the nutritious need to billions of world's populations. Rice is a prime foodstuff in the Asian sub-continent. Monitoring and management of agriculture systems are indispensable for food security measures and allied policies measures. It is a fact that agriculture system has been undesirably affected by climate change activities (viz. unseasonal rainfall, alteration in crop seasons, etc.) and extreme weather events (viz. drought, flood, rainstorms, etc.) (Patel et al., 2012; Dutta et al., 2015). So, assessing the health of the crop at real-time could make differences to upgrade farmer's income as well as to alleviate the associated risks. Over the last few decades, Remote Sensing (RS) techniques have been revitalized the way of agriculture system to monitor and assess the crop health. Owing to its specific abilities, RS data has been successfully deployed in the agriculture domain for innumerable kinds of study. For

instance, RS data has been used for crop acreage mapping and estimation, crop type discrimination, yield prediction, biomass estimation, health monitoring, phenological study, biochemical and biophysical parameters estimation (i.e. chlorophyll (Chl) and nitrogen (N) content, FAPAR (Fraction of Absorbed Photosynthetically Active Radiation), Leaf Area Index (LAI)) etc. (Goel et al., 2003; Sullivan et al., 2004; Gitelson et al., 2005; Ranjan and Parida, 2019; Parida and Ranjan, 2019a,b).

Biochemical and canopy biophysical parameters (Chl, N, LAI, FAPAR, etc.) have a distinct grandness to understand the crops biogeochemical cycling, health, and physiographic growth parameters (Lin et al., 2015; Zhang et al., 2019). Various studies have been suggested that biochemical and biophysical parameters have an optimistic linear relation with crop productivity (Scharf et al., 2006; Miao et al., 2007; Varvel et al., 2007). In particular, Chl of foliage has a substantial relationship with N content of leaves, as it is an important element of chlorophyll (Alchanatis et al., 2005). Spatio-temporal alteration in Chl

**Abbreviations:** RS, Remote Sensing; GPS, Global Positioning System; NPS, Near-proximal Sensor; IRS, Indian Remote Sensing; MODIS, MODerate-resolution Imaging Spectro-radiometer; NDVI, Normalized Difference Vegetation Index; EVI, Enhanced Vegetation Index; RVI, Ratio Vegetation Index; Chl, Chlorophyll; N, Nitrogen; NBI, Nitrogen Balance Index; NVI, Nitrogen Vegetation Index; EF, Empirical Formula; LR, Linear Regression; MR, Multiple Regression; RMSE, Root Mean Square Error; MAD, Mean Absolute Deviation.

<sup>\*</sup> Corresponding author.

E-mail address: [avinash.ranjan07@yahoo.com](mailto:avinash.ranjan07@yahoo.com) (A.K. Ranjan).

<https://doi.org/10.1016/j.rsase.2020.100293>

Received 23 August 2019; Received in revised form 14 December 2019; Accepted 8 February 2020

Available online 12 February 2020

2352-9385/© 2020 Elsevier B.V. All rights reserved.



# Floristic analysis and dominance pattern of sal (*Shorea robusta*) forests in Ranchi, Jharkhand, eastern India

Rahul Kumar<sup>1</sup> · Purabi Saikia<sup>1</sup>

Received: 20 November 2017 / Accepted: 27 April 2018 / Published online: 7 November 2018  
© Northeast Forestry University and Springer-Verlag GmbH Germany, part of Springer Nature 2018

**Abstract** The present study describes the floristic composition and dominance pattern of sal forests in Ranchi, Jharkhand, eastern India. Vegetation was studied in 47 belt transects (50 × 100 m) that had 137 plant species (110 identified and 27 unidentified) belonging to 51 families. The family Fabaceae with 17 species (8 spp. belonging to subfamily Faboideae, 6 spp. to Caesalpinioideae and 3 spp. to Mimosoidiae) contributed the most to diversity, followed by Rubiaceae (8 spp.) and Euphorbiaceae (6 spp.). Tree density in sal was inversely related to species richness. Total tree density ( $\geq 10$  cm GBH) in the studied forests was 397 individuals  $\text{ha}^{-1}$ , with a basal cover of 262.50  $\text{m}^2 \text{ha}^{-1}$ . Important plants of conservation concern are *Pterocarpus marsupium* Roxb, *Andrographis paniculata* (Burm.f.) Wall, *Sterculiaurens* Roxb., *Tinospora cordifolia* (Willd.) Miers, and *Asparagus densiflorus* (Kunth) Jessop. Phanerophytes had the highest percentage (71%, with percentage deviation from normal life form of + 25) followed by therophyte (15%, with percentage deviation + 2). Observed percentage deviation from normal life form was much lower (with + 2 percentage deviation) in both chamaephytes (8%) and therophytes

(15%), suggesting that the studied sal forests are favorable for supporting various plants species. The forest management strategies should focus on the increasing demands for different timber and non-timber forest products to conserve the plant diversity of these natural forests.

**Keywords** Sal forests · Species richness · Life form · Jharkhand

## Introduction

Sal (*Shorea robusta* C.F. Gaertn.) is a tropical tree species native to South Asia from Myanmar in the east to Bangladesh, Nepal and India in the west and covers more than 12 million hectares of forest area (Tiwari 1995). Although, the general distribution of sal is governed by climate, its local distribution is regulated largely by geological conditions and soil (Troup 1921). On the basis of edaphic conditions and microclimate, the phenology of sal forests ranges from deciduous to evergreen and extends from tropical to subtropical. Sal has been described as deciduous (Cooke 1958; Kirtikar and Basu 1975; Tiwari 1995), semi-deciduous (Bor 1953), evergreen (Krishnaswamy and Mathauda 1954; Singh and Singh 1992; Borchert 2000) or deciduous or borderline between evergreen and deciduous (Joshi 1980). In addition to timber and fuel wood, sal produces fodder (Panday 1982; Gautam 1990; Pandey and Yadama 1990; Mathema 1991; Upadhyay 1992; Thacker and Gautam 1994; Fox 1995; Shakya and Bhattarai 1995; Edwards 1996; Gautam and Devkota 1999), leaves for plates (Rajan 1995; Gautam and Devkota 1999), seed for oil (Venkat and Sharma 1978; Sharma 1981), feed (Rai and Shukla 1977; Sinha and Nath 1982), resin or latex from heartwood (FRIB 1947) and tannin and gum from bark

Project funding: This work was supported by Science and Engineering Research Board (SERB) under Young Scientist Scheme (Ref. No. YSS/2015/000479 dated 12th January 2016).

The online version is available at <http://www.springerlink.com>

Corresponding editor: Chai Ruihai.

✉ Purabi Saikia  
purabi.saikia@cuja.ac.in

<sup>1</sup> Department of Environmental Sciences, Central University of Jharkhand, Brambe, Ranchi 835205, Jharkhand, India



## Treatment of monazite processed effluent to recover rare earth metals (REMs)

Archana Kumari<sup>a,b</sup>, Sunidhi Singh<sup>c</sup>, Kavita Parmar<sup>c</sup>, Devendra Deo Pathak<sup>b</sup>, Manis Kumar Jha<sup>a\*</sup>

<sup>a</sup> Metal Extraction and Recycling Division, CSIR-National Metallurgical Laboratory, Jamshedpur- 831007, India

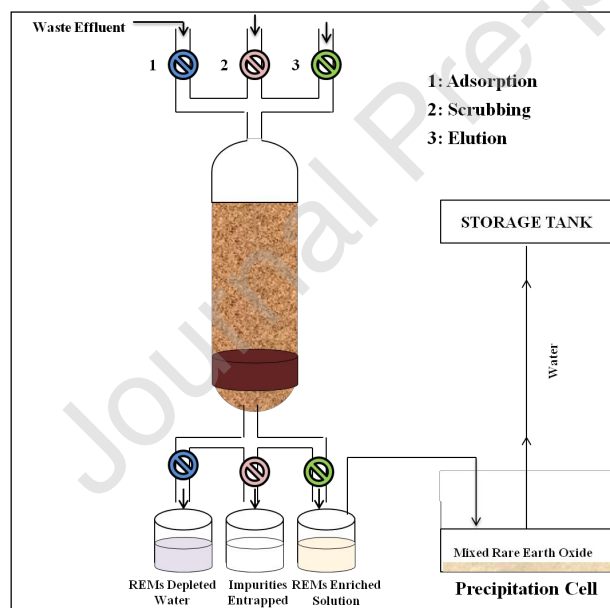
<sup>b</sup> Department of Applied Chemistry, Indian Institute of Technology (ISM), Dhanbad-826004, India

<sup>c</sup> Department of Environmental Sciences, Central University of Jharkhand, Ranchi-835205, India

\*Corresponding author:

E-mail address: mkjha@nmlindia.org (Dr. M.K. Jha), FAX +91-657-2345213

### Graphical Abstract



### Highlights

- Human health risk due to REMs in mine water and effluent.
- Processing of monazite effluent to reduce human health risks.
- Amberlite IR120 Na used to recuperate light REMs.
- Significantly enriched the REMs in solution for recovery.
- Pure REMs oxides can be prepared from enriched solution of REMs by precipitation.

### Abstract

Improper disposal of effluent generated in rare earth mining areas and ore processing industries results in loss of REMs and miserably affects the ecosystem. Thus, their appropriate treatment is required, which can be achieved via environmentally feasible processes. In this connection, systematic scientific adsorption studies were carried out to separate REMs using cationic resin, Amberlite IR120 Na from the effluent generated during monazite processing for REMs recovery. To optimize feasible conditions for REMs recovery, bench scale studies were carried out varying different process parameters viz. pH, contact time, resin dose, etc. It was observed that adsorption of 92.63% La, 92.79% Ce, 91.45% Nd, 90.95% Pr and 95.09% Sm was achieved at aqueous/ resin (A/R) ratio 25 mL/g, pH 1.3 and contact time 10 min. Loading capacity of resin was found to hold 48.57 mg REMs/g resin. The adsorption data followed the second order reaction ( $(t/q) = (1/h) + (1/q_e)(t)$ ) and Langmuir adsorption isotherm ( $(1/q) = [(1/k_1 q_m)(1/C_e)] + (1/q_m)$ ). The loaded REMs was effectively eluted using 15% H<sub>2</sub>SO<sub>4</sub> in 10 min. The REMs enriched solution was treated to get pure REM oxides as precipitate. This technical application will be useful for REMs recovery as well as to mitigate environmental pollution.

**Keywords:** Effluent; Advance Separation; Rare Earth Extraction; Environment; Adsorption.

### 1. Introduction

Huge mine-water, industrial effluent, rinse water and various lean-grade aqueous solution containing rare earth metals (REMs) create environmental problem as well as loss of valuable



# Nitrous Oxide (N<sub>2</sub>O) Estimation from Tropical Rice Paddy Under the Influence of Growth-Regulating Compounds

Nirmali Bordoloi<sup>1</sup> · Kushal Kumar Baruah<sup>2</sup> · Jinnashri Devi<sup>3</sup>

Received: 30 August 2019 / Revised: 11 March 2020 / Accepted: 21 March 2020  
© University of Tehran 2020

## Abstract

Nitrous oxide (N<sub>2</sub>O) is an important long-lived greenhouse gas and is a dominant contributor to stratospheric ozone depletion. Mitigating N<sub>2</sub>O emission from the rice paddies is one of the important challenges to global food security and climate change research while sustaining optimum productivity. We conducted a 2-year experiment to investigate the effect of different plant growth regulators (PGRs) on N<sub>2</sub>O emission to the atmosphere. The PGRs namely abscisic acid and cytozyme (20 mg L<sup>-1</sup>), kinetin (10 and 20 mg L<sup>-1</sup>) and tea extract (1:20 w/w) along with distilled water as control were sprayed at the tillering and panicle initiation stages of rice crop. Abscisic acid and kinetin (10 and 20 mg L<sup>-1</sup>) were found to bring about a significant ( $p < 0.01$ ) reduction in N<sub>2</sub>O emission over control plants primarily through regulation of leaf growth, plant biomass, stomatal frequency, and xylem vessel size of rice plants. Cytozyme and kinetin application enhanced the flag leaf photosynthetic rate and grain yield through maximum partitioning of photosynthates to the developing grains. The PGRs were found to regulate the transport process of N<sub>2</sub>O, through manipulation of physiological and anatomical processes of rice plants. The present study indicates that kinetin (10 mg L<sup>-1</sup>) may be a sustainable mitigation measure for N<sub>2</sub>O emission reduction with efficient grain productivity and highest net revenue.

## Article Highlights

- Effects of growth regulators on N<sub>2</sub>O emission from rice field were studied.
- The growth regulators influenced the transport mechanism of N<sub>2</sub>O to the atmosphere.
- Kinetin and abscisic acid were effective in reducing N<sub>2</sub>O emission.
- Kinetin and cytozyme enhanced the photosynthesis and increased grain productivity.

**Keywords** Rice paddy · Nitrous oxide · Growth regulators · Photosynthesis and yield

---

**Electronic supplementary material** The online version of this article (<https://doi.org/10.1007/s41742-020-00257-2>) contains supplementary material, which is available to authorized users.

---

✉ Kushal Kumar Baruah  
kkbaruah14@gmail.com

<sup>1</sup> Department of Environmental Sciences, Central University of Jharkhand, Brambe, Ranchi 835205, India

<sup>2</sup> School of Earth and Environmental Sciences, Royal Global University, Guwahati, Assam 781035, India

<sup>3</sup> Department of Environmental Science, Tezpur University, Tezpur, Assam 784028, India

## Introduction

Greenhouse gas (GHG) induced climate change is the most pressing challenges faced by the humanity and is becoming serious risks for the ecosystem. Although GHG is minor constituents of the atmosphere but the increasing concentration of GHG enhance the absorption of longwave radiation emitted by the earth's surface. As a result, it increases the global temperature and affect the environment and human health. Many international treaties were signed to reduce the concentration of GHG in the atmosphere but to attain this universal goal reduction on a local, regional and national level is also important (Arslan 2012). Among the GHGs, N<sub>2</sub>O is a powerful greenhouse gas contributing to climate change and receiving more attention due to its strong global

# Magnetic Cobalt Oxide Nanoparticles: Sucrose-Assisted Self-Sustained Combustion Synthesis, Characterization, and Efficient Removal of Malachite Green from Water

Jhilirani Mohanta, Banashree Dey, and Soumen Dey\*

Cite This: <https://dx.doi.org/10.1021/acs.jced.0c00131>

Read Online

ACCESS |



Metrics &amp; More



Article Recommendations



Supporting Information

**ABSTRACT:** Designing a stable and efficient adsorbent for removal of pollutants such as dyes is of serious concern nowadays. In view of that, magnetic cobalt oxide nanoparticles (CONP) were synthesized in a multigram scale using a modified self-propagator combustion method triggered by sucrose as the fuel. The material was characterized by Fourier-transform infrared spectroscopy, X-ray diffraction, vibrating sample magnetism (VSM), scanning electron microscopy (SEM)–energy-dispersive system, high-resolution transmission electron (HRTEM),  $\text{pH}_{\text{ZPC}}$ , and Brunauer–Emmett–Teller surface area. SEM and HRTEM images confirm the presence of distinct pore channels. Room temperature VSM reveals weak hysteresis, indicating that the CONP is a soft but robust magnetic material.  $\text{pH}_{\text{ZPC}}$  was found to be 6.45. Removal of malachite green from simulated water was tested in a batch mode and found to be promising. Physiochemical parameters such as pH, contact time, dose, and temperature were optimized. The maximum Langmuir adsorption capacity was found to be 238.10 mg/g. Adsorption is best described by the Langmuir isotherm model ( $R^2 = 0.999$ ) and pseudo-second order kinetics ( $R^2 = 0.999$ ). Regeneration (83%) with dilute acid enables its successive use. Its magnetic nature facilitates the rapid separation of the CONP after adsorption using a hand-held magnet. Easy synthetic protocols, robustness, high removal efficiency, and reusability make the material an ideal future choice for dye detoxification.



## 1. INTRODUCTION

Dyes are molecules which connect themselves to the fabric surface to impart a permanent color.<sup>1</sup> Nowadays, dyes are used in various industries such as textile, food, paint, paper, pulp, leather treatment, silk, jute, wool, and cotton. Discharge of waste dyes to waterbodies result in considerable environmental and health problems.<sup>2–6</sup> Dyes are toxic to aquatic life because of their mutagenic, carcinogenic, teratogenic, and genotoxic properties.<sup>4,7,8</sup> In addition, dyes significantly reduce sunlight penetration in waterbodies. Hence, the need to address the problem emerges.

Several chemical, biological, and physical methods have been developed such as chemical reduction, photo-degradation, electrochemical, oxidation, coagulation–flocculation, membrane separation, Fenton oxidation, and adsorption.<sup>9,10,63–69</sup> Among all, adsorption is considered to be one of the best techniques. It offers advantages such as an easy operation technique, high separation efficiencies, and cost effectiveness.<sup>11–14</sup> Among various adsorbents, metal oxide-based nanoparticles and composites were shown to be effective for dye removal. Metal oxide, owing to its small size, high surface area, and robustness is an ideal choice. Synthesis of various metal oxides was attempted by various methods such as sol–gel, chemical vapor deposition, co-precipitation, mechanical alloying, micelle synthesis, combustion, and microwave

heating.<sup>15–18,42–44,57–59,72,74</sup> Among all, the combustion method is easy, rapid, and cost effective. Such reactions are self-propagator and exothermic in nature. High purity and homogeneous powders are obtained with a fine particle size.<sup>19,20,30–33</sup>

Magnetic nanoscale iron oxide, flower-like iron oxide, and magnetic  $\text{MnO}-\text{Fe}_2\text{O}_3$  composites were used earlier for dye removal.<sup>20–22</sup>  $\text{ZnO}$  and  $\text{SnO}_2$  nanoparticles were synthesized by the precipitation method and used for adsorption of commercial dyes.<sup>23</sup> Manganese-based porous, magnetic oxide nanoparticles are known.<sup>24,25</sup>  $\text{ZnCr}_2\text{O}_4$  nanoparticles were synthesized via a sol–gel method and tested for azo dyes.<sup>26</sup> Iron oxide nanoparticles were synthesized via a hydrolysis technique and were found to be efficient for removal of Congo red.<sup>27</sup> Alumina and mixed  $\text{Al}-\text{Co}$  oxide were effective for removal of color black G and Congo red.<sup>28,29</sup> Tungsten oxide nanoparticles and  $\text{SrTiO}_3$  nanoparticles were synthesized by the solution combustion method and used in removal of

Received: February 5, 2020

Accepted: March 26, 2020



# Determination of concentration of total sodium and potassium in surface and ground water using a flame photometer

Payal Banerjee<sup>1</sup> · Bably Prasad<sup>2</sup>

Received: 15 March 2019 / Accepted: 30 March 2020 / Published online: 19 April 2020  
© The Author(s) 2020

## Abstract

In this paper, we have investigated 18 water samples collected from various sources, e.g., surface, underground and river water, as specimens for their sodium and potassium ions content in and around Dhanbad, a mining town, using the flame photometry. We have plotted the contour maps to show the spatial distributions of the dissolved sodium and potassium cations in the groundwater and surface water sources in and around the Dhanbad city to identify the relative contributions of human and natural phenomena to it. Along with it, water quality index (WQI) is calculated to evaluate whether the collected surface, ground and river water samples are fit for human consumption for the residents of those areas. The water of Maithan Dam has been observed to have the least sodium and potassium concentrations of 16 mg/l and 7 mg/l, respectively, which make it most suitable for human consumption. The water of Rani Talab Pond has the highest sodium and potassium contents of 49 mg/l and 24 mg/l. WQI values of all the samples are found to be less than 50, which indicates they are safe to consume by the humans. Reduction in the use of pesticides, potassium permanganate and water softeners is recommended to maintain WQI of the Dhanbad city within safe limit.

**Keywords** Flame photometer · Sodium · Potassium · Surface water · Underground water

## Introduction

The possibility of employment of characteristic emission from excited atoms in quantitative analysis of elements for analytical chemical science was first experimentally studied by Bunsen and Kirchhoff. This very principle was actually employed for the development of instruments such as flame photometer for analytical chemical science experiments for quantitative analysis of potassium and sodium alkali metal ions. For the detection of trace metals all across the world, atomic emission is considered as an effective tool. In order to develop a robust and quantitative atomic emission-based method, there are many considerations that need to be taken into accounts such as proper selection of atomization and excitation source, proper wavelength along with slit width selection, minimization of outside chemical

and spectral interference and techniques to standardization. Progress in the development of flame photometer is accelerated with the introduction of nebulizer, which enables the introduction of the sample in the form of aerosol inside the air/acetylene flame. At that time, emission was dispersed by quartz prism spectrograph, and emission was recorded photographically. As a result of this, a low-cost, highly sensitive instrument such as flame photometer was developed for the precise determination of alkali metal ions content in the samples.

Other precise techniques such as atomic absorption spectroscopy (Parker 1972) (AAS), inductively coupled plasma atomic emission spectroscopy (ICP-AES) were also developed alongside to increase the resolution of other metal ions detection. Flame photometer has a high resolution for the detection of alkali metal ions such as sodium ( $\text{Na}^+$ ) and potassium ( $\text{K}^+$ ). Later in the field of analytical spectrophotometers, the concept of the introduction of photomultiplier tube in the grating-based spectrophotometers to AAS was significant.

Flame photometer actually works by atomizing a solution sample into a flame and separates the characteristic spectra of an element along with measurement of emission. Low

✉ Bably Prasad  
drbablyprasad@yahoo.com

<sup>1</sup> Department of Applied Chemistry, Central University of Jharkhand, Ranchi, Jharkhand 835205, India

<sup>2</sup> Natural Resources and Environment Management, CSIR-CIMFR, Dhanbad Jharkhand-826015, India

RESEARCH

Open Access



# Remote Sensing approach to evaluate anthropogenic influences on Forest Cover of Palamau Tiger Reserve, Eastern India

Binita Kumari, Arvind Chandra Pandey\*  and Amit Kumar 

## Abstract

**Background:** Tropical forests have been experiencing remarkable rates of transformation over the past century as they are getting degraded or decimated to a great extent by anthropogenic activities. This study aims at investigating the long-term forest cover transformation in Palamau Tiger Reserve (PTR), Jharkhand, India, using Landsat TM, ETM<sup>+</sup>, and OLI satellite images during 1975–2015. The forest cover was delineated utilizing various keys of visual interpretation techniques.

**Results:** The forest cover was primarily decreased in the north-eastern and north-western parts in PTR. In order to identify the anthropogenic disturbance in the forest reserve, human settlement density was mapped using high-resolution Google Earth imagery. The results showed a positive correlation between human population density and settlement density. Five major affected sites with an outer buffer of 2 km were demarcated in order to deduce the anthropogenic influences in major non-forested sites in PTR. It was observed that the forest change was maximum at site 3 (Ranidah, area 61.06 km<sup>2</sup>, – 6.47% change) followed by site 2 (Saidup, area 124.38 km<sup>2</sup>, – 7.65% change), where settlement units were also high (2638 and 2621 settlement units, respectively). At site 1 (Barkheta, area 81.59 km<sup>2</sup>), – 1.99% change was observed, and at site 4 (Samadh Tola, area 9.15 km<sup>2</sup>), 1.03% change was observed having moderate settlement units (2422 and 1892 settlement units, respectively). Areas with the low level of human settlements (1038 settlement units) observed the least change, i.e., at site 5 (Netarhat, area 48.52 km<sup>2</sup>), 0.58% change was observed mainly during the years.

**Conclusions:** The forest cover exhibited an overall decrease of 14.55 km<sup>2</sup> (– 1.34% change) with episodic variation during 1975–2015 in PTR, Eastern India. A significant forest disturbance occurred primarily in the north-eastern and north-western parts of PTR along the forest fringe due to the high population and settlement density. The study highlighted the potential use of freely available multi-temporal satellite observations in forest management.

**Keywords:** Population density, Settlement density, Remote sensing and GIS, Palamau Tiger Reserve

\* Correspondence: [arvindchandrap@yahoo.com](mailto:arvindchandrap@yahoo.com)

Department of Geoinformatics, Central University of Jharkhand, Ranchi, Jharkhand 835205, India



# Mixed lineage kinase 3 promotes breast tumorigenesis via phosphorylation and activation of p21-activated kinase 1

Subhasis Das<sup>1</sup> · Rakesh Sathish Nair<sup>1</sup> · Rajakishore Mishra<sup>2</sup> · Gautam Sondarva<sup>1</sup> · Navin Viswakarma<sup>1</sup> · Hazem Abdelkarim<sup>3</sup> · Vadim Gaponenko<sup>3</sup> · Basabi Rana<sup>1,4,5</sup> · Ajay Rana<sup>1,4,5</sup>

Received: 17 August 2018 / Revised: 28 November 2018 / Accepted: 7 December 2018  
© Springer Nature Limited 2019

## Abstract

Mixed lineage kinase 3 (MLK3), a MAP3K member has been envisioned as a viable drug target in cancer, yet its detailed function and signaling is not fully elucidated. We identified that MLK3 tightly associates with an oncogene, PAK1. Mammalian PAK1 being a Ste20 (MAP4K) member, we tested whether it is an upstream regulator of MLK3. In contrast to our hypothesis, MLK3 activated PAK1 kinase activity directly, as well as in the cells. Although, MLK3 can phosphorylate PAK1 on Ser133 and Ser204 sites, PAK1S133A mutant is constitutively active, whereas, PAK1S204A is not activated by MLK3. Stable overexpression of PAK1S204A in breast cancer cells, impedes migration, invasion, and NFκB activity. In vivo breast cancer cell tumorigenesis is significantly reduced in tumors expressing PAK1S204A mutant. These results suggest that mammalian PAK1 does not act as a MAP4K and MLK3-induced direct activation of PAK1 plays a key role in breast cancer tumorigenesis.

## Introduction

Mixed lineage kinase 3 (MLK3) also known as MAP3K11 belongs to a large family of MAP3Ks, called the mixed lineage kinases (MLKs) because their catalytic domains contain signature sequences of both Ser/Thr and Tyr kinases [1, 2]. The biochemical analyses hitherto, have shown that MLKs are functional Ser/Thr kinases and activate

downstream MAPK pathways, however their tyrosine kinase activities if any, are still not known [1, 3]. There are nine mammalian MLK members and based on the functional domains and sequence similarities, they are classified in three sub-groups: the mixed lineage kinases (MLKs), dual-leucine zipper kinases (DLKs), and zipper sterile- $\alpha$ -motif kinases (ZAKs) [1]. MLK3 belongs to the MLK sub-group and has been implicated in various cancers [4–6] and neurodegenerative diseases [7, 8]. The pan-MLK inhibitor went to clinical trials for Parkinson's disease, however the trial was abruptly stopped due to unknown reasons [8]. The role of MLK3 in cancer is an emerging area and earlier we reported that MLK3 kinase activity and transcripts were downregulated by estrogen in breast cancer, providing a survival advantage to ER+ breast cancer cells [4]. We also reported that the kinase activity of MLK3 was downregulated by HER2 amplification and MLK3 activity was essential to promote cell death in HER2+ breast cancer cells by anti-HER2 therapies [9]. However, in triple-negative breast cancer cells, MLK3 activation promotes migration and invasion, and MLKs inhibitor blocked cancer cell migration/invasion [10]. Conceivably, MLK3 and other MLK family members are important therapeutic targets in various diseases, including cancer, yet, their upstream regulators and downstream signaling pathways are not fully elucidated.

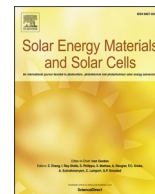
These authors contributed equally: Subhasis Das, Rakesh Sathish Nair

**Supplementary information** The online version of this article (<https://doi.org/10.1038/s41388-019-0690-0>) contains supplementary material, which is available to authorized users.

✉ Ajay Rana  
arana@uic.edu

- <sup>1</sup> Department of Surgery, Division of Surgical Oncology, University of Illinois at Chicago, Chicago, IL 60612, USA
- <sup>2</sup> Center for Life Sciences, School of Natural Sciences, Central University of Jharkhand, Ranchi, Jharkhand 835205, India
- <sup>3</sup> Department of Biochemistry and Molecular Genetics, University of Illinois at Chicago, Chicago, IL 60607, USA
- <sup>4</sup> University of Illinois Hospital & Health Sciences System Cancer Center, University of Illinois at Chicago, Chicago, IL 60612, USA
- <sup>5</sup> Jesse Brown VA Medical Center, Chicago, IL 60612, USA





## Dependence of photoactivity of niobium pentoxide (Nb<sub>2</sub>O<sub>5</sub>) on crystalline phase and electrokinetic potential of the hydrocolloid

Neha Kumari<sup>a,b</sup>, Kumar Gaurav<sup>a,b</sup>, S.K. Samdarshi<sup>a,b,\*</sup>, A.S. Bhattacharyya<sup>a,c</sup>, Samrat Paul<sup>d</sup>, BijuMani Rajbongshi<sup>e</sup>, Kaustubha Mohanty<sup>f</sup>

<sup>a</sup> Centre for Excellence in Green and Efficient Energy Technology, Central University of Jharkhand, Ranchi, 835205, Jharkhand, India

<sup>b</sup> Department of Energy Engineering, Central University of Jharkhand, Ranchi, 835205, Jharkhand, India

<sup>c</sup> Department of Nanotechnology, Central University of Jharkhand, Ranchi, 835205, Jharkhand, India

<sup>d</sup> Department of Energy Engineering, North-Eastern Hill University, Shillong, 793022, India

<sup>e</sup> Department of Chemical Engineering, Indian Institute of Technology, Delhi, 110016, India

<sup>f</sup> Department of Chemical Engineering, Indian Institute of Technology, Guwahati, 781039, India

### ARTICLE INFO

#### Keywords:

Niobium pentoxide  
Photoactivity  
Monoclinic  
Recombination  
Hydrocolloids

### ABSTRACT

Multiphase crystallite complex of the most popular photocatalyst – TiO<sub>2</sub> has consistently shown better UV and/or visible photoactivity than its pristine monophasic counterparts. An identical behaviour is reported in the studies conducted on ZnO as well. This motivated the present study i) to explore the possibility to establish this as generic behavior for all such materials, and ii) to look for a better material with high photocatalytic activity. The choice of niobium pentoxide for the purpose lies in its uniqueness in terms of its existence in different oxidation states and crystalline phases. Additionally it offers a novel and promising alternative to the existing photoactive nanomaterials due to its apposite band gap, band edge location, stability, sorption characteristics and recyclability. Herein, an attempt has been made to prepare niobium pentoxide with different crystalline phases, including mixed, and analyze their photoactivity in UV and visible ranges. The results show that niobium pentoxide, calcined between 500–800°C, crystallizes predominantly in orthorhombic and 900°C and above in monoclinic phase. The results reveal that under both UV and visible radiation the monophasic (monoclinic phase) niobia has high photoactivity as compared to the other phases in degradation of aqueous probe pollutant. This result is contrary to the expected result. The samples have been characterized by X-ray diffraction (XRD), UV-VIS spectroscopy (UV-VIS DRS), X-ray photoelectron spectroscopy (XPS), photoluminescence (PL) spectroscopy, transmission electron microscopy (TEM), and scanning electron microscopy (SEM) to arrive at a conclusive explanation of the results. The sorption characteristics of the hydrocolloid system, among others, have been found to be responsible for this behavior.

### 1. Introduction

Solar energy driven heterogeneous photocatalysis promises to be one of the most attractive options for environmental remediation, hydrogen production, and carbon valorization [1–4]. Photovoltaic techniques also offers robust method for addressing depleting fossil fuels problems [5–7]. The most explored photoactive nanomaterials for the purpose are extrinsic/intrinsic TiO<sub>2</sub> and ZnO and their respective homo-/hetero-phase complexes and composites, due to their suitable band edge location, stability, sorption characteristics in aqueous medium and other physico-chemical characteristics [8–11]. But overall yield of the process

for both of them have been reported to be low, which has been ascribed to high recombination of photogenerated charge carriers, narrow absorption spectrum and poor sorption characteristics in aqueous medium [1,12]. It, consequently, has kept the interest and intensity in the search for a suitable candidate photocatalytic nanomaterial phase/phase complex composite and/or structure still on [7,13]. Also, the study of the sorption characteristics in terms of electrokinetic potential and its correlation with photoactivity of such hydrocolloid systems still remains an area of interest [14].

Niobium pentoxide promises to be a good material with remarkable and proven performance in electrochromic and bio-sensing applications

\* Corresponding author. Centre for Excellence in Green and Efficient Energy Technology, Central University of Jharkhand, Ranchi, 835205, Jharkhand, India.  
E-mail address: [sanjoy.samdarshi@cuja.ac.in](mailto:sanjoy.samdarshi@cuja.ac.in) (S.K. Samdarshi).

<https://doi.org/10.1016/j.solmat.2020.110408>

Received 26 August 2019; Received in revised form 15 December 2019; Accepted 12 January 2020

Available online 21 January 2020

0927-0248/© 2020 Elsevier B.V. All rights reserved.

# Experimental Determination of the Thermal Performance of an Intermediate Temperature Solar Box Cooker with a Hybrid Cooking Pot

Atul A. Sagade<sup>a,d,\*</sup>, S. K. Samdarshi<sup>a,b,†</sup>, P.J. Lahkar<sup>c,1</sup>, Narayani A. Sagade<sup>d</sup>

<sup>a</sup> Center for Energy Engineering, Central University of Jharkhand, Ranchi 835205, Jharkhand, India

<sup>b</sup> Centre of Excellence in Green and Efficient Energy Technology, Central University of Jharkhand, Ranchi 835205, Jharkhand, India

<sup>c</sup> Tejpur University, Aasam, India

<sup>d</sup> Solar Energy Research Laboratory, Pandharpur-413304, Maharashtra, India

## Abstract:

The performance improvement of the solar box cookers is possible using different techniques and design changes. One of them is new or advance designs of cooking utensil/pot. New designs of the cooking pot enhance the heat transfer to the food leading to reduced cooking time. The present work depicts the performance of an Intermediate Temperature Solar Box Cooker (ITSBC) using a hybrid cooking pot (HCP). The ITSBC is tested with new design of the cooking pot equipped with top glazed lid. The COR is used as a thermal performance parameter (TPP) and determined experimentally using heating and open sun cooling tests. The inter-cooker performance comparison of the ITSBC is done using a newly designed HCP and a conventional cooking pot (CCP).

It is shown that the thermal performance of intermediate temperature solar box cooker (ITSBC) improves with a hybrid cooking pot (HCP) because of reduction in heat loss with the additional benefit of visualization of the solar cooking activity.

**Keywords:** Solar cookers, modified utensils for solar cookers, thermal performance of solar cookers, Cooker Opto-Thermal Ratio, thermal performance parameters

## 1. Introduction:

Many designs of solar box cookers (SBCs) have been designed, fabricated and investigated to enhance their thermal performance using different techniques. Some of them

---

\* Corresponding Authors Email: [atulsagade@gmail.com](mailto:atulsagade@gmail.com) ; Mobile no. 9763707309

† Corresponding Authors Email: [drsksamdarshi@rediffmail.com](mailto:drsksamdarshi@rediffmail.com) ; Mobile no. 9431701210

<sup>1</sup> Current Affiliation: Dhemaji Polytechnic, Silapathar, Assam, India.



# Turbulence of tropical cyclone ‘Fani’ in the Bay of Bengal and Indian subcontinent

Shubham Kumar<sup>1</sup> · Preet Lal<sup>1</sup> · Amit Kumar<sup>1,2</sup>

Received: 25 August 2019 / Accepted: 25 April 2020 / Published online: 11 May 2020  
© Springer Nature B.V. 2020

## Abstract

The present study is focused on the movement and impact of extremely severe tropical cyclone ‘Fani,’ which developed in the Bay of Bengal near the Equator during April 2019 and caused a severe impact on landmass due to high wind speed (max.180 km/h) and extreme precipitation (150–300 mm/day). The multi-satellite-based study exhibited that the cyclone remained in the oceans for a longer duration (7 days; 70% of its life span) since its formation, providing a substantial strength and moisture to travel a very long trajectory (2136 km on the ocean and 1040 km on land). The high-intensive *Fani* cyclone had severely affected a large area in the eastern Indian subcontinent (primarily Odisha, West Bengal, Assam in India and Bangladesh). The precipitation pattern over the landmass was estimated using temporal tropical rainfall measurement mission (TRMM) satellite dataset. The TRMM-based study exhibited a very high-intensity precipitation (>300 mm/day) in the Bay of Bengal, whereas high- (150–300 mm/day) to low-intensity precipitation (< 50 mm/day) was observed in the coastal Andhra Pradesh, Odisha and West Bengal due to the influence of extremely severe cyclonic storm during the landfall and its progression on the landmass. The tropical cyclone significantly affected the agricultural land (128,019 km<sup>2</sup>; 57% of total area) and least affected the built-up land (2758 km<sup>2</sup>; 1.2% of total area) in the region. Nevertheless, the cyclonic impact on built-up land was extensive as it devastated human life, property and assets, with the high-speed wind, torrential rain and extensive flooding. The premonsoon cyclone is a sporadic history in BoB, and *Fani* was one of the most influential cyclones of the region. The study provides the nature of the 10th most severe cyclone in the Indian subcontinent in the last 52 years, through its movement, wind direction and impact in terms of heavy rainfall and on land use/land cover in the region.

**Keywords** Tropical cyclones · *Fani* · North Indian oceans · LULC · TRMM

---

✉ Amit Kumar  
amit.iirs@gmail.com; amit.kumar@uj.ac.in

Shubham Kumar  
shubhamgeoinfo@gmail.com

Preet Lal  
preetlal2011@gmail.com

<sup>1</sup> Department of Geoinformatics, Central University of Jharkhand, Ranchi, Jharkhand, India

<sup>2</sup> IUCN - Commission on Ecosystem Management (South Asia), Gland, Switzerland



# Polarimetric decomposition methods for LULC mapping using ALOS L-band PolSAR data in Western parts of Mizoram, Northeast India

Bikash Ranjan Parida<sup>1</sup> · Shyama Prasad Mandal<sup>1</sup>Received: 22 January 2020 / Accepted: 1 May 2020 / Published online: 9 May 2020  
© Springer Nature Switzerland AG 2020

## Abstract

The rapid advancement of remote sensing and availability of polarimetric SAR (PolSAR) data have facilitated to monitor the land use land cover (LULC) dynamics. In the recent past, polarimetric decomposition theorems are applied widely to perform LULC classification with the help of machine learning techniques. In this study, we utilized ALOS PALSAR-1 L-band quad polarimetric data for performing polarimetric decomposition, textural information extraction, and to generate LULC maps over the western part of Mizoram state, northeast India. The study area comprises three districts, namely Mamit, Lunglei, and Lawngtlai. We adopted two representative full-polarimetric decomposition models: classical model-based Freeman–Durden and Yamaguchi decomposition. These methods decompose the coherency matrix of PolSAR images into surface, double-bounce, and volume scattering. Textural measures, such as variance, contrast, entropy, homogeneity, dissimilarity, and uniformity are also retrieved using grey-level co-occurrence matrix (GLCM) for LULC classification. For LULC classification, we employed a support vector machine classifier and calculated the area statistics of LULC. The outcomes were checked with the help of confusion matrix derived for six classes, such as built-up, deciduous forest, evergreen forest, scrubland, bareland, and waterbody. Each LULC class is separated using the scattering properties of PolSAR images. Results exhibited that Yamaguchi four-component decomposition (overall accuracy 90% and kappa coefficient 0.88) gives relatively better LULC classification results than the Freeman–Durden three-component decomposition (overall accuracy 87% and kappa coefficient 0.84). Use of textural images of GLCM has supported the classification accuracy at par with the Yamaguchi model. Integration of polarimetric information offers a new dimension in LULC classification and produces high accuracy maps. This approach overcomes the limitations of optical data in cloud covering areas, and furthermore, it provides better classification accuracy.

**Keywords** L-band SAR · Polarimetric SAR · Polarimetric decompositions · GLCM · Support vector machines · LULC mapping

## 1 Introduction

The alteration of terrestrial surface by human activities is typically known for Land use land cover (LULC) change. Over the last few decades, the LULC is changing rapidly around the globe [1]. It is widely documented that the alterations of LULC have caused severe environmental problems, such as floods, landslides, deforestation, loss of

biodiversity, and urbanization, among others [2–7] due to mismanagement of agriculture, forest, urban, wetland, and forest. So, LULC maps are very essential for understanding any unprecedented changes in agriculture [8–10], forest ecosystems [7, 11], biodiversity/ecological process [6], environmental process, and hazard assessment [4]. LULC change information is essential for providing vital input to

✉ Bikash Ranjan Parida, bikashrp@gmail.com | <sup>1</sup>Department of Geoinformatics, School of Natural Resource Management, Central University of Jharkhand, Ranchi 835205, India.





# Nitrate-leaching and groundwater vulnerability mapping in North Bihar, India

Pankaj Kumar Gupta<sup>1</sup> · Binita Kumari<sup>2</sup> · Saurabh Kumar Gupta<sup>2</sup> · Deepak Kumar<sup>3</sup>

Received: 17 August 2019 / Accepted: 15 May 2020 / Published online: 28 May 2020  
© Springer Nature Switzerland AG 2020

## Abstract

Aquifer vulnerability assessment is crucial for studying the impact of increasing pollution load scenarios on the quantification of contaminant concentration with movement of plume for protecting groundwater resources. Only a few recent studies have focused on the performance evaluation of vulnerability assessment methods using process-based modeling approach. However, the moisture flow and pollutant transport through partially saturated zone plays a crucial role under varying hydrogeological conditions, which are generally ignored in index-based methods. Thus, the objective of this research is to evaluate the vulnerability of groundwater resources to nitrate in Samastipur, Darbhanga and Madhubani districts of Bihar State, India, using soil moisture flow and solute transport modeling. Richard's equation integrated with the classical advection dispersion equation is simulated using HYDRUS 1D by incorporating a constant head and atmospheric boundary conditions. The time taken to reach the nitrate peak concentration at groundwater table is considered to estimate vulnerability index (VI). Results have shown that high risk in terms of nitrate-leaching vulnerability in southern part of study area is dominated by Gangetic kankar in subsurface. Further, high pollution risk was reported in eastern north part of study area having alluvial deposition in subsurface. The main causes of high risk were due to the short depth of water table, little discharge and more hydraulic conductivity presence in the subsurface media. Moreover, comparatively low vulnerability was observed in area having clay capping of 2–4 m from surface. This research may help in better implementation of agricultural, soil–water conservation practices and urban/industrial infrastructure development in and around the study area.

**Keywords** Vadose zone · Groundwater resource · Pollution · Nitrate · Vulnerability · Clay capping

## Introduction

Pollution of natural water bodies such as lake, pond and rivers through application of agrochemicals in cultivated lands is major concern to fulfill safe drinking water demands of citizens of a country (Gupta and Sharma 2019; Gupta 2020a, b; Gupta and Yadav 2020; Gupta et al. 2020). Nitrate is one of the well-known agrochemicals used in irrigation practices, which possibly will leach into subsurface and ultimately reach underlying groundwater resources (Zhu et al. 2005; Siyal et al. 2012). High value of concentration of nitrate in drinking water may cause health hazardous, especially methemoglobinemia in infants (Spalding and Exner 1993; Fewtrell 2004).

Numerous studies have been published on pollution risk assessment using statistical/overlay/index-based modeling. Almasri and Kaluarachchi (2007) used GIS to characterize the spatial distribution of nitrogen-N causes and underlying groundwater pollution loadings. Similarly, De Paz

✉ Pankaj Kumar Gupta  
pk3gupta@uwaterloo.ca

Binita Kumari  
binita.kumari@cuja.ac.in

Saurabh Kumar Gupta  
srbkr72@gmail.com

Deepak Kumar  
deepak.civil.iitdelhi@gmail.com

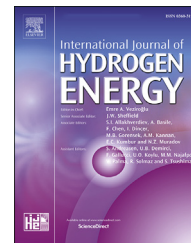
<sup>1</sup> Faculty of Environment, University of Waterloo, Waterloo, ON, Canada

<sup>2</sup> Department of Geoinformatics, Central University of Jharkhand, Ranchi 835205, India

<sup>3</sup> Department of Soil and Water Conservation Engineering, College of Technology, G.B. Pant University of Agriculture and Technology, Pantnagar 263153, India

Available online at [www.sciencedirect.com](http://www.sciencedirect.com)

ScienceDirect

journal homepage: [www.elsevier.com/locate/ije](http://www.elsevier.com/locate/ije)

# Analysis of ignition delay by taking Di-tertiary-butyl peroxide as an additive in a dual fuel diesel engine using hydrogen as a secondary fuel

Chandra Bhushan Kumar <sup>a,\*</sup>, D.B. Lata <sup>b</sup>, Dhaneshwar Mahto <sup>a</sup>

<sup>a</sup> Department of Mechanical Engineering, Birla Institute of Technology, Mesra, Ranchi 835215, India

<sup>b</sup> Department of Energy Engineering, Central University of Jharkhand, Ranchi 835205, India

## HIGHLIGHTS

- The polytropic index get increased by addition of (Di-tert butyl peroxide) DTBP.
- 5% Di tertiary butyl peroxide reduces Ignition delay.
- Hydrogen based Modified Heisenberg-Hase equation shows variation up to 11.96%.
- Ignition delay based on DTBP by modified Heisenberg-Hase equation shows variation up to 18.01%.

## ARTICLE INFO

### Article history:

Received 15 November 2019

Received in revised form

23 March 2020

Accepted 27 March 2020

Available online 22 April 2020

### Keywords:

Hydrogen fuel

Alternative fuel

DTBP (Di-tertiary-butyl-peroxide)

Dual-fuel diesel engine

Ignition delay

## ABSTRACT

Ignition delay (ID) is one of the important parameters that make influenced on the combustion process inside the cylinder. This ignition delay affects not only the performances but also the noise and emissions of the engine. In this regards the experiments were conducted on single cylinder 4–stroke compression ignition research diesel engine, power 3.50 kW at constant speed 1500 rpm Kirloskar model TV1 with base fuel as diesel and hydrogen as secondary fuel with and without Di-tertiary-butyl-peroxide (DTBP). Experiments were conducted to measure the ignition delay of the dual fuel diesel (DFD) engine at different load conditions and substitution of diesel by hydrogen with or without DTBP and then it was compared with predicted ID given by Hardenberg-Hase equation and modified Hardenberg-Hase equation.

The experimental values of ignition delay were compared with theoretical ignition delay which was predicted on the basis of Hardenberg-Hase equation by considering mean cylinder temperature, pressure, activation energy and cetane number and variations are found in between 6.60% and 21.22%. While, the Hardenberg-Hase equation was modified (by considering variation in activation energy) for DFD engine working on diesel as primary fuel and hydrogen as secondary fuel shows variations 1.20%–11.96%. Furthermore, with DTBP it gives variation up to 18.01%. It was found that ID decreases with increase in percentage of DTBP and hydrogen in air-fuel mixture. This might be due to the cetane improver nature of DTBP, pre-ignition reaction rate and energy release rate of hydrogen fuel. The polytropic index get increased by addition of (Di-tert butyl peroxide) DTBP. Similarly, 5% Di tertiary butyl peroxide reduces Ignition delay.

© 2020 Hydrogen Energy Publications LLC. Published by Elsevier Ltd. All rights reserved.

\* Corresponding author.

E-mail address: [cb19bit@yahoo.co.in](mailto:cb19bit@yahoo.co.in) (C.B. Kumar).

<https://doi.org/10.1016/j.ijhydene.2020.03.212>

0360-3199/© 2020 Hydrogen Energy Publications LLC. Published by Elsevier Ltd. All rights reserved.





# Probing of incomplete fusion dynamics in $^{14}\text{N} + ^{124}\text{Sn}$ system and its correlation with various entrance channel effects

Amritraj Mahato<sup>1</sup>, D. Singh<sup>1,a</sup>, Pankaj K. Giri<sup>1</sup>, Sneha B. Linda<sup>1</sup>, Harish Kumar<sup>2</sup>, Suhail A. Tali<sup>2</sup>, M. Afzal Ansari<sup>2</sup>, R. Kumar<sup>3</sup>, S. Muralithar<sup>3</sup>, R. P. Singh<sup>3</sup>

<sup>1</sup> Department of Physics, Central University of Jharkhand, Ranchi 835 205, India

<sup>2</sup> Department of Physics, Aligarh Muslim University, Aligarh 202 002, India

<sup>3</sup> Inter-University Accelerator Centre, Aruna Asaf Ali Marg, New Delhi 110 067, India

Received: 30 September 2019 / Accepted: 24 March 2020 / Published online: 18 May 2020  
© Società Italiana di Fisica and Springer-Verlag GmbH Germany, part of Springer Nature 2020  
Communicated by Tohru Motobayashi

**Abstract** Measurements of excitation functions were done for the evaporation residues populated in  $^{14}\text{N} + ^{124}\text{Sn}$  system at low energy. The present analysis shows the appearance of incomplete fusion by the breakup of non- $\alpha$  cluster structured projectile  $^{14}\text{N}$  into  $\alpha + ^{10}\text{B}$ . A correlation between the combined effects of total asymmetry and  $Z_P Z_T$  has been studied through three new parameters total asymmetry ( $S_{TAS}$ ), Coulomb asymmetry parameters;  $Z_P Z_T / S_{TAS}$  and  $Z_P Z_T \cdot S_{TAS}$ . These new parameters were found more sensitive and effective to encounter the combined effects of coulomb interactions and entire asymmetry effect of the system on incomplete fusion dynamics. The complete fusion and total fusion cross-sections of two systems  $^{14}\text{N} + ^{124}\text{Sn}$  and  $^{16}\text{O} + ^{124}\text{Sn}$  have been reduced using two different standard reduction procedures, which shows that the incomplete fusion probability for reactions induced by projectile  $^{16}\text{O}$  is generally larger than  $^{14}\text{N}$  induced reactions. The experimental fusion functions are found to be suppressed as compared to universal fusion function for systems  $^{14}\text{N} + ^{124}\text{Sn}$  and  $^{16}\text{O} + ^{124}\text{Sn}$ . The different values of suppression factor for projectiles  $^{14}\text{N}$  and  $^{16}\text{O}$  indicate that the probability of  $\alpha$ -breakup is different for these projectiles. Further, the total fusion functions for systems  $^{14}\text{N} + ^{124}\text{Sn}$  and  $^{16}\text{O} + ^{124}\text{Sn}$  agree well with the universal fusion function. However, the present results clearly show that the shell closure of nuclei also affect the low energy incomplete fusion dynamics along with the structure of projectile.

## 1 Introduction

Comprehensive studies of heavy ion induced reactions have been done by nuclear physicists [1–4]. The effect of incomplete fusion (ICF) on the fusion process has been widely studied by theoretical and experimental investigators [5–8]. Complete fusion (CF) is a dominant reaction mode in heavy ion interactions at projectile energy just above the Coulomb barrier and well beyond it. However, the significant contribution of ICF has also been observed at above barrier energies in some investigations [9–11]. In the CF process, the fusion of entire projectile with the target takes place, where the input angular momentum ( $\ell$ ) associated with the system is less than the critical angular momentum i.e.  $\ell < \ell_{\text{crit}}$ . In case of ICF, the projectile breaks up into its fragments before fusion and only a part of the projectile fuses with the target whereas the remaining part behaves as a spectator (fast  $\alpha$ -particle). At relatively higher values of impact parameter and energy of the incident projectile ICF takes place in the collision of the projectile with the target. The dependence of ICF dynamics on entrance channel mass-asymmetry has been studied earlier [12]. Recently, several investigators have shown great interest to study the dependence of ICF dynamics on various entrance channel parameters in search of a unique set of parameters which can explain the characteristics of ICF dynamics [13–15]. These studies show that the onset of ICF dynamics does not depend on a single entrance channel parameter, while it depends on various entrance channel parameters. Several dynamical models have been proposed to explain the gross features of ICF dynamics. The Sumrule and Break-up Fusion (BUF) models are the most popular theoretical models for ICF dynamics. The Sumrule model has been proposed by Wilczynski et al. [16]. This model suggests that ICF is mainly focused in the window of  $\ell$ -space above the

<sup>a</sup> e-mail: dsinghcuj@gmail.com (corresponding author)



# Corrosion Behavior of Newly Developed High-Strength Bainitic Railway Wheel Steels

A.P. Moon, K. Chandra Sekhar, S. Mahanty, S. Sangal, and K. Mondal

(Submitted November 26, 2019; in revised form April 14, 2020; published online May 18, 2020)

**High-strength bainitic wheel steels based on a new steel composition, namely MS2 [0.47% C, 0.87% Mn, 0.51% Si, 0.02% Mo, 0.03% Cu, 0.031% S, 0.033% P and rest Fe (weight percent)], were prepared by austempering treatment at 400 °C for 10, 30, 60 and 120 min. Corrosion behavior of the bainitic MS2 steels and normalized ferritic–pearlitic MS2 steel was studied and compared with that of the conventional ferritic–pearlitic wheel steel. Immersion test, electrochemical polarization and salt fog tests were carried out in 3.5% NaCl. Bainitic steels prepared with higher holding duration during austempering exhibited improved corrosion resistance on salt fog exposure. In contrast, bainitic steels prepared with lower holding duration during austempering resulted in better corrosion resistance on electrochemical polarization test. Salt fog test revealed gradual improvement in corrosion resistance for the bainitic steels with the successive holding. Improved corrosion behavior for the bainitic steel was related to the tiny and uniform spreading of iron carbide in the ferritic matrix resulting in the uniform coverage of the protective oxide layer on the steel surface. The enrichment of Si on the corroded surface of bainitic steel favored the formation of supermagnetic  $\alpha$ -FeOOH of smaller particle size, improving the protective character of the rust against corrosion. Corrosion mechanisms for the ferritic–pearlitic and bainitic wheel steels were put forward.**

**Keywords** bainitic steels, corrosion behavior, ferritic–pearlitic steel, polarization, railway wheel

## 1. Introduction

Railway steel components, such as rail, axle and wheel, undergo corrosion over a period of time (Ref 1–4). Wheel is considered to be the most stressed components of railway vehicles. Wheel steels guide the train on the tracks through curves and switches. Conventional wheel steels based on ferritic–pearlitic microstructure could carry axle load up to 25 tonnes and above (Ref 2). Corrosion is very dangerous for the reliability and service life of railway wheels. Damages due to corrosion could lead to embrittlement of wheels. Corrosion damages on the wheel surface are also susceptible to cracks and contribute to wear. Pinchuk et al. (Ref 3) have suggested that “white layers,” grain size variation and structure streakiness of wheel steel promote corrosion rate. White layer is hard and brittle layer and results from severe plastic deformation of the austenitic phase at low temperature, and sometimes, it develops at a considerably higher temperature. They have also reported that nonmetallic inclusions are likely sources of corrosion nucleation and their effect depends on the nature of inclusion. Corrosion of various parts of a wheel usually takes place under

static condition (non-running condition). Particularly, the static state of the wheel allows water collection, salt and pollutant inside the pockets of the rim-plate junction of the wheel. Miscellaneous factors, such as atmospheric, wet, gaseous, seawater, stress fretting and stray current, contribute to the corrosion of wheel (Ref 3, 4).

It has been observed that nucleation of fatigue cracks on the metal surface could not occur before 90% of normal service life of metal has elapsed. But, corrosion has the potential to introduce fatigue cracks very early (Ref 4). Oxides formed on the tread part of a wheel during corrosion of steel change properties of the surface (strength, plasticity and wear resistance) and influence the interaction between railway wheel and rail during the running operation.

It has been observed that wheel steel during manufacturing undergoes different degrees of plastic deformation and develops heterogeneous grain size at different locations of the wheel steel, resulting in varied corrosion behavior in different sections. The heterogeneous plastic deformation, which develops along the rim width during manufacturing of railway wheels, results in higher corrosion during operation in the roll zone than the cavetto part of the wheel (Ref 4).

In railway wheel, the plastic deformation is heterogeneous along its depth resulting different degrees of grains elongation. In cavetto zone, the degree of deformation,  $\epsilon$ , is 65–75% and it reduces to 22–25% at the middle of tread and increases up to 90% in the roll zone (Ref 3, 4). This results in variation in grain size, and banding of wheel steel structure influences the corrosion rate at different locations of wheel steels (Ref 3).

Many investigations show that the evidence of corrosion is more likely at rim width region of the wheel steel (Ref 3, 4). Pits arising from corrosion trigger the fatigue crack and lead to fracture of the tread portion of the wheel steel. Ren et al. (Ref 5) have recommended a critical corrosion pit depth (300  $\mu\text{m}$ ) on the wheel steel based on their experimentation and FEM analysis and considered corrosion as a key problem for the

A.P. Moon, Tata Steel Limited, Jamshedpur, Jharkhand 831001, India; K. Chandra Sekhar, Department of Metallurgical and Materials Engineering, Indian Institute of Technology, Roorkee 247667, India; S. Mahanty, Department of Applied Physics, Central University of Jharkhand, Brambe 835205, India; and S. Sangal and K. Mondal, Department of Materials Science and Engineering, Indian Institute of Technology, Kanpur 208 016, India. Contact e-mail: abhijeet.moon@tatasteel.com.



# A Comparative Study on Shear Strength and Deformation Behaviour of Clayey and Sandy Soils Reinforced with Glass Fibre

Suchit Kumar Patel · Baleshwar Singh

Received: 31 December 2019 / Accepted: 27 April 2020 / Published online: 6 May 2020  
© Springer Nature Switzerland AG 2020

**Abstract** In this investigation, the shear strength and specimen deformation behaviour of glass fibre-reinforced clayey and sandy soils have been compared based on the results of consolidated undrained and consolidated drained triaxial tests, respectively under varying moulded states. The clayey soil specimens were moulded with varying dry unit weight, whereas sandy soil specimens were moulded at relative densities ranging from 35 to 85%. For any moulded state, no peak is noted in the stress–strain curves of reinforced clayey soil up to 20% axial strain. In case of the reinforced sandy soil, clear peak is observed well before 20% axial strain with post-peak stress reduction at all relative densities. Reinforced clayey soil shows bulging at all dry unit weights. For the reinforced sandy soil, bulging failure is noted at 35% relative density, whereas shear failure occurs at relative densities of 65% and 85%. At all dry unit weights, under undrained condition, the reinforced clayey soil exhibits only positive pore water pressure indicating contractive behaviour at all axial strains.

Under drained condition, the reinforced sandy soil of 35% relative density shows contractive behaviour, while the specimens of 65% and 85% relative densities indicate contractive response at smaller axial strain followed by dilative behaviour at higher strain. The increase of shear strength is up to 0.75% and 3% fibre content in the clayey and sandy soils, respectively irrespective of moulded states. At respective optimum fibre reinforcements, the benefit of glass fibre reinforcement is greater for the sandy soil. The possible environmental impact and field application of glass fibre-reinforced soil have also been discussed.

**Keywords** Glass fibre · Dry unit weight · Relative density · Shear strength · Failure mode

## List of Symbols

$B$	Foundation width
$FC$	Fibre contribution
OMC	Optimum moisture content
MDU	Maximum dry unit weight
$C_u$	Coefficient of uniformity
$C_c$	Coefficient of curvature
$D$	Foundation depth
$D_r$	Relative density
$ESP$	Effective stress path
$H$	Height of earth retaining structure
$K_a$	Active earth pressure coefficient
$N_c, N_q$ and $N_\gamma$	Bearing capacity factors
$Q$	Ultimate bearing capacity

---

S. K. Patel (✉)  
Department of Transport Science and Technology,  
Central University of Jharkhand, Ranchi,  
Jharkhand 835205, India  
e-mail: suchit.patel@cuja.ac.in

B. Singh  
Department of Civil Engineering, Indian Institute of  
Technology Guwahati, Guwahati, Assam 781039, India  
e-mail: baleshwar@iitg.ac.in

# Gold-Catalyzed Oxidative Alkyne Functionalization by N-O/S-O/C-O Bond Oxidants

Sabyasachi Bhunia,<sup>a,\*</sup> Partha Ghosh,<sup>a</sup> Snigdha Rani Patra<sup>a</sup>

<sup>a</sup>Department of Chemistry, Central University of Jharkhand, Ranchi, Jharkhand 835205, India

E-mail: [sabyasachi.bhunia@cuja.ac.in](mailto:sabyasachi.bhunia@cuja.ac.in)

**Abstract:** Since the beginning of this century, homogeneous gold-catalyzed alkyne transformations have been an active area of research in pursuit of developing efficient synthetic methodologies. This emerging area of research which at the beginning exploited the mild Lewis acid character of gold and its propensity to form  $\pi$ -complex with alkyne, has been reinvigorated upon the discovery of gold-catalyzed oxidative alkyne functionalization in 2007. The gold-catalyzed alkyne oxidation enabled direct access to  $\alpha$ -oxo gold carbenes and gold alkynal complex with versatile reactivity which has been applied to achieve transformations including but not limited to oxyarylation, C–H, X–H (X = N, O) insertion, cyclization, cycloaddition, ring expansion, and various cascade reactions. This review provides a comprehensive summary of methods, applications and mechanistic insight of gold-catalyzed oxidative alkyne functionalization by N–O/S–O/C–O bond oxidants covering the literature reports appeared since 2007.

1 Introduction

2 Oxidative 1,2-difunctionalizations of alkynes

3 Oxyarylation through Friedel–Crafts type reaction and [3,3]-sigmatropic rearrangement

3.1 Intramolecular Friedel–Crafts type cyclization through internal oxidation

3.2 Intramolecular Friedel–Crafts type cyclization by external oxidant

3.3 Intermolecular Friedel–Crafts type reaction

3.4 [3,3]-Sigmatropic rearrangement

4 Alkyne oxidative X–H insertions

4.1 Intramolecular X–H insertion

4.1.1  $sp^3$  C–H insertion

4.1.1.1  $sp^3$  C–H insertion through  $\alpha$ -oxo gold carbene path

4.1.1.2  $sp^3$  C–H activation through non-carbene path.

4.1.2 N–H insertion

4.1.3 O–H insertion

4.2 Intermolecular X–H Insertion

5 Alkyne oxidative cycloaddition reaction

6 Alkyne oxidative cyclopropanation reaction

7 Alkyne oxidative 1,2-insertion/migration into  $\alpha$ -oxo gold carbene

7.1 1,2-alkyl, aryl, thiol, alkenyl, alkynyl, benzoyloxy or acyloxy and 1,2-enynyl migration into  $\alpha$ -oxo gold carbene or alkenyl gold species

7.2 1,2-H migration into  $\alpha$ -oxo gold carbene

7.3 Oxidative ring-expansion through 1,2-migration of C–C bond

8. Alkyne oxidation and sequential cascade reaction

8.1 Intermolecular trapping of  $\alpha$ -oxo gold carbene

8.2 Intermolecular trapping of  $\alpha$ -oxo gold carbene & subsequent annulation reaction

8.3 Intramolecular trapping of  $\alpha$ -oxo gold carbene & simultaneous cascade sequences

9 Gold-catalyzed enantioselective oxidative alkyne functionalization

10 Conclusions

**Keywords:** alkyne oxidation;  $\alpha$ -oxo gold carbene; oxygenated alkenyl gold; oxidative alkyne functionalization; C–H insertion

## 1 Introduction

Discovery of new efficient ways to construct complex carbo- & hetero-cycles from simple and readily available precursors has been an ever continuing pursuit in organic chemistry. A very attractive way to meet this demand would be through transition metal catalyzed transformation of doubly unsaturated alkynes. Among the transition metals gold in particular has found wide application due to its propensity to form  $\pi$  complex with alkyne together with mild Lewis acidity.<sup>1,2,3</sup> At the beginning of homogeneous gold catalysis,<sup>4,5,6,7,8,9</sup> alkyne substrates were extensively